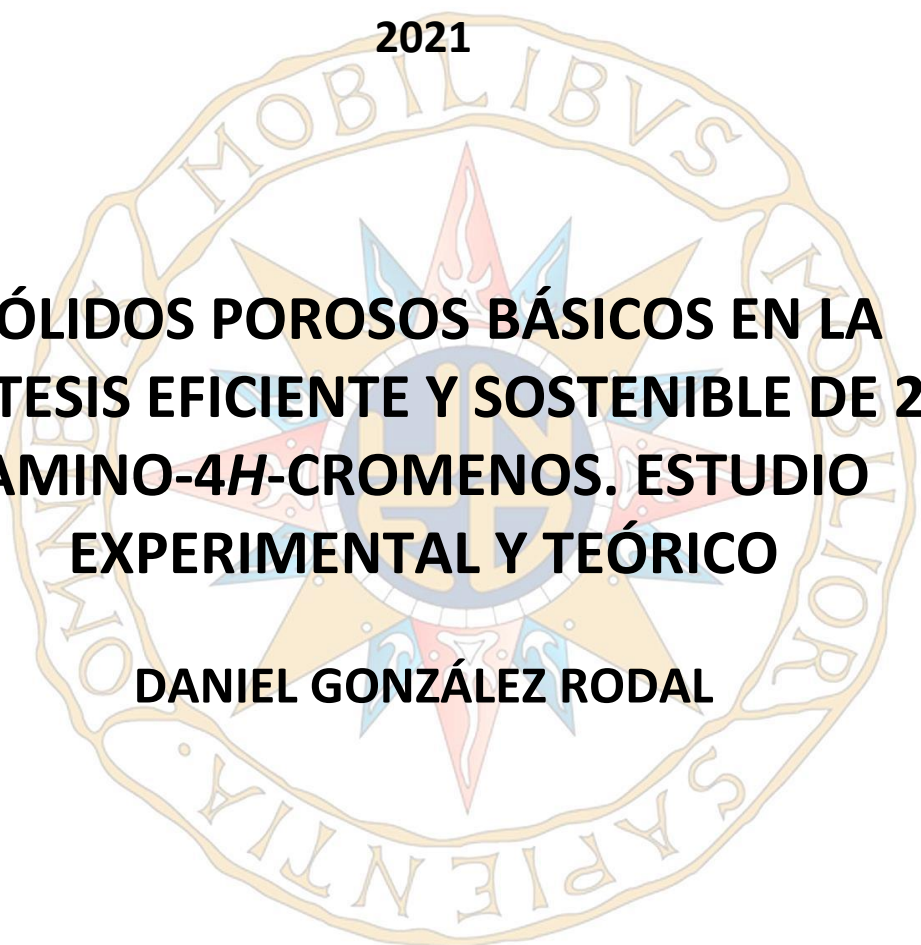


TESIS DOCTORAL

2021

The seal of the University of Zaragoza is a circular emblem. It features a central shield with a crown on top, surrounded by a sunburst. The shield is divided into four quadrants with various symbols. The entire emblem is encircled by a gold border containing the Latin motto 'SAPIENTIA MOBILIBVS' at the top and 'MAGIS BONA' at the bottom.

**SÓLIDOS POROSOS BÁSICOS EN LA
SÍNTESIS EFICIENTE Y SOSTENIBLE DE 2-
AMINO-4H-CROMENOS. ESTUDIO
EXPERIMENTAL Y TEÓRICO**

DANIEL GONZÁLEZ RODAL

PROGRAMA DE DOCTORADO EN CIENCIAS

DIRECTORES:

MARÍA ELENA PÉREZ MAYORAL

JOSE ANTONIO LÓPEZ PEINADO

*“¿Cuáles son las tres leyes más importantes del químico?
Eso sí me lo había enseñado Ben.
Etiquetar con claridad. Medir dos veces. Comer en otro sitio.”*

*Patrick Rothfuss
El Nombre del Viento*

A Ana

AGRADECIMIENTOS

En primer lugar, me gustaría agradecer a mis directores, la Dra. Elena Pérez Mayoral y el Dr. Antonio José López Peinado, por toda la entrega, motivación, apoyo, dedicación, cariño y empuje que han hecho posible la realización de este trabajo.

A la Universidad Nacional de Educación a Distancia y al Departamento de Química Inorgánica y Química Técnica y todos sus miembros, por darme la oportunidad de desarrollar este trabajo, en especial a la Dra. María Luisa Rojas Cervantes y a la Dra. M^a Ángeles García Fernández, por toda la ayuda que me han brindado durante estos años.

Al Dr. Jacek Przepiórski, a la Dra. Gemma Isabel Turnes Palomino, a la Dra. Maria Ziolk y a la Dra. Izabela Sobczak, por su inestimable ayuda en la preparación y caracterización de los materiales descritos en el presente trabajo.

A la Dra. Elena Soriano Santamaría por su tutela, cariño y paciencia durante mis primeros pasos en el mundo de la Química Computacional.

A mis compañeras, Marina y Agata, por haber sido un espejo en el que mirarme.

A Po Kai, Chesco y todos los compañeros que me han acompañado en algún tramo de este camino tan largo.

A Cons, Ana, Bibi, Valbuena, Ángel, Nani, Raúl, Patri, Tamara, Jose y Adri, por apuntalarme tantas veces.

A Sura y Ziggy, por haberlo hecho todo más fácil.

A la familia de Ana, por todo el ánimo que siempre me han transmitido.

A toda mi familia, por su aliento pese a la distancia.

A mis padres, Teté y Lito, por su amor, fuerza y apoyo incondicional que me han permitido alcanzar mis metas.

Ana, esta tesis es tan tuya como mía. Gracias por todo.



Departamento de Química Inorgánica y Química Técnica
Facultad de Ciencias
Universidad Nacional de Educación a Distancia

Dña ELENA PÉREZ MAYORAL, Profesora Titular de Química Inorgánica y **D. ANTONIO J. LÓPEZ PEINADO**, Catedrático de Química Inorgánica, en el Departamento de Química Inorgánica y Química Técnica, de la Facultad de Ciencias de la UNED,

INFORMAN:

Que **D. DANIEL GONZÁLEZ RODAL** ha realizado su Tesis Doctoral en el grupo de investigación de “*Catálisis no Convencional Aplicada a la Química Verde*”, bajo nuestra dirección, en el Departamento de Química Inorgánica y Química Técnica, de la Facultad de Ciencias, en la UNED.

Durante la realización de este trabajo Daniel se ha mostrado como una estudiante responsable, de trato impecable, tanto con sus superiores como con sus compañeros de laboratorio; es un estudiante trabajador que ha demostrado sobradamente su interés y buen hacer. Daniel destaca por ser un investigador en formación perseverante, resolutivo y autónomo con la motivación, constancia y aptitudes que requiere la labor investigadora.

Daniel es un estudiante altamente cualificado; es graduado en Ciencias Criminológicas y de la Seguridad Pública (Universidad de Santiago de Compostela, 2011) y Licenciado en Ciencias Químicas (UNED, 2014), además de haber superado el Postgrado en Ciencia y Tecnología Química, con especialidad en Química Inorgánica (UNED, 2015). Ha realizado, además, una estancia de investigación, durante los meses de enero a junio de 2018, en la Nanyang Technological University of Singapore, financiada por EURASIACAT (Advanced Education European-Asiatic Program in Materials Science and Catalysis), lo que sin duda ha contribuido enormemente a su formación como investigador.

La formación de Daniel en Química está avalada por la comunicación de los resultados obtenidos en numerosos congresos, tanto nacionales como internacionales, por la publicación de un capítulo de libro y de artículos científicos, en revistas internacionales especializadas de alto índice de impacto en su categoría:

1. E. Pérez-Mayoral, M. Godino-Ojer and D. González-Rodal. Bifunctional Porous Catalysts in the Synthesis of Valuable Products: Challenges and Prospects, chapter 2, 27-80. In: "Nanocatalysis: applications and technologies", Eds. V. Calvino-Casilda, A. López-Peinado, R.M. Martín-Aranda, E. Pérez-Mayoral; Taylor & Francis Group, 2019, CRC Press, New York. DOI: <https://doi.org/10.1201/9781315202990>
2. D. González-Rodal, J. Przepiorski, A. J. López Peinado, E. Pérez-Mayoral. Basic-carbon nanocatalysts in the efficient synthesis of chromene derivatives. Valorization of both PET residues and mineral sources. Chem. Eng. J. **2020**, *382*, 122795.
DOI: [10.1016/j.cej.2019.122795](https://doi.org/10.1016/j.cej.2019.122795)
Índice de impacto: 10,652 (2019); Categoría: ENGINEERING, CHEMICAL, 4/143, Q1; ENGINEERING, ENVIRONMENTAL, 2/53, Q1.
3. D. González-Rodal, G. Turnes Palomino, C. Palomino Cabello, E. Pérez-Mayoral. Amino-grafted Cu and Sc Metal-Organic Frameworks involved in the green synthesis of 2-amino-4*H*-chromenes. Mechanistic understanding. Micropor. Mesopor. Mat. **2021**, *323*, 111232.
DOI: [10.1016/j.micromeso.2021.111232](https://doi.org/10.1016/j.micromeso.2021.111232)
Índice de impacto: 4,551 (2019); Categoría: CHEMISTRY, APPLIED 13/71, Q1.

Otros artículos relacionados con esta Tesis Doctoral:

4. F. D. Velázquez-Herrera, D. Gonzalez-Rodal, G. Fetter, E. Perez-Mayoral. Towards highly efficient hydrotalcite/hydroxyapatite composites as novel catalysts involved in eco-synthesis of chromene derivatives. Appl Clay Sci. **2020**, *198*, 105833.
DOI: [10.1016/j.clay.2020.105833](https://doi.org/10.1016/j.clay.2020.105833)
Índice de impacto: 4,605 (2019); Categoría: MINERALOGY, 2/30, Q1
5. F. D. Velázquez-Herrera, D. Gonzalez-Rodal, G. Fetter, E. Perez-Mayoral. Enhanced catalytic performance of highly mesoporous hydrotalcite/SBA-15 composites involved in chromene multicomponent synthesis, Micropor. Mesopor. Mat. **2020**, *309*, 110569.
DOI: [10.1016/j.micromeso.2020.110569](https://doi.org/10.1016/j.micromeso.2020.110569)
Índice de impacto: 4,551 (2019); Categoría: CHEMISTRY, APPLIED 13/71, Q1

Por todo ello, informamos que esta Tesis Doctoral titulada “SÓLIDOS POROSOS BÁSICOS EN LA SÍNTESIS EFICIENTE Y SOSTENIBLE DE 2-AMINO-4H-CROMENOS. ESTUDIO EXPERIMENTAL Y TEÓRICO”, realizada por D. Daniel González Rodal, bajo nuestra dirección, en el laboratorio del Departamento, reúne todos los requisitos, por lo que autorizamos su presentación y posterior defensa pública.

Madrid, 1 de mayo de 2021

Fdo.: Elena Pérez Mayoral

Fdo.: Antonio J. López Peinado

Las investigaciones realizadas se han financiado con cargo al proyecto de investigación concedido por MICINN (CTM2014-5668-R).

ESTRUCTURA DE LA TESIS DOCTORAL

La presente Tesis Doctoral se estructura en los siguientes Capítulos:

Capítulo I: Introducción

Capítulo II: Objetivos

Capítulos III-VI: Resultados obtenidos, discusión y conclusiones del estudio realizado.

Capítulo VII: Sección Experimental.

Y finalmente la bibliografía consultada.

Con el objetivo de optar a la mención internacional de la Tesis Doctoral, algunos apartados de la Memoria se han escrito en inglés, concretamente los capítulos del II al VII.

El **Capítulo I** consiste en una breve introducción acerca del **estado del arte** en la investigación de los materiales estudiados y sus diversas aplicaciones. Además, se detalla la relevancia de los 2-amino-4*H*-cromenos, compuestos objeto de síntesis en el presente trabajo. Se incluye también un resumen sobre los principales conceptos acerca de la Química Verde y por qué resulta de relevancia en el desarrollo de este trabajo. Finalmente, se resumen aspectos destacados en relación a la Química Computacional.

El **Capítulo II** recoge los objetivos principales de la presente Tesis Doctoral.

En el **Capítulo III** se describe una familia de **carbones activados de carácter básico**, preparados a partir de tereftalato de polietileno como precursor de la matriz carbonosa, permitiendo el reciclado de residuos plásticos en su síntesis, y fuentes minerales naturales —caliza, magnesita y dolomita— como precursoras de las distintas especies activas —CaO y/o MgO—. Estos materiales actúan como nanocatalizadores ecoeficientes en la síntesis de 2-amino-4*H*-cromenos. Además, se detalla el estudio mecanístico de la reacción catalizada por clústers de CaO, la especie que presenta mayor actividad catalítica. La caracterización de los materiales sintetizados se ha llevado a cabo en colaboración con el grupo de investigación del Prof. Jacek Przepiórski (West Pomeranian University of Technology).

En el **Capítulo IV** se describen dos familias de redes metaloorgánicas —de Cu y Sc— funcionalizadas con aminas utilizando dos metodologías distintas, de forma que se consigue una funcionalización total o parcial de la superficie del material poroso. Estos materiales catalizan de forma eficiente la síntesis de 2-amino-4*H*-cromenos, mejorando los rendimientos de los materiales descritos en el capítulo anterior. Además, se comenta el estudio mecanístico llevado a cabo. La síntesis de los materiales MIL-100 y la caracterización se ha llevado a cabo en colaboración con el grupo de investigación de la Prof. Gemma Turnes Palomino (Universidad de las Islas Baleares).

En el **Capítulo V** se describen una serie de catalizadores basados en sílices mesoporosas tipo SBA-15, funcionalizadas con distintos silanos comerciales que presentan grupos amino en su estructura química, empleando el método post-sintético. Se describe la actuación de estos materiales como catalizadores en la síntesis eficiente y selectiva de 2-amino-4*H*-cromenos, permitiendo el empleo de unas condiciones de reacción más suaves y mejorando las conversiones hacia el producto deseado. Los resultados obtenidos se han racionalizado mediante un estudio mecanístico que relaciona la etapa limitante del proceso con el carácter ácido-base de los catalizadores, siendo más activos aquellos que presentan una mayor basicidad. La caracterización por FTIR de los materiales sintetizados se ha llevado a cabo en colaboración con el grupo de investigación de la Prof. Gemma Turnes Palomino (Universidad de las Islas Baleares).

El **Capítulo VI** describe la preparación de catalizadores síliceos del tipo MCF, con metales (Nb, Ta) en su estructura, incorporados durante su síntesis a partir de distintas sales del correspondiente metal (etóxidos y oxalatos). Se detalla la funcionalización de los materiales mediante grafting y cómo estos catalizadores mejoran enormemente los rendimientos y selectividad del proceso con respecto a aquellos obtenidos con los materiales previamente preparados. La caracterización de los materiales sintetizados se ha llevado a cabo en colaboración con el grupo de investigación de la Prof. María Ziolek (Adam Mickiewicz University).

En el **Capítulo VII** se detallan los materiales y equipos utilizados, así como los procedimientos y metodologías experimentales, además de los datos espectroscópicos de los productos sintetizados.

Y, finalmente, se muestra la bibliografía consultada en la elaboración del presente documento.

Índice de abreviaturas

ZAPTMS: [3-(2- aminoethylamino) propyl] trimethoxysilane

AES: Atomic Emission Spectroscopy

ATD: Análisis Térmico Diferencial

APTMS: (3-aminopropil)trimetoxisilano (*(3-aminopropyl)trimethoxysilane*)

APTES: (3-aminopropyl)triethoxysilane

atm: atmósferas

BET: Brunauer-Emmett-Teller

B3LYP: Funcional de densidad Becke, 3-parámetros, Lee-Yang-Parr

BTC: 1,3,5-benzenetricarboxylate

CA: Carbones Activados

CAL: Caliza (*Limestone*)

CC: Coupled-Clusters

CCSD: Coupled Cluster Single-Double

CGTO: Orbitales Tipo Gaussianos Contraídos (*Contracted Gaussian-Type Orbitales*)

CI: Configuration Interactions

COF: Covalent Organic Frameworks

CUS: Coordinatively Unsaturated Metal Sites

D: diámetro (*diameter*)

DEAPTMS: [3-(diethylamino)propyl]trimethoxysilane

DET: Diethylenetriamine

DFT: Teoría del Funcional de Densidad (*Density Functional Theory*)

DMF: Dimetilformamida (*Dimethylformamide*)

DTA: Análisis Térmico Diferencial (*Differential Thermal Analysis*)

DOL: Dolomita (*Dolomite*)

E_{Coul}: Energía de Coulomb

EN: Ethylenediamine

EPA: Agencia de Protección Medioambiental (*Environmental Protection Agency*)

E_T: Energía cinética

E_v: Energía de interacción electrón-núcleo

E_{xc}: Energía de correlación-intercambio

feiQue: Federación Empresarial de la Industria Química Española

FTIR: Espectroscopía Infrarroja por Transformada de Fourier (*Fourier-Transform Infrared Spectroscopy*)

g(E): Gradiente de energía

GTO: Orbitales Tipo Gaussianos (*Gaussian-Type Orbitals*)

H: Matriz Hessiana

HF: Hartree-Fock

HTC: Carbonización hidrotermal (*Hydrothermal Carbonization*)

I+D+i: Investigación, desarrollo e innovación

ILs: Líquidos Iónicos (*Ionic Liquids*)

INE: Instituto Nacional de Estadística

IRC: Intrinsic Reaction Coordinate

IUPAC: Unión Internacional de Química Pura y Aplicada (*International Union of Pure and Applied Chemistry*)

K: Kelvin

KS: Kohn-Sham

MAG: Magnesita (*Magnesite*)

MAPTMS: (3-metilaminopropil)trimetoxisilano (*(3-methylaminopropyl)trimethoxysilane*)

MC: Mecánica Cuántica

MCF: Mesoporous Cellular Foam

MCM-41: Mobile Composition of Matter 41

MCR: Reacción Multicomponente (*Multicomponent reactions*)

MM: Mecánica Molecular

MMEN: N,N'-dimethylenediamine

MOF: Redes Metaloorgánicas (*Metal-Organic Framework*)

MPn: Moller and Plesser

MW: Microondas (*Microwave*)

MWCNTs: Nanotubos de carbono de pared múltiple (*Multi Wall Carbon Nanotubes*)

nm: nanómetro (*nanometer*)

NMR: Resonancia Magnética Nuclear (*Nuclear Magnetic Resonance*)

PBC: Condiciones Periódicas de Contorno (*Periodic Boundary Conditions*)

PET: Tereftalato de Polietileno (*Polyethylene Terephthalate*)

PIB: Producto Interior Bruto

PZC: Point of Zero Charge

QF: Química Fina

QV: Química Verde

RC: Reactant Complex

SBA-15: Santa Barbara Amorphous 15

SBU: Unidades de Construcción Secundaria (*Secondary Building Units*)

SCF: Campo Autoconsistente (*Self-Consistent Field*)

SE: Métodos Semiempíricos (*Semi Empirical Method*)

SEM: Microscopía Electrónica de Barrido (*Scanning Electron Microscopy*)

SEP: Superficie de Energía Potencial

SNC: Sistema Nervioso Central

STO: Orbitales de Slater (*Slater-Type Orbitals*)

TEM: Microscopía de Transmisión Electrónica (*Transmission Electron Microscopy*)

TEOS: Tetraortoetilsilicato (*Tetraethyl ortosilicate*)

TG: Termogravimetría (*Thermogravimetry*)

TMB: 1,3,5-trimetilbenceno

TNF α : Factor de Necrosis Tumoral α (*Tumour Necrosis Factor Alpha*)

US: Ultrasonidos

UV-Vis: Ultraviolet-Visible Spectroscopy

TS: Estado de transición (*Transition Structure*)

VOCs: Compuestos Orgánicos Volátiles (*Volatile Organic Compounds*)

XRD: Difracción de Rayos X (*X-Ray Diffraction*)

XRF: Fluorescencia de Rayos X (*X-Ray Fluorescence*)

Índice de figuras

Figura 1. Datos clave del sector químico español.

Figura 2. Doce Principios de la Química Verde.

Figura 3. Green ChemisTREE.

Figura 4. Influencia del proceso Haber-Bosch en el crecimiento de la población mundial.

Figura 5. Estructura base de los a) cromenos y b) isocromenos.

Figura 6. Compuestos con estructura base de cromeno extraídos de especies vegetales (*Ageratina Pichinchenis*, familia *Asteraceae*, izquierda; y *Amyris Brenesii*, familia *Rutaceae*, derecha).

Figura 7. Estructura de cromenos con aplicaciones farmacéuticas: a) *hematoxilina*, b) AX-024, c) HA-14-1.

Figura 8. Flores de *Haematoxylum campechianum* y sección de un glomérulo de un riñón de mamífero teñido con una mezcla de hematoxilina (núcleos, color violáceo) y eosina (citoplasma, color rosado).

Figura 9. Plegamiento de las láminas microcristalinas que generan la estructura de un CA.

Figura 10. Representación gráfica de la distribución de los distintos tipos de poro en un CA.

Figura 11. Isotermas de adsorción según la clasificación de la IUPAC.

Figura 12. Ciclos de histéresis según la clasificación de la IUPAC.

Figura 13. Representación de diversos grupos funcionales en la superficie de un CA.

Figura 14. Perfil de energía libre en la reacción de condensación entre 2-amino-5-clorobenzaldehído y acetoacetato de etilo catalizada por MgO.

Figura 15. Esquema estructural de un MOF.

Figura 16. Ejemplos de ligandos orgánicos con grupos carboxilos habitualmente utilizados en la síntesis de MOFs.

Figura 17. Número de publicaciones por año, desde 1990 hasta 2018, en las que aparece la terminología “Metal-Organic Framework” según la base de datos de la Web of Science.

Figura 18. Ejemplos de diversas unidades inorgánicas (los poliedros azules corresponden a unidades inorgánicas metal-oxígeno, mientras que los polígonos y poliedros rojos delimitan las

correspondientes SBUs) y orgánicas (los polígonos y poliedros verdes corresponden a las SBUs) de MOFs derivados de ligandos carboxílicos. Las esferas rojas corresponden a átomos de oxígeno, las verdes de nitrógeno y las negras de carbono.

Figura 19. Expansión reticular. Manteniendo la misma topología, la adición de ligandos orgánicos a la SBU de partida, permite aumentar el tamaño de poro del material.

Figura 20. MOF-200 (izquierda) y MOF-210 (derecha). Las esferas naranjas y amarillas indican los diferentes espacios en el interior del material.

Figura 21. Propiedades y aplicaciones de MOFs en catálisis heterogénea.

Figura 22. Imágenes SEM (a y b) y TEM (c y d) de SBA-15.

Figura 23. Interacciones precursor-surfactante no iónico en la síntesis de nanoestructuras mesoporosas silíceas.

Figura 24. Síntesis de SBA-15.

Figura 25. Modelo de estructura coralina de los materiales MCF.

Figura 26. Imágenes TEM de sílices MCF con distintos tamaños medios de poro (a: 6,3 nm, b: 11,5 nm, c: 26,4 nm y d: 42,1 nm).

Figure 27. Thermogravimetric profile of PET/CAL 30:70 sample.

Figure 28. XRD patterns of PET/CAL 30:70 recently synthesized, PET/CAL 30:70(1), stored under atmospheric conditions, PET/CAL 30:70(2), and re-calcined PET/CAL 30:70(3).

Figure 29. N₂ adsorption/desorption isotherms for PET/CAL hybrid materials.

Figure 30. TEM images of the samples with different PET/CAL ratio: a) PET/CAL 30:70, b) PET/CAL 50:50, c) PET/CAL 70:30 y and d) PET/CAL 83:17.

Figure 31. Synthesis of 2-amino-4*H*-chromenes **1** catalysed a) by PET/CAL hybrid materials, and b) by PET/CAL 100:00 and Norit RX3, both at 323 K, under solvent-free conditions.

Figure 32. Synthesis of 2-amino-4*H*-chromenes **1** catalysed by PET/CAL 30:70 hybrid materials, at 323 K, under solvent-free conditions.

Figure 33. Synthesis of 2-amino-4*H*-chromenes **1** catalysed by PET/CAL 70:30 hybrid material, at 303 K, under solvent-free conditions.

Figure 34. Synthesis of 2-amino-4*H*-chromenes **1** catalysed by PET/CAL 30:70(2), PET/DOL 30:70 and PET/MAG 30:70 hybrid materials, at 323 K, under solvent-free conditions

Figure 35. Synthesis of 2-amino-4*H*-chromenes **1** catalysed by PET/CAL 30:70(1) and PETb/CAL 30:70 hybrid materials, at 323 K, under solvent-free conditions.

Figure 36. Free-energy profiles computed for the uncatalysed and catalysed synthesis of chromenes **1**.

Figure 37. Optimized transition structures TS_{R-11} for the first step of the reaction in the formation of chromenes **1**. a) TS_{R-11} in the absence of any catalyst. b) $TS_{R-11(CaO)}$ in the presence of CaO. Relevant distances are expressed in Å.

Figure 38. Optimized transition structures TS_{I1-I2w} TS_{I2-I3w} for the catalysed synthesis of chromenes **1**. a) $TS_{I1-I2w(CaO)}$ and b) $TS_{I2-I3w(CaO)}$. Relevant distances are expressed in Å.

Figure 39. X-Ray diffractograms of amino-grafted a) CuBTC and b) MIL-100(Sc) samples.

Figure 40. Nitrogen adsorption-desorption isotherms for amino-grafted a) CuBTC and b) MIL-100(Sc) samples.

Figure 41. FTIR spectra for amino-grafted a) CuBTC and b) MIL-100(Sc) samples.

Figure 42. FTIR spectra of CO adsorbed at 100 K on bare and amino-grafted a) CuBTC and b) MIL-100(Sc) samples. IR absorption bands in 2240-2080 cm^{-1} region.

Figure 43. Thermogravimetric profile of a) EN-M/CuBTC sample and b) CuBTC sample.

Figure 44. Synthesis of 2-amino-4*H*-chromenes **1**, from 2-hydroxybenzaldehyde **2** and ethyl cyanoacetate **3**, catalysed by a) amino-grafted CuBTC and MIL-100(Sc) at 323 K, b) EN-M/CuBTC and EN-M/MIL-100(Sc) at 303 K, c) DET/CuBTC and MMEN-M/MIL-100(Sc) at 323 K and d) DET/CuBTC and MMEN-M/MIL-100(Sc) at 303 K. Reaction conditions: 25 mg of catalysts, 2/3 molar ratio = 2:4, solvent-free conditions.

Figure 45. Reduced models simulating a) bare CuBTC, b) EN or EN-M/CuBTC and c) DET/CuBTC catalysts.

Figure 46. Optimized TS for the aldolization reaction between 2-hydroxybenzaldehyde **2** and ethyl cyanoacetate **3** (*keto* form) catalysed by a) EN/CuBTC and b) DET/CuBTC. Relevant distances are expressed in Å.

Figure 47. Optimized transition structures for the aldolization reaction between 2-hydroxybenzaldehyde **2** and ethyl cyanoacetate **3** (*enol* form) catalysed by a) EN/CuBTC and b) DET/CuBTC. Relevant distances are expressed in Å.

Figure 48. Optimized TS for the aldolization reaction between 2-hydroxybenzaldehyde **2** and ethyl cyanoacetate **3** catalysed by EN/CuBTC. a) Cu...O=C and b) Cu...N≡C interactions. Relevant distances are expressed in Å.

Figure 49. A) Adsorption/desorption isotherms of amino-grafted SBA-15 catalysts. B) XRD patterns for SBA-15 and amino-grafted SBA-15 catalysts.

Figure 50. FTIR spectra for amino-grafted SBA-15 samples.

Figure 51. Synthesis of 2-amino-4*H*-chromenes **1** catalysed by amino-grafted/SBA-15 catalysts at a) 323 K and b) 303 K. Reaction conditions: 25 mg of catalysts, **2/3** molar ratio = 2:4, solvent-free conditions.

Figure 52. Synthesis of chromenes **1** catalysed by amino-grafted SBA-15 catalysts, a) after 180 min of reaction time, at 323 and 303 K. b) Conversion values and selectivity variation to isomer **1a** using APTES/SBA-15 as catalyst at 323 K. Reaction conditions: 25 mg of catalysts, **2/3** molar ratio = 2:4, solvent-free conditions.

Figure 53. Catalyst amount influence in the synthesis of chromenes **1** catalysed by amino-grafted SBA-15 materials: a) **2/3** molar ratio = 4:8, b) **2/3** molar ratio = 6:12. Reaction conditions: 25 mg of catalysts, 303 K, solvent-free conditions.

Figure 54. Synthesis of 4*H*-chromenes **9** by using different 5-substituted-2-hydroxy-aldehydes **5** and ethyl cyanoacetate **3**, catalysed by DEAPTMS/SBA-15. Reaction conditions: 25 mg of catalysts, 303 K, **6/3** molar ratio = 2:4, solvent-free conditions.

Figure 55. a) Reduced models of amine-based catalysts. b) Reactant complexes indicating the reactants-amine interactions.

Figure 56. Optimized transition structures for the aldol reaction between 2-hydroxybenzaldehyde **2** and ethyl cyanoacetate **3** catalyzed by amino-grafted mesoporous silicas when amine function acting as individual catalytic sites: a) TS_{APTMS}, b) TS_{MAPTMS}, and c) TS_{DEAPTMS}. Relevant distances are expressed in Å.

Figure 57. Free-energy profiles for the aldolization reaction between 2-hydroxybenzaldehyde **2** and ethyl cyanoacetate **3** catalyzed by amino-grafted mesoporous silicas. a) Amines as individual catalytic sites. b) Amines with the assistance of the silica matrix.

Figure 58. Influence of catalytic support. Optimized TS for the aldol reaction between 2-hydroxybenzaldehyde **2** and ethyl cyanoacetate **3** catalyzed by amino-grafted mesoporous silicas. a) Silica cluster, b) TS_{MAPTMS-SBA}, and c) TS_{DEAPTMS-SBA}. Relevant distances are expressed in Å.

Figure 59. Adsorption/desorption isotherms of a) TaMCF(*Et*), b) 2APTMS/NbMCF(*Et*) and 2APTMS-TaMCF(*Et*) catalysts.

Figure 60. DTA/TG curves for a) 2APTMS/NbMCF(*Et*), and b) 2APTMS/TaMCF(*Et*). Curves normalized to 5 mg of the sample.

Figure 61. FTIR spectra of a) MCF supports and b) MCF and NbMCF (*Ox*) materials after evacuation at 373 K.

Figure 62. FTIR spectra of 2APTMS/NbMCF(*Et*) and 2APTMS/TaMCF(*Et*) after evacuation at 373 K: a) from 500 cm^{-1} until 4000 cm^{-1} and b) from 500 cm^{-1} until 2000 cm^{-1} .

Figure 63. UV-Vis spectra of a) NbMCF(*Et*) and b) TaMCF(*Et*) catalysts dried at 373 K.

Figure 64. SEM images from a) MCF, b) NbMCF(*Ox*) and c) 2APTMS/NbMCF(*Ox*).

Figure 65. Synthesis of 2-amino-4*H*-chromenes **1**, catalysed by a) amino-grafted MCF and NbMCF (*Ox*), and b) amino-grafted NbMCF(*Et*) and TaMCF(*Et*) catalysts. Reaction conditions: 25 mg of catalysts, 323 K, 2:4, **2/3** molar ratio = 2:4, solvent-free conditions.

Figure 66. Synthesis of 2-amino-4*H*-chromenes **1** a) catalysed by MCF and NbMCF(*Ox*) catalysts at 303 K. b) Conversion of **1a** and **1b** and c) selectivity to **1a** catalysed by 2APTMS/NbMCF(*Ox*) at 303 K.

Figure 67. Synthesis of 2-amino-4*H*-chromenes **1** catalysed by amino-grafted NbMCF(*Ox*), NbMCF(*Et*) and TaMCF(*Et*) catalysts at a) 303 K. Reaction conditions: 25 mg of catalysts, 2/3 molar ratio = 2:4, solvent-free conditions

Figure 68. Catalyst amount influence in the synthesis of chromenes **1** catalysed by amino-grafted MCF and Nb/MCF catalysts: a) **2/3** ratio 2:4 (catalyst amount: 50 mg) and b) **2/3** ratio 4:8 (catalyst amount: 25 mg) at 303 K.

Figure 69. Synthesis of 2-amino-4*H*-chromenes **9** catalysed by 2APTMS/NbMCF(*Et*). Reaction conditions: 25 mg of catalysts, 323 K, **6/3** molar ratio = 2:4, solvent-free conditions.

Índice de tablas

Tabla 1. Análisis de la generación de contaminantes en relación con la cantidad de producto anual generado en los diversos sectores químicos industriales.

Tabla 2. Procesos catalíticos que emplean catalizadores heterogéneos en sus transformaciones químicas.

Tabla 3. Métodos utilizados en Química Computacional

Tabla 4. Clasificación de métodos en función de la variable de la que depende y ejemplos de funcionales de cada categoría.

Tabla 5. Métodos habitualmente empleados en el estudio teórico de sólidos (zeolitas tipo ferrierita).

Table 6. Chemical composition (in wt. %, calculated as oxides) of the used minerals (based on supplier's data).

Table 7. Calcium oxide content and pH_{PZC} for PET/CAL, PET/MAG and PET/DOL samples.

Table 8. Textural parameters for the PET/CAL samples.

Table 9. Synthesis of chromenes **1** catalysed by PET/CAL 30:70 and PET/CAL 0:100, at 323 K, under solvent-free conditions.

Table 10. Catalyst textural properties.

Table 11. Composition of the amino-grafted MOFs catalysts under study.

Table 12. Synthesis of chromenes **7** and **8** from 2-hydroxybenzaldehydes and cyano compounds catalysed by amino-grafted CuBTC.

Table 13. Interactions of the reagents with metal centres in remaining CUS for amino-grafted CuBTC.

Table 14. Amount of nitrogen and textural parameters in SBA-15 samples.

Table 15. Textural parameters and N content for the samples under study.

Índice de esquemas

Esquema 1. Síntesis de quinolinas vs quinolonas catalizada por CAs ácidos a través de la condensación Friedländer.

Esquema 2. Condensación Friedländer entre 2-amino-5-clorobenzaldehído y acetilacetato de etilo, y modelos computacionales de las interacciones π,π -stacking en la formación de enlaces C-C.

Esquema 3. Síntesis de quinoxalinas a partir de *o*-fenilendiamina y α -hidroxicetonas catalizada por CAs. Estructuras optimizadas del ataque nucleofílico de *o*-fenilendiamina a la acetoína a) en ausencia de catalizador, b) catalizada por grupos -CO₂H, c) -SO₃H y d) -PO₃H.

Esquema 4. Síntesis de quinolinas por condensación de Friedländer a partir de 2-aminobenzaldehídos y compuestos carbonílicos, catalizada por materiales PET/MAG.

Esquema 5. Síntesis de quinoxalinas a partir de *o*-fenilendiamina y α -hidroxicetonas a 373 K, a 373 K, catalizada por Basolites.

Esquema 6. Inserción de grupos funcionales en la estructura de una sílice mesoporosa durante el proceso de síntesis.

Esquema 7. Anclaje de grupos funcionales en la superficie de una SBA-15 mediante una metodología post-sintética.

Esquema 8. Reacción de Henry entre *p*-nitrobenzaldehído y acetona catalizada por SBA-15 modificada con grupos funcionales ácidos y amino.

Scheme 9. Synthesis of 2-amino-4*H*-chromenes **1** from 2-hydroxybenzaldehyde **2** and ethyl acetoacetate **3**, at 323 K, catalysed by basic carbon materials.

Scheme 10. Synthesis of HA **14-1** (**4a** and **4b**) from 5-bromo-2-hydroxybenzaldehyde **5** and ethyl acetoacetate **3**, at 323 K, catalysed by basic carbon materials.

Scheme 11. Reaction pathway in the catalysed synthesis of chromenes **1** by ILs.

Scheme 12. Probably reaction pathway for the synthesis of chromenes **1** catalysed by CaO.

Scheme 13. Synthesis of chromenes **8** and **9** from 5-substituted 2-hydroxybenzaldehydes and cyano compounds, at 303 or 323 K, under solvent-free conditions.

Scheme 14. Synthesis of 5-substituted-2-hydroxybenzaldehydes **9** from different 5-substituted-2-hydroxy-aldehydes **6** and **3**, at 303 K, under solvent-free conditions.

SUMMARY OF THE THESIS “POROUS SOLIDS IN THE EFFICIENT AND SUSTAINABLE SYNTHESIS OF 2-AMINO-4*H*-CHROMENES. EXPERIMENTAL AND THEORETICAL STUDY”

Multicomponent reactions (MCR) are of great interest both from an academic and an industrial point of view. The use of MCR in organic synthesis constitutes one of the most useful tools, allowing access to complex heterocyclic systems in a simple, efficient and selective operation.

Chromenes, more specifically 2-amino-4*H*-chromenes, are bioactive oxygenated heterocycles of great interest to the pharmaceutical industry due to their therapeutic properties, constituting the basic structure of several commercial drugs. One of the easier synthetic routes to obtain chromenes is based on the MCR between 2-hydroxybenzaldehyde and nitriles with active methylene groups. However, this MCR usually requires the use of solvents, involves long reaction times and, in some cases, complex isolation and purification processes. That is why the development of new active and selective catalytic systems in the sustainable synthesis of this type of compounds is essential. This thesis presents the study of porous materials of different nature, structure, composition and porosity, modified to act as highly efficient catalysts in the selective synthesis of 2-amino-4*H*-chromenes —with excellent conversion values at short reaction times—, under solvent-free and mild reaction conditions, significantly reducing the environmental impact that such synthesis usually implies.

The synthesized catalysts are grouped into different families:

PET/CAL materials prepared by pyrolysis of polyethylene terephthalate (PET) and limestone (CAL) mixtures in different proportions. For comparative purposes, analogous materials were also prepared from natural magnesite (MAG) and natural dolomite (DOL). The minerals used in the synthesis have provided the active species — CaO and/or MgO—. The carbonaceous support has been obtained both from commercial PET and from plastic waste.

Metallo-organic frameworks (MOFs), with basic properties, modified with amines of different nature, from the corresponding MOFs using two different post-synthetic (grafting) methodologies. The starting MOFs were MIL-100-Sc, synthesized

following the adapted methodologies described in the literature and a commercial MOF (CuBTC, Basolite® C300).

Mesoporous silicas — Santa Barbara Amorphous 15 (SBA-15), Mesoporous Cellular Foam (MCF)— synthesized following the procedures described in the literature for this type of materials. As in the case of MOFs, the silicas prepared were functionalized by grafting with amino groups of different nature, using different commercial silanes. In the case of MCF materials, during their synthesis, different metal atoms were incorporated into their structure, obtaining the materials denoted as T/MCF —where T is Nb or Ta—, using two different metal sources, oxalates and ethoxides.

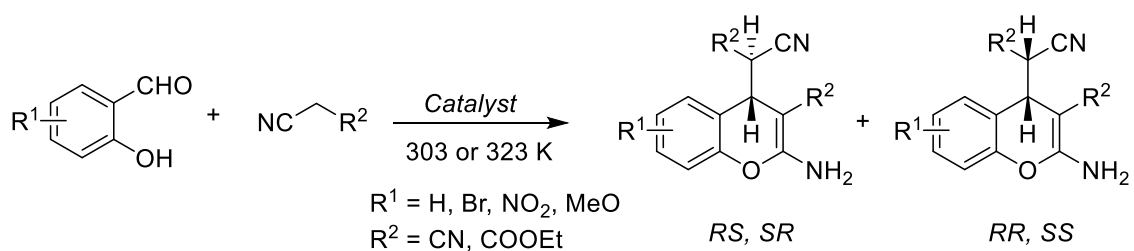
All of these catalysts were characterized by various techniques. Their textural parameters were obtained by their N₂ adsorption/desorption isotherms. The materials have shown a high surface area in all cases, being especially high in MOFs, followed by siliceous materials —even higher in MCF materials— and, finally, carbon materials. In the case of the first three types of catalysts, the surface area decreases proportionally to the functionalization of the materials, while in the case of PET/CAL catalysts, the starting PET ratio was the crucial factor that determines this value.

The nature of the surface groups present in the solids was studied by FTIR. In the case of MOFs, differences were observed in their functionalization, depending not only on the used amine but also on the used methodology. In the case of CuBTC, a partially functionalized material was obtained, while in the case of MIL-100 (Sc) all of the metal centers were coordinated with the amines. The SBA-15 catalysts showed a high functionalization degree, although differences between them depend on the silane used, showing the catalysts modified with (3-methylaminopropyl)trimethoxysilane (MAPTMS) the lowest degree of functionalization. Similarly, the used silane is the differential factor in MCF materials, having (3-aminopropyl)trimethoxysilane (APTMS) materials a higher functionalization degree in comparison to [3-(2- aminoethylamino) propyl] trimethoxysilane (2APTMS) materials. These results were confirmed by determining the chemical composition of the catalysts, obtained by elemental analysis so that the amount of N present in the catalysts could be compared with the expected degree of functionalization.

Furthermore, their structure was studied by X-Ray Diffraction (XRD) and their morphology by Transmission Electron Microscopy (TEM) and Scanning Electron Microscopy (SEM). Using these techniques, it was determined the existence of two active species in the PET/CAL catalysts —CaO and Ca(OH)₂—, whose presence is determined according to the degree of hydration of the materials. The micrographs showed how the morphology of the PET/CAL catalysts is directly related to their composition, with the Ca species appearing as dispersed cubic structures on the carbonaceous support. The support has shown different structures, from amorphous agglomerates to strands, always depending on the amount of PET present in the starting mixture. In the XRD analysis of the MOFs, it should be noted how functionalization has barely altered their degree of crystallinity, maintaining the initial structure in most cases. On the other hand, the SBA-15 siliceous catalysts have maintained their hexagonal structure after functionalization, as evidenced by their diffractograms. In the case of TMCF catalysts, their TEM and SEM images show that their morphology is coral-type, typical of MCF materials. Besides, Ultraviolet-Visible Spectroscopy (UV-Vis) studies were carried out for TMCF materials to study the differences in the metal coordination with the siliceous structure, appearing tetra, penta and octacoordinate species.

Finally, thermogravimetric studies and differential thermal analysis (DTA) were carried out to determine their thermal stability, being all the materials stable until a higher temperature range than the used in the studied synthesis.

The prepared materials were tested for the synthesis of 2-amino-4*H*-chromenes, by MCR, under mild reaction conditions, between various 2-hydroxy benzaldehydes and nitriles with active methylene groups as indicated below. Additionally, the influence of the amount of catalyst and the effect of temperature on the reaction was studied.



All the prepared materials were highly efficient catalysts in the synthesis of 2-amino-4*H*-chromenes. In the case of PET/CAL materials, although the carbonaceous

support is involved in the reaction, CaO and Ca(OH)₂ are the predominant catalytic species. When the Ca content increase, the corresponding samples present higher catalytic activity. If the synthesis reaction is carried out at a temperature of 323 K, the most active PET/CAL catalysts reach conversion values close to 100% after 2 h of reaction, decreasing when the temperature is reduced. The influence of temperature has been observed in the other families of catalysts, however, the greater catalytic activity of those notably affects this dependence.

In the case of MOFs, at 303 K, the most active catalysts reach almost quantitative conversion values after 2 h of reaction. These times are significantly reduced when working at 323 K. These catalysts showed superior catalytic performance. In fact, half amount of MOFs (25 mg) was used, regarding the above mentioned carbon catalysts (50 mg). The CuBTC-derived catalysts showed higher catalytic activity than MIL-100-Sc, due to the differences in the functionalization of the metal centers and the different textural properties. The basicity of the used amine in the modification of the materials notably affects the catalytic activity. In general, the highest conversions were obtained in the presence of the most basic materials.

In the case of siliceous catalysts, both the SBA-15 and MCF samples were found to be highly active catalysts when working at 323 K, affording almost quantitative conversion values in just 30 min, in the presence of the most efficient catalysts. At 303 K these catalysts have also shown excellent conversion values, especially the TMCF catalysts. In the case of functionalized SBA-15 catalysts, the most active samples have been those that present a higher concentration of basic centers, directly related to the presence of amino groups. In the case of TMCF catalysts, those functionalized with 2APTMS resulted as the best catalysts. The presence of the additional amino group probably is behind the enhanced catalytic performance. The presence of metal centers in the structure of mesoporous silica increases its catalytic activity, probably due to the interaction between metal atoms and reactants. In addition, a greater catalytic activity has been observed for the catalysts that incorporated the Nb centers from the corresponding oxalate as the metal source, in comparison to those that used ethoxides.

All materials were selective to the most stable chromene isomer (RS, SR) in a 2:1 ratio. In most of the studied cases, the selectivity to RS, SR isomer increases with time,

reaching values close to 90%, probably due to the epimerization of the thermodynamically less stable isomer to the most stable one.

In all cases, a higher amount of catalyst is related to higher conversion values, as might be expected. In this sense, the most active catalysts, highlighting 2APMS/NbMCF (*Ox*), carried out the synthesis using less than 2% of catalyst amount referred to the weight of the reactant, in the absence of any solvent and at 303 K, reaching quantitative conversions after 2 h of reaction time.

The experimental results obtained are supported by the computational studies carried out, using the computational software Gaussian 09, through the Density Functional Theory (DFT) methodology. The obtained results allowed us to clarify how the different catalysts can act in each case. Based on our previous studies, the reaction could take place through the sequence: aldolization, heterocyclization, dehydration, and, finally, Michael addition, being the rate-limiting step the activation of the starting nitrile.

RESUMEN DE LA TESIS “SÓLIDOS POROSOS BÁSICOS EN LA SÍNTESIS EFICIENTE Y SOSTENIBLE DE 2-AMINO-4H-CROMENOS. ESTUDIO EXPERIMENTAL Y TEÓRICO”

Las reacciones multicomponente (MCR, *por sus siglas en inglés*) presentan gran interés tanto desde el punto de vista académico como industrial. El uso de MCR en síntesis orgánica constituye una de las herramientas más útiles, permitiendo el acceso a sistemas heterocíclicos complejos en una operación sencilla, eficiente y selectiva.

Los cromenos, más concretamente los 2-amino-4*H*-cromenos, son heterociclos oxigenados bioactivos de gran interés para la industria farmacéutica por sus propiedades terapéuticas, constituyendo la estructura base de diversos fármacos comerciales. Una de las rutas sintéticas más sencillas para la obtención de cromenos se basa en la MCR entre 2-hidroxibenzaldehído y nitrilos con grupos metilenos activos. Sin embargo, esta MCR habitualmente requiere el uso de disolventes, implica tiempos de reacción prolongados y, en algunos casos, procesos de aislamiento y purificación tediosos. Es por ello por lo que resulta fundamental el desarrollo de nuevos sistemas catalíticos activos y selectivos en la síntesis sostenible de este tipo de compuestos. En esta tesis se presenta el estudio de materiales porosos de distinta naturaleza, estructura, composición y porosidad, modificados para que puedan actuar como catalizadores altamente eficientes en la síntesis selectiva de 2-amino-4*H*-cromenos — con excelentes rendimientos a tiempos cortos de reacción —, en ausencia de disolventes y bajo condiciones de reacción suaves, reduciendo de manera significativa el impacto ambiental.

Los catalizadores sintetizados se agrupan en las diferentes familias:

Materiales PET/CAL, preparados mediante pirólisis de mezclas de tereftalato de polietileno (PET), y roca caliza (CAL), en distintas proporciones. Con fines comparativos se prepararon también materiales análogos a partir de magnesita natural (MAG) y dolomita natural (DOL). Los minerales empleados en la síntesis de estos catalizadores conducen por tratamiento térmico a las especies activas —CaO y MgO—. El soporte carbonoso se ha preparado tanto a partir de PET comercial como a partir de residuos plásticos, ofreciendo una alternativa sostenible al uso de dichos residuos.

Redes metaloorgánicas (MOFs), con propiedades básicas, modificadas con aminas de distinta naturaleza, a partir de los correspondientes MOFs, empleando dos metodologías post-sintéticas (*grafting*) distintas. Los MOFs de partida son MIL-100-Sc, previamente sintetizado siguiendo el protocolo experimental adaptado descrito en la literatura para MOFs similares, y un MOF comercial (CuBTC, Basolite® C300).

Sílices mesoporosas — Santa Barbara Amorphous 15 (SBA-15), Mesoporous Cellular Foam (MCF)— sintetizadas siguiendo los procedimientos descritos en la literatura para este tipo de materiales. Al igual que en el caso de las redes metaloorgánicas, las sílices preparadas se han funcionalizado mediante *grafting* con grupos amino de diferente naturaleza, empleando distintos silanos comerciales. En el caso de los materiales MCF, se han incorporado en su estructura, durante su síntesis, distintos átomos metálicos, dando lugar a los materiales T/MCF —donde T es Nb o Ta— empleando dos fuentes metálicas distintas, oxalatos o etóxidos.

Todos estos catalizadores se caracterizaron mediante diversas técnicas. Sus parámetros texturales fueron obtenidos mediante sus isothermas de adsorción/desorción de N₂. En todos los casos, los materiales han mostrado una elevada área superficial, siendo esta especialmente elevada en el caso de los MOFs, seguida de los materiales silíceos —siendo mayor en los materiales MCF— y, por último, de los materiales de carbón. En el caso de los tres primeros, el área superficial decrece de forma proporcional al grado de funcionalización de los materiales, mientras que en el caso de los catalizadores PET/CAL, la proporción de PET de partida es determinante en la porosidad del material.

La naturaleza de los grupos superficiales presentes en los sólidos fue estudiada mediante espectroscopía infrarroja por transformada de Fourier (FTIR, *por sus siglas en inglés*). En el caso de los MOFs, se observaron diferencias en su funcionalización, dependiendo no sólo de la amina utilizada, sino también del método empleado. En el caso de CuBTC se pudieron obtener materiales parcialmente funcionalizados, mientras que en el caso de MIL-100(Sc) la mayoría de los centros metálicos están funcionalizados con las aminas. Los catalizadores SBA-15 mostraron elevados grados de funcionalización, aunque existen diferencias en función del silano utilizado, siendo el catalizador funcionalizado con (3-metilaminopropil)trimetoxisilano (MAPTMS) el que

presenta un menor grado de funcionalización. Del mismo modo, el grado de funcionalización en los materiales MCF depende del silano empleado. Así, los materiales APTMS/MCF mostraron un mayor grado de incorporación del silano (3-aminopropil)trimetoxisilano (APTMS) al soporte silíceo.

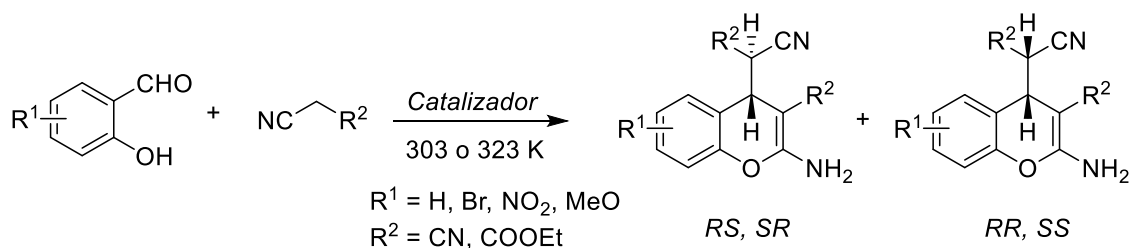
Estos resultados fueron confirmados mediante la determinación de la composición química de los catalizadores, obtenida mediante análisis elemental.

Además, se estudió su estructura mediante XRD y su morfología mediante TEM y SEM. Esto permitió determinar la existencia de dos especies activas en los catalizadores PET/CAL —CaO y Ca(OH)₂—, en función del grado de hidratación de los materiales. Las micrografías mostraron cómo la morfología de los catalizadores PET/CAL está directamente relacionada con su composición, apareciendo diferentes especies de Ca como estructuras cúbicas dispersas sobre el soporte carbonoso. Así, se han observado distintas estructuras, desde aglomerados amorfos hasta hebras, siempre dependiendo de la cantidad de PET presente en la mezcla de partida. En el análisis por XRD de los MOFs cabe destacar cómo la funcionalización apenas ha alterado su grado de cristalinidad, manteniendo la estructura inicial en la mayoría de los casos. Por otro lado, los catalizadores silíceos SBA-15 han mantenido su estructura hexagonal inalterada después de la funcionalización, tal y como evidencian sus difractogramas. En el caso de los catalizadores TMCF, sus imágenes TEM y SEM evidencian que su morfología es coralina, típica de este tipo de materiales. Además, se realizaron estudios de UV-Vis en los materiales TMCF para estudiar las diferencias en la coordinación de los metales con la estructura silícea, observándose especies tetra, penta y octacoordinadas.

Finalmente, se realizaron estudios termogravimétricos y análisis térmico diferencial (DTA) para determinar la estabilidad térmica de los materiales, resultando todos los materiales estables hasta un rango de temperaturas muy superior al utilizado en la síntesis estudiada.

Los materiales preparados se ensayaron en la síntesis de 2-amino-4*H*-cromenos, mediante la MCR, entre diversos 2-hidroxi-benzaldehídos y nitrilos con grupos metileno activos, en condiciones suaves de reacción, tal y como se representa a continuación.

Además, se estudió la influencia de la cantidad de catalizador y el efecto de la temperatura en la reacción.



Todos los materiales preparados son catalizadores altamente eficientes en la síntesis de 2-amino-4*H*-cromenos. En el caso de los materiales PET/CAL, aunque el soporte carbonoso está involucrado en la reacción, CaO y Ca(OH)₂ son las especies catalíticas predominantes, por lo que al aumentar su contenido, se observa la formación de los correspondientes cromenos con mayor conversión. Si la reacción de síntesis se lleva a cabo a una temperatura de 323 K, los catalizadores PET/CAL más activos conducen a valores de conversión próximos al 100% a las 2 h de reacción, viéndose este rendimiento mermado al reducir la temperatura. Esta influencia de la temperatura ha sido observada en las demás familias de catalizadores, sin embargo, la mayor actividad catalítica de estos reduce de forma significativa su influencia.

En el caso de los MOFs, a 303 K, los catalizadores más activos conducen a valores de conversión casi cuantitativos a las 2 h de reacción. Estos tiempos se reducen sensiblemente si la temperatura empleada es de 323 K. Además, la utilización de estos catalizadores permite trabajar empleando cantidades menores en un 50% con respecto a las de los catalizadores de carbón —25 mg en lugar de 50 mg—. Los catalizadores derivados de CuBTC mostraron mayor actividad catalítica que MIL-100-Sc modificados, debido a las diferencias en la funcionalización de los centros metálicos y a las diferentes propiedades texturales. La basicidad de la amina empleada en la modificación de los materiales afecta a la actividad catalítica. En general, las mayores conversiones fueron obtenidas en presencia de los materiales más básicos.

Los catalizadores silíceos, tanto los derivados de SBA-15 como de MCF, a 323 K, condujeron a rendimientos especialmente elevados, cercanos al 100% en apenas 30 min en el caso de los catalizadores más eficientes. De igual forma, a 303 K los rendimientos son excelentes, especialmente con los catalizadores TMCF. En el caso de los

catalizadores de SBA-15 funcionalizados, los más activos son aquellos que han mostrado una mayor concentración de centros básicos, directamente relacionado con la presencia de grupos amino provenientes del silano utilizado en su síntesis. En el caso de los catalizadores TMCF, aquellos funcionalizados con [3-(2- aminoetilamino) propil] trimetoxisilano (2APTMS) han mostrado una mayor actividad catalítica, muy probablemente debido al grupo amino adicional. La presencia de los centros metálicos en la estructura de la sílice mesoporosa aumenta su actividad catalítica muy probablemente debido a la interacción entre los átomos metálicos y los reactivos. Además, se ha observado una mayor actividad catalítica en los catalizadores que incorporaron en su síntesis los centros metálicos a partir del correspondiente oxalato como precursor metálico, con respecto a los que utilizaron etóxidos.

Todos los materiales fueron selectivos hacia la formación del isómero más estable (RS, SR) en relación 2:1. En la mayoría de los casos estudiados, la selectividad a hacia el isómero más estable del correspondiente cromeno aumenta con el tiempo, alcanzando valores cercanos al 90%, probablemente debido a la epimerización del isómero termodinámicamente menos estable al más estable.

En todos los casos, una mayor cantidad de catalizador se traduce en mayores valores de conversión, tal y como cabría esperar. En este sentido, los catalizadores más activos, destacando el 2APMS/NbMCF(Ox), han permitido llevar a cabo la síntesis con cantidades inferiores al 2% en peso con respecto a los reactivos, en ausencia de disolvente y a temperaturas próximas a la ambiente, alcanzando conversiones casi cuantitativas en menos de 2 h de tiempo de reacción.

Los resultados experimentales obtenidos se ven respaldados con en el estudio computacional realizado, empleando el software de química computacional Gaussian 09, a través de la metodología de la Teoría del Funcional de Densidad (DFT). Estos resultados han permitido clarificar el modo de actuación de los diferentes catalizadores. Basándonos en resultados previos de nuestro grupo, la reacción podría tener lugar a través de la secuencia: aldolización, heterociclación, deshidratación, y, finalmente, adición de Michael, siendo la etapa limitante la activación del nitrilo de partida.

Contenido

CAPÍTULO I. INTRODUCCIÓN	3
I.1 Química Fina (QF) vs Química Verde (QV)	4
<i>I.1.1 Química Verde</i>	5
I.2 Catálisis	11
<i>I.2.1 Importancia de la catálisis en cifras</i>	14
I.3 Cromenos	15
<i>I.3.1 Metodologías de síntesis</i>	18
<i>I.4.1 Estructura y propiedades de los CAs</i>	19
<i>I.4.2 Precursores convencionales y estrategias sintéticas</i>	24
<i>I.4.3 Aplicaciones de los CAs</i>	27
I.5 Redes Metalorgánicas (MOFs)	34
<i>I.5.1 Propiedades de MOFs</i>	36
<i>I.5.2 Síntesis de MOFs</i>	36
<i>I.5.3 Aplicaciones de MOFs</i>	41
I.6 Sílices Mesoporosas	45
<i>I.6.1 Santa Barbara Amorphous 15 (SBA-15)</i>	45
<i>I.6.2 Mesoporous Cellular Foam (MCF)</i>	47
<i>I.6.3 Modificación de los materiales mesoordenados</i>	49
<i>I.6.4 Aplicaciones de las sílices mesoporosas</i>	51
I.7 Química Computacional	54
<i>I.7.1 Superficie de Energía Potencial (SEP)</i>	54
<i>I.7.2 Métodos de cálculo</i>	55
<i>I.7.3 Conjunto de funciones de base</i>	62
<i>I.7.4 Aproximaciones teóricas al estudio con sólidos</i>	66
CAPÍTULO II. OBJETIVOS	73
II.1. Sintetizar los sólidos objeto de estudio	73
<i>II.1.1. Carbones Activados (CAs)</i>	73
<i>II.1.2. Redes metalorgánicas (MOFs)</i>	73
<i>II.1.3. Sílices mesoporosas</i>	73
II.2. Caracterizar los materiales sintetizados	74
II.3 Evaluar la actividad catalítica de los diferentes catalizadores	74
II.4 Realizar un estudio computacional del mecanismo de reacción mediante cálculos teóricos	74

CAPÍTULO III. CARBONES BÁSICOS COMO CATALIZADORES EN LA SÍNTESIS SOSTENIBLE Y EFICIENTE DE DERIVADOS DE CROMENOS. VALORIZACIÓN DE RESIDUOS DE PET Y FUENTES MINERALES	77
III.1 RESULTS AND DISCUSSION.....	79
<i>III.1.1 S Synthesis and characterization of the catalysts</i>	<i>79</i>
<i>III.1.2 Catalytic performance</i>	<i>83</i>
<i>III.1.3 Computational study</i>	<i>89</i>
III.2 CONCLUSIONS.....	94
CAPÍTULO IV. REDES METALOORGÁNICAS DE Cu Y Sc FUNCIONALIZADAS CON GRUPOS AMINO IMPLICADAS EN LA SÍNTESIS VERDE DE 2-AMINO-4H-CROMENOS.....	97
IV. 1 RESULTS AND DISCUSSION.....	99
<i>IV.1.1 Synthesis and characterization of the catalysts.....</i>	<i>99</i>
<i>IV.1.2 Catalytic performance.....</i>	<i>104</i>
<i>IV.1.3 Computational study.....</i>	<i>109</i>
CAPÍTULO V. SÍLICES MESOPOROSAS BÁSICAS EN LA SÍNTESIS VERDE DE 2-AMINO-4H-CROMENOS	117
V.1 RESULTS AND DISCUSSION	119
<i>V.1.1 Synthesis and characterization of the catalysts.....</i>	<i>119</i>
<i>V.1.2 Catalytic performance.....</i>	<i>122</i>
V.2 CONCLUSIONS	132
CAPÍTULO VI. SÍLICES MESOPOROSAS TMCF (T = Nb, Ta) FUNCIONALIZADAS CON GRUPOS AMINO. UN TIPO DE CATALIZADORES ALTAMENTE EFICIENTES EN LA SÍNTESIS DE 2-AMINO-4H-CROMENOS.....	135
VI.1 RESULTS AND DISCUSSION	137
<i>VI.1.1 Synthesis and characterization of the catalysts.....</i>	<i>137</i>
VI.2 CONCLUSIONS	149
ESQUEMA INTEGRADOR	151
CAPÍTULO VII. SECCIÓN EXPERIMENTAL	157
VII.1 EQUIPMENTS.....	157
VII.2 CHEMICAL REAGENTS AND SOLVENTS	159
VII.3 GENERAL PROCEDURES.....	162
<i>VII.3.1 Synthesis and functionalization.....</i>	<i>162</i>
<i>VII.3.2 Characterization techniques.....</i>	<i>166</i>
<i>VII.3.3 Catalytic performance</i>	<i>169</i>
<i>VII.3.4 Computational studies</i>	<i>169</i>
VII.4 SPECTROSCOPIC DATA	171
BIBLIOGRAFÍA.....	177

CAPÍTULO I

INTRODUCCIÓN

CAPÍTULO I. INTRODUCCIÓN

Hoy en día no se puede concebir el desarrollo social y tecnológico, que ha permitido alcanzar los estándares sociales, económicos y de bienestar de los que actualmente disfrutamos, sin la contribución de la industria química.

Considerando los datos proporcionados por la Federación Empresarial de la Industria Química Española (feiQue)¹, en España la industria química es un sector constituido por aproximadamente 3.100 empresas que facturan alrededor de 57 mil millones de euros, aportando casi un 6 % del PIB español (un 13 % del PIB industrial), generando más de medio millón de puestos de trabajo y siendo el segundo mayor exportador de la economía española tras el sector de la automoción. En cuanto a inversión en investigación, desarrollo e innovación (I+D+i), la industria química supone un 26 % total de las inversiones, aportando hasta un 22,5 % del personal investigador (Figura 1). La industria química es, además, la mayor inversora en protección medioambiental, con un 20 % del total invertido. Dentro del sector químico, la industria farmacéutica es el subsector más representativo, abarcando un 22 % del total en la distribución sectorial de la cifra de negocios².



Figura 1. Datos clave del sector químico español¹.

Este desarrollo ha sido posible, en parte, gracias a la contribución de la catálisis. Actualmente, el 95% del volumen total de los productos sintetizados requiere del uso de catalizadores, y un 70% de los procesos industriales han incorporado el uso de catalizadores en alguna de sus etapas. Es por ello que el 80 % del valor añadido en la industria química se basa en tecnologías catalíticas³. La catálisis es, hoy por hoy, el principal sector tecnológico de la industria química, lo que la ha convertido en uno de los grandes motores globales de desarrollo económico. Sin embargo, la contribución económica, tecnológica y social de la industria química no debe enmascarar la problemática que supone la producción de residuos. Atendiendo a las cifras proporcionadas por las Naciones Unidas, la producción de cada kilogramo de productos farmacéuticos implica la producción de, al menos, 25 kilogramos de emisiones y deshechos⁴. Por esta razón, el desarrollo de nuevos procesos químicos más eficientes, inocuos para el medioambiente y de menor coste económico y energético es un reto importante de gran repercusión social.

I.1 Química Fina (QF) vs Química Verde (QV)

Actualmente, uno de los campos de gran relevancia en la industria química es la Química Fina (QF), que se encarga del desarrollo y síntesis de compuestos de *gran valor añadido*. Estos compuestos son moléculas orgánicas de estructura compleja que pueden contener diversos grupos funcionales y heteroátomos estructurales, conformando productos o intermedios para una aplicación específica⁵. Si bien la producción de este tipo de compuestos es bastante limitada, menor a 1000 toneladas al año, su coste es muy elevado, debido principalmente a que requiere el uso de procedimientos muy específicos de síntesis, así como protocolos tediosos de aislamiento y purificación de los productos de reacción⁶. Además, en sus procesos de producción y fabricación se plantean una serie de desventajas, como es el uso de disolventes nocivos, tanto para la salud como para el medioambiente, que al final del proceso generan efluentes altamente contaminantes. Por otra parte, son procesos que tienen lugar a través de rutas sintéticas complejas, que transcurren en varias etapas, generándose un gran número de subproductos y deshechos y, por tanto, dando lugar al producto deseado con baja selectividad.

Resulta evidente que el desarrollo y evolución de nuevas tecnologías químicas ha supuesto numerosos avances sociales, mejorando directamente la calidad y esperanza de vida actuales. Sin embargo, la emisión excesiva de residuos altamente contaminantes ha generado una situación de alarma medioambiental. En este contexto surge la Química Verde (QV), tratando de dar una respuesta a la necesidad de diseñar nuevos procesos químicos fundamentales para el desarrollo tecnológico, y que resulten, al mismo tiempo, medioambientalmente sostenibles.

1.1.1 Química Verde

Los primeros antecedentes a la concepción del término QV surgen, en el año 1991, de la mano del Prof. Barry Trost, al enunciar el concepto de *Economía Atómica*^{7,8}. Se plantea la necesidad de cuantificar la cantidad de contaminantes generados en una reacción química, siendo la economía atómica un factor para la estimación de la eficiencia de una reacción. Se define como el total de átomos contenidos en los productos de una reacción con respecto al total de átomos, ambos en peso, contenidos en los reactivos de partida (**Ecuación 1**).

$$\% \text{ Economía Atómica} = \frac{\text{Peso molecular del producto de reacción}}{\text{Peso molecular de los reactivos utilizados}} \times 100 \quad (1)$$

Este concepto se convirtió inmediatamente en una herramienta especialmente útil en la evaluación rápida de las cantidades de residuos generados en un proceso químico. Además, contribuyó en la implantación de la idea de que, en el diseño de aproximaciones sintéticas eficientes, se debe tratar de conseguir que la mayor parte de los átomos de los reactivos de partida se encuentren presentes en el producto final, reduciendo al mínimo las etapas sintéticas y la formación de subproductos y residuos. Sin embargo, esta idea excluía de los cálculos otros elementos a considerar en una reacción química, tales como disolventes, reacciones secundarias, subproductos generados e incluso combustibles empleados⁹.

Es por ello por lo que el Prof. Roger A. Sheldon amplía el análisis de la producción de residuos mediante la definición del *Factor E*, que relaciona la cantidad de residuos generados con la masa de productos obtenidos en un mismo proceso (**Ecuación 2**).

$$\text{Factor } E = \frac{\text{Masa de residuos (Kg)}}{\text{Masa de productos (Kg)}} \quad (2)$$

De esta forma, un aumento en el valor del *Factor E* implicaría un aumento en la producción de residuos con respecto a la obtención de productos. Así, un proceso completamente sostenible produciría valores de *Factor E* próximos a cero¹⁰. El análisis mediante la aplicación del *Factor E* de diversos sectores industriales en los que intervienen reacciones químicas ha puesto de manifiesto que existen determinadas industrias, como la industria farmacéutica o la QF, que generan una mayor cantidad relativa —en ocasiones 50 o 100 veces mayor— de residuos que de productos generados, mientras que otras más estigmatizadas, como la industria petroquímica, muestran valores de *Factor E* mucho menores (**Tabla 1**)¹¹.

Tabla 1. Análisis de la generación de contaminantes en relación con la cantidad de producto anual generado en los diversos sectores químicos industriales.

Sector Industrial	Cantidad de Producto generado (ton/año)	Factor E
Industria Petroquímica	106 - 108	0,1
Producción de productos a gran escala	104 - 106	1 - 5
Química Fina	102 - 104	5 - 50
Industria Farmacéutica	10 - 103	25 - 100

Sin embargo, el modelo de *Factor E* seguía presentando una serie de limitaciones al pasar por alto otros parámetros a tener en cuenta, como pueden ser el grado de toxicidad de los reactivos empleados o de los deshechos producidos. Esto ha sido subsanado con la introducción del *Factor de Impacto* o *Factor Q*, que cuantifica el impacto medioambiental que supone cada uno de los reactivos y productos implicados en una reacción, así como el coste económico en función de los precios de mercado. Esta consideración económica resulta indispensable, ya que en la definición de *desarrollo sostenible* se asume que el precio de un producto debe reflejar tanto su coste de producción como sus costes medioambientales y sociales¹². Sin embargo, esta evaluación objetiva y cuantitativa de los procesos químicos no siempre resulta sencilla, ya que es necesario valorar también otros parámetros tales como localización, instalaciones y volumen de producción. Por ello, actualmente, la evaluación del impacto medioambiental de un proceso químico, especialmente en procesos de QF, se realiza

mediante la utilización conjunta de los *Factores Q y E*, dando lugar al *Factor QE* o *Factor Medioambiental*, que consiste en el producto de ambos términos. La aplicación de este modelo es la más efectiva para limitar la emisión y utilización de productos contaminantes, permitiendo una química compatible con un desarrollo sostenible. Esto ha contribuido a que, en la actualidad, especialmente en los países de mayor desarrollo, las legislaciones vigentes sean especialmente exigentes y restrictivas en relación con el transporte, almacenamiento, producción y vertido, tanto de efluentes como de residuos sólidos nocivos para ser humano y el medioambiente.

En este contexto, en el año 1998, los profesores Paul T. Anastas y John C. Warner establecieron las bases del que sería el avance más significativo en materia de sostenibilidad con la publicación del libro *Green Chemistry: Theory and Practice*¹³. La publicación de esta obra supuso un cambio diametral de enfoque: *el sector químico industrial no debería ceñirse exclusivamente a tratar de arreglar los problemas derivados de un crecimiento descontrolado, sino que debería desarrollarse en sintonía con la sostenibilidad*. Por ello, debe tratar de rediseñar los procesos químicos desde su propia base, intentando, siempre que sea posible, utilizar materias primas renovables y bajo condiciones de reacción suaves. Todo ello derivaría en un sector más seguro, limpio y eficiente en términos energéticos, desde la síntesis de productos hasta la eliminación de residuos^{14, 15}.

La QV se fundamenta en 12 Principios (**Figura 2**), que son la hoja de ruta que definirá el devenir de una Química responsable, que permita un desarrollo sostenible compatible con los progresos en investigación, diseñando nuevas rutas sintéticas respetuosas con el medio ambiente que minimicen el impacto medioambiental¹⁶. Tal y como el propio Anastas —actualmente miembro de la Agencia de Protección del Medio Ambiente (EPA, *por sus siglas en inglés*)— la define “es una química más efectiva, eficiente y elegante. Dicho sencillamente, es una química mejor”.



Figura 2. Doce Principios de la Química Verde.

Los Doce Principios de la QV son:

1. **Prevención de emisión de residuos.** Resulta más sencillo evitar la producción de residuos, mientras sea posible, que su posterior eliminación.
2. **Economía atómica.** Es posible minimizar las pérdidas mediante el desarrollo de procesos que impliquen la obtención de productos con un número de átomos lo más cercano posible al de los reactivos de partida.
3. **Reducción de la toxicidad en la síntesis química.** El uso de productos químicos de escaso o nulo peligro para la salud del ser humano y/o el medio ambiente minimiza el riesgo de daño.
4. **Diseño de compuestos químicos más seguros.** Los productos químicos deben ser sintetizados, sin perder las propiedades para las que fueron diseñados, de forma que ofrezcan la menor toxicidad posible.
5. **Ahorro de disolventes y sustancias auxiliares.** La adición de sustancias auxiliares implica un problema añadido a la contaminación, así que su uso debe estar limitado a los casos en los que resulten indispensables, tratando de emplear siempre los que menor toxicidad presenten.

6. **Eficiencia energética.** Las condiciones en las que se realiza un proceso químico son un factor especialmente relevante, sobre todo a la hora de escalar dicho proceso a nivel industrial. Cuanto más suaves sean las condiciones de reacción empleadas, mayor será el ahorro energético y, por tanto, menor el coste económico y ambiental.
7. **Empleo de materias primas renovables.** Siempre que se consiga mantener un rendimiento adecuado en los productos deseados se deben emplear materias renovables, que permiten ahorrar costes y tiempos de producción, además de reducir la aparición de productos contaminantes.
8. **Reducción de la derivación innecesaria.** Se debe favorecer el trazado de rutas sintéticas sencillas, disminuyendo también el número de reactivos en la medida de los posible, para así reducir el coste económico del proceso y la generación de contaminantes.
9. **CATÁLISIS.** Tal y como se detalla en el Capítulo I.2, el uso de catalizadores permite el incremento de la velocidad y selectividad de las reacciones químicas, además de favorecer la aplicación de los restantes Principios.
10. **Diseño de productos biodegradables.** Se ha de buscar la toxicidad mínima o nula de los productos generados, además de intentar que su tratamiento y almacenaje posterior, para su eliminación, sean lo menos costosos económica y ecológicamente.
11. **Prevención de la contaminación mediante análisis en tiempo real.** El empleo de técnicas de monitorización de los procesos que ocurren durante el transcurso de las reacciones químicas puede ayudar a evitar la formación de productos no deseados o tóxicos.
12. **Prevención de accidentes mediante el incremento de la seguridad química.** No solo las medidas de seguridad deben implementarse y mejorarse, si no que la síntesis de productos más seguros favorecerá la prevención de accidentes.

Hasta hace relativamente poco tiempo, la industria química había centrado su actividad exclusivamente en la extracción y procesamiento de materias primas, ya fueran naturales o sintéticas, y en su transformación en otras sustancias con el objetivo de satisfacer las diferentes necesidades humanas. Actualmente, la preocupación

mundial por el medio ambiente suma a su actividad normal la obligación de implantar los procedimientos necesarios para desarrollar su actividad de tal manera que ocasionen el menor impacto en el entorno. La lucha contra la degradación medioambiental es una realidad acuciante a la que se debe hacer frente, tal y como establecen los 17 objetivos y metas de desarrollo sostenible establecidos por las Naciones Unidas¹⁷. Entre ellos se incluyen las inversiones en industria, innovación e infraestructuras, en sinergia con un desarrollo sostenible y las actuaciones para frenar el calentamiento global. Es por ello que la aplicación estricta y exhaustiva de los Doce Principios de la QV para la mejora de los procesos industriales actuales resulta fundamental para el cumplimiento de parte de estos objetivos antes del plazo establecido: 2030.



Figura 3. Green ChemistREE.

En el año 2018, conmemorando el 20º aniversario de la concepción de los 12 Principios de la QV e inspirado en diagramas de árbol que ilustran la diversidad de productos a partir de materias primas, Anastas *et al*¹⁸, han presentado el Green ChemisTREE (**Figura 3**), como escaparate de la diversidad de investigación y logros derivados de la QV. Cada rama del árbol representa a cada uno de los 12 Principios, mientras que las hojas son las distintas áreas de investigación y desarrollo relevantes para ese Principio.

Existen numerosos ejemplos en los que se aplican los Principios fundamentales de la QV en procesos industriales para la obtención de productos farmacéuticos. Entre ellos se encuentra la síntesis de *simvastatina*, en la que se introdujo una etapa de catálisis enzimática, optimizando el proceso global y reduciendo así los residuos generados, así como el coste de producción¹⁹. Otro ejemplo relevante es la síntesis de *sitagliptina*, que mediante un proceso enzimático redujo la producción de residuos, mejoró el rendimiento y la seguridad del proceso, y eliminó la necesidad de uso del catalizador metálico²⁰.

I.2 Catálisis

Tal y como se muestra en los *12 Principios de la QV* (apartado I.1.1), la catálisis es un sector de especial relevancia industrial, siendo uno de los pilares fundamentales para una química más sostenible. El desarrollo de nuevos nanomateriales que pueden actuar como catalizadores contribuye al conocimiento y desarrollo de nuevas metodologías de menor impacto ambiental (9º Principio de la QV).

En general, las reacciones químicas implican cambios en la disposición y enlace de los átomos en las moléculas y, por lo tanto, alteraciones en el estado de ordenamiento de un sistema. Estos cambios tienen lugar con evolución o absorción de calor y una disminución de la energía libre. La velocidad de un determinado proceso depende, entonces, de la ruta de reacción por la que los reactivos se convierten en productos.

Un catalizador se define como una sustancia que aumenta la velocidad de una reacción, disminuyendo considerablemente la energía de activación de conversión de reactivos en productos, no siendo consumido durante el proceso, y proporcionando caminos de reacción alternativos a los procesos sin catalizar. Por lo tanto, la velocidad de un proceso catalizado depende del catalizador empleado.

Aunque existen diferentes clasificaciones de los tipos de catálisis —por ejemplo, atendiendo a las características del proceso químico que catalizan, se diferencia entre catálisis ácido-base, redox o enzimática, entre otros— la más general es la que diferencia entre catálisis homogénea y catálisis heterogénea. Esta clasificación hace referencia a si el catalizador implicado en una reacción se encuentra en la misma fase que el resto de las especies químicas —catálisis homogénea— o no —catálisis heterogénea—. Los catalizadores heterogéneos más comúnmente empleados están constituidos por sólidos de distinta naturaleza, a menudo inorgánicos, con diferente composición, morfología y textura, y propiedades. La catálisis heterogénea es clave en la industria química moderna. Se emplea en diferentes áreas en la fabricación de productos químicos y farmacéuticos de interés e incluso en la producción de productos de QF, sustituyendo en muchos casos a procesos anticuados que usan cantidades estequiométricas de reactivos nocivos, dando paso así a tecnologías más limpias²¹.

El uso de catalizadores heterogéneos en procesos industriales supone una serie de ventajas evidentes frente a las disoluciones con catalizadores homogéneos. Entre ellas cabe destacar: i) **facilidad de separación** del catalizador de los reactivos y productos; ii) **mayor robustez del catalizador**, tolerando rangos de temperatura y presión superiores; iii) **menor capacidad corrosiva**, lo que permite prolongar el tiempo de vida medio de los equipos en la industria; iv) **menor toxicidad**, ya que no se trata de compuestos volátiles, siendo algunos de ellos incluso inocuos para el ser humano; v) **posibilidad de reutilización o regeneración**, reduciendo el coste, el tiempo de operación y minimizando la producción de residuos.

En la **Tabla 2** se muestran algunos ejemplos de procesos catalíticos industriales modernos que involucran catalizadores heterogéneos.

Tabla 2. Procesos catalíticos que emplean catalizadores heterogéneos en sus transformaciones químicas²¹.

Proceso	Transformación química	Catalizador
Reformado con vapor	$\text{CH}_4 + \text{H}_2\text{O} \rightarrow \text{CO} + 3\text{H}_2$	Ni/Al ₂ O ₃
	$\text{C}_n\text{H}_m + n\text{H}_2\text{O} \rightarrow n\text{CO} + (n+m/2)\text{H}_2$	Ni/CaAl ₂ O ₄
Síntesis de metanol	$\text{CO} + 2\text{H}_2 \rightarrow \text{CH}_3\text{OH}$	Cu/ZnO/Al ₂ O ₃
	$\text{CO}_2 + 3\text{H}_2 \rightarrow \text{CH}_3\text{OH} + \text{H}_2\text{O}$	
Hidrogenación selectiva	Hidrogenación parcial de ésteres de glicerol con ácidos grasos C18	Ni/SiO ₂
Hidrodesulfuración	$\text{C}_4\text{H}_4\text{S}$ (tiofeno) + 2H ₂ → C ₄ H ₆ + H ₂ S	Co o Ni MoS ₂ /Al ₂ O ₃ o WS ₂ /Al ₂ O ₃
Deshidrogenación oxidativa	$\text{C}_2\text{H}_5\text{CH}=\text{CH}_2 + \frac{1}{2} \text{O}_2 \rightarrow \text{CH}_2=\text{CHCH}=\text{CH}_2 + \text{H}_2\text{O}$	Fe ₂ O ₃ , Cr ₂ O ₃ , BiPO ₄
Oxidación de eteno	$\text{C}_2\text{H}_4 + \frac{1}{2}\text{O}_2 \rightarrow \text{C}_2\text{H}_4\text{O}$ (óxido de etileno)	(Cs + Cl) Ag/α-Al ₂ O ₃

Un aspecto importante a tener en cuenta es la selectividad del proceso. La selectividad del catalizador es de suma importancia en el desarrollo de procesos industriales, tanto por razones económicas como ambientales²². En el caso de los catalizadores heterogéneos, la ruta de reacción operativa está condicionada, en gran medida, por su química superficial, lo que constituye el origen de la selectividad del catalizador. Como ejemplo se puede citar la hidrogenación de monóxido de carbono en condiciones apropiadas en presencia de diferentes catalizadores: mientras que el proceso catalizado por níquel conduce selectivamente a metano, en presencia de catalizadores de cobre o rutenio se obtienen selectivamente metanol o hidrocarburos superiores, respectivamente.

En este contexto, el desarrollo de nuevos nanomateriales que puedan actuar como catalizadores heterogéneos de procesos químicos de interés es un campo de investigación muy activo, que contribuye al conocimiento y desarrollo de nuevas metodologías de menor impacto ambiental. El uso de catalizadores permite adaptarse a los nuevos modelos de producción establecidos desde el Parlamento Europeo, basados en la normativa sobre economía circular establecida el 18 de abril de 2017²³. Con esta nueva legislación se pretende reducir la producción de residuos al mínimo, con lo que aquellos productos, como son los catalizadores heterogéneos, que permitan su reutilización durante varios ciclos y que puedan ser retirados sin necesidad de usar productos contaminantes adicionales, adquieren un gran valor añadido.

1.2.1 Importancia de la catálisis en cifras

Para poner de relieve el impacto de la catálisis como uno de los grandes motores globales de desarrollo económico, la mejor opción es recurrir a las cifras. El mercado global de catalizadores alcanzó valores próximos a los 19 mil millones de dólares en 2018, con una previsión cercana a los 24 mil millones de dólares en 2024²⁴. Según la revisión realizada por Hagen³, en 2015 las estimaciones sugerían que la catálisis contribuía a un 35 % del PIB mundial²⁵, mientras que más del 80 % de los productos manufacturados implicaban el uso de catalizadores en alguna de sus etapas de procesado²⁶.

Todas estas cifras ponen de manifiesto la importancia de la catálisis para el desarrollo económico y social. Sin las aportaciones de la industria química, en todos sus sectores, la esperanza de vida actual apenas superaría los 40 años. El ejemplo más claro de esto es la relación intrínseca que tiene la mayor explosión demográfica mundial en la Historia, a partir de 1920, con uno de los procesos químicos más famosos y ampliamente utilizados que implica el uso de catalizadores: el proceso Haber–Bosch para la obtención de amoníaco. En este proceso se emplean catalizadores de hierro pulverizado con promotores de distintos óxidos (Al, K, Ca, Mb y Mg). Dicho proceso es la base para la producción de fertilizantes en masa, tal y como se concibe actualmente. Hasta 2002 implicaba la utilización de más de 500 millones de toneladas de fertilizantes, que empleaban un 1 % de la energía total mundial producida año²⁷. Este desarrollo sumado a los avances logrados en medicina incrementó, en menos de 80 años, la población mundial desde menos de dos mil millones hasta los más de seis mil millones en el año 2000²⁸, alcanzando un incremento cercano al 350 % (**Figura 4**). Dichos fertilizantes fueron responsables de mantener a la mitad de la población mundial, y se espera que esta cifra alcance los dos tercios²⁹. Todo ello deriva en que más del 50% del nitrógeno presente en el organismo proceda de procesos industriales.

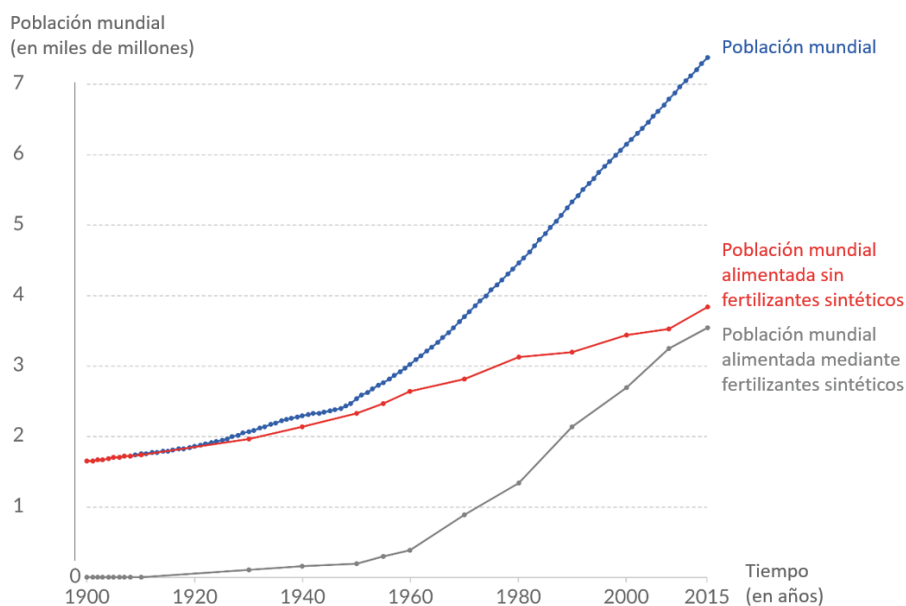


Figura 4. Influencia del proceso Haber-Bosch en el crecimiento de la población mundial³⁰.

En esta Tesis Doctoral se han desarrollado tres familias de catalizadores heterogéneos basados en materiales de carbono, redes metaloorgánicas (MOF, *por sus siglas en inglés*) y sílices mesoporosas modificadas, capaces de catalizar la síntesis de 2-amino-4H-cromenos. En este contexto, en los apartados siguientes, se incluye una descripción general de la estructura, propiedades y aplicaciones de este tipo de materiales.

1.3 Cromenos

Una amplia gama de productos de QF contienen gran variedad de sistemas heterocíclicos en su estructura. La importancia de los compuestos heterocíclicos radica principalmente en sus aplicaciones farmacológicas o tecnológicas³¹, aunque también están presentes en diversos aditivos alimentarios, colorantes, productos cosméticos o fragancias, entre muchos otros^{32, 33}. Aunque hasta 2008 se habían registrado más de 24 millones de compuestos con estructura heterocíclica³⁴, un gran número de ellos se encuentran presentes en la naturaleza, actuando de forma activa en diferentes procesos biológicos ampliamente estudiados. Entre ellos, destacan especialmente los cromenos.

Los cromenos o benzopiranos son compuestos heterocíclicos oxigenados, formados por un anillo bencénico fusionado con un anillo de pirano (**Figura 5**). Existen,

por tanto, dos isómeros según la nomenclatura aceptada por la Unión Internacional de Química Pura y Aplicada (IUPAC, *por sus siglas en inglés*), el 1-benzopirano o cromeno y el 2-benzopirano o isocromeno.

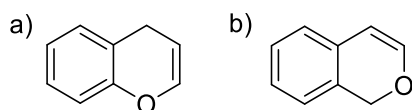


Figura 5. Estructura base de los a) cromenos e b) isocromenos.

Los cromenos forman parte de productos naturales presentes en hojas, tallos y raíces de diversas especies vegetales, entre las que se incluyen varias de las familias *Rutaceae*, *Liliaceae*, *Cyperaceae* y *Asteraceae*, especialmente la *Astereae*, *Eupatorieae*, *Heliantheae*, *Inuleae* y *Senecioneae*³⁵ (**Figura 6**).

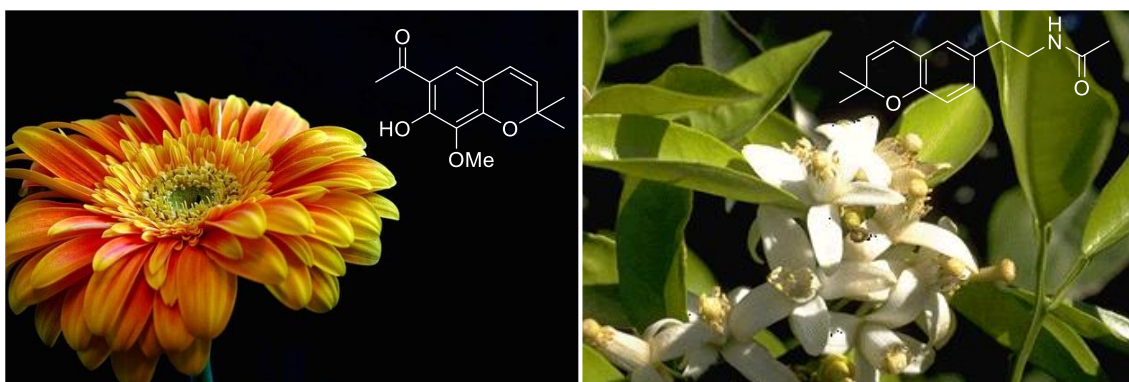


Figura 6. Compuestos con estructura base de cromeno extraídos de especies vegetales (*Ageratina Pichinchenis*, familia *Asteraceae*³⁶, izquierda; y *Amyris Brenesii*, familia *Rutaceae*, derecha³⁷).

Otro ejemplo de cromeno, en este caso sintético, con aplicaciones farmacéuticas como inmunomodulador sobre los linfocitos T, es el fármaco AX-024, que ha mostrado un gran potencial en el tratamiento de enfermedades autoinmunes como la esclerosis múltiple, psoriasis, artritis, enfermedad de Chron o lupus (**Figura 7b**).

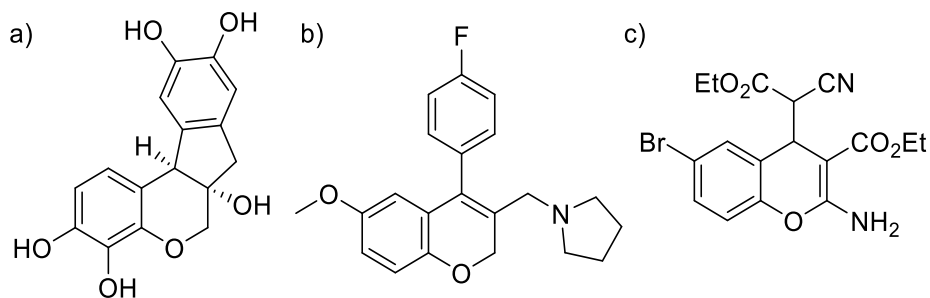


Figura 7. Estructura de cromenos con aplicaciones farmacéuticas: a) *hematoxilina*, b) AX-024³⁸, c) HA-14-1.

El papel de los cromenos en la industria farmacéutica adquiere especial relevancia debido a sus propiedades terapéuticas, ya que han mostrado actividad como agentes antibacterianos, anticoagulantes, antifúngicos, antiinflamatorios, antihistamínicos, antidiuréticos, antioxidantes, antiprotozoarios, antitumorales, antivirales, antihipertensivos o antiproliferativos, entre otros³⁹. Un ejemplo de producto natural con aplicación médica, que contiene el esqueleto de cromeno, es la *hematoxilina* (**Figura 7a**), aislado de la leguminosa *Haematoxylum campechianum*, que se emplea habitualmente como colorante en citología e histología en el diagnóstico de lesiones malignas⁴⁰ (**Figura 8**).

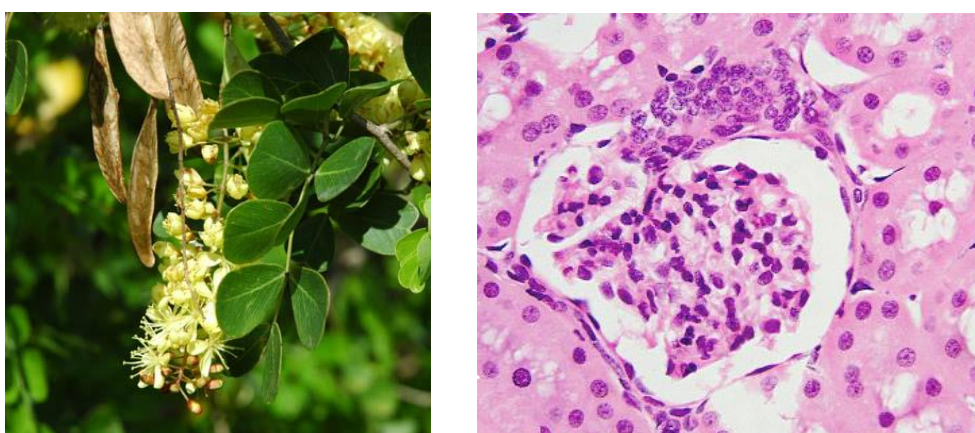


Figura 8. Flores de *Haematoxylum campechianum* y sección de un glomérulo de un riñón de mamífero teñido con una mezcla de hematoxilina (núcleos, color violáceo) y eosina (citoplasma, color rosado)⁴¹.

En la familia de los cromenos destacan especialmente los 2-amino-4*H*-cromenos y sus derivados, ya que forman la estructura base de numerosos fármacos comerciales (**Figura 8**). A modo de ejemplo, se puede citar el fármaco HA-14-1⁴² (**Figura 7c**). Este compuesto actúa inhibiendo el comportamiento antiapoptótico de las proteínas Bcl-2, las cuales se expresan en un gran número de procesos cancerígenos y se encuentran relacionadas con los mecanismos de resistencia a dichos tratamientos.

Los cromenos forman parte de compuestos que se emplean también en el tratamiento de enfermedades inflamatorias mediadas por el factor de necrosis tumoral α (TNF α , *por sus siglas en inglés*), tales como la artritis reumatoide o psoriásica. Son también destacados anestésicos locales y agentes antileishmaniasis⁴³, muestran fototoxicidad ante diversos hongos y bacterias⁴⁴, y se han descrito como inhibidores de bacterias Gram positivas y Gram negativas⁴⁵. Por otra parte, son candidatos potenciales para el tratamiento de trastornos de la salud mental tales como la esquizofrenia⁴⁶ o la

enfermedad de Alzheimer⁴⁷, ya que muchos de sus derivados resultan activos sobre el sistema nervioso central (SNC). Su versatilidad permite que incluso tengan aplicación en otros sectores industriales, tales como la agroquímica o la cosmética⁴⁸.

1.3.1 Metodologías de síntesis

Actualmente, se han descrito diferentes rutas sintéticas en la preparación de 2-amino-4H-cromenos incluyendo tanto la utilización de organocatalizadores homogéneos clásicos —aminas orgánicas^{49, 50}—, como de heterogéneos, entre los que se incluyen algunos como fosfato de circonio⁵¹, resinas de intercambio aniónico —Amberlita A-21⁵²—, hidrotalcitas dopadas con estaño⁵³ o tamices moleculares 3A⁵⁴, entre otros.

Las reacciones multicomponente (MCR, *por sus siglas en inglés*) presentan gran interés tanto desde el punto de vista académico como industrial. La utilización de MCR en síntesis orgánica y química médica permite la preparación de moléculas de gran complejidad estructural, en una operación sencilla, por lo que se consideran rutas de reacción altamente eficientes. En general, se caracterizan por ser procesos rápidos, convergentes, de alta economía atómica y elevada formación de enlaces dando lugar a gran diversidad molecular⁵⁵. Sin embargo, en función de la metodología elegida, este tipo de síntesis a menudo requiere el uso de disolventes, empleando altas cantidades de sólidos inorgánicos usados como catalizadores del proceso, tiempos de reacción prolongados y, en algunos casos, métodos complejos de aislamiento y purificación de los productos de reacción, originando residuos altamente contaminantes, un consumo energético alto y, por lo tanto, un elevado impacto ambiental. En este contexto, el diseño de nuevas rutas sintéticas más eficientes y selectivas, que permitan mantener la producción de este tipo de compuestos, minimizando el daño ecológico, es una necesidad urgente. Recientemente, en nuestro grupo de investigación se han descrito nuevos sistemas catalíticos activos, selectivos y eficientes en la síntesis de 2-amino-4H-cromenos. Entre ellos se encuentran los líquidos iónicos⁵⁶ (ILs, *por sus siglas en inglés*), metalosilicatos mesoporosos bifuncionales^{57,58} o composites hidrotalcita/hidroxiapatita⁵⁹ e hidrotalcita/SBA-15⁶⁰.

I.4 Carbones activados (CAs)

Se define como carbonos activados (CAs) a aquellos materiales de escala nanométrica que han sido preparados mediante carbonización de diversos productos orgánicos, entre ellos residuos vegetales procedentes de biomasa de alto contenido en carbono o compuestos orgánicos de síntesis⁶¹. R. Von Ostrejko se considera el inventor del primer carbón activado, en 1909⁶².

Su composición química se basa, fundamentalmente, en carbono, aunque habitualmente contienen distintos heteroátomos, tales como oxígeno, nitrógeno o hidrógeno, entre otros. Se trata de materiales con estructura no gráfica, carbonosa y microcristalina. Estos materiales presentan, además, varias características interesantes, tales como la porosidad controlable, conductividad eléctrica, estabilidad física y química, química superficial modificable, y posibilidad de presentar diferentes metodologías de preparación⁶³.

I.4.1 Estructura y propiedades de los CAs

La estructura de los CAs se conforma de microcristales elementales que constituyen unidades laminares bidimensionales de planos hexagonales de átomos de carbono, replegadas sobre sí mismas, sin orden cristalográfico aparente, generando espacios que dan lugar a la porosidad y evitan que se adquiera conformación gráfica **(Figura 9)**^{64, 65}.



Figura 9. Plegamiento de las láminas microcristalinas que generan la estructura de un CA⁶⁶.

La propiedad física más destacable de los CAs es su porosidad, que facilita el acceso de los reactivos a los centros activos disponibles⁶⁷, resultando, por tanto, materiales con altas capacidades como adsorbentes. Esta porosidad les confiere una elevada área superficial, que puede alcanzar más de $2000 \text{ m}^2\cdot\text{g}^{-1}$. Generalmente, los CAs presentan una distribución de tamaño de poro no uniforme que les permite adsorber moléculas de muy diverso tamaño (**Figura 10**)⁶⁵.

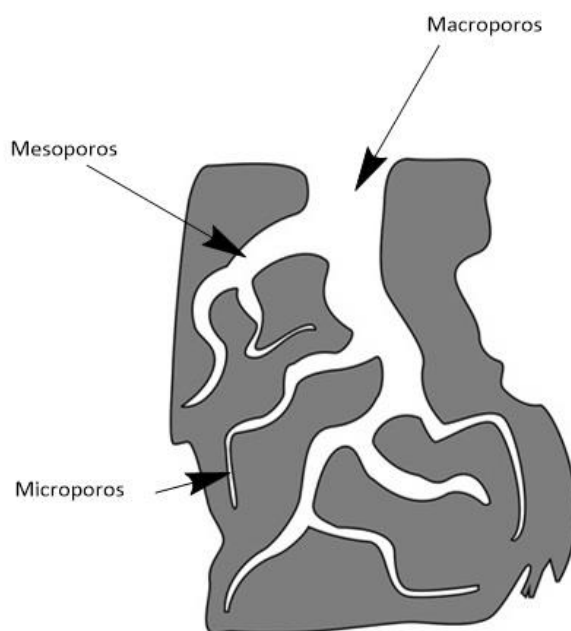


Figura 10. Representación gráfica de la distribución de los distintos tipos de poro en un CA⁶⁸.

Atendiendo a la clasificación efectuada por la IUPAC⁶⁹, los materiales porosos, en general, se clasifican en tres grupos en función de su diámetro de poro:

- i) *Microporosos*: diámetro de poro de tamaño menor a 2 nm.
- ii) *Mesoporosos*: diámetro de poro comprendido entre 2 nm y 50 nm.
- iii) *Macroporosos*: diámetro de poro de tamaño mayor a 50 nm.

Cada uno de estos poros realiza una función específica. En los CAs predomina la presencia de microporos, que son los principales responsables de sus elevadas superficies específicas y contribuyen activamente a sus propiedades adsorbentes. Para que este proceso tenga lugar, las moléculas acceden al material a través de los macroporos, que realizan una función de transporte. Posteriormente, los mesoporos — poros de transición— facilitan el transporte de las moléculas más pequeñas hacia los microporos, donde se produce la adsorción, aunque también participan en la adsorción

de las moléculas de mayor tamaño⁶³. Las diferencias en las propiedades adsorbentes de los materiales de carbón se ven perfectamente representadas en sus isothermas de adsorción-desorción, que muestran las cantidades de gas adsorbidas por un material en función de la presión ejercida sobre el mismo. De esta forma, a altas presiones se producirá en primer lugar el llenado de los microporos, seguido de los mesoporos y de, finalmente, los macroporos. Esto ha permitido a la IUPAC establecer diferencias y generalizar ocho modelos distintos de isothermas de adsorción-desorción⁶⁹, pudiendo así clasificar a los materiales adsorbentes, en función de a qué modelo se ajusta más su comportamiento (**Figura 11**).

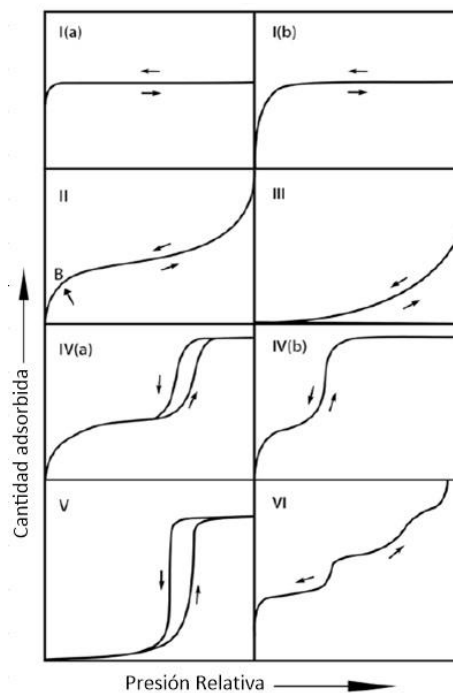


Figura 11. Isothermas de adsorción según la clasificación de la IUPAC⁶⁹.

Otro aspecto que debe ser considerado a la hora de clasificar las isothermas de adsorción-desorción es el denominado ciclo de histéresis (**Figura 12**), que es la diferencia entre las cantidades de gas adsorbidas por los materiales durante el proceso de adsorción, frente a las desorbidas durante el proceso de desorción, a presiones iguales. La presencia de uno de estos ciclos en la isoterma de adsorción-desorción se debe a la aparición de procesos de condensación capilar en el interior de los mesoporos, lo que permite la identificación de geometrías y distribuciones de tamaños de poro determinados⁷⁰.

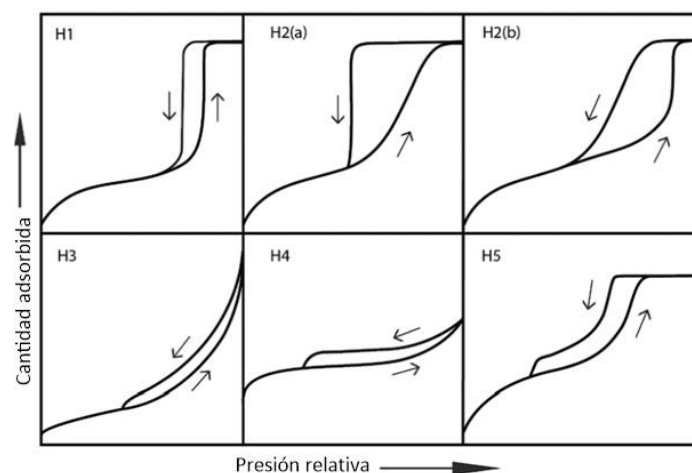


Figura 12. Ciclos de histéresis según la clasificación de la IUPAC⁶⁹.

La morfología de los poros presentes en los materiales porosos permite llevar a cabo una segunda clasificación, en función de la forma originada durante la etapa de cristalización. Se establecen tres modelos de poro: a) cilíndricos, b) cuello de botella y c) en forma de hendidura^{70, 71}.

Las propiedades estructurales que muestran los CAs están determinadas por las condiciones de síntesis empleadas. Tanto sus propiedades texturales como su química superficial pueden modificarse para un uso específico, lo que les confiere gran versatilidad. Sin embargo, no siempre unas características texturales similares en dos CAs distintos equivalen a la misma capacidad de adsorción para un mismo adsorbato, debido a muchos otros factores, como puede ser su composición química⁷².

Anteriormente se ha citado la estructura no gráfica de los CAs. Es precisamente esta estructura, con su sistema de electrones π de los planos basales, la responsable de la basicidad de estos materiales. La concentración y naturaleza de los grupos funcionales orgánicos, así como los diferentes heteroátomos que estos contienen —principalmente O, N, H, Cl, S—, sobre la superficie del carbono, contribuyen a los cambios en su carácter ácido-base y propiedades redox, siendo los grupos oxigenados los más ampliamente investigados, debido al hecho de que el oxígeno combinado con los átomos de carbono forma una amplia variedad de componentes orgánicos con distintas funciones ácido-base.

La relevancia de la composición química de un CA se debe al papel que juegan en el anclaje químico de los adsorbatos los centros activos presentes en la superficie del

material, generados por átomos de carbono con electrones deslocalizados⁷³, así como a los heteroátomos de los grupos funcionales superficiales. La química superficial de los CAs se puede modificar por la introducción de diversos grupos funcionales, que modifican sustancialmente sus propiedades redox y ácido-base (**Figura 13**). Por tanto, su carácter ácido-base dependerá directamente tanto de la concentración, distribución y tipo de grupos ácidos o básicos en superficie, pudiendo presentar incluso un carácter anfótero.

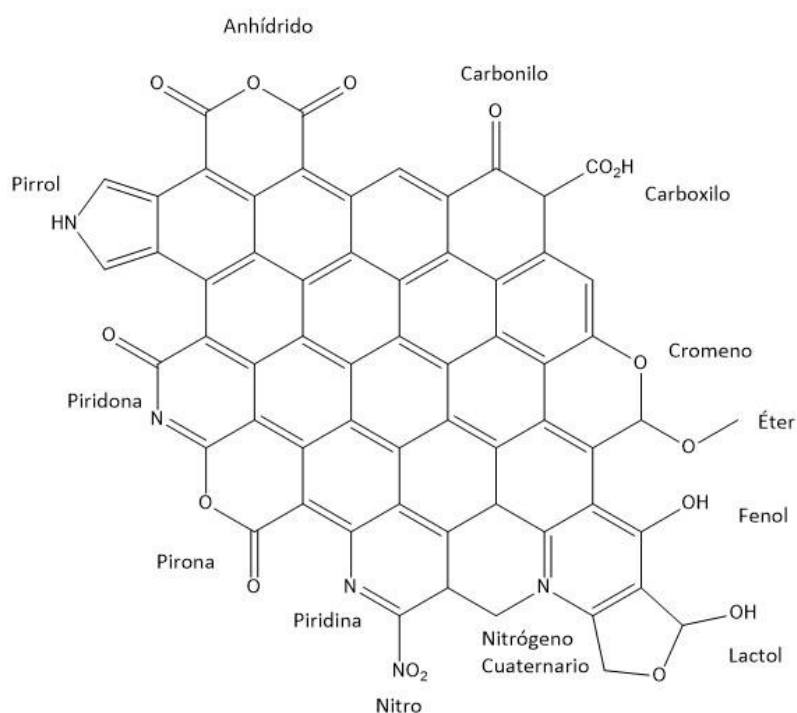


Figura 13. Representación de diversos grupos funcionales en la superficie de un CA.

El método de modificación más habitual para la introducción de grupos oxigenados en la superficie del CA^{74, 75} es la oxidación. En el proceso de oxidación seca se emplean gases oxidantes tales como vapor de agua, dióxido de carbono, oxígeno u ozono, generalmente a altas temperaturas. En cambio, en la oxidación húmeda se emplean disoluciones oxidantes, tales como ácido nítrico, ácido sulfúrico, peróxido de hidrógeno o agua clorada, en condiciones suaves. Generalmente, la oxidación aumenta los grupos ácidos, disminuyendo así el carácter básico de los CAs. Este proceso ocurre en los sitios más susceptibles de ser oxidados, como los defectos en la superficie del CA o en las cadenas laterales alifáticas del CA, es decir, en los átomos de carbono periféricos

en la superficie. Debido a que estos grupos funcionales pueden generarse en la entrada de los poros, este proceso puede bloquear alguno de ellos⁶³.

Es igualmente posible la introducción de otros heteroátomos en la red carbonosa, tales como B, N, S y P, lo que puede modificar el área superficial y las propiedades electrónicas de los materiales, además de influir en la aplicación de los CAs como catalizadores, por ejemplo⁷⁶.

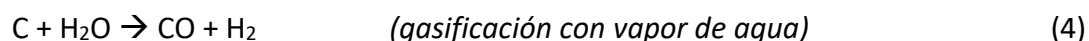
1.4.2 Precursores convencionales y estrategias sintéticas

Tradicionalmente, la preparación de CAs se ha relacionado con la carbonización/activación de materiales típicamente lignocelulósicos y carbón mineral — carbón bituminoso, lignito, y antracita— como precursores. Sin embargo, casi todos los materiales orgánicos que contienen carbono se pueden utilizar como precursores en la preparación de CAs, dependiendo, en gran medida, de su disponibilidad y coste. Otros precursores habitualmente utilizados han sido los residuos de petróleo, la turba, la cáscara de coco, la cáscara de nuez, los huesos de frutas o restos óseos animales^{64, 77}.

Los principales métodos para la producción de CAs son:

Activación física

Los procesos de pirólisis/activación son la ruta más habitual en la síntesis de CAs porosos. El procedimiento de activación física consta de dos etapas bien diferenciadas: en una primera etapa, el material precursor se carboniza generalmente a temperaturas comprendidas entre 673 K y 1123 K y en atmósfera inerte, con el fin de que se produzca la deshidratación completa del mismo para generar la estructura porosa deseada. En una segunda etapa se efectúa un tratamiento térmico a altas temperaturas, del rango de 1073 K a 1273 K, en presencia de agentes oxidantes, habitualmente H₂O, NH₃ CO₂ y aire⁷⁸, o mezclas de estos gases, que reaccionan con los átomos de carbono de la matriz^{64, 79, 80, 81}. Durante este procedimiento se pierden los átomos de carbono más insaturados, que se eliminan en forma de CO, de manera que se incrementa el tamaño de poro y se aumenta la accesibilidad a los microporos del material⁸². Las reacciones que se producen en la activación de un material de carbón se muestran en las ecuaciones 3-6.



La activación con CO_2 producirá una distribución de tamaño de microporos estrecha, mientras que la activación con vapor de agua generará CAs con una distribución de tamaño de poro más amplia y un volumen de microporos menor. Las reacciones de los agentes activantes gaseosos, así como los productos de reacción gaseosos producen la quimisorción del oxígeno en la superficie, conduciendo la formación de grupos funcionales superficiales oxigenados. En el tratamiento con NH_3 también se introducirán grupos superficiales que contengan N, aunque este tipo de activación suele combinarse con otros gases oxidantes, como el CO_2 , para así mejorar el desarrollo de la porosidad^{81, 83, 84, 85, 86}.

Cabe mencionar la importancia del material inorgánico contenido en los precursores—en particular sales, óxidos y metales de la serie de los metales alcalinos, metales alcalinotérreos y metales de transición—, ya que en algunos de ellos pueden actuar como catalizadores eficaces de las reacciones de gasificación.

Activación química

El procedimiento de activación química puede ocurrir en dos etapas o en una sola, aunando los procesos de carbonización y de activación. Para ello, antes del tratamiento térmico en atmósfera inerte, a temperaturas entre 673 K y 1173 K, se debe añadir un agente químico, mediante impregnación del precursor carbonoso, que actuará como activante, disminuyendo la formación de materia volátil y alquitranes, evitando así la oclusión de los poros generados. Los activantes habitualmente utilizados son agentes deshidratantes tales como ácidos, cloruros o hidróxidos, entre los que destacan H_3PO_4 , H_2SO_4 , ZnCl_2 , NaOH o KOH , entre otros^{87, 88}. Otros agentes químicos que se pueden utilizar, aunque menos comunes, son HNO_3 , HCl , H_2O_2 , FeCl_3 y KMnO_4 ^{64, 79, 80, 81, 89}. Tanto el H_3PO_4 como el ZnCl_2 son ejemplos de agentes químicos que son activos a temperaturas relativamente bajas, alrededor de 723-773 K, siendo particularmente

eficaces para los precursores lignocelulósicos. El ZnCl_2 se comporta como un catalizador deshidratante de las estructuras lignocelulósicas, actuando así como plantilla para la generación de microporos. Esto significa que el volumen de microporos desarrollado es similar al volumen de ZnCl_2 introducido en la partícula, creando una microporosidad uniforme^{64, 79, 80, 89}. En el caso del H_3PO_4 , los mecanismos de desarrollo de porosidad son diferentes ya que el ácido promueve la deshidratación, despolimerización, reacciones de condensación y reticulación en el precursor lignocelulósico, formando estructuras enlazadas por grupos éster de fosfato. La inserción de los grupos fosfato crea una expansión que, después de la eliminación del ácido, deja la matriz en un estado expandido con una estructura de poro accesible^{64, 79}. Es por ello que el ZnCl_2 desarrolla tanto microporos anchos como mesoporos pequeños, mientras que el H_3PO_4 desarrolla esencialmente microporosidad con algunos mesoporos más grandes e incluso macroporos^{79, 89}.

El uso de sales de metales alcalinos —óxidos, hidróxidos o carbonatos— para preparar CAs requiere de mayores temperaturas, generalmente entre 973-1173 K. Las sales alcalinas no actúan como agentes deshidratantes, lo que implica que no reaccionan con el precursor sino con el carbón resultante del proceso de carbonización⁷⁹. El mecanismo de reacción para el desarrollo de porosidad con sales alcalinas generalmente implica los siguientes pasos: i) inicialmente, se produce una reacción redox donde los átomos de carbono del carbón formado se oxidan CO o CO_2 , produciendo porosidad, siendo esta gasificación catalizada por el metal alcalino, y posteriormente ii) la reducción de la sal de metal alcalino que produce los átomos metálicos que serán intercalados entre las capas de grafeno, expandiendo la estructura de carbono^{79, 89}.

Tanto el activante elegido como la atmósfera inerte empleada van a influir en las características texturales y estructurales del material, así como en su capacidad de regeneración⁸². Tras realizar el proceso de calcinación-activación, en atmósfera inerte, es necesario un lavado posterior, para eliminar los restos sobrantes de activante que no hayan reaccionado, generalmente con agua destilada. Aunque la activación química permite la producción de CAs con elevadas áreas superficiales, la etapa de lavado hace que el proceso sea lento, caro y con un consumo energético elevado, con el

correspondiente impacto medioambiental. Por otro lado, los CAs obtenidos a mayores temperaturas permiten un peor control de su porosidad.

Es importante reseñar que ambos procesos de activación —física y química— se pueden utilizar de forma simultánea.

Otros métodos

Otros métodos de síntesis de CAs destacados son: i) la carbonización hidrotermal (HTC, *por sus siglas en inglés*), en la que el precursor se trata termoquímicamente en presencia de agua subcrítica⁹⁰; ii) calentamiento bajo irradiación de microondas (MW, *por sus siglas en inglés*), que ofrece la ventaja de acelerar las reacciones químicas a temperaturas más bajas, proporcionando además un calentamiento uniforme en comparación con la calefacción convencional⁹¹; iii) preparación de geles de carbón preparados mediante síntesis sol-gel, a través de reacciones de policondensación/polimerización en disoluciones acuosas de hidroxibencenos —resorcinol, fenol, floroglucinol o cresol— con aldehídos —formaldehído o furfural—, catalizadas por agentes químicos, como Na₂CO₃, NaOH, HCl o ácido acético, entre otros^{92, 93, 94}; iv) métodos que emplean sólidos inorgánicos como agentes directores de la estructura (*hard template*) —zeolitas, sílices, arcillas, entre otros—^{95, 96}; o v) aquellos que usan agentes tensioactivos como plantillas (*soft template*)^{97, 98}.

1.4.3 Aplicaciones de los CAs

El elevado poder adsorbente y su bajo coste de producción convierten a los CAs en materiales ampliamente utilizados en numerosos sectores. Hoy en día, muchos productos comerciales de uso cotidiano están compuestos por CAs. Se emplean en la potabilización de aguas para consumo humano⁹⁹, en los procesos de producción en la industria alimentaria¹⁰⁰, purificación de biogás^{101, 102}, en medicina en el tratamiento de intoxicaciones provocadas por la ingesta de venenos^{103, 104}, en sistemas para la filtración de aire¹⁰⁵ y aguas residuales¹⁰⁶, o para el control de emisiones tanto de gases nocivos como de vertidos¹⁰⁷, entre muchas otras aplicaciones.

I.4.3.1 Aplicaciones de los CAs en catálisis

Actualmente, el diseño de nuevos nanomateriales que actúen de forma eficiente en procesos químicos de interés es un campo de investigación muy activo, debido a su gran repercusión e impacto industrial.

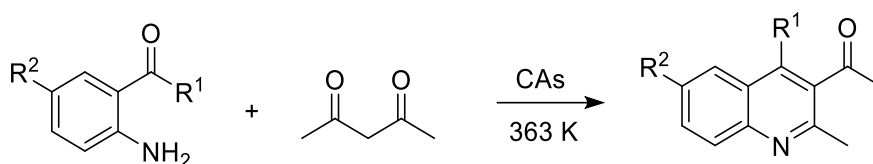
Durante mucho tiempo, los materiales de carbono se han utilizado en el campo de la catálisis como catalizadores o incluso como soportes de catalizadores¹⁰⁸. Entre las principales características de los CAs para su aplicación en catálisis se encuentran: i) su elevada estabilidad térmica, que les permite ser utilizados a altas temperaturas, ii) alta estabilidad química, tanto en medio ácido como básico, iii) baja capacidad de corrosión, iv) destacado carácter hidrofóbico, v) facilidad de recuperación de la mezcla de reacción y, vi) desde un punto de vista económico, su reducido precio.

En este contexto, los materiales de carbón se han investigado ampliamente en la síntesis de productos de QF, particularmente como soportes de nanopartículas metálicas, siendo una alternativa económica y sostenible a otros catalizadores sólidos^{109, 110, 111}. La alta dispersión y estabilidad de las fases metálicas en los CAs es posible principalmente debido a sus elevadas áreas superficiales y grupos funcionales en su superficie. En este contexto, tanto las propiedades texturales como la química superficial de los CAs influyen en su actividad como catalizadores. Algunos CAs comerciales se emplean en numerosos procesos de interés. Destaca su uso como catalizadores en procesos de hidrogenación, debido a las excelentes propiedades de dispersión de las partículas metálicas. En general, son soportes más baratos en comparación con la alúmina o la sílice, y además permiten recuperar la fase activa eliminando el soporte mediante calcinación.

Muy recientemente, se ha descrito una nueva generación de materiales carbonosos preparados a partir de otros precursores emergentes, como son los MOFs y otros polímeros de naturaleza orgánica, denominados “Covalent Organic Frameworks” (COF, *por sus siglas en inglés*), con propiedades fisicoquímicas mejoradas, útiles en la síntesis de productos de alto valor añadido⁶³. Estos materiales de carbón porosos presentan áreas superficiales extremadamente altas, volúmenes de poro grandes y, en

algunos casos, contienen especies metálicas altamente dispersas, todas estas propiedades de gran importancia para su aplicación en catálisis.

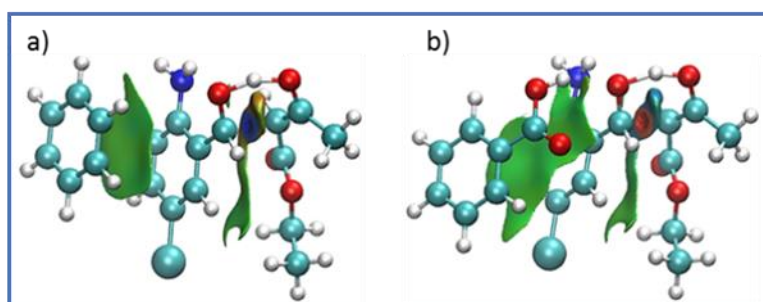
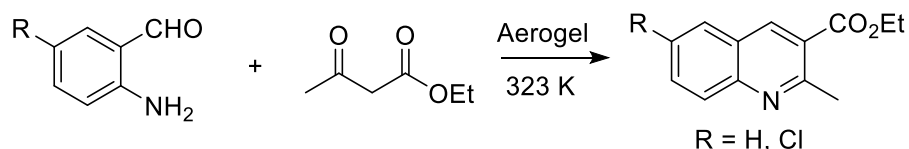
A este respecto, nuestro grupo de investigación posee amplia experiencia en la utilización de materiales carbonosos como catalizadores, o soportes de fases activas, en la síntesis de compuestos de QF, especialmente en la síntesis de sistemas heterocíclicos de interés. Entre ellos destacan CAs ácidos¹¹² y aerogels de carbón, sintetizados por polimerización resorcinol-formaldehído, libres de metales¹¹³ empleados en la síntesis de quinolinas y compuestos relacionados a través de la condensación de Friedländer (Esquema 1)¹¹⁴.



Esquema 1. Síntesis de quinolinas catalizada por CAs ácidos a través de la condensación Friedländer¹¹².

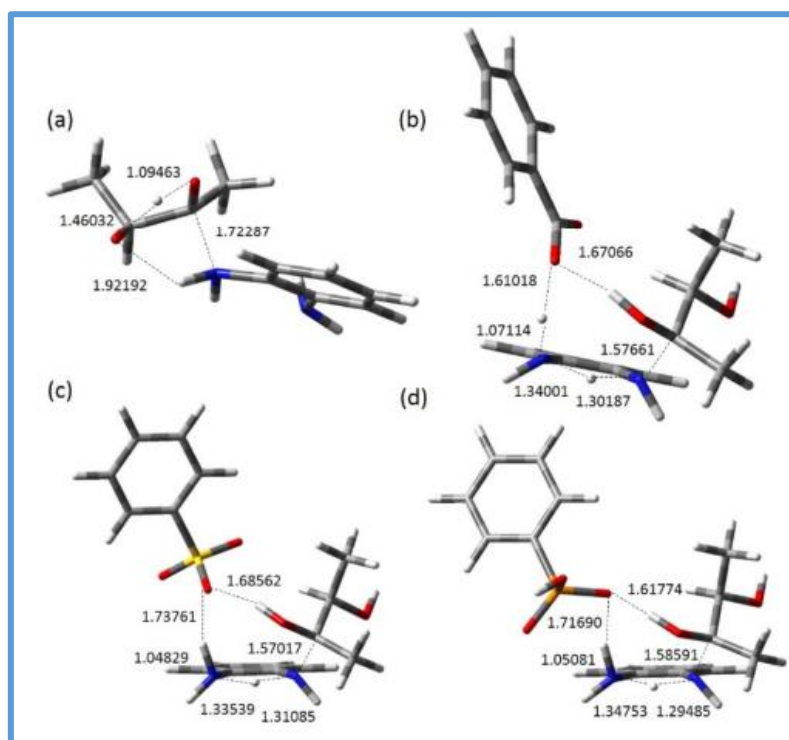
El estudio realizado ha permitido racionalizar el mecanismo por el que tiene lugar el proceso. En el caso de los materiales carbonosos derivados de los CAs comerciales — Norit RX3 y Merck— funcionalizados con grupos ácidos, -CO₂H y -SO₃H, se pudo comprobar que las funciones -SO₃H, presentes en las muestras Norit/S y Merck/S, están involucrados en la formación preferente de la correspondiente quinolina, mientras que otras funciones oxigenadas —grupos -CO₂H— en superficie (Norit/N), son probablemente responsables de selectividades más bajas. El estudio teórico realizado, mediante cálculos computacionales *ab initio*, investigando la primera etapa de la reacción de Friedländer, que consiste en la reacción de aldolización entre o-aminobenzofenona y acetilacetato de etilo, en presencia de modelos reducidos de que simulan los centros activos en los catalizadores estudiados —C₆H₅-SO₃H o C₆H₅-CO₂H—, sugiere que la formación de los aldoles correspondientes se produce a través de una red de intercambio de hidrógenos que tiene lugar durante la formación del enlace C-C en el aldol correspondiente; estas migraciones de H se completan en el caso de C₆H₅-CO₂H pero no en C₆H₅-SO₃H. Esta red de enlaces de H le confiere gran flexibilidad al complejo reactivos-catalizador y podría ser responsable de la baja estereoselectividad del proceso.

Por otra parte, el estudio experimental y teórico realizado en la reacción catalizada por aerogeles de carbón¹¹² confirmó que la reacción es fuertemente dependiente tanto de la porosidad del material como de su química superficial. Fue posible demostrar que tanto la acidez de los materiales como interacciones de π,π -stacking, relativamente fuertes, entre la superficie del carbón y los reactivos podrían ser responsables de la reactividad observada (**Esquema 2**).



Esquema 2. Condensación Friedländer entre 2-amino-5-clorobenzaldehído y acetilacetato de etilo, y modelos computacionales de las interacciones π,π -stacking en la formación de enlaces C-C¹¹³.

Muy recientemente, nuestro grupo de investigación ha descrito también diferentes series de materiales carbonosos, con una química superficial similar y alta microporosidad desarrollada, activos y selectivos en la síntesis verde de benzodiazepinas¹¹⁵ y quinoxalinas¹¹⁶ (**Esquema 3**). Los resultados obtenidos confirman, una vez más, que ambas reacciones son controladas por la combinación de la porosidad del material y la fuerza ácida de las funciones oxigenadas en superficie. El estudio realizado ha permitido esclarecer el mecanismo por el que tiene lugar la formación de quinoxalinas, catalizada por los materiales carbonosos investigados, que tendría lugar a través de las siguientes etapas: i) reacción de iminación entre reactivos, ii) sucesivas tautomerías imina-enamina y ceto-enólica, iii) heterociclación con iv) posterior deshidratación y, finalmente v) aromatización.

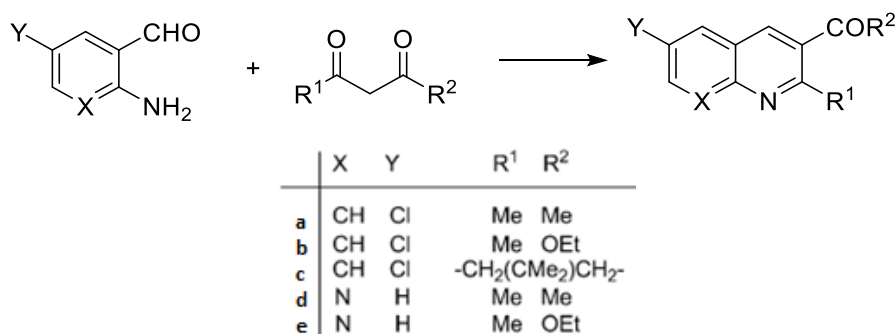


Esquema 3. Síntesis de quinoxalinas a partir de *o*-fenilendiamina y α -hidroxicetonas catalizada por CAs. Estructuras optimizadas del ataque nucleofílico de *o*-fenilendiamina a acetoina a) en ausencia de catalizador, b) catalizada por grupos $-\text{CO}_2\text{H}$, c) $-\text{SO}_3\text{H}$ y d) $-\text{PO}_3\text{H}$.

La reacción de condensación de Friedländer también se ha investigado en presencia de otros materiales carbonosos como aerogeles de carbón o incluso nanotubos de carbono de pared múltiple (MWCNTs, *por sus siglas en inglés*) dopados con metales de transición, en los que la especie activa predominante está constituida por nanopartículas de Co^0 o Cu^0 en el caso de los materiales dopados^{117, 118} y por CoO en el caso de los materiales sintetizados por impregnación con disoluciones de sales de cobalto de los soportes carbonosos¹¹⁹.

Merece destacar también el estudio descrito por Godino-Ojer *et al*¹²⁰ sobre la síntesis selectiva de quinolinas, mediante condensación Friedländer, catalizada por carbones básicos con MgO soportado (**Esquema 4**). Se trata de composites preparados por pirolisis de tereftalato de polietileno (PET, *por sus siglas en inglés*) y magnesia (MAG) en distintas proporciones, en los que el MgO es la especie catalítica predominante mientras que el material carbonoso actúa como soporte aportando

porosidad al sistema. El análisis computacional del mecanismo de la reacción (**Figura 14**), en este caso, sugiere que el MgO se comporta como un catalizador dual, activando ambos compuestos carbonílicos de partida, estando implicado en todas y cada una de las etapas de reacción involucradas en la formación de la correspondiente quinolina, estabilizando las especies intermedias y promoviendo la reacción.



Esquema 4. Síntesis de quinolinas por condensación de Friedländer a partir de 2-aminobenzaldehídos y compuestos carbonílicos, catalizada por materiales PET/MAG.

En primer lugar, se estudiaron los distintos modos de adsorción de acetato de etilo en el clúster de MgO. En los tres escenarios estudiados, los cálculos sugieren que la adsorción se produce a través del HC=O, formando un complejo reactivo estable, mientras la interacción a través del oxígeno del éster conduce a un complejo metaestable, menos estable que los reactivos aislados. En todos los casos la quimisorción disociativa de los complejos reactivos resulta favorable energéticamente. Posteriormente, la segunda especie reaccionante, el aldehído, se une al complejo interaccionando a través del par solitario de oxígeno carbonílico con Mg²⁺. En la **Figura 14** se muestran los tres posibles estados de transición, teniendo en cuenta los tres posibles modos de interacción del nucleófilo que conducen a los respectivos intermedios **I1a-c**, respectivamente. Las estructuras de transición muestran cómo, durante el transcurso de esta etapa, el protón adsorbido permanece fuertemente unido al catalizador y forma un enlace fuerte del H con el oxígeno del aceptor carbonílico. El mecanismo de la **Figura 14** muestra cómo la reacción sigue, previsiblemente, la secuencia: i) activación por quimisorción disociativa, ii) aldolización, iii) heterociclación mediada por una molécula de H₂O, iv) primera deshidratación y v) segunda deshidratación.

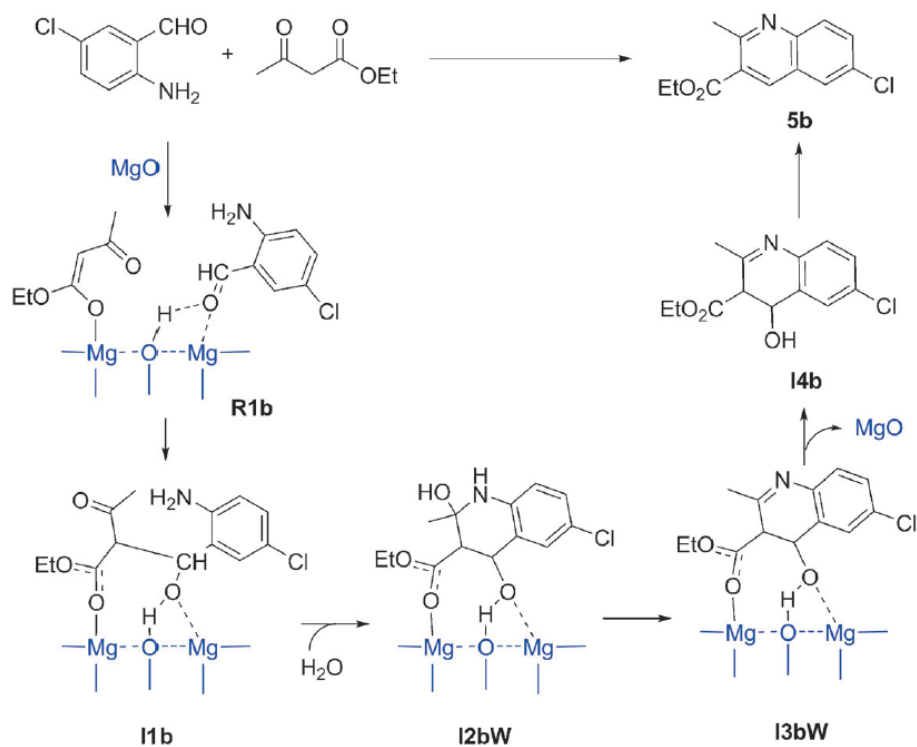
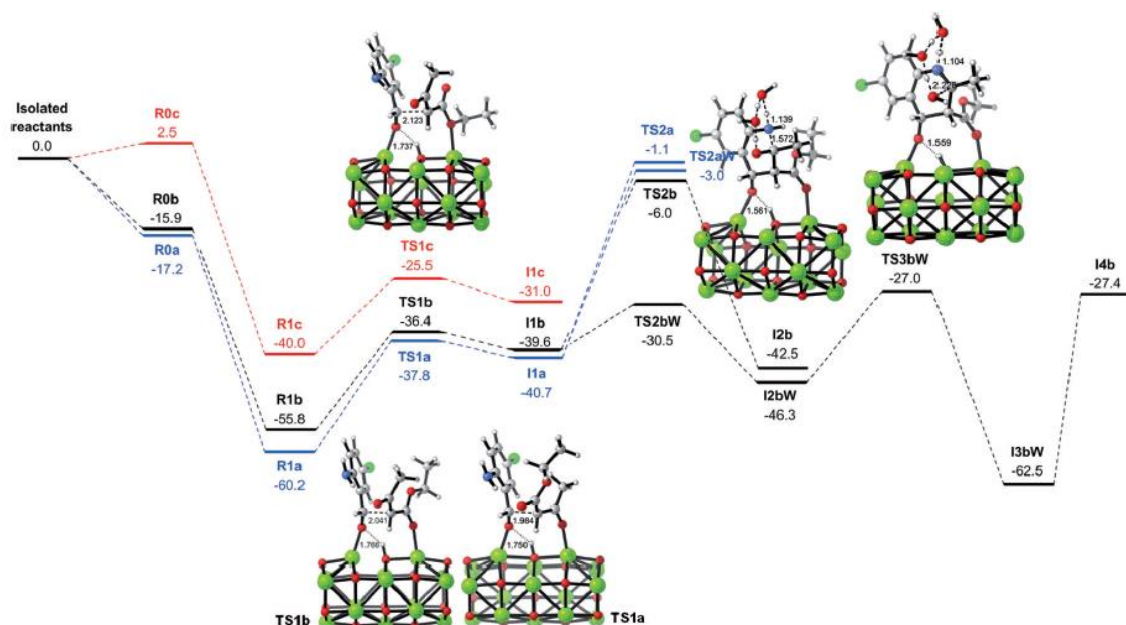


Figura 14. Perfil de energía libre y posible mecanismo de reacción en la reacción de condensación entre 2-amino-5-clorobenzaldehído y acetoacetato de etilo catalizada por MgO¹²⁰.

En nuestro grupo de investigación se han sintetizado, caracterizado y testado otros materiales carbonosos, impregnados con metales alcalinos, en la síntesis de compuestos de QF como es el caso de las chalconas¹²¹ o en la alquilación de imidazoles^{122, 123}, promovida también por radiación microondas^{124, 125, 126}, y en la síntesis de γ -lactamas *N*-sustituidas¹²⁷, entre otros ejemplos.

1.5 Redes Metalorgánicas (MOFs)

Los MOFs son materiales sólidos cristalinos porosos reticulares, constituidos por iones metálicos coordinados a ligandos orgánicos multidentados. La diferente coordinación da lugar a estructuras unidimensionales, bidimensionales o tridimensionales (**Figura 15**)¹²⁸.

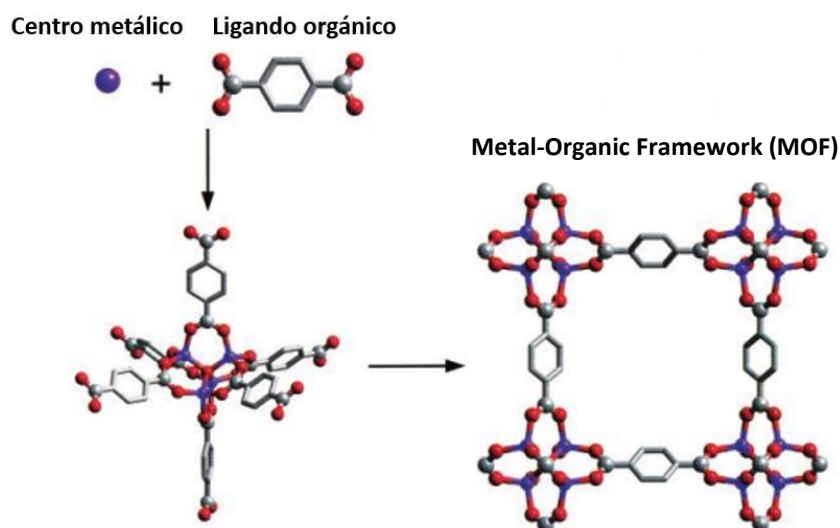


Figura 15. Ensamblaje estructural de un MOF mediante la copolimerización de iones metálicos con ligandos orgánicos¹²⁹.

En relación con los elementos constituyentes de los MOFs, si bien el Zn^{2+} y el Cu^{2+} son los cationes metálicos más utilizados¹³⁰, también se suelen utilizar muchos otros metales de transición, como el Y, Sc o elementos lantánidos¹³¹. En el caso de los ligandos orgánicos, entre los más utilizados se encuentran los compuestos con grupos carboxílicos¹³² (**Figura 16**) o nitrógeno estructural.

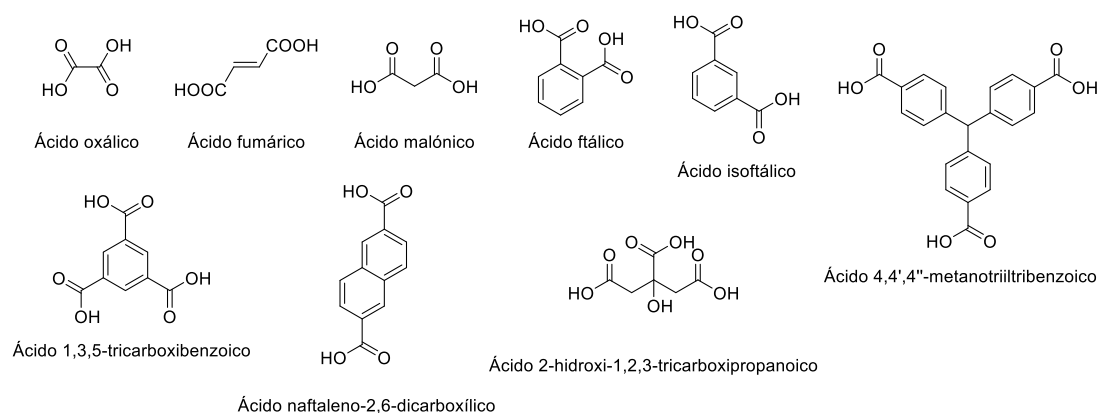


Figura 16. Ejemplos de ligandos orgánicos con grupos carboxilos habitualmente utilizados en la síntesis de MOFs¹³².

Kitagawa *et al*¹³³, en 1998, clasificaron los MOFs en tres generaciones de acuerdo con su flexibilidad y estabilidad:

- i) Primera generación: redes microporosas, sostenidas exclusivamente por moléculas huésped que colapsan durante la extracción de éstas, debido a las fuertes interacciones electrostáticas que se establecen en la estructura.
- ii) Segunda generación: compuestos estructuralmente estables y robustos, con porosidad definida y permanente, sin necesidad de la presencia de moléculas huésped. Las moléculas adsorbidas se pueden extraer fácilmente a bajas temperaturas.
- iii) Tercera generación: MOFs con estructura flexible y dinámica, que actúan en respuesta a estímulos externos tales como luz, campo eléctrico o moléculas huésped, de forma que modifican sus canales o poros de forma reversible.

Inicialmente, la mayor parte de la investigación en este tipo de materiales se centró en el desarrollo de nuevos tipos y estructuras, así como en su aplicación como adsorbentes de diversos gases. Sin embargo, actualmente, el gran conocimiento acumulado sobre este tipo de materiales permite el control de la composición, estructura, funcionalidad y porosidad de los mismos, de tal forma que pueden ser diseñados para aplicaciones específicas. En la **Figura 17** se muestra el incremento exponencial en el número de publicaciones sobre MOFs desde los años 90.

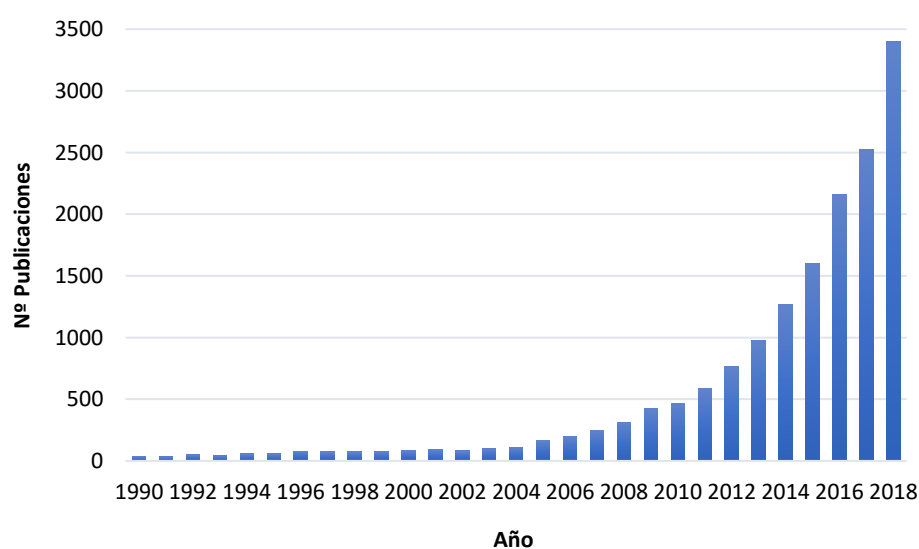


Figura 17. Número de publicaciones por año, desde 1990 hasta 2018, en las que aparece la terminología “Metal-Organic Framework” según la base de datos de la Web of Science¹³⁴.

1.5.1 Propiedades de MOFs

La conformación particular de los MOFs, centros metálicos y ligandos orgánicos, les otorga la capacidad de adaptar su tamaño de poro y su entorno químico a las necesidades para las que se sintetice el material. Esto puede llevarse a cabo durante el proceso de síntesis mediante un diseño adecuado con cationes o ligandos específicos o, incluso, mediante modificaciones post-sintéticas¹³⁵. Existe, además, la posibilidad de funcionalizar con múltiples grupos funcionales de naturaleza variada la superficie de un MOF, ampliando las posibilidades que puede ofrecer un mismo material.

En la síntesis de MOFs se pueden utilizar un amplio abanico de cationes metálicos, así como de ligandos orgánicos. Estos ligandos otorgan una elevada rigidez a la estructura del material, pudiendo incluso ser sustituidos por otros, manteniendo la topología estructural. Asimismo, presentan una ventaja con respecto a otros materiales porosos como sílices mesoordenadas o zeolitas, ya que no requieren el uso de plantillas durante su síntesis¹³⁶.

Los MOFs son materiales que presentan áreas superficiales elevadas, alcanzando incluso valores de $7400 \text{ m}^2 \cdot \text{g}^{-1}$, así como una porosidad mayor al 50% del volumen del cristal, superior a la de los materiales porosos tradicionales. Además, la versatilidad que ofrecen en su síntesis permite la modificación de diversas propiedades, como su difusividad e incluso su estabilidad térmica o química¹³⁷.

1.5.2 Síntesis de MOFs

La estructura de un MOF puede diseñarse a partir de unidades moleculares, de estructura rígida y bien definida, de forma que se mantenga la integridad estructural del MOF a lo largo del procedimiento de síntesis¹³⁸. Esta metodología se conoce como *síntesis reticular*¹³⁹ y se basa en la utilización de Unidades de Construcción Secundarias (SBUs, *por sus siglas en inglés*) como bloques moleculares a partir de los que se elaboran las redes que conforman la estructura del material final. Las SBUs son figuras geométricas que representan los clústers inorgánicos o las esferas de coordinación enlazadas por ligandos orgánicos, cuyo uso fue adoptado de las estructuras zeolíticas¹⁴⁰

(Figura 18). Aunque estas estructuras se pueden observar en distintos compuestos moleculares, habitualmente se sintetizan artificialmente bajo condiciones específicas.

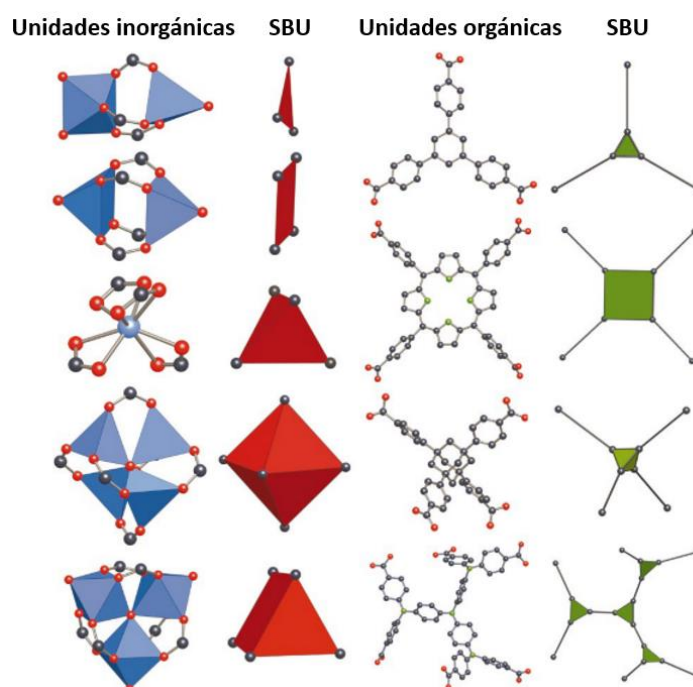


Figura 18. Ejemplos de diversas unidades inorgánicas (los poliedros azules corresponden a unidades inorgánicas metal-oxígeno, mientras que los polígonos y poliedros rojos delimitan las correspondientes SBUs) y orgánicas (los polígonos y poliedros verdes corresponden a las SBUs) de MOFs derivados de ligandos carboxílicos. Las esferas rojas corresponden a átomos de oxígeno, las verdes de nitrógeno y las negras de carbono¹³⁹.

En la síntesis de MOFs se debe prestar especial atención, tanto a la selección de los iones metálicos y ligandos orgánicos como al ensamblaje entre sí de ambos componentes, de forma que se pueda obtener una estructura final bien definida¹⁴¹ y evitar una posible descomposición del ligando orgánico. Por tanto, la disponibilidad del ion metálico para adquirir la geometría buscada, además de las características del ligando orgánico, tales como quiralidad o ángulos de enlace son los factores determinantes en la síntesis de un MOF. Las condiciones de reacción son otro factor importante a considerar, especialmente la temperatura de reacción, ya que influirá en la coordinación del ion metálico. Del mismo modo, la elección del disolvente o la cinética de reacción debe ser adecuada para que la nucleación y el crecimiento de las fases se produzcan de forma adecuada¹⁴². Por ello, en ocasiones, se incorporan compuestos aminados durante los procedimientos de síntesis, sin que formen parte del producto final, con el fin de favorecer la reacción mediante la desprotonación del ligando

orgánico, siendo ésta la etapa anterior a la formación del enlace de coordinación con el ion metálico¹⁴¹.

En general, la longitud de los ligandos empleados no afecta a las características de las distintas SBUs mientras se mantenga el mismo grado de conectividad de dichos ligandos. De esta forma, se pueden modificar las estructuras de los MOFs mediante un proceso conocido como *expansión reticular*, consistente en la variación de la longitud de los ligandos, produciendo estructuras con las mismas características geométricas, pero con diferencias en sus características texturales (**Figura 19**).

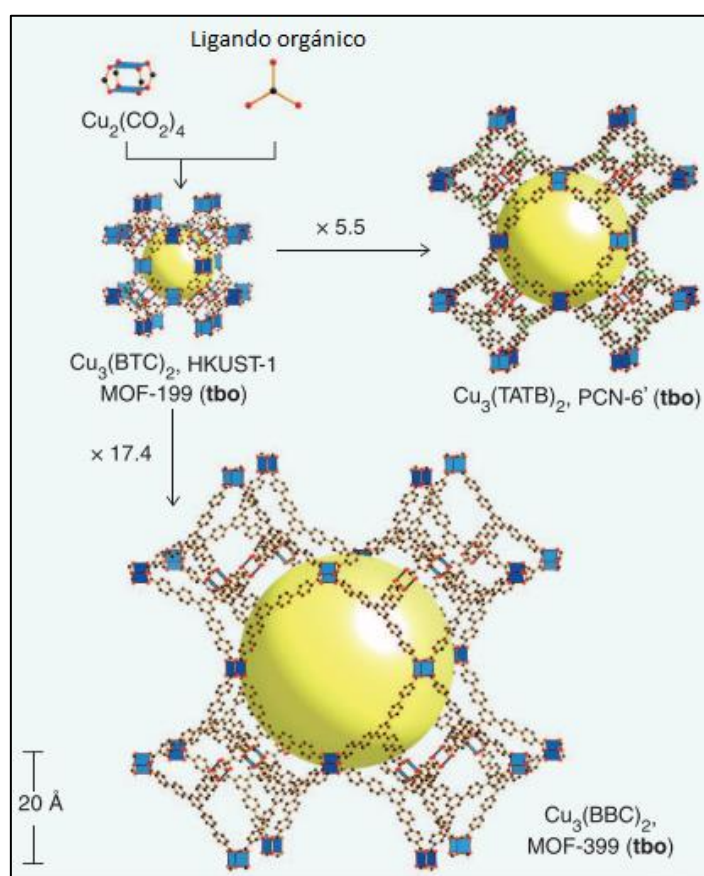


Figura 19. Expansión reticular. Manteniendo la misma topología, la adición de ligandos orgánicos a la SBU de partida, permite aumentar el tamaño de poro del material¹³⁷.

En cuanto a la metodología de síntesis a nivel operacional, existen diversas alternativas, si bien todas permiten obtener MOFs de manera sencilla, económica y con altos rendimientos. A continuación, se detallan los posibles métodos de síntesis que pueden emplearse¹⁴³:

Síntesis termal

Es la metodología más ampliamente utilizada y la que presenta una mayor eficiencia a la hora de obtener MOFs. En función del disolvente empleado se diferencia entre síntesis hidrotermal, cuando se utiliza H₂O, o solvotermal, siendo los disolventes más empleados etanol, *N,N'*-dimetilanilina, *N,N'*-dimetilformamida o DMF, entre otros.

El procedimiento a seguir consiste en el tratamiento térmico de disoluciones de ligandos orgánicos y sales metálicas en agua o disolventes orgánicos a relativamente bajas temperaturas (rango habitual de 353 K a 533 K) en un espacio confinado, frecuentemente un autoclave. Existen diversos factores que deben tenerse en cuenta durante la síntesis termal de MOFs que resultan cruciales en la estructura final del producto, tales como las características del ligando, la tendencia de los iones metálicos a adoptar determinadas geometrías y las condiciones de reacción —temperatura, concentraciones de sal y ligando, disolvente elegido, pH e incluso rampa de enfriamiento—.

El principal problema de la síntesis termal es que no es apta para materiales de partida que sean térmicamente sensibles¹⁴⁴. Es además un procedimiento tedioso, ya que habitualmente requiere de tiempos prolongados, incluso días o semanas.

Síntesis bajo irradiación microondas (MW)

La principal ventaja que plantea este método con respecto a los métodos termal¹⁴⁵, es la mayor velocidad de reacción del proceso¹⁴⁶ y de tiempos de cristalización. En este caso la transferencia energética en el calentamiento depende directamente de las propiedades dieléctricas del disolvente utilizado, en lugar de deberse a procesos de conducción o convección, pudiendo por tanto alcanzarse altas temperaturas en periodos de tiempo muy cortos. Permite, además, un mayor control de morfologías, estructuras y tamaños de los MOFs^{147, 148}. En ocasiones, esta metodología se ha empleado en combinación con síntesis termal, como paso previo¹⁴⁹.

Síntesis promovida por Ultrasonidos (US)

La metodología de síntesis por sonicación se basa en el aumento de presión y temperatura que se produce por el fenómeno de la cavitación acústica, el cual permite

acelerar el tiempo de reacción, además de producir monocristales de MOFs de pequeño tamaño¹⁵⁰. La cavitación acústica consiste en la formación de cavidades en forma de burbujas de gas o vapor en fluidos, que crecen y colapsan a una velocidad mayor que la del sonido, emitiendo ondas de choque o de presión abrupta. En las pequeñas zonas donde se localiza el colapso de estas burbujas, también llamadas *hot spots*, se alcanzan temperaturas de 4500-5000 K y presiones superiores a 1000 atm¹⁵¹, de forma que las velocidades de calefacción y enfriamiento son extremadamente rápidas.

Síntesis en ausencia de disolvente

Aunque las metodologías de síntesis bajo irradiación microondas o ultrasonidos permiten reducir los tiempos de síntesis respecto a los métodos termal, ambas requieren la utilización de disolventes. El método de síntesis en ausencia de disolventes es una técnica novedosa de menor impacto medioambiental, que se basa en la molienda de reactivos mediante el uso de un molino de bolas mecánico¹⁴³. Aunque el uso de este procedimiento no es muy utilizado, ya existen algunos ejemplos en la literatura de materiales cristalinos sintetizados empleando este método^{152, 153}.

Síntesis por evaporación lenta

La primera etapa del procedimiento es análoga a la de la síntesis termal, preparando de forma similar disoluciones de ligandos orgánicos y sales metálicas. La diferencia reside en que el crecimiento de los cristales se produce mientras se evapora el disolvente con el tiempo¹⁵⁴.

En este tipo de síntesis resulta fundamental controlar tanto la saturación del sistema, de forma que se alcance el estado de nucleación y posterior crecimiento cristalino, como la solubilidad de los reactivos, que se ve afectada por la temperatura.

Aunque esta técnica es la menos utilizada en la síntesis de MOFs, destaca por su sencillez y ahorro energético, aunque habitualmente los tiempos de cristalización son prolongados, en ocasiones incluso de meses¹⁵⁵.

Síntesis por difusión lenta

Esta metodología permite el contacto lento entre dos especies diferentes en disolución, una conteniendo la sal metálica y la otra el ligando orgánico, de forma que difunden en

sentido opuesto. Habitualmente, entre ambas disoluciones, se ubica una capa de disolvente puro que permita separar ambas fases, o incluso geles actuando como fases intermedias, para ralentizar la difusión. Este método permite obtener cristales de gran tamaño y calidad, apropiados para estudios de difracción de monocristal¹⁵⁶. Sin embargo, la duración del procedimiento es indeterminada, pudiendo requerir de tiempos prolongados que van desde unas horas hasta incluso meses.

Síntesis por precipitación directa

Este procedimiento consiste en la adición directa de una disolución que contiene la sal metálica sobre otra que contiene el ligando. Las condiciones habituales suelen ser presión atmosférica y temperaturas variables, lo que lo convierte en una metodología simple, rápida y económica.

Métodos alternativos

Aunque habitualmente, los MOFs se sintetizan mediante reacción directa entre la sal metálica y el ligando orgánico, existen rutas alternativas, como las modificaciones post-sintéticas¹⁵⁷ o la síntesis empleando precursores tipo oxoclusters¹⁵⁸ e incluso metaloligandos¹⁵⁹.

1.5.3 Aplicaciones de MOFs

Tras el descubrimiento de los MOFs, durante los primeros años, la investigación se centró en el desarrollo de nuevas estructuras y topologías. Sin embargo, debido a su diversidad estructural, una vez se comenzaron a conocer en profundidad sus propiedades, el estudio de sus posibles aplicaciones creció exponencialmente.

Aunque se han descrito numerosas aplicaciones de este tipo de sólidos, como son: liberación controlada de fármacos o moléculas biológicas¹⁶⁰, preparación de materiales luminiscentes como pigmentos orgánicos¹⁶¹ o elaboración de membranas para procesos de separación permeoselectiva¹⁶²; en esta memoria se han destacado las aplicaciones de MOFs principalmente en el almacenaje y separación de gases y en catálisis, esta última por su relación con el presente trabajo.

Tal y como ya se ha mencionado, los MOFs son los materiales cristalinos que presentan los valores más altos de área específica, de acuerdo con el modelo Brunauer-Emmett-Teller (BET), con un valor de $6240 \text{ m}^2 \cdot \text{g}^{-1}$ en el caso del MOF-210¹⁶³. Del mismo modo, aplicando la expansión isorreticular, se han podido preparar materiales con un 90% de espacio vacío, lo que ha permitido obtener materiales de densidad extremadamente baja, como el MOF-200, con un valor de $0,22 \text{ g} \cdot \text{cm}^{-3}$ (**Figura 20**). Estas características han convertido a los MOFs en materiales ampliamente utilizados en la captación de gases contaminantes atmosféricos, especialmente CO_2 , y en el almacenamiento de gases empleados para la obtención de energía, como CH_4 o H_2 .

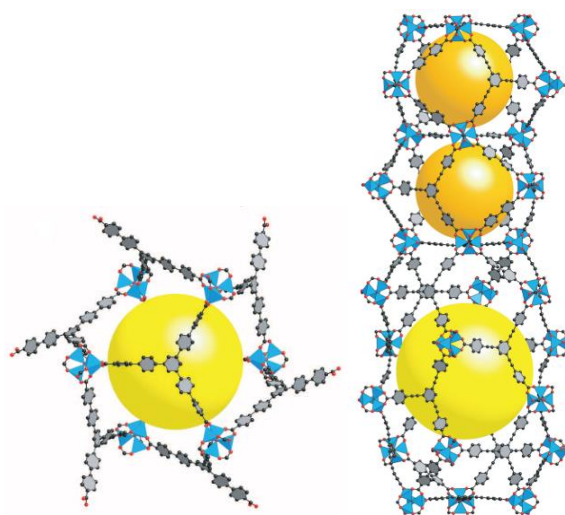


Figura 20. MOF-200 (izquierda) y MOF-210 (derecha). Las esferas naranjas y amarillas indican los diferentes espacios en el interior del material¹⁶³.

Su utilización en la separación de gases se fundamenta en la adsorción selectiva de moléculas gaseosas en función de su tamaño y forma, aumentando su efectividad en los casos en que el material adsorbente interacciona de forma diferente con los distintos compuestos de una mezcla gaseosa. Debido a la problemática medioambiental actual derivada de la necesidad de controlar las emisiones de CO_2 por parte de la industria, existe un gran interés en el desarrollo de MOFs que adsorban selectivamente este gas. Actualmente se están empleando diversas modificaciones del MOF-74, de estructura formada por canales hexagonales. Los estudios realizados sobre el MOF-74 de Mg con mezclas de gases de CO_2 y CH_4 muestran como las moléculas de CO_2 son atrapadas en los poros, mientras que las de metano difunden a través de ellos. Se ha logrado sintetizar el MOF-74 con hierro como centro metálico, material que ha presentado actividad

redox, pudiendo adsorber selectivamente moléculas de O₂. Sin embargo, los dos MOFs que han mostrado resultados más prometedores en la adsorción de CO₂, con aplicación en la reducción de emisiones en vehículos de combustión interna, son el MOF-177 y MOF-200, con capacidades de 1470 mg·g⁻¹ a 3.5 MPa y 2437 mg·g⁻¹ a 5 MPa, respectivamente¹⁶³. Estos resultados permitirían retener una cantidad de CO₂ de 9 a 17 superior a la cantidad de un tanque de gasolina estándar.

En cuanto a sus posibilidades en el almacenaje de CH₄, la tecnología de utilización de MOFs para aumentar la capacidad de recipientes de combustibles, ya se encuentra actualmente en uso. La empresa BASF comercializa MOFs¹⁶⁴ que duplican, e incluso, en ocasiones, triplican, la cantidad de CH₄ almacenada en un recipiente vacío, a temperatura ambiente y hasta 8 MPa¹⁶³. En el caso de la adsorción de H₂, el proceso de adsorción puramente física implica que la interacción con las moléculas de hidrógeno es demasiado débil, lo que limita su aplicabilidad. Sin embargo, diversos MOFs han mostrado potencial¹⁶⁵, por lo que actualmente se están tratando de realizar modificaciones sobre los mismos, dopando su estructura con metales alcalinos¹⁶⁶ o empleando MOFs con centros metálicos abiertos en la estructura¹⁶⁷, con el fin de mejorar su capacidad.

1.5.3.1 Aplicaciones de los MOFs en catálisis

Los MOFs se han descrito también como catalizadores heterogéneos, debido a su alta porosidad y a la gran concentración de centros, metálicos o no, activos disponibles. Tal y como se ha mencionado se puede variar su composición, incluyendo distintas funcionalidades en los ligandos orgánicos, permitiendo así la preparación de catalizadores bifuncionales, con una actuación sinérgica de dos especies activas diferentes¹⁶⁸. Esta estrategia, en combinación con el ajuste de tamaño de poro adecuado, permite la modificación del entorno de los centros catalíticos en los MOFs, aumentando la selectividad hacia la formación del producto deseado de forma eficaz, siendo este tipo de catalizadores de gran interés en catálisis asimétrica^{169, 170}.

Un gran inconveniente que muestran los MOFs para su aplicación en la catálisis es su baja estabilidad térmica, por lo que habitualmente se emplean como catalizadores en QF, bajo condiciones de reacción suaves¹⁷¹.

Entre las distintas estrategias que se han descrito para la modificación de este tipo de sólidos se encuentran: i) incorporación de catalizadores homogéneos en su estructura para ser transformados en catalizadores heterogéneos¹⁷², ii) estabilización de la estructura de catalizadores con durabilidad limitada¹⁷², iii) encapsulación de especies catalíticas en la estructura reticular del MOF¹⁷³, iv) modificación de los centros metálicos mediante métodos post-sintéticos (*grafting*)¹⁷⁰ y uso como catalizadores enantioselectivos en función del tamaño del sustrato¹⁷⁰.

En la **Figura 21** se muestra un resumen de las distintas aplicaciones de los MOFs gracias a las posibilidades que facilitan sus propiedades.

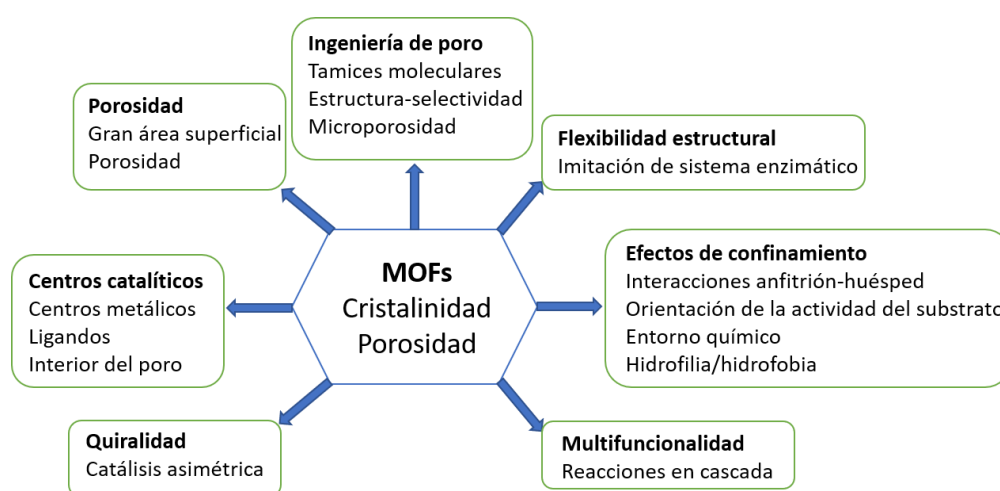
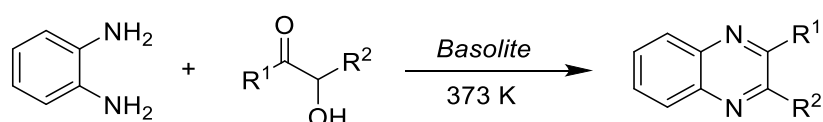


Figura 21. Propiedades y aplicaciones de MOFs en catálisis heterogénea¹⁷⁴.

Muy recientemente, en nuestro grupo de investigación se han descrito diferentes Basolitas comerciales —Basolite® C300 (CuBTC, BTC = 1,3,5-benzenetricarboxylate), F300 (FeBTC) y Z1200 (ZnZIF-8)— activas en la condensación Friedländer, para la síntesis de quinoxalinas distintamente funcionalizadas^{175, 176, 177} y en la síntesis de quinoxalinas¹⁷⁸ (**Esquema 5**).



Esquema 5. Síntesis de quinoxalinas a partir de *o*-fenilendiamina y α -hidroxicetonas, a 373 K, catalizada por Basolites.

I.6 Sílices Mesoporosas

El primer material mesoporoso silíceo preparado artificialmente fue descrito en 1969 por Chiola *et al*, aunque las limitaciones técnicas de la época no permitieron la caracterización suficientemente exhaustiva para describirlo por completo¹⁷⁹. No fue hasta 1992 cuando científicos de la Mobil Corporation descubrieron la Mobile Composition of Matter 41 (MCM-41), revolucionaron el campo de la nanoquímica, de gran interés y relevancia hoy en día. El descubrimiento de las sílices mesoporosas resultó un antes y un después en el desarrollo de nuevos nanomateriales con aplicaciones industriales, aumentando exponencialmente el número de investigaciones dedicadas a la síntesis de nuevas estructuras silíceas¹⁸⁰. El uso de estas sílices como catalizadores permitió superar las limitaciones de las zeolitas, materiales principalmente microporosos, que impiden las transformaciones de moléculas voluminosas.

El presente trabajo se centra en el desarrollo de diferentes sílices mesoporosas basadas en la estructura de Santa Barbara Amorphous 15 (SBA-15) y Mesoporous Cellular Foam (MCF).

I.6.1 Santa Barbara Amorphous 15 (SBA-15)

Zhao *et al*¹⁸¹ describieron la obtención de SBA-15 por vez primera en 1998, empleando el copolímero no iónico Pluronic 123 como agente director de la estructura mesoporosa, en medio ácido. El desarrollo de SBA-15 supuso un avance con respecto a su predecesora, MCM-41, ya que mostraba una mayor estabilidad térmica, un mayor grosor de sus paredes y un tamaño de sus canales más grande^{182, 183}.

Las sílices SBA-15 son materiales de estructura hexagonal ordenada, tal y como se observa en sus imágenes de Microscopía Electrónica de Barrido (SEM, *por sus siglas en inglés*) y de Microscopía de Transmisión Electrónica (TEM¹⁸⁴, *por sus siglas en inglés*) (**Figura 22**), con dos sistemas porosos consistentes en poros cilíndricos de diámetro uniforme, interconectados por una red de microporos. El tamaño de los mesoporos oscila entre 3 - 40 nm, con un grosor de pared de 3,1 - 6,4 nm^{185, 186}. Los microporos tienen un diámetro de unos 0,5 - 1,5 nm, y su proliferación está directamente

relacionada con la temperatura de síntesis empleada¹⁸⁷. Su área BET es elevada, con valores comprendidos entre 400 - 900 m²·g.

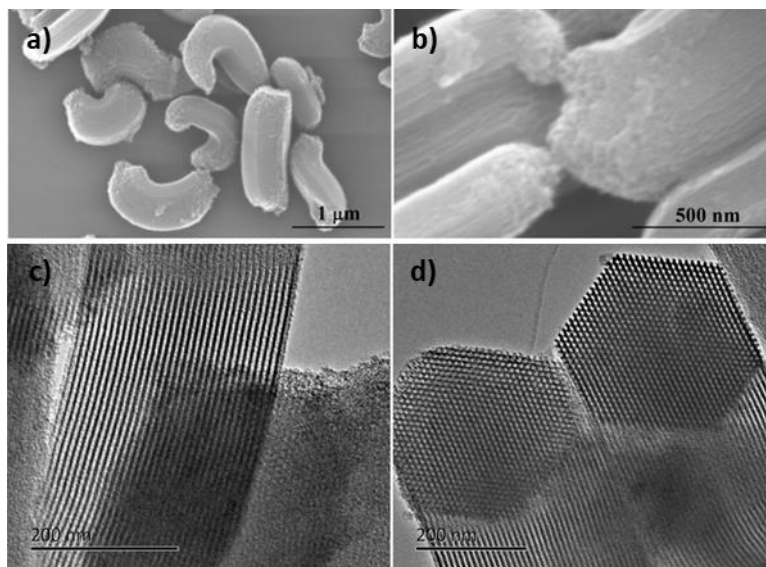


Figura 22. Imágenes SEM (a y b) y TEM (c y d) de SBA-15¹⁸⁸.

El procedimiento de síntesis de la SBA-15 consta de varias etapas diferenciadas¹⁸⁹. En una primera, se prepara una disolución de tetraortoetilsilicato (TEOS) con el surfactante Pluronic 123 ((EO)₂₀(PO)₇₀(EO)₂₀), a pH ácido. De esta forma, el TEOS, precursor silíceo, se hidroliza alrededor de las moléculas del surfactante, que hace de plantilla, generando una red polimérica formada por óxido de silicio. El carácter no iónico del Pluronic 123 le permite interactuar con las especies inorgánicas a través de enlaces de hidrógeno o formando dipolos, tal y como se muestra en la **Figura 23**.

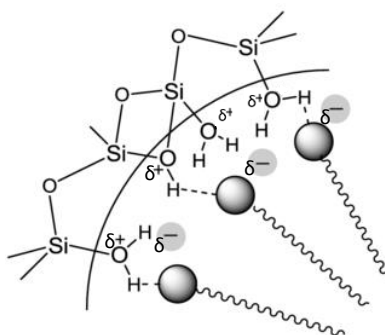


Figura 23. Interacciones precursor-surfactante no iónico en la síntesis de nanoestructuras mesoporosas silíceas¹⁹⁰.

Las condiciones de temperatura y pH son cruciales en la etapa de síntesis, así como las concentraciones de los reactivos empleadas, ya que influirán la morfología del

material final. De esta forma, modificando los parámetros de síntesis se podrán obtener diferentes SBA-15 con porosidad diversa, pero manteniendo su forma característica. Cabe reseñar que el pH ácido es un factor clave, ya que no solo permite la obtención de un tamaño de poro uniforme, sino que a valores de pH mayores de 2 no se forma el gel silíceo. La segunda etapa consiste en el proceso de envejecimiento, en el que el gel obtenido se introduce en un autoclave, a 373 K, en condiciones estáticas, durante 24 h. Durante este proceso, el gel se contrae y aglomera, adquiriendo rigidez. Finalmente, el surfactante se elimina mediante calcinación a 823 K, en atmósfera de aire, durante 5 h, para así obtener el material final¹⁹¹ (**Figura 24**).

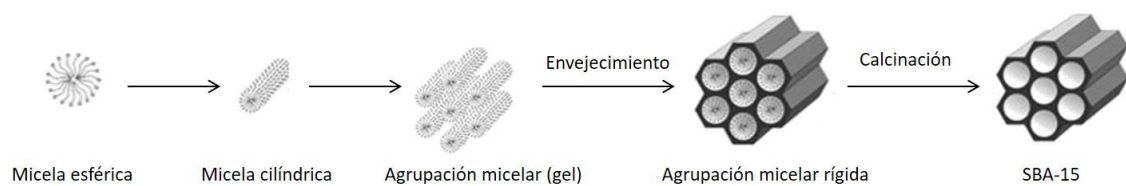


Figura 24. Síntesis de SBA-15.

1.6.2 Mesoporous Cellular Foam (MCF)

Las sílices mesoporosas MCF son materiales de estructura mesocelular ordenada que muestran dos sistemas porosos diferenciados: oquedades esféricas, cuyo tamaño está comprendido entre 24 - 42 nm, las cuales están interconectadas por ventanillas de menor tamaño, entre 9 - 22 nm. Esta porosidad les otorga áreas superficiales especialmente elevadas, alcanzando valores de incluso 1000 m²-g, con paredes gruesas y una distribución homogénea de tamaño de poro^{192, 193}. La morfología de los materiales es de tipo coralino¹⁹⁴ (**Figura 25**).

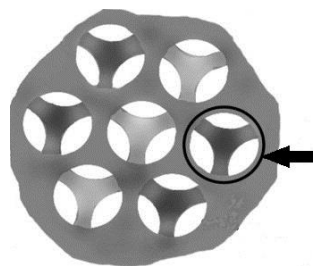


Figura 25. Modelo de estructura coralina de los materiales MCF.

Fueron sintetizados por primera vez en 1999 por Schmidt-Winkel *et al*¹⁹⁵, a raíz del desarrollo de la SBA-15. En general, la síntesis de estos materiales se lleva a cabo en diversas etapas. En primer lugar, se forma una microemulsión del surfactante Pluronic 123 en una disolución de ácido clorhídrico y 1,3,5-trimetilbenceno (TMB). A continuación, se adiciona el TEOS, precursor silíceo, el cual se hidroliza en la superficie de las agrupaciones de TMB/P123, generando etanol. Este etanol se comporta como co-surfactante, de forma que se establece una red polimérica con óxido de silicio como unidad. La relación entre TMB/P123 será el factor determinante en la estructura de MCF. Si esta relación es de 0,2 o menor, la estructura se ordenaría formando de SBA-15. Otros parámetros a tener en cuenta son las concentraciones de ácido clorhídrico y TEOS, ya que una baja concentración de ácido (< 0,8 M) generaría trazas de estructuras tipo SBA-15, incluso a relaciones TMB/P123 = 0,5¹⁹⁴, mientras que una cantidad de TEOS mayor de lo necesario generaría materiales con una distribución de poro más ancha. Con el fin de controlar el tamaño de las ventanillas de interconexión se emplea fluoruro de amonio, manteniendo siempre una relación $\text{NH}_4/\text{Si} = 0,03$ ¹⁹².

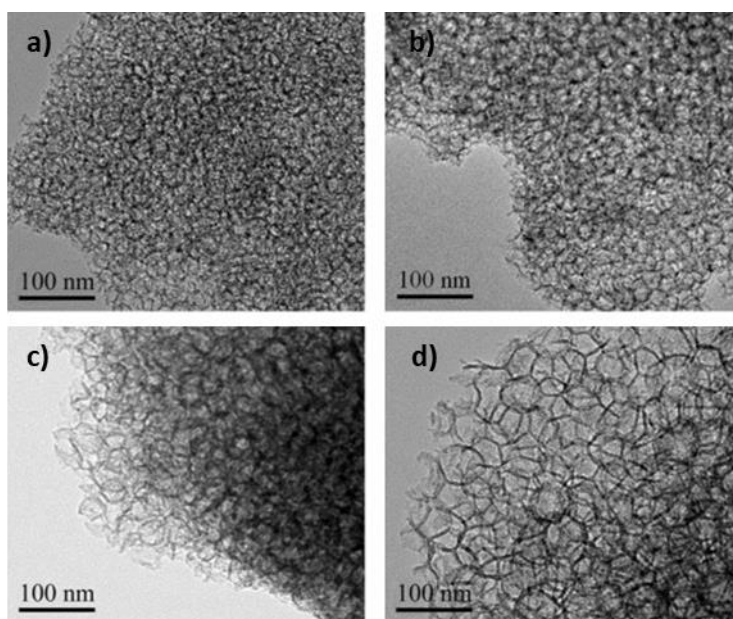


Figura 26. Imágenes TEM de sílices MCF con distintos tamaños medios de poro: a) 6,3 nm, b) 11,5 nm, c) 26,4 nm y d) 42,1 nm).

Una etapa crucial es el proceso de envejecimiento, que se realiza en autoclave, bajo condiciones estáticas y en un rango de temperaturas comprendido entre 373 – 393 K, durante 24 h. En el transcurso de este proceso se produce una aglomeración de las gotas de la microemulsión que generarán los poros del material silíceo. Es una etapa

fundamental, debido a que influirá tanto en el tamaño (**Figura 26**) como la distribución de poros en la estructura final, de forma que cuanto mayor sea la temperatura dentro del rango establecido, mayor será el tamaño y volumen de poros y ventanillas, pero menor su área superficial BET y viceversa.

La última etapa en el proceso de síntesis de MCF es la calcinación, en la que, para la obtención del material final, se retira la plantilla mediante calentamiento a 773 K durante 8h en presencia de aire¹⁹⁶Error! Marcador no definido.

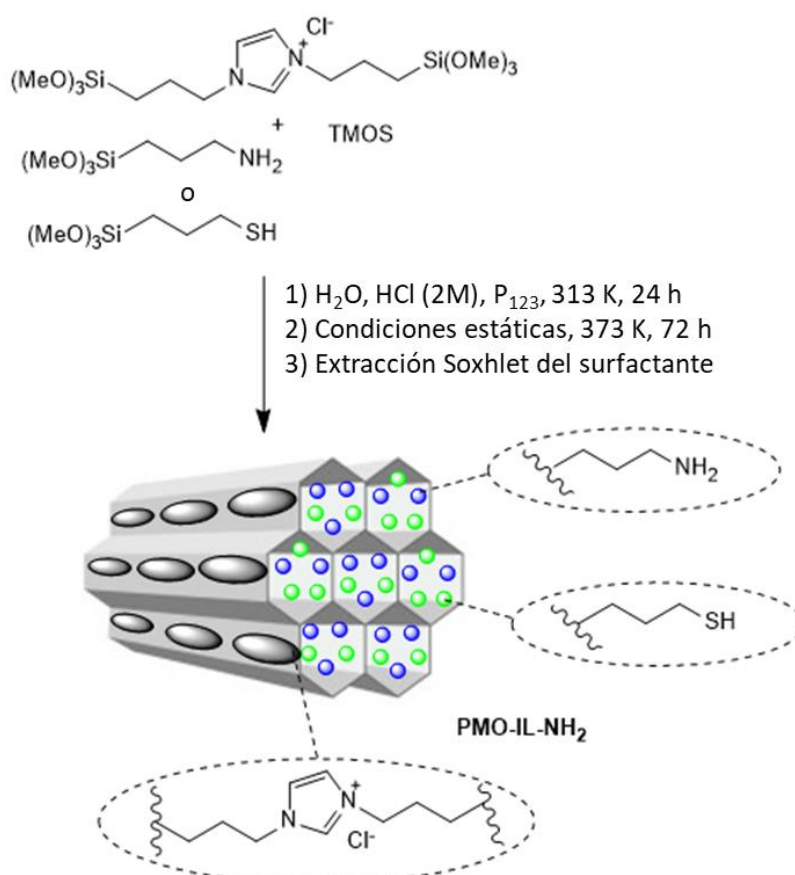
1.6.3 Modificación de los materiales mesoordenados

Las propiedades que presentan las sílices mesoporosas hace de ellas unos materiales útiles y muy versátiles en diversas áreas, entre las que destaca la catálisis. Esto se debe a que poseen una elevada área superficial, además de una gran resistencia térmica. Sin embargo, el carácter ligeramente ácido de las mismas, apenas les confiere actividad catalítica por sí solas. Es por ello por lo que resulta fundamental su funcionalización, ya sea anclando a su superficie compuestos orgánicos o inorgánicos, o variando la composición del material durante el proceso de síntesis. Los dos métodos principales para la síntesis de sílices mesoporosas son:

- a) **síntesis directa (*one-pot synthesis*)**: el procedimiento consta de una única etapa en la que se incorporan los precursores de los sitios activos a la mezcla de reacción durante el proceso de síntesis del material. Aunque esta metodología facilita el procedimiento a nivel técnico y permite la obtención de materiales con una distribución de los centros activos más homogénea sobre su superficie, puede ralentizar o incluso limitar la formación de las estructuras ordenadas¹⁹⁷.
- b) **post-síntesis (*grafting*)**: la presencia de grupos silanoles (Si-OH) en la superficie de los materiales silíceos permite que estos actúen como punto de anclaje de diversos grupos orgánicos. En este procedimiento es necesaria la síntesis previa del soporte silíceo, que será funcionalizado en una o varias etapas posteriores. Si bien esta metodología ofrece como ventaja la obtención de materiales más ordenados, manteniendo las propiedades del soporte prácticamente inalteradas, la posible inserción de los compuestos orgánicos empleados en la funcionalización

dentro de los canales porosos puede producir una oclusión parcial o incluso total de los mismos^{198, 199}.

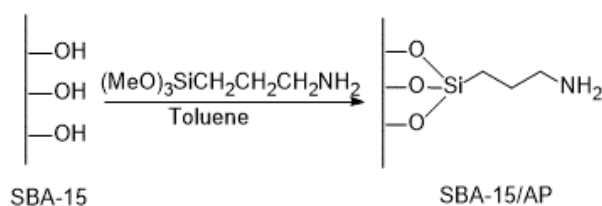
Las fases activas empleadas para la funcionalización de las sílices mesoporosas pueden ser de naturaleza diversa. Entre las más frecuentemente utilizadas se encuentran los átomos metálicos que pueden incorporarse directamente en la mezcla de reacción inicial, de forma que sustituyen las posiciones de los átomos de Si, otorgando un mayor carácter ácido al material, así como propiedades redox. Existen diversos ejemplos de sílices mesoporosas descritas en la literatura, empleando átomos de Al, Nb, Mo o Ti, entre otros. También se pueden encontrar numerosos ejemplos de sílices modificadas con óxidos metálicos, destacando W, Mo y Re, útiles en reacciones de metátesis de olefinas e hidrodesulfuración. El procedimiento habitual es la incorporación del óxido en la superficie de la sílice previamente sintetizada, de forma que el metal se localiza en la interfase, aumentando su accesibilidad con respecto a las sílices dopadas.



Esquema 6. Inserción de grupos funcionales en la estructura de una sílice mesoporosa durante el proceso de síntesis²⁰⁰.

En cuanto al anclaje de compuestos orgánicos y complejos organometálicos, también se pueden encontrar numerosos estudios al respecto en la literatura. El procedimiento de inmovilización en estos casos también se puede llevar a cabo durante la síntesis de la propia sílice, mediante la adición de un organosilano funcional, produciendo entonces el proceso de co-condensación, de forma que el organosilano se incorpora a la red cristalina de la sílice (**Esquema 6**).

Una alternativa a esta metodología es la inclusión de los organosilanos durante el proceso de síntesis, pero en su última etapa previa al calcinado, para la eliminación del surfactante. De esta forma, se produce un desplazamiento del tensoactivo por el organosilano, dando lugar a la sílice funcionalizada. Si la funcionalización se realiza sobre la sílice ya sintetizada, en un proceso de **grafting** (**Esquema 7**), la ausencia o presencia de agua interfacial delimita que los organosilanos se unan exclusivamente en los lugares disponibles, o que estos sean hidrolizados y puedan sufrir reacciones de autoensamblaje, cubriendo gran parte de la superficie de la sílice.



Esquema 7. Anclaje de grupos funcionales en la superficie de una SBA-15 mediante una metodología post-sintética¹⁰⁸.

1.6.4 Aplicaciones de las sílices mesoporosas

Las propiedades de las sílices mesoporosas permiten su aplicación en diversos campos de investigación, entre los que se pueden destacar la adsorción de contaminantes, su uso en biomedicina y su aplicación en catálisis. En este contexto, se han desarrollado numerosos nanomateriales útiles en la adsorción de gases contaminantes como, por ejemplo, CO₂, compuestos orgánicos volátiles e incluso para la descontaminación de agua. Así, las sílices mesoporosas funcionalizadas con grupos amino, han demostrado su eficacia en la adsorción de CO₂^{201, 202, 203, 204, 205}. Sin embargo, no solo el CO₂ genera un importante impacto medioambiental, si no que existen otros gases con compuestos

orgánicos volátiles (VOCs, *por sus siglas en inglés*) que suponen un peligro para la salud del ser humano. En este sentido, diversos autores han demostrado la eficacia de las sílices mesoporosas en la eliminación de hidrocarburos contaminantes^{206, 207}.

Tanto SBA-15 como MCM-41 modificadas con grupos tiol y amino²⁰⁸ se han descrito también en la eliminación de iones de metales pesados, altamente contaminantes y tóxicos para el ser humano, además de en procesos de descontaminación y purificación de aguas.

Por otra parte, las sílices mesoporosas se han estudiado en procesos de liberación controlada de fármacos. La elevada porosidad y área superficial de estos materiales facilitan el transporte de principios activos insolubles en agua, a través de la conversión de la forma cristalina en la fase amorfa del fármaco^{209, 210}. El primer estudio al respecto fue la utilización de la MCM-41 en el transporte de ibuprofeno²¹¹. Posteriormente se describió la utilización de SBA-15 modificada para el transporte de cefalexina, un antibiótico del grupo de las cefalosporinas utilizado para tratar infecciones bacterianas del tracto respiratorio²¹²; o la MCM-41 modificada para el transporte de sulfadiazina, que es un tipo de sulfonamida empleada como antibacteriana para la prevención de infecciones en quemaduras de segundo y tercer grado²¹³. Entre los grandes desafíos en biomedicina, a los que la investigación con sílices mesoporosas puede dar respuesta, destacan el desarrollo de sistemas que permitan monitorizar los efectos terapéuticos de fármacos anticancerígenos²¹⁴ o la ingeniería de tejidos en la reparación ósea²¹⁵.

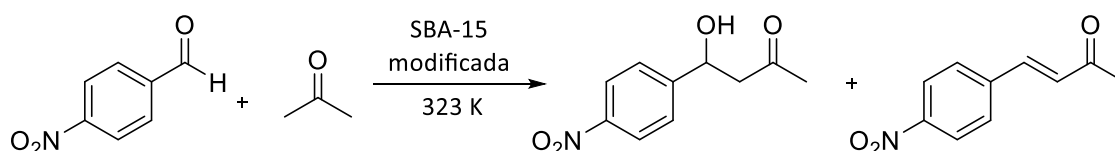
1.6.4.1 Aplicaciones de las sílices mesoporosas en catálisis

Las sílices mesoporosas se han convertido en uno de los materiales más investigados y utilizados en el diseño de catalizadores heterogéneos. Su elevada área superficial, así como el tamaño y distribución de sus poros, las convierten en materiales idóneos para permitir la transformación de sustratos de volumen considerable^{216, 217, 218}.

El uso de sílices mesoordenadas con fines catalíticos ofrece la posibilidad de que la multifuncionalización superficial permita la síntesis de una gran diversidad molecular. Además, estos nanomateriales utilizados como soportes de fases activas proporcionan un alto rendimiento catalítico y una acentuada selectividad, debido principalmente al

aumento de la superficie de contacto que contribuye a los rendimientos globales de los productos deseados²¹⁹. Entre las distintas aplicaciones industriales de estos catalizadores destaca la refinación de petróleo, incluyendo todos los procesos químicos que conlleva, su utilización en la producción de productos petroquímicos²²⁰, o su aplicación en la obtención de numerosos productos de QF²⁰⁰.

El carácter habitualmente ácido de las sílices —ya sea por funcionalización con grupos $-SO_3H$ o por dopaje con metales de transición, óxidos metálicos o heteropoliácidos— las convierte en catalizadores activos en la síntesis de heterociclos de gran complejidad estructural. Nuestro grupo posee amplia experiencia en la aplicación de sílices mesoporosas, con distintas propiedades ácido-base como catalizadores heterogéneos en gran variedad de transformaciones orgánicas y, particularmente, en la síntesis de productos de QF (**Esquema 8**)^{58, 109, 221, 222, 223}.



Esquema 8. Reacción de Henry entre *p*-nitrobenzaldehído y acetona catalizada por SBA-15 modificada con grupos funcionales ácidos y amino.

Así, se han descrito diferentes sílices mesoporosas del tipo SBA-15, MCM-41 o MCF funcionalizadas, dopadas o no con metales —Al, Nb, Ta—, en la condensación de Knoevenagel²²⁴, reacciones de isomerización (safrol²²⁵ y eugenol²²⁶) y acetalización. Son de gran relevancia los ejemplos de sílices mesoporosas de carácter básico descritas en la reacción Friedländer. Tal es el caso de la reacción entre 2-amino aril cetonas²²⁷ y compuestos 1,3-dicarbonílicos catalizados por sílices mesoporosas MCM-41 con grupos amino²²⁸. Recientemente nuestro grupo ha publicado una revisión en la que se pone de manifiesto la utilidad de este tipo de materiales como nanocatalizadores activos en reacciones de formación de enlaces C-C y C-heteroátomo, en cascada, implicadas en la síntesis de sistemas heterocíclicos biológicamente activos²²⁹.

I.7 Química Computacional

La Química Computacional surge en paralelo a la Química teórica, como una evolución de la misma, tratando de darle soporte técnico mediante el uso de software y la introducción de aproximaciones, para así dar respuesta a las complejas ecuaciones matemáticas que definen las reacciones químicas. El objetivo principal de la Química Computacional es, por tanto, predecir las propiedades moleculares de los sistemas químicos. El desarrollo y aplicación de esta tecnología ha permitido el avance en la investigación de las propiedades y comportamientos moleculares, ya sean estructurales, energéticos o electrónicos, entre las que se incluyen las siguientes:

- *Geometría molecular*, cuyo objetivo es predecir distancias y ángulos de enlace, permitiendo caracterizar la estructura de distintas moléculas y macromoléculas.
- *Energía de las distintas especies químicas*, como son los intermedios de reacción, estados de transición o estados excitados.
- *Propiedades termodinámicas*.
- *Reactividad química*, cuantificada como índices de reactividad mediante la determinación de la geometría y estabilidad relativa de los intermedios o estados de transición involucrados en las distintas etapas de una reacción, permitiendo así caracterizar mecanismos de reacción.
- *Propiedades espectroscópicas, eléctricas y magnéticas*.
- *Propiedades físicas de las fases condensadas y materiales*.

I.7.1 Superficie de Energía Potencial (SEP)

La *Superficie de Potencial (SEP)* de una reacción se define como la expresión de la energía respecto a una o varias variables posicionales, expresadas en este caso de forma continua como una superficie, es decir, la envoltura de las fuerzas de interacción entre átomos de una molécula.

Los métodos de cálculo computacional se fundamentan en la determinación de las SEP de las moléculas, para así obtener la variación de la energía potencial total del sistema en función de las coordenadas de posición de los núcleos que lo forman. De esta forma, la SEP proporciona información estructural y química de las moléculas

implicadas, como pueden ser el gradiente de energía $g(E)$, que es la variación de la energía potencial del sistema respecto a las coordenadas nucleares del sistema, o la matriz hessiana H , que se obtiene a partir de la segunda derivada de la energía con respecto a las coordenadas internas. Existen diferencias entre los métodos computacionales para calcular las SEP y, por lo tanto, las propiedades moleculares del sistema a estudiar²³⁰. La representación gráfica de una SEP en un modelo multiatómico resulta casi imposible, ya que sería necesaria una superficie multidimensional que se vería incrementada con el número de variables independientes, en este caso las tres dimensiones de cada átomo participante en la reacción. Para solventar este problema, generalmente se estudian tan solo dos variables independientes por átomo. De todos los puntos que constituyen la SEP, existen ciertos puntos críticos que proporcionan información especialmente relevante, que se denominan puntos estacionarios. Entre ellos están:

- *Mínimo global*: se define como el estado energético más bajo que indica la conformación más estable. Por tanto, solo existe un mínimo global por molécula.
- *Mínimo local*: cualquier mínimo energético distinto al anterior, de forma que cualquier variación geométrica independientemente de la dirección, proporcionará una geometría de mayor energía. Su gradiente es nulo y un cálculo de la segunda derivada en las coordenadas nucleares, proporcionará en todos los casos resultados positivos.
- *Punto de silla*: punto de transición entre dos mínimos de energía. Un punto de silla de orden 1 correspondería a un estado de transición (TS, *por sus siglas en inglés*), a partir del cual existiría un incremento energético en todas las direcciones de la SEP excepto una. Si se realiza un cálculo de la segunda derivada en las coordenadas nucleares de dicho punto, se observa cómo son todas positivas excepto una, la cual se asocia a la coordenada de reacción.

1.7.2 Métodos de cálculo

La clasificación de los diversos métodos de cálculo empleados en Química Computacional establece dos grandes bloques, en función del nivel de aproximación en

la resolución de la ecuación de Schrödinger: i) los métodos de mecánica molecular y ii) los de mecánica cuántica. A su vez, estos métodos se clasifican en métodos *ab initio*, métodos semiempíricos (SE) y métodos basados en la Teoría del Funcional de Densidad (DFT, *por sus siglas en inglés*). Todos ellos presentan ventajas e inconvenientes, con lo que la elección de uno u otro, a la hora de afrontar un cálculo, dependerá de diversas variables, tales como el sistema que se desee analizar, los recursos informáticos y equipos de los que se disponga y la exactitud requerida en el estudio a realizar. En la **Tabla 3** se representan los distintos métodos y sus características²³¹.

Tabla 3. Métodos utilizados en Química Computacional

Método	Fundamento	Aplicación	Ventajas	Inconvenientes
Mecánica Molecular	Potenciales Interacción	1-10 ⁵ átomos	Gran rapidez	Aplicabilidad limitada
Ab Initio	Ecuación Schrödinger y Función de Onda	1-10 ² átomos. Todas las propiedades	Exactitud y precisión controlable	Lento y complicado de utilizar
Semiempírico	Ecuación Schrödinger y Función de Onda o T. Khon-Sham y densidad electrónica	1-10 ⁴ átomos. Todas las propiedades	Rápido, fácil de usar, fiables en moléculas orgánicas	Errores no sistemáticos, escasa fiabilidad en moléculas con metales
DFT	T. Khon-Sham y densidad electrónica	1-10 ³ átomos. Todas las propiedades	Más rápido que ab initio	Exceso de métodos DFT disponibles. Sin pautas de mejora

I.7.2.1 Métodos de Mecánica Molecular (MM)

Se trata de métodos fundamentados en las leyes de la mecánica clásica, de forma que consideran a la molécula exclusivamente como un núcleo, sin tener en cuenta los electrones y sus interacciones. El modelado matemático se basa, por tanto, en la representación de los diversos átomos como un conjunto de esferas de radios diferentes y con cargas parciales, manteniéndose unidas mediante enlaces elásticos. De esta forma, la energía molecular queda definida como un sumatorio de las distintas vibraciones de tensión (E_r), flexión (E_θ) y torsión (E_ω), así como de interacciones electrostáticas (E_{Coul}) y fuerzas de van der Waals (E_{vdw}) (**Ecuación 7**).

$$E = E_r + E_\theta + E_\omega + E_{Coul} + E_{vdw} \quad (7)$$

La calidad de los parámetros empleados influirá directamente en la calidad de los resultados, ya que todos los términos del sumatorio están basados en parámetros empíricos. Las funciones de energía potencial empleadas, así como la parametrización en la evaluación de los diversos métodos de MM, generan lo que se denomina *campo de fuerza*. Generalmente, los métodos MM se limitan a la obtención de la geometría molecular en equilibrio, no aportando información sobre la distribución electrónica molecular. Los campos de fuerza más utilizados actualmente se han desarrollado empleando cálculos cuánticos de alto nivel y ajustándose a los valores experimentales²³².

I.7.2.2 Métodos de Mecánica Cuántica (MC)

Este tipo de métodos fundamentan la descripción de los modelos moleculares en función de las interacciones explícitas entre núcleos y electrones. De esta forma, el comportamiento de un sistema para una sola molécula está descrito por una función de onda Ψ , que incluye todas las coordenadas tanto de electrones (r) como de núcleos (R). El estudio de las propiedades de un sistema poliatómico en el estado estacionario es la solución de la ecuación de Schrödinger independiente del tiempo. En dicha ecuación aparece también H , que es el operador Hamiltoniano, asociado a la energía del sistema de electrones y núcleos, y que contiene términos de movimiento y de atracción y repulsión entre las partículas que constituyen el sistema. El término restante E es el correspondiente a la energía total del sistema en el estado estacionario (**Ecuación 8**).

$$\hat{H}(R, r) \cdot \Psi(R, r) = E(R, r) \cdot \Psi(R, r) \quad (8)$$

La resolución analítica de esta ecuación solo es posible para sistemas sencillos, por lo que su traslado a sistemas complejos requiere de la introducción de diversas aproximaciones. La aproximación de Born-Oppenheimer o aproximación adiabática supone que la diferencia másica entre núcleos y electrones es de, cuanto menos, 10^3 , con lo que la diferencia en la velocidad de movimiento será del mismo orden. De esta forma, matemáticamente es posible separar el hamiltoniano como sumatorio de dos términos, uno nuclear y otro electrónico, ya que el movimiento electrónico está limitado por una geometría nuclear definida (**Ecuación 9**).

$$H = \sum_{i=1}^N \left[-\frac{1}{2} \nabla_i^2 + \sum_{A=1}^M -\frac{Z_A}{r_{iA}} \right] + \sum_{i=1}^N \sum_{j>1}^N \frac{1}{r_{ij}} \quad (9)$$

donde N corresponde al número de electrones del sistema, Z se define como la carga nuclear, M es el campo de cargas nucleares e i, j son los electrones correspondientes a cada capa del sistema.

El primer término del sumatorio se corresponde con la energía cinética de un electrón, mientras que los siguientes definen las interacciones interatómicas: i) el potencial de atracción entre un electrón y un núcleo y ii) la interacción entre dos electrones. Por tanto, la energía total del sistema (E), queda definida como la suma de la energía electrónica, E_e , con la constante de repulsión electrónica dependiente de la geometría del sistema (**Ecuación 10**).

$$E = E_e + \sum_{A=1}^M \sum_{B>A}^M \frac{Z_A Z_B}{R_{AB}} \quad (10)$$

Será, por tanto, el nivel de aproximación matemático-empírico en la resolución de la ecuación de Schrödinger el que delimite las diferencias entre los distintos métodos de cálculo:

1.7.2.3 Métodos ab initio

Son métodos que se basan en la resolución aproximada de la ecuación de Schrödinger exclusivamente con métodos teóricos, empleando como información empírica únicamente los datos definidos para las constantes físicas fundamentales, para así obtener la energía y función de onda electrónicas del sistema en evaluación²³².

El método de cálculo *ab initio* más ampliamente extendido es la teoría de Hartree-Fock (HF), que se fundamenta en que el movimiento de cada electrón es independiente del resto, estableciendo el efecto del potencial como un promedio generado por los restantes electrones. La función de onda Ψ queda expresada en forma de un determinante de Slater, con lo que la aplicación de esta aproximación permite la construcción del operador monoeléctrico F (**Ecuación 11**).

$$F = \sum_{i=1}^N \left[-\frac{1}{2} \nabla_i^2 + \sum_{A=1}^M -\frac{Z_A}{r_{iA}} \right] + \sum_{j=1}^N (J_i - K_i) \quad (11)$$

La solución de dicha ecuación permitirá la obtención del conjunto de orbitales ortonormales χ_i que establezcan la energía mínima del sistema en estado estacionario (**Ecuación 12**).

$$F\chi_i = \varepsilon_i\chi_i \quad (12)$$

Para la obtención del conjunto de funciones monoeléctricas que proporcionen la función de onda más adecuada se recurre al principio variacional, según el que cualquier función correctamente definida para un sistema proporciona un valor de energía mayor o igual al valor exacto del estado fundamental. La aplicación de este principio da lugar a las ecuaciones de HF, donde aparecen los términos correspondientes a los operadores coulombianos —expresan los potenciales de interacción de un electrón con la nube electrónica promedio, generada por los restantes electrones— y de intercambio, J y K —expresan la energía de intercambio electrónico que se genera por el carácter asimétrico de la función de onda—. La resolución de las ecuaciones HF se efectúa mediante la aplicación del método del campo autoconsistente (SCF, *por sus siglas en inglés*), que es un método iterativo en el que se selecciona un conjunto de valores de χ_i de partida con los que se calcula ε_i . Estos valores se van modificando hasta que este ε_i alcanza su valor mínimo.

El método HF tiene una limitación importante en el cálculo de la energía con exactitud, debido a que la repulsión electrónica puntual se simplifica con la utilización de la repulsión promedio, que constituye una aproximación poco precisa. A esta diferencia entre energía exacta y promedio se le denomina energía de correlación. El cálculo de esta energía de correlación ha propiciado el desarrollo de diversos métodos post HF, tales como el método “Configuration Interactions” (CI) —que expresa la función de onda como un conjunto de determinantes²³³—, el método Moller-Plesset (MP n) —que utiliza como función de onda sin perturbar la función de HF²³⁴—, o más recientemente el método de “Coupled-Cluster” (CC)²³⁵, que posteriormente evolucionó al método “Coupled Cluster Single-Double” (CCSD). Estos métodos, de forma más o menos exhaustiva, han permitido describir la correlación electrónica de forma bastante

adecuada, pudiendo así predecir las propiedades moleculares con bastante exactitud, ya que la utilización de métodos *ab initio* más exactos derivaría en requerimientos de hardware de altas prestaciones y un mayor consumo de tiempo de cálculo.

1.7.2.4 Métodos semiempíricos (SE)

Se trata de métodos químico-cuánticos que emplean tanto valores teóricos como experimentales para el cálculo de los valores de energía y orbitales moleculares. Esto se realiza mediante el reemplazo de los valores esperados de la función de onda por formas paramétricas ajustadas estadísticamente mediante la obtención de grandes volúmenes de datos experimentales —geometrías moleculares y calores de formación— además de datos teóricos proporcionados por otros métodos, ya sean *ab initio* o DFT²³⁶.

Aunque la velocidad de cálculo es mucho mayor debido al uso de estos valores, la fiabilidad en moléculas poco representativas o con propiedades moleculares no tenidas en cuenta durante la parametrización, disminuye abruptamente. Es, por tanto, una metodología especialmente ligada a la experiencia previa y que requiere de confirmación mediante otros métodos de mayor exactitud.

El método más ampliamente conocido y utilizado es el PM6, que consiste en una aplicación semi empírica del método HF y muestra una gran fiabilidad en la predicción de geometrías y entalpías de reacción de compuestos orgánicos.

1.7.2.5 Métodos de la Teoría del Funcional de la Densidad (DFT)

La DFT fue desarrollada por los profesores Pierre C. Hohenberg y Walter Kohn en 1964²³⁷. Actualmente son los métodos más ampliamente utilizados en Química Computacional²³⁸. Tratan de dar solución a la ecuación de Schrödinger considerando la energía de correlación de manera alternativa, pero sin que suponga un coste computacional especialmente elevado. Para ello, definen la energía del estado fundamental de un sistema electrónico sustituyendo la función de onda polieletrónica Ψ por una magnitud observable, la densidad electrónica ρ . Esto se traduce, matemáticamente, en que la energía electrónica del sistema se convierte en función de la densidad $E[\rho(r)]$, conduciendo a las ecuaciones Kohn-Sham (KS)²³⁹. Estas ecuaciones guardan gran similitud con las HF ya que la densidad electrónica se expresa a partir de

orbitales moleculares, quedando la energía electrónica en el estado fundamental, E , definida como el sumatorio de la energía cinética (E_T), la energía de interacción electrón-núcleo (E_V), la energía de Coulomb (E_{Coul}) y la energía de correlación-intercambio (E_{XC}). Así, todos los términos dependen de la densidad electrónica, con excepción de la E_T (**Ecuación 13**).

$$E = E_T + E_V + E_{Coul} + E_{XC} \quad (13)$$

Por tanto, la aplicación de la teoría DFT permite calcular tanto la suma de energías de intercambio como de correlación de un gas de electrones uniforme, simplemente conociendo su densidad.

En los últimos años se han desarrollado numerosos métodos DFT, fundamentalmente debido a que la forma analítica del funcional de correlación de intercambio $Exc[\rho]$ es desconocida, por lo que pueden existir tantos funcionales DFT como aproximaciones propuestas. Esto ha generado que muchos de los métodos DFT se aproximen a un enfoque más cercano a la metodología semi empírica, ya que los funcionales correspondientes contienen parámetros ajustados a datos experimentales.

Los métodos DFT se pueden clasificar en función de la sofisticación y desarrollo de los mismos, atendiendo a las variables de las que depende (**Tabla 4**).

Tabla 4. Clasificación de métodos en función de la variable de la que depende y ejemplos de funcionales de cada categoría.

Método	Variable de la que depende	Aplicación
LDA	ρ	VWM
GGA	ρ, ∇	HCTH, PBEPBE, BPW91, BLYP, OLYP, mPWPW91, mPWPBE, mPWLYP
Híbridos	$\rho, \nabla\rho + HF$	TPSSH, HCTHhyb, mPW1LYP, mPW1PW91, mPW3PBE, O3LYP, B1B95, B1B95, B3PW91, PBE1KCIS, PBEh1PBE, X3LYP, B3LYP
Meta-GGA	$\rho, \nabla\rho, \tau$	M06L, VSXC, TPSS, τ -HCTH, BB95, PBEKCIS, N12, MN12L
Dispersión corregida	$\rho, \nabla\rho, \tau + HF$	M06, xB97, cam-B3LYP, LC-xPBE, LC-BLYP, B2PLYP, M11, N12SX, MN12SX

ρ = densidad; $\nabla\rho$ = gradiente de densidad; τ =energía cinética; HF=intercambio Hartree-Fock

Sin embargo, el uso de estos métodos no está exento de inconvenientes, como pueden ser las dificultades a la hora de determinar cuál es el funcional óptimo para analizar cada sistema. Además, muchos funcionales presentan errores sistemáticos, como puede ser la no consideración de la energía de dispersión, que resultaría fundamental en el análisis de determinados sistemas. Por último, a diferencia de los métodos *ab initio*, no permiten el refinamiento sistemático de resultados. Todo ello conlleva que, una vez más, la experiencia acumulada y el contraste con resultados experimentales o métodos *ab initio* resulte crucial en la determinación del funcional DFT que más se adecúe a las necesidades en cada caso.

Actualmente, el funcional híbrido B3LYP es el de uso más extendido, ya que su exactitud y rendimiento son adecuados en la gran mayoría de cálculos.

1.7.3 Conjunto de funciones de base

La elección adecuada de un conjunto de funciones de base es un elemento crucial en los métodos mecanocuánticos moleculares, ya que los orbitales moleculares se expresan como combinación lineal de estas funciones. Resulta imposible la utilización de un conjunto infinito de funciones de base, lo que permitiría la obtención de la solución exacta dentro del procedimiento de cálculo seleccionado, por lo que es necesario, a nivel práctico, la elección de un conjunto finito de funciones de base normalizadas. Dos aspectos que deben valorarse en su elección son tanto el tipo de funciones elegidas como su número²⁴⁰.

En los siguientes apartados se comentan brevemente los principales tipos de funciones de base que se utilizan:

1.7.3.1 Orbitales de Slater (STO, por sus siglas en inglés)

Estas funciones se definen por la **Ecuación 14**:

$$X_{nlm} = N_{\zeta} r^{n-1} e^{-\zeta r} Y_l^m \quad (14)$$

donde ζ = constante relacionada con la carga efectiva nuclear, determinable variacionalmente; N_{ζ} = constante de normalización; r = radio del orbital; Y = armónico

esférico; n = número cuántico principal efectivo; l = número cuántico azimutal; m = número cuántico magnético.

La dependencia exponencial con la distancia se asemeja a un orbital hidrogenoide, de forma que, cuando $\zeta = 1$, coincide con los orbitales hidrogenoides 1s, 2p y 3d. Es por este motivo que fueron las primeras funciones utilizadas en el desarrollo de los orbitales atómicos. Este tipo de orbitales permiten cálculos precisos de sistemas atómicos y diatómicos empleando métodos semiempíricos. Sin embargo, presentan el inconveniente de que no permiten la resolución analítica y rápida de las integrales bielectrónicas, debido al elevado coste computacional. Además, el término polinomial en r supone que los orbitales no son ortogonales, ya que no presenta nodos en la función de distribución radial.

1.7.3.2 Orbitales Gaussianos (GTO, por sus siglas en inglés)

Estas funciones están definidas por la **Ecuación 11**:

$$X_{nlm} = N_{\zeta} r^{n-1} e^{-\zeta r^2} Y_l^m \quad (11)$$

cuyos términos son idénticos a los de los orbitales de Slater, con la única diferencia de la modificación en el término exponencial, en este caso elevado al cuadrado, lo que constituye una ventaja de los GTO frente a los STO. Esto se debe a que el producto de dos gaussianas es una gaussiana centrada en las dos anteriores, de forma que sus integrales son igualmente gaussianas, permitiendo una resolución analítica. Sin embargo, el problema de este tipo de orbitales es que todas las gaussianas presentan una pendiente cero en el núcleo, lo cual es físicamente incorrecto, ya que cualquier orbital diverge en esa posición. Una solución a este problema es la utilización de gaussianas de corto rango para simular un comportamiento divergente en el núcleo.

Las funciones de base se pueden clasificar en función de la complejidad del conjunto de funciones descritas por los orbitales atómicos. Esta clasificación fue descrita por el profesor John A. Pople^{241, 242}:

- **Conjunto de funciones de base mínima**

En este tipo de conjuntos se utiliza una única función de base por cada orbital atómico ocupado en el estado fundamental del átomo correspondiente, empleando de esta forma el número mínimo de funciones de base necesarias por átomo. Sin embargo, este tipo de funciones no genera resultados del todo satisfactorios, lo que suele requerir del uso de bases con un mayor número de funciones. Para ello se puede tanto aumentar el número de funciones que representan los orbitales de las capas ocupadas como utilizar funciones que incluyan el número cuántico azimutal.

Un ejemplo de este tipo de conjuntos de base es la STO-3G, donde STO se aproxima mediante un Orbital Gaussiano Contraído (CGTO, *por sus siglas en inglés*) de 3 gaussianas.

- **Conjunto de bases extendidas**

Dentro de este tipo de conjuntos podemos encontrar dos tipos:

- a) *Conjuntos de base doble ζ , triple ζ , cuádruple ζ , ..., n-tuple ζ .* En estos conjuntos se aumenta el tamaño de la base mediante el remplazo de cada función del conjunto mínimo por n funciones.
- b) *Conjuntos de base de valencia desdoblada o Split-valence.* En estos conjuntos cada orbital atómico queda definido por n funciones de base, tal y como se ha descrito en el apartado anterior, mientras que cada orbital interno se define por una única función de base.

Un ejemplo de este tipo de conjuntos sería la base 6-31G, en el que el orbital interno se representa mediante una función de 6 gaussianas y los orbitales de valencia por dos funciones —una de 3 gaussianas y otra de 1 gaussiana—. Otra base característica es la 6-311G, en la que el orbital interno se representa mediante una función de 6 gaussianas y los orbitales de valencia por tres funciones —una de 3 gaussianas y otras dos de 1 gaussiana cada una de ellas—. La gran ventaja de los conjuntos de bases de valencia extendidos es que ofrecen una mejor descripción de las propiedades moleculares del sistema. Sin embargo, su problema radica en que no permiten una descripción completamente exacta de las energías moleculares relativas,

lo que hace que no sean adecuadas para su utilización en métodos multiconfiguracionales.

- **Conjunto de funciones polarizadas**

Para subsanar las limitaciones de los conjuntos de base extendidas se recurre, además, al uso de funciones de polarización, que son funciones con el mismo número cuántico principal pero correspondientes a un momento angular superior, de forma que permiten describir correctamente los cambios de densidad electrónica de un átomo en su entorno molecular.

Las funciones de polarización suelen estar descritas mediante una única gaussiana, como en el caso de la 6-31G(d) o 6-31G*, que es similar a 6-31G pero añadiendo un conjunto de funciones tipo *d* para los átomos del segundo periodo. La inclusión de funciones adicionales de polarización mejora el cálculo de las propiedades moleculares, ya que el conjunto añadido de gaussianas de segundo orden equivale a un conjunto de cinco funciones *d* puras.

Otro ejemplo es la base 6-31G(d,p) o 6-31G**, que añade, además del conjunto de funciones tipo *d* para los átomos de segundo periodo, un conjunto de orbitales *p* para los hidrógenos. De esta forma se contempla un momento angular mayor del requerido para la descripción del átomo, permitiendo modificar la forma del orbital.

- **Conjunto de funciones difusas**

Son funciones con los mismos números cuánticos *s* y *p* que las funciones de la capa de valencias, pero con una mayor extensión espacial. Es decir, son funciones gaussianas de exponente pequeño. Resultan especialmente importantes en sistemas en los que la distribución electrónica se encuentra expandida, como en el caso de los aniones.

Ejemplos de conjuntos de funciones difusa son las bases 6-31+G(d,p) o 6-31+G** —que añade funciones difusas a los átomos pesados— o 6-31++G(d,p) o 6-31++G** —similar a la base 6,31+G** pero añadiendo una función difusa a los átomos de hidrógeno²⁴³.

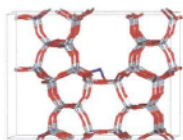
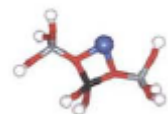
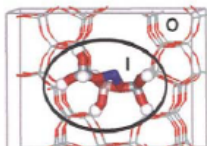
El principal problema que presentan todos estos conjuntos de funciones es que todos sus exponentes y coeficientes de contracción de bases se optimizaron sin

contemplar los efectos de la correlación electrónica. Esto resulta contradictorio con el hecho de que estas funciones se utilizan habitualmente en cálculos post Hartree-Fock, en los que sí entran en juego los efectos de la correlación electrónica. Es por ello que Dunning *et al* desarrollaron conjuntos tales como CC-pVDC, CC-pVTZ, CC-pVQZ, CC-pV5Z o CC-pV6Z, de alto momento angular que subsanan esta problemática^{244, 245}.

1.7.4 Aproximaciones teóricas al estudio con sólidos

Existen tres tipos de modelos que se aplican en la descripción teórica de sólidos: i) el método de condiciones periódicas de contorno o PBC, ii) el método de aproximación al modelo del clúster y iii) el método de aproximación al modelo del clúster embebido, que es un modelo combinado de los dos anteriores²⁴⁶. Todos ellos presentan una serie de ventajas e inconvenientes que propician su aplicación en determinados casos. A modo de resumen, en la **Tabla 5** se comparan los tres modelos en el estudio de zeolitas.

Tabla 5. Métodos habitualmente empleados en el estudio teórico de sólidos (zeolitas tipo ferrierita)²⁴⁶.

Modelo	Ventajas	Inconvenientes
<p>Periódico</p> 	<ul style="list-style-type: none"> · Todos los átomos se tratan al mismo nivel teórico. · Condiciones de contorno periódicas apenas afectan a la función de onda. · Optimización completa de la geometría. · Interacciones de largo alcance implícitamente incluidas. 	<ul style="list-style-type: none"> · Computacionalmente exigente para sistemas con celdas unitarias de gran tamaño o de gran número de átomos.
<p>Conjuntos de bases centradas en el átomo</p>	<ul style="list-style-type: none"> · Comparación directa con clústeres modelo de estudio. 	<ul style="list-style-type: none"> · Alto coste computacional.
<p>Conjuntos de bases de onda plana</p>	<ul style="list-style-type: none"> · Eficiencia computacional. 	<ul style="list-style-type: none"> · El uso de funcionales híbridos resulta prohibitivo a nivel computacional.
<p>Clúster</p> 	<ul style="list-style-type: none"> · Clústeres de tamaño pequeño permiten el uso de métodos HF fiables. 	<ul style="list-style-type: none"> · Condiciones de contorno problemáticas: efectos sobre geometría y función de onda.
<p>Híbrido</p>  <p>I: región interna O: región externa</p>	<ul style="list-style-type: none"> · Optimización completa de la geometría. · Descripción correcta de la relajación de la red. · Interacciones de largo alcance incluidas. · Posibilidad de uso de métodos HF. 	<ul style="list-style-type: none"> · Efectos de los enlaces de los clústeres sobre la función de onda.

I.7.4.1 Condiciones Periódicas de Contorno (PBC, por sus siglas en inglés)

El modelo de PBC es un procedimiento riguroso y coherente en el caso de materiales cristalinos. Se basa en forzar dichas condiciones y resolver la correspondiente ecuación de Schrödinger. Para ello, inicialmente se debe definir una celda unidad, lo que resulta un proceso simple en materiales cristalinos puros, como el α -cuarzo, que es la forma estructural más estable del cuarzo, hasta temperaturas de 846 K, pudiendo obtenerse la celda unidad de este tipo de cristales mediante Difracción de Rayos-X (XRD, *por sus siglas en inglés*) o estudios de difracción de neutrones. Las posiciones atómicas de esta celda se relacionan entre sí por elementos de simetría definidos por el grupo espacial cristalográfico. De esta forma se reduce, en gran medida, el coste computacional, ya que se evita el cálculo sistemático de los distintos componentes de energía total de la celda unidad, que ya estarían, de este modo, relacionados por simples reglas de simetría.

A la hora de diseñar la celda unidad que defina al sólido objeto de estudio, es importante ser especialmente cauto con las peculiaridades propias del material, teniendo en cuenta sus parámetros específicos, de forma que los cálculos obtenidos ofrezcan resultados aceptables. A modo de ejemplo, en el caso de los materiales silíceos, hay que considerar la presencia de los grupos hidroxilo que pueda haber presentes, ya que podrían originar la presencia de puentes de hidrógeno.

Resulta evidente, por tanto, que la principal ventaja del enfoque PBC es que permite tener en cuenta la naturaleza expandida del material partiendo de una celda unidad suficientemente definida y de tamaño adecuado. Sin embargo, este método presenta como principal desventaja la limitación de su aplicabilidad a métodos de cálculo DFT como nivel máximo de método teórico, ya que resulta complicado extender los métodos más altos de correlación basados en la expansión de la función de onda — métodos MP2— para el estudio del estado sólido. Recientemente, se han obtenido diversos avances al respecto, basados en la implementación periódica del método MP2 en el programa CRYSCOR, así como métodos basados en la aproximación de fase aleatoria en el programa VASP, aunque todos ellos adolecen de ser largos en exceso y no permitir una optimización coherente de las geometrías debido a que el gradiente analítico de energía aún no se ha implementado²⁴⁷.

Muchos de los programas de cálculo que habitualmente se utilizan, emplean conjuntos de bases de onda plana, que difieren de las funciones de tipo gaussiano, explicadas anteriormente, y que son bases localizadas centradas en el átomo. En el caso de las de onda plana, se utiliza un número finito de funciones, por debajo de un valor de energía específico, que se elige para un cálculo determinado, para así facilitar ciertas operaciones integrales que resultarían más arduas con funciones localizadas. A nivel práctico, es habitual utilizar las funciones de onda plana en combinación con un pseudopotencial, de forma que las ondas planas describen únicamente la densidad de carga de valencia²⁴⁸. La aproximación debida al pseudopotencial simplifica considerablemente el cálculo, ya que implica un menor número de electrones. Esto se debe a que solamente los electrones de valencia químicamente activos se tratan explícitamente, mientras que los electrones internos (*core*) se concentran en torno a los núcleos atómicos, de forma que se consideran en conjunto con los núcleos, como núcleos rígidos no polarizables. El uso del pseudopotencial resulta fundamental debido al gran tamaño de las funciones de onda derivadas de esta situación, así como gradientes de densidad cercanos a los núcleos que no resultan fáciles de definir con una base de onda plana. Además, la aplicación de una base de onda plana garantiza la convergencia de forma suave y monótona a la función de onda objetivo.

La aplicación de la metodología PBC en combinación con una base de onda plana con pseudopotencial está ampliamente extendida entre diversos programas de cálculo – Abinit, Castep, Cp2k, NWChem, Quantum Espresso o Vasp, citando algunos –, mientras que muchos otros, entre los que se incluyen Gaussian, Crystal Freon, Scigrees o Turbomole, emplean funciones de tipo gaussiano centradas en el átomo.

1.7.4.2 Modelo de aproximaciones del clúster

A diferencia del método PBC, que se centra inicialmente en la definición de la estructura del sólido, este método se focaliza en la superficie del sólido. Para ello se define como elemento representativo una región de la superficie en torno a un sitio específico o centro activo que interese analizar, considerando la topología del sólido. Resulta fundamental tener en cuenta diversos factores a la hora de aplicar el modelo, que pudieran derivar en defectos estructurales y electrónicos en las terminaciones del

clúster, tales como perturbaciones en la función de onda debido a los límites del clúster, restricciones estructurales y problemas con interacciones de largo alcance.

La principal ventaja de este método con respecto al método PBC es que serán los recursos informáticos utilizados la única limitación al nivel de sofisticación del método teórico adoptado. Esto se debe a que, una vez que el clúster está completamente definido, se puede tratar de modo habitual a cualquier otra molécula regular, empleando los métodos altamente sofisticados de mecánica cuántica estándar, para así analizar sus características fisicoquímicas. Es importante mencionar que las interacciones de largo alcance, si afectan a las propiedades del clúster, pueden ser un inconveniente en la aplicación del método. Por tanto, solo debe utilizarse cuando las propiedades sean de naturaleza local²⁴⁶.

I.7.4.3 Modelo de aproximaciones del clúster embebido

Este modelo, más reciente que los anteriores, combina tanto las ventajas del enfoque de aproximaciones del clúster, pudiendo aplicar un nivel teórico alto, como las limitaciones geométricas impuestas por la aproximación PBC, aunque sin llegar a hacer uso de la periodicidad²⁴⁹. El modelo PBC puede ser evitado si se adopta un clúster de tamaño suficiente como para imitar correctamente el entorno del sitio activo. Sin embargo, aunque se localice en un centro activo determinado, el uso de este enfoque provoca un crecimiento exponencial en el número de orbitales atómicos con el tamaño del clúster. Por ello se han desarrollado una serie de nuevos métodos que tratan de describir con un mayor nivel la zona químicamente relevante, siendo la zona externa descrita por un método inferior y, por tanto, con un menor coste computacional. Entre ellos destaca el método ONIOM²⁵⁰, que subdivide en distintos fragmentos o capas el sistema de interés, siendo analizada cada una con un nivel de cálculo diferente. En esta división, la parte principal y más importante del sistema es la capa interna, que se describe con el nivel más alto de cálculo, y se denomina como "sistema de modelo". El resto de capas se definen con métodos teóricos de menor coste computacional, reduciendo así el coste global de cálculo del sistema.

CAPÍTULO II

OBJETIVOS

CAPÍTULO II. OBJETIVOS

El objetivo general de esta Tesis Doctoral es el diseño, síntesis y caracterización de nuevos materiales porosos de carácter básico, y su utilización como catalizadores en la síntesis de heterociclos oxigenados relevantes para la industria farmacéutica.

Más concretamente, los objetivos específicos de este trabajo son los siguientes:

II.1. Sintetizar los sólidos objeto de estudio

II.1.1. Carbones Activados (CAs)

Se sintetizará la familia de materiales PET/CAL, por pirólisis de mezclas de PET, y roca caliza (CAL), en distintas proporciones, siguiendo los procedimientos descritos en la literatura. Se prepararán también materiales análogos a partir de MAG y dolomita (DOL), para su comparación.

II.1.2. Redes metaloorgánicas (MOFs)

Se prepararán dos series de redes metaloorgánicas, con propiedades básicas, modificadas con aminas de distinta naturaleza, a partir de los correspondientes MOFs empleando el método post-sintético (*grafting*). Se partirá de MIL-100-Sc, que se sintetizará adaptando los procedimientos descritos en la literatura y un MOF comercial (CuBTC, Basolite® C300).

II.1.3. Sílices mesoporosas

Se sintetizarán distintas familias de sílices mesoporosas —SBA-15, T/MCF (donde T es Nb o Ta)— siguiendo los procedimientos descritos en la literatura para este tipo de materiales. Al igual que en el caso de las redes metaloorgánicas (*objetivo* II.1.2.), las sílices preparadas se funcionalizarán con grupos amino de diferente naturaleza, mediante el método post-sintético (*grafting*), empleando distintos silanos comerciales.

II.2. Caracterizar los materiales sintetizados

La caracterización de los sólidos obtenidos se llevará a cabo por diversas técnicas. Para la obtención de sus parámetros texturales, se realizará mediante adsorción/desorción de N₂. Se realizarán estudios termogravimétricos y análisis térmico diferencial (TG-ATD) para la determinación de su estabilidad térmica. La naturaleza de los grupos superficiales presentes en los materiales se estudiará por FTIR. Su estructura se estudiará mediante XRD y su morfología mediante TEM y SEM. La determinación de su composición química se estudiará mediante análisis elemental, y la espectrometría de fluorescencia de Rayos X (XRF, *por sus siglas en inglés*) para la determinación de sus centros metálicos.

II.3 Evaluar la actividad catalítica de los diferentes catalizadores

Los materiales preparados se ensayarán en la síntesis de 2-amino-4H-cromenos, mediante la MCR, entre diversos 2-hidroxi benzaldehídos y diferentes nitrilos con grupos metileno activos, en condiciones suaves de reacción. Adicionalmente, se realizarán estudios acerca de la influencia de la cantidad de catalizador y del efecto de la temperatura en la reacción. Finalmente, se estudiará la posible reutilización de los catalizadores más eficientes.

II.4 Realizar un estudio computacional del mecanismo de reacción mediante cálculos teóricos

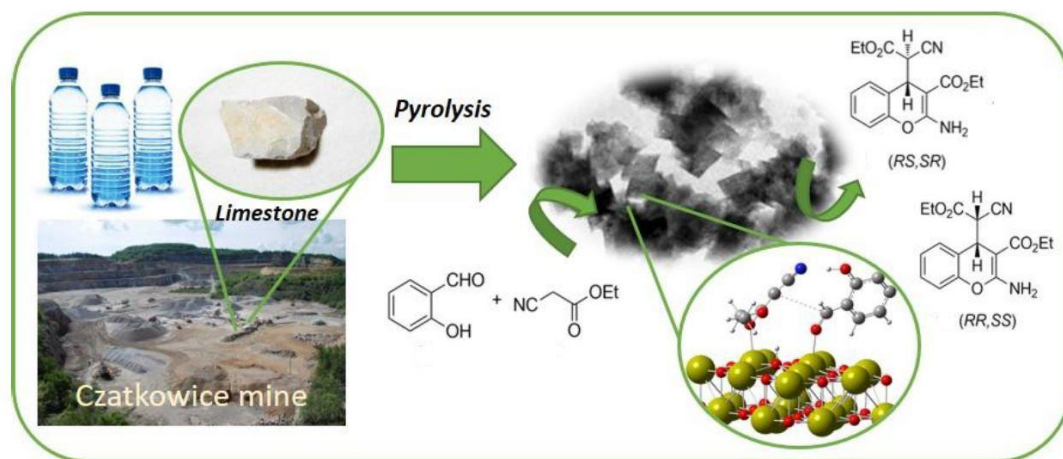
Los resultados experimentales obtenidos se racionalizarán empleando el software de química computacional Gaussian 09, a través de la metodología DFT. En combinación con los resultados teóricos permitirán clarificar las diferencias de actividad y selectividad mostradas por los distintos materiales en la síntesis de cromenos.

CAPÍTULO III

CARBONES BÁSICOS COMO CATALIZADORES EN LA SÍNTESIS SOSTENIBLE Y EFICIENTE DE DERIVADOS DE CROMENOS

CAPÍTULO III. CARBONES BÁSICOS COMO CATALIZADORES EN LA SÍNTESIS SOSTENIBLE Y EFICIENTE DE DERIVADOS DE CROMENOS. VALORIZACIÓN DE RESIDUOS DE PET Y FUENTES MINERALES

CHAPTER III. BASIC-CARBON NANOCATALYSTS IN THE EFFICIENT SYNTHESIS OF CHROMENE DERIVATIVES. VALORIZATION OF BOTH PET RESIDUES AND MINERAL SOURCES



ABSTRACT

Novel series of calcium oxide (calcium hydroxide)/carbon composites applied to the green and efficient synthesis of 2-amino-4*H*-chromenes, from 2-hydroxybenzaldehydes and ethyl cyanoacetate, under mild and solvent-free conditions, is herein reported for the first time. These basic hybrid materials are easily prepared by direct thermal pyrolysis of limestone and PET mixtures. Different Ca phases, CaO or Ca(OH)₂, were independently detected, since CaO/carbon composites initially formed can be easily hydrated, under atmospheric conditions, but also dehydrated by re-calcination. CaO-containing samples present enhanced catalytic performance, the observed reactivity being attributed to the catalyst basicity.

The reaction under study probably occurs through cascade reactions following aldolization - heterocyclization - dehydration - Michael addition sequence, strongly favoured by the presence of the truly active phase, CaO, as experimental and theoretical has been demonstrated. The methodology herein reported can be framed in the circular economy domain opening the possibility of synthesizing valuable compounds from carbon-based catalysts prepared by using plastic residues as PET source.

III.1 RESULTS AND DISCUSSION

In this chapter, a new family of calcium oxide (calcium hydroxide)/carbon composites were synthesized, characterized and applied to the green and efficient synthesis of 2-amino-4*H*-chromenes **1**, from 2-hydroxybenzaldehydes **2** and ethyl cyanoacetate **3**, under mild and solvent-free conditions (**Scheme 9**, see *III.1.2 Catalytic Performance*). These hybrid materials are easily prepared by direct thermal pyrolysis of limestone and (PET), as commented below. Additionally, some mechanistic considerations are also reported.

III.1.1 Synthesis and characterization of the catalysts

The carbonaceous catalysts were synthesized by following the experimental procedure previously reported by Przepiórski *et al.*²⁵¹, detailed in *Chapter VII (Section VII.3.1)*. The precursor materials used in this research were commercially available: PET, limestone (CAL), magnesite (MAG), and dolomite (DOL). The PET was acquired from Elana S.A. (Poland) whereas the minerals were mined from different deposits in Poland. CAL deposit was located in Czatkowice, MAG deposit near Grochów, and DOL was mined from deposits located near Ząbkowice. CaCO₃ and MgCO₃ are the major components for CAL (96.3%) and MAG (81.6%), respectively, whereas DOL is mainly composed of both carbonates, CaCO₃ and MgCO₃ in a 52.6/41.5 [wt.%/wt.%] ratio. The minerals contained naturally included other components, as summarized in **Table 6**.

The catalysts were prepared by direct pyrolysis of mixtures of PET/CAL, varying the PET/CAL —ratio 100:0, 83:17, 70:30, 50:50, 30:70 and 0:100—. An extra catalyst was prepared with the same methodology as PET/CAL 30:70 but replacing commercial PET by PET residues from plastic bottles, and it was named as PETb/CAL 30:70. In addition, PET/MAG 30:70 and PET/DOL 30:70 catalysts were also synthesized.

Table 6. Chemical composition (in wt. %, calculated as oxides) of the minerals (based on supplier's data).

Component	Mineral		
	MAG	DOL	CAL
CaO	1.83	29.44	53.80
MgO	41.20	19.75	0.71
SiO ₂	4.21	1.43	2.13
Fe ₂ O ₃	2.57	0.14	0.11
Al ₂ O ₃	1.18	0.11	0.08

Firstly, thermogravimetric analysis was carried out to initial PET/CAL mixtures. In this regard, two mass drops appeared at approximately 623 K and 873 K, corresponding to thermal degradation of both, PET and limestone, according to previous studies²⁵¹. The same thermal treatment was used for analysing the catalysts, obtained after several days stored under atmospheric conditions. The corresponding thermograms showed a new weight loss presence at, approximately, 625 K (**Figure 27**). This new drop was assigned to the dehydration of Ca(OH)_2 to CaO , according to several studies reported at similar temperatures²⁵².

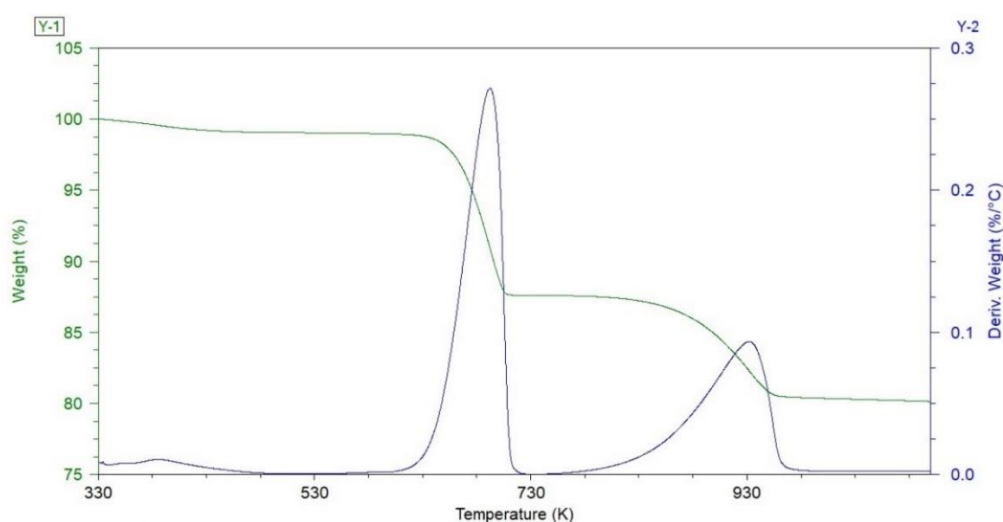


Figure 27. Thermogravimetric profile of PET/CAL 30:70 sample.

Table 7 shows the CaO loading determined by TG experiments and point of zero charge (pH_{PZC}) values for the investigated samples. These values, which are close to 12, confirm the remarked basic character of the samples, as expected.

Table 7. Calcium oxide content and pH_{PZC} for PET/CAL, PET/MAG and PET/DOL samples.

Sample	CaO content (wt. %)	pH_{PZC}	Cristal size (nm)
PET/CAL 0:100	100	--	189
PET/CAL 30:70	87	12.03	140
PET/CAL 50:50	66	12.06	95
PET/CAL 70:30	57	12.38	-
PET/CAL 83:17	35	12.12	61
PET/MAG 30:70	78 ^[a]	10.23	-
PET/DOL 30:70	88 ^[b]	12.19	-

[a] MgO content. [b] MgO + CaO content determined by TG.

The investigated materials were also characterized by XRD. The obtained diffraction patterns confirmed the presence of CaO, formed by thermal decomposition of CaCO_3 —the major component in limestone—, as well as silica traces, from raw mineral²⁵¹. **Figure 28** shows the XRD patterns of three different PET/CAL 30:70 samples: PET/CAL 30:70 (1), which corresponds to the recently prepared catalyst; PET/CAL 30:70 (2), which is the catalyst after several days stored under atmospheric conditions; and PET/CAL 30:70 (3), as recalcined PET/CAL 30:70 (2) sample.

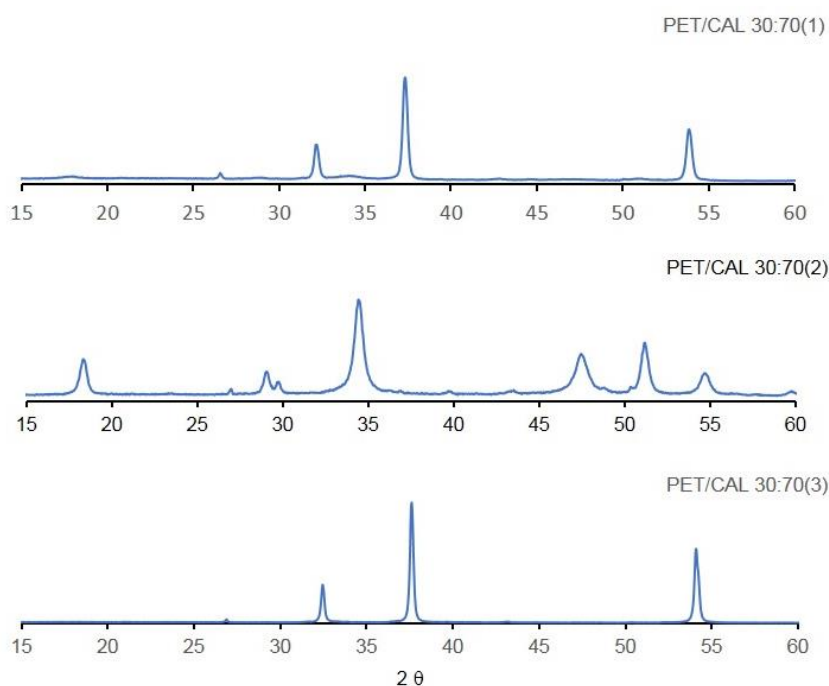


Figure 28. XRD patterns of PET/CAL 30:70 recently synthesized, PET/CAL 30:70(1), stored under atmospheric conditions, PET/CAL 30:70(2), and re-calcined PET/CAL 30:70(3).

The obtained results showed that PET/CAL 30:70(1) and PET/CAL 30:70(3) present almost the same composition, being CaO the main metallic phase. However, PET/CAL 30:70(2) contains a new phase, Ca(OH)_2 , probably formed by hydration under atmospheric conditions, this results in good agreement with the TG results. It is important to remark that there are no extra diffraction peaks, so it demonstrates that the carbonaceous support is amorphous and do not contribute to the crystallinity. The crystal size of Ca phases increases proportionally with CAL content in the initial mixtures and it was calculated by using the Scherrer equation, such as it was summarized in **Table 7**.

Textural parameters of the catalysts were determined by N₂ adsorption-desorption. All the obtained isotherms were an overlapping type I – type IV, showing a remarkable H3 type hysteresis loop (**Figure 29**). The microporosity character of the materials is related to the carbonaceous phase amount, these materials also showing certain mesoporosity. It is important to note that the carbonized PET sample in absence of CAL showed a weak capacity of N₂ adsorption, according to the previous studies²⁵¹.

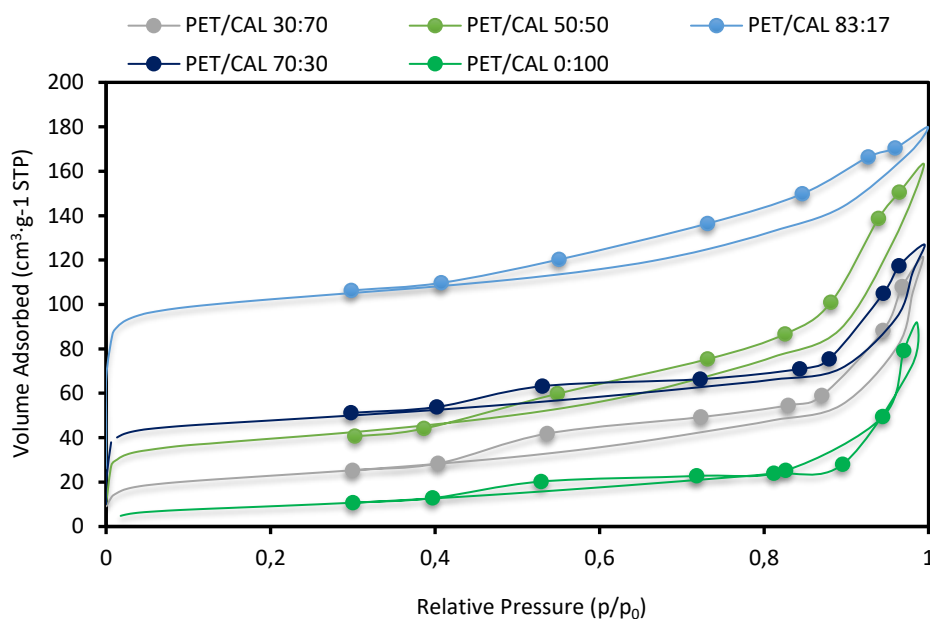


Figure 29. N₂ adsorption/desorption isotherms for PET/CAL hybrid materials.

In general, the porosity is higher for the samples with the higher PET content, S_{BET} (79–326 m²·g⁻¹) and V_{micro} increasing when the CAL amount decreases. In this regard, all the textural parameters are summarized in **Table 8**.

Table 8. Textural parameters for the PET/CAL samples.

Catalyst	t-plot				(p/p ₀ = 0,95)	Dubinin-Radushkevich		BJH
	S_{BET} (m ² ·g ⁻¹)	S_{Total} (m ² ·g ⁻¹)	S_{External} (m ² ·g ⁻¹)	S_{Micro} (m ² ·g ⁻¹)	V_{T} (cm ³ ·g ⁻¹)	V_{micro} (cm ³ ·g ⁻¹)	V_{meso} (cm ³ ·g ⁻¹)	D (Å)
PET/CAL 0:100	33	35	35	0	0.11	0.02	0.09	142
PET/CAL 30:70	79	78	57	21	0.13	0.04	0.09	118
PET/MAG 30:70	158	176	107	69	0.32	0.07	0.25	--
PET/DOL 30:70 ^[27,28]	106	114	90	24	0.22	0.05	0.17	-
PETb/CAL 30:70	113	113	27	86	0.11	0.04	0.07	217
PET/CAL 50:50	131	131	67	64	0.20	0.06	0.14	112
PET/CAL 70:30	159	158	52	106	0.15	0.08	0.07	118
PET/CAL 83:17	326	327	74	253	0.26	0.16	0.10	89
PET/CAL 100:0 ^[26]	34	37	3	34	0.02	0.02	0.00	-
Norit RX3	1306	1468	191	1277	-	-	-	-

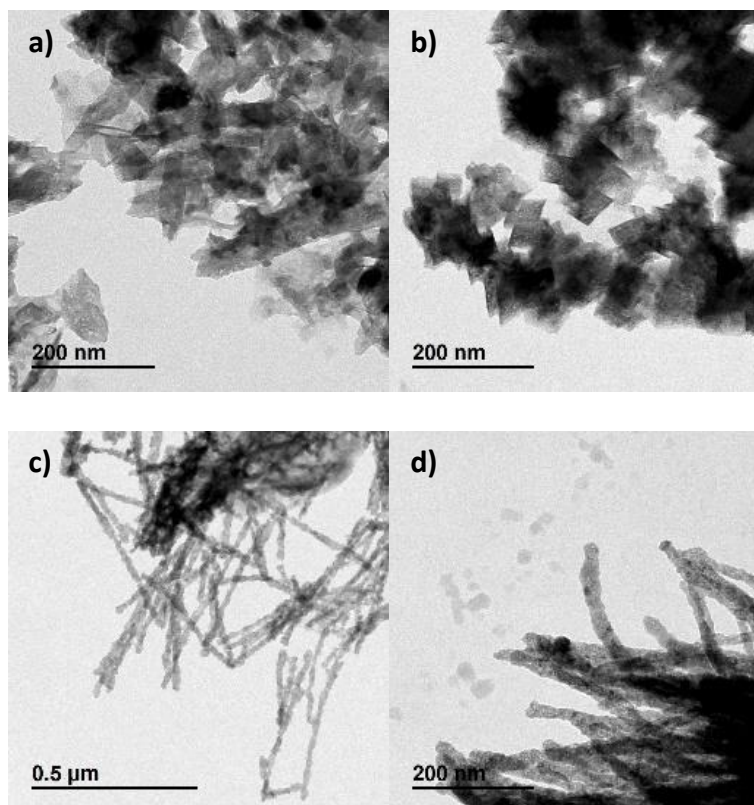
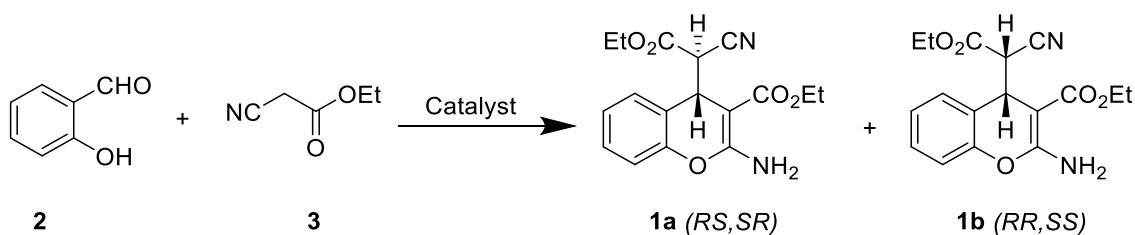


Figure 30. TEM images of the samples with different PET/CAL ratio: a) PET/CAL 30:70, b) PET/CAL 50:50, c) PET/CAL 70:30 y and d) PET/CAL 83:17.

Figure 30 shows the TEM images of the samples. It can be seen that the composition has a remarkable influence on the morphology of the materials. The Ca phases —CaO and Ca(OH)₂— appeared as cubic structures heterogeneously dispersed over amorphous carbon. When the PET/CAL ratio is 30:70, the amorphous carbon is deposited in the cavities of the predominant cubic Ca phase while when the PET amount is increased, some carbonaceous agglomerates appeared covering the Ca phase surface (**Figure 30a**). Furthermore, the materials with higher PET amount showed thread structures, with Ca phases dispersed between them (**Figure 30c and 30d**).

III.1.2 Catalytic performance

The catalysts were firstly tested in the synthesis of 2-amino-4*H*-chromenes **1**, between 2-hydroxybenzaldehyde **2** and ethyl cyanoacetate **3**, under solvent-free conditions, at 323 K (**Scheme 9**) and atmospheric pressure, as it is detailed in the experimental (**Chapter VII**). It is noteworthy that the blank experiment, in the absence of any catalyst, led to chromenes **1** in only 1 % of conversion, after 3 h of reaction time.



Scheme 9. Synthesis of 2-amino-4H-chromenes **1** from 2-hydroxybenzaldehyde **2** and ethyl acetoacetate **3**, at 323 K, catalysed by basic carbon materials.

Figure 31a shows conversion values to chromenes **1** vs time in the presence of PET/CAL catalyzes. All the materials led to mixtures of chromenes **1** as diastereomeric mixtures of **1a/1b** isomers, in approximately 2:1 ratio, compound **1a** being the most thermodynamically stable isomer and, therefore, the major compound. Note that conversion to **1** depends on the Ca loading in PET/CAL samples, conversion diminishing when the PET/CAL ratio increases. The most active catalyst was PET/CAL 30:70, affording almost quantitative conversion of chromenes **1** after 3h of reaction time. There were no significant differences between the other PET/CAL samples, probably due to the amorphous carbon phase is covering the Ca species.

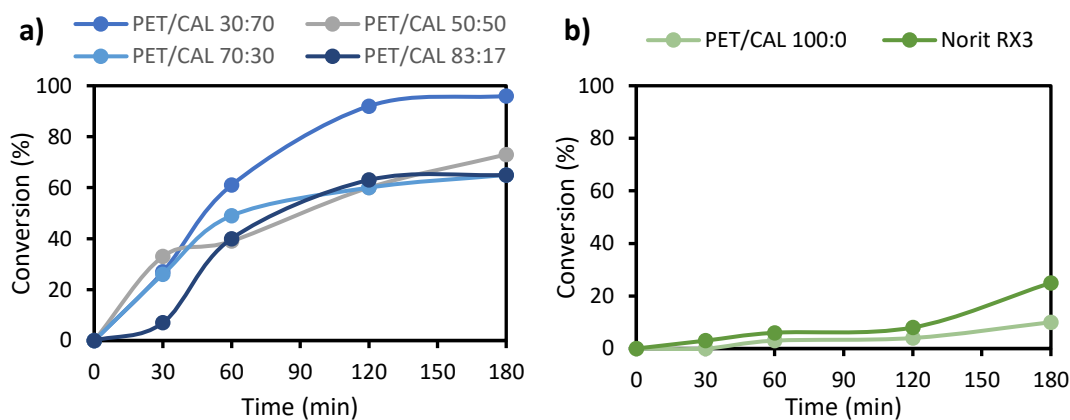


Figure 31. Synthesis of 2-amino-4H-chromenes **1** catalysed by a) PET/CAL hybrid materials, and b) by PET/CAL 100:00 and Norit RX3. Reaction conditions: 50 mg of catalysts, 323 K, **2/3** molar ratio = 2:4, solvent-free conditions.

The sample PET/CAL 100:0, prepared from PET, was also tested in the reaction. The results showed that the catalytic activity of the carbon matrix could be neglected at the shortest reaction times. When comparing this behaviour with other microporous carbon material (**Figure 31b**), Norit RX3, an increase of conversion values to **1** was observed —approximately 10% in case of PET/CAL 100:0 vs approximately 20% for Norit

RX3, after 3 h of reaction time—, probably due to its higher surface area (34 vs 1306 $\text{m}^2\cdot\text{g}^{-1}$, for PET/CAL 100:0 and Norit RX3, respectively, **Table 8**).

Interestingly, the raw limestone —mainly composed of CaCO_3 — was not active in the synthesis of **1**, reaching only 3% of conversion after 2 h of reaction time, under the same experimental conditions. Therefore, in order to confirm that CaO in PET/CAL catalysts is the predominant catalytic specie, PET/CAL 0:100, prepared by pyrolysis of CAL, was also tested. It is noteworthy that both PET/CAL 0:100 and PET/CAL 30:70 gave similar conversion values to **1**, with a slight decrease in the case of non-supported material. One of the main problems when working with metallic oxides is leaching²⁵³, so the presence of catalytic support turns into a crucial factor to guarantee heterogeneous catalysis. For this reason, we carried out the reaction, using PET/CAL 30:70 catalyst, removing it from the reaction mixture by filtering after 15 min of reaction time (**Table 9**). In this regard, while PET/CAL 0:100 sample was totally solubilized in the reaction medium, the presence of a small amount of carbon in PET/CAL 30:70 catalyst confirms that it certainly works as a heterogeneous catalyst.

Table 9. Synthesis of chromenes **1** catalysed by PET/CAL 30:70 and PET/CAL 0:100. Reaction conditions: 50 mg of catalysts, 323 K, 2/3 molar ratio = 2:4, solvent-free conditions.

Catalysts	Time (min)			
	15	30	60	120
PET/CAL 30:70	32	42	57	92
PET/CAL 30:70*	31	35	43	57
PET/CAL 0:100	25	38	56	87

*Catalyst removed from the reaction mixture after 15 min.

All these results suggested that the Ca phases are the main active catalytic species. Thus, the catalytic behaviour is conditioned by the dispersion and Ca loadings as well as the porosity of each material. The active centres of the catalysts with higher PET/CAL ratios, probably are less accessible due to the presence of the amorphous carbon phase. On the other hand, the microporosity and its related higher surface area contribute to the conversion to chromenes **1**, as suggested by the PET/CAL 83:17 results (**Figure 31a**).

As above mentioned, the CaO in PET/CAL materials can be easily transformed into $\text{Ca}(\text{OH})_2$ by hydration under atmospheric conditions (**Figure 27**). Having this in mind, three different PET/CAL 30:70 samples were tested: PET/CAL 30:70(1) —recently

prepared and stored under an inert atmosphere, in which the main phase is CaO—, PET/CAL 30:70(2) —prepared days ago and stored under ambient conditions, where calcium phase is mainly Ca(OH)₂—, and PET/CAL 30:70(3) —recalcined from PET/CAL 30:70(2)—. The obtained results showed a decrease in conversion for PET/CAL 30:70 (2) in comparison to PET/CAL 30:70(1) and PET/CAL 30:70 (3) (**Figure 32**). This could be related to the presence of Ca(OH)₂, which performs as a catalyst although loading to lower conversions.

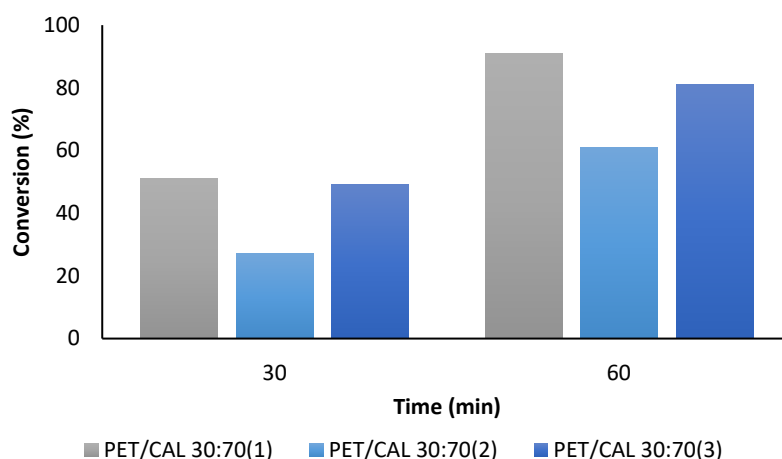


Figure 32. Synthesis of 2-amino-4H-chromenes **1** catalysed by PET/CAL 30:70 hybrid materials. Reaction conditions: 50 mg of catalysts, 323 K, **2/3** molar ratio = 2:4, solvent-free conditions.

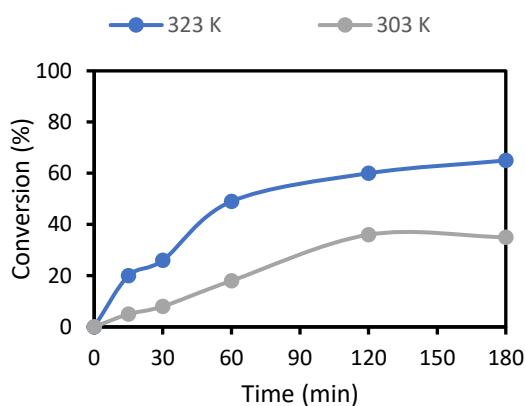


Figure 33. Synthesis of 2-amino-4H-chromenes **1** catalysed by PET/CAL 70:30 hybrid material. Reaction conditions: 50 mg of catalysts, 323 K vs 303 K, **2/3** molar ratio = 2:4, solvent-free conditions.

Following ongoing investigations, we studied the influence of the temperature and the catalyst amount in the reaction. First of all, the reaction was carried out at a lower temperature, 303 K, closer to room temperature, using PET/CAL 30:70 as a

catalyst. The chromenes **1** were obtained with lower conversion values but maintaining the selectivity, as expected (**Figure 33**).

Also, the influence of the catalyst amount was checked by using 25 mg and 12 mg of PET/CAL 30:70 instead of 50 mg, at 323 K. As expected, when the quantity of the catalyst was reduced, conversion to chromenes **1** underwent a remarkable decrease — 49% and 34% of conversion, after 1 h of reaction time, when using 25 mg and 12 mg, respectively—, without observing any changes in the selectivity. These results are in agreement with the previous ones when using the samples with a high PET/CAL ratio, pointing out that the sample with the lowest Ca content works as an efficient catalyst in chromenes **1** synthesis.

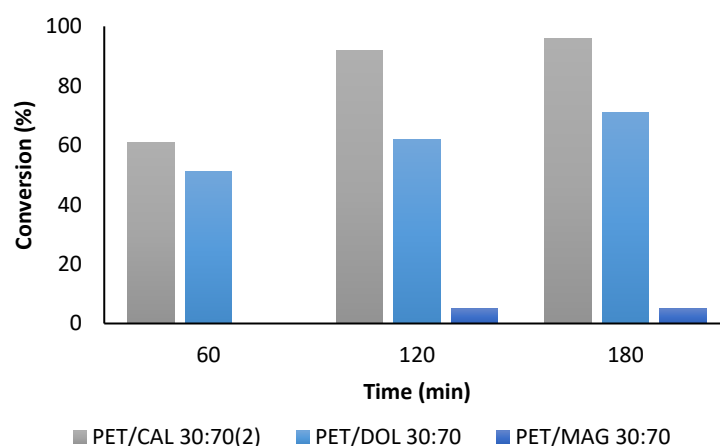


Figure 34. Synthesis of 2-amino-4H-chromenes **1** catalysed by PET/CAL 30:70(2), PET/DOL 30:70 and PET/MAG 30:70 hybrid materials. Reaction conditions: 50 mg of catalysts, 323 K, **2/3** molar ratio = 2:4, solvent-free conditions.

Based on previous studies of our research group concerning the use of similar catalysts in the Friedländer reaction¹²⁰, we also prepared the corresponding samples derived from MAG and DOL, following the experimental protocol previously reported by Przepiórski *et al.* resulting in PET/MAG 30:70²⁵⁴ and PET/DOL 30:70 hybrid materials²⁵⁵. Both samples PET/MAG 30:70 and PET/DOL 30:70 resulted active in the synthesis of chromenes **1** although leading to lower conversion values to chromenes **1**. In this sense, when using PET/MAG 30:70 catalyst conversion to **1** was lower than 5% after 3 h of reaction time, whereas PET/DOL 30:70 sample reached similar conversion values than PET/CAL 30:70 catalyst (**Figure 34**). These results strongly suggest that the reaction is mainly controlled by the basicity of the active specie, which is the corresponding metal

oxide. Both PET/CAL 30:70 and PET/DOL 30:70 samples showed similar pH_{PZC} , with values close to 12, while PET/MAG 30:70 presented a pH_{PZC} of approximately 10 (Table 7).

As it was anticipated, an additional catalyst —PETb/CAL 30:70—, in which PET residues from plastic bottles were used instead of commercial PET, was prepared following the same methodology reported for PET/CAL 30:70 sample and, subsequently, tested in chromenes **1** synthesis. Diastereomeric mixtures of chromenes **1a/1b** (approximately 2:1 ratio) were obtained in the presence of PETb/CAL 30:70 catalyst, at 323 K, with similar conversions than that for PET/CAL 30:70 sample (Figure 35). These results are especially relevant because of the potential application of highly polluting plastic residues as efficient carbon-based catalysts, allowing the valorisation of such residues in the frame of the circular economy domain.

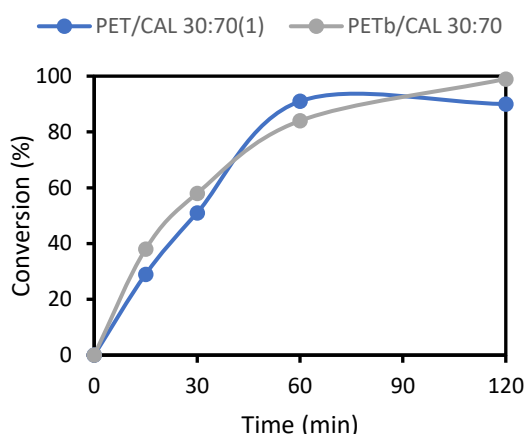
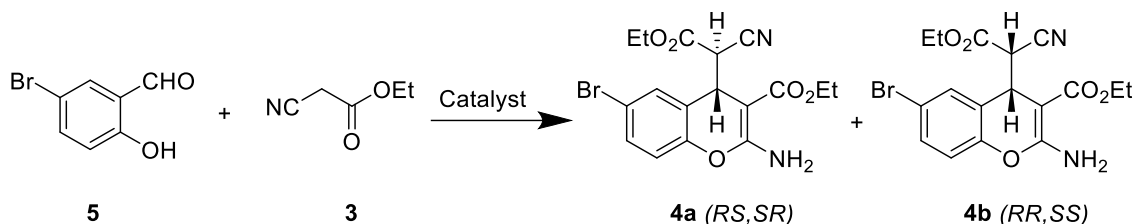


Figure 35. Synthesis of 2-amino-4*H*-chromenes **1** catalysed by PET/CAL 30:70(1) and PETb/CAL 30:70 hybrid materials. Reaction conditions: 50 mg of catalysts, 323 K, **2/3** molar ratio = 2:4, solvent-free conditions.

Finally, the PET/CAL hybrid materials were tested in the synthesis of ethyl 2-amino-6-bromo-4-(1-cyano-2-ethoxy-2-oxoethyl)-4*H*-chromene-3-carboxylate **4** (HA-14-1), which is an agonist for Bcl-2 receptors. This Bcl-2 protein is expressed in most types of cancer, so HA 14-1 presents great potential in therapy for cancer treatment^{42, 256, 257}. HA 14-1 synthesis was carried out between 5-bromo-2-hydroxybenzaldehyde **5** and ethyl cyanoacetate **3**, under same reaction conditions mentioned above at 323 K, catalysed by PET/CAL 30:70(2) and PET/DOL 30:70 (Scheme 10), HA 14-1 being obtained

with almost total conversion (99 %), after only 2 h of reaction time, as a diastereomeric mixture of **4a/4b** in a 2:1 ratio.

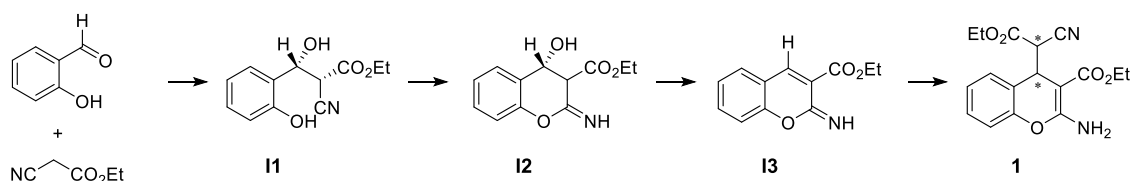


Scheme 10. Synthesis of HA 14-1 (**4a** and **4b**) from 5-bromo-2-hydroxybenzaldehyde **5** and ethyl acetoacetate **3**. Reaction conditions: 50 mg of catalysts, 323 K, **5/3** molar ratio = 2:4, solvent-free conditions.

III.1.3 Computational study

Considering these results, the reaction mechanism was investigated by computational methods through DFT methodology, analysing every step of the reaction as an elementary reaction, in gas phase, at 298 K. All the involved reactions were simulated in the presence and the absence of the catalytic specie. The selected representation of the catalytic specie was a cubic metallic cluster of (CaO)₂₀, which is large enough to host all the reactant structures and the most active Ca phase²⁵⁸.

Based on our previous studies using ionic liquids (ILs) as catalysts involved in the chromene synthesis, the catalysed reaction probably follows the pathway: i) aldol formation from chemisorbed reactants to generate **I1**, ii) heterocyclization to obtain **I2**, iii) dehydration to produce **I3**, and finally iv) Michael addition of a second ethyl cyanoacetate **3** molecule, leading to chromenes **1** as mixtures of the corresponding diastereomers (**Scheme 11**).



Scheme 11. Reaction pathway in the catalysed synthesis of chromenes **1** by ILs.

In **Figure 36** it is shown the free-energy profiles of the catalysed and uncatalysed processes, pointing out the relevance of the catalyst. A remarkable decrease of the free energy values during the first steps of the reaction, as the limiting steps, was

observed, the presence of CaO having a strong kinetic effect. Regarding the global free-energy balance, it can be concluded that the uncatalyzed reaction has a negative balance, while the catalysed one has a positive balance.

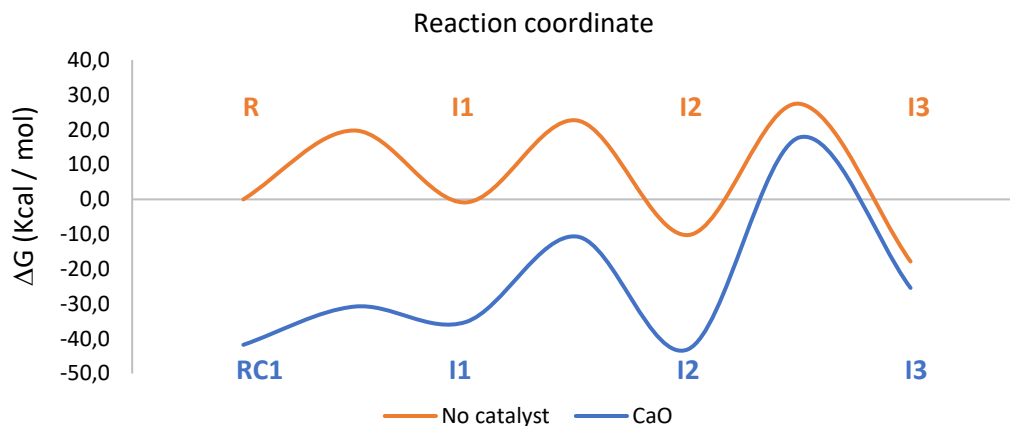
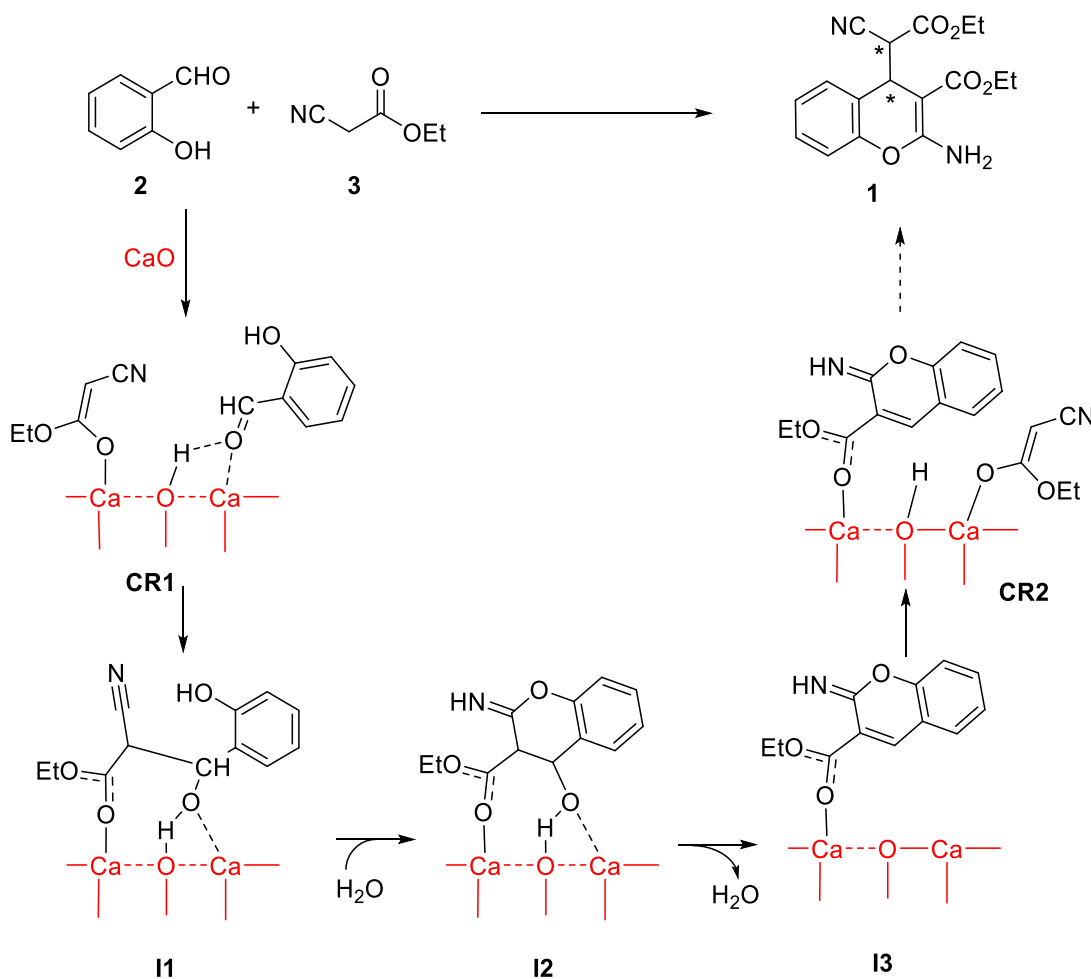


Figure 36. Free-energy profiles computed for the uncatalysed and catalysed synthesis of chromenes **1**.



Scheme 12. Plausible reaction pathway for the synthesis of chromenes **1** catalysed by CaO.

Our group has experience working with alkaline earth oxides (CaO and MgO), which present Lewis basicity and acidity, related to surface Ca cations²⁵⁹ and O anions²⁶⁰, as reported in previous adsorption experiments²⁶¹. The investigated PET/CAL catalysts could act then as bifunctional acid-base catalysts, activating simultaneously both electrophile —2-hydroxybenzaldehyde **2**— and nucleophile —ethyl cyanoacetate **3**—. This behaviour has been previously observed in the quinoline synthesis in the presence of MgO catalysts¹²⁰. Based on that, we propose the initial formation of reactant complex **CR1** as the crucial stage, where ethyl cyanoacetate **3** is activated by dissociative chemisorption, giving the corresponding enolate, which is anchored to the CaO surface, whereas 2-hydroxybenzaldehyde **2**, is interacting with the Lewis acid centre (**Scheme 12**).

Notable differences were found when comparing the corresponding catalysed and uncatalysed TS (**Figure 37**) proposed for the first step of the reaction —**TS_{R-11}(CaO)** and **TS_{R-11}**—. It is remarkable that **TS_{R-11}(CaO)** is more advanced TS to forming C-C bonds, as it can be observed from the C-C distances—2.1319 Å vs 2.6006 Å—. On the other hand, in case of **TS_{R-11}**, the enolic proton is hardly transferred to the acceptor, the carbonyl group in compound **2**, whereas in **TS_{R-11}(CaO)**, this proton is strongly bound to the cluster surface. Remarkably, the activation barrier for the catalysed process is much lower than for uncatalysed one —8.8 Kcal/mol lower—.

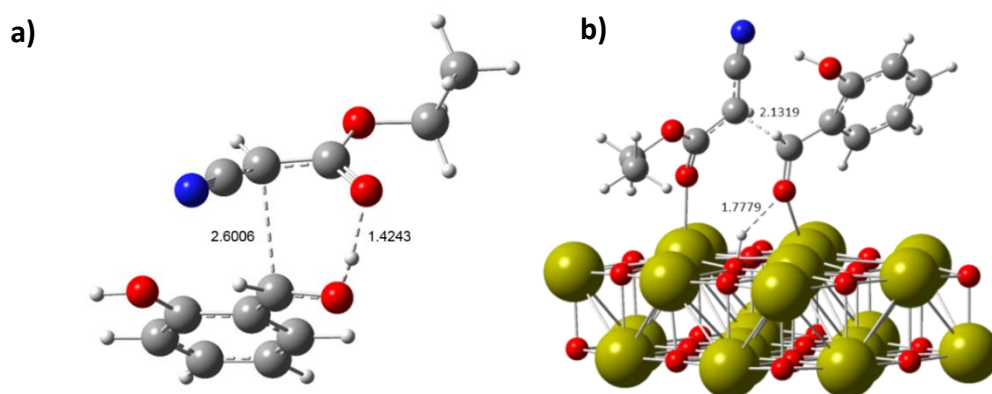


Figure 37. Optimized transition structures TS_{R-11} for the first step of the reaction in the formation of chromenes **1**. a) TS_{R-11} in the absence of any catalyst. b) $TS_{R-11}(CaO)$ in the presence of CaO. Relevant distances are expressed in Å.

Both heterocyclization of **I1** to **I2** and subsequent dehydration to **I3** are assisted by one water molecule, the presence of water being observed in all the investigated samples as demonstrated by TG experiments. There are some previous studies concerning the water effect in condensation and dehydration reactions²⁶². Our group has observed this water assistance in the mentioned quinolines synthesis by using MgO-based catalysts¹²⁰ and amino-grafted mesoporous silicas²²². Thus, the participation of one water molecule in **TS_{I1-I2}** and **TS_{I2-I3}**, in absence of any catalyst, drastically reduces the activation barrier —18.8 Kcal/mol and 12.2 Kcal/mol, respectively—, diminishing the ring strain during the proton transference. Considering the water participation in the catalysed process, the corresponding optimized structures for both elementary steps —**TS_{I1-I2w(CaO)}** and **TS_{I2-I3w(CaO)}**— are showed in **Figure 38**.

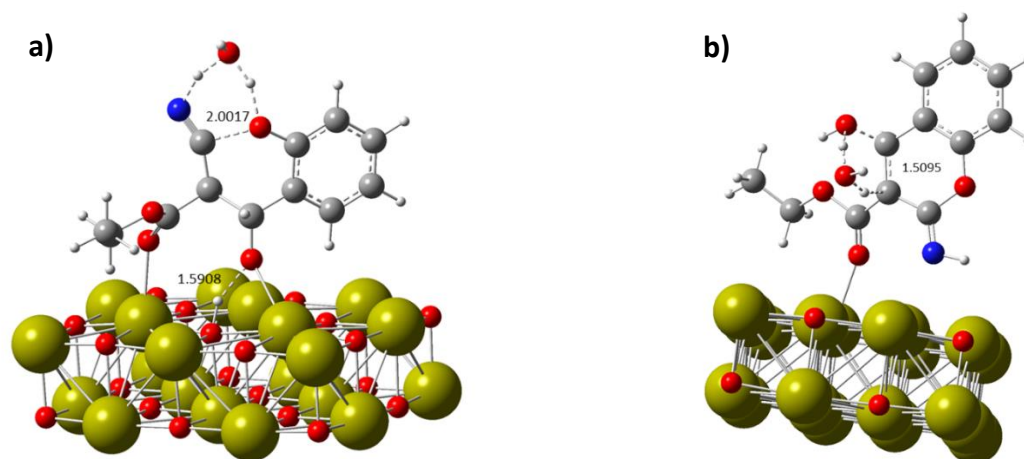


Figure 38. Optimized transition structures **TS_{I1-I2w}** **TS_{I2-I3w}** for the catalysed synthesis of chromenes **1**. a) **TS_{I1-I2w(CaO)}** and b) **TS_{I2-I3w(CaO)}**. Relevant distances are expressed in Å.

It is remarkable that the **I2** intermediate changes its adsorption mode for the dehydration process to allow the accessibility to the —OH group for dehydration, the imine moiety being in the surroundings of Lewis acid centres (**Figure 38**). This new interaction is produced with a notable lower free energy barrier —29.2 Kcal/mol— than those calculated for **TS_{I2-I3w(CaO)}** indicating the desorption and re-adsorption before dehydration. The last step, Michael addition of a second ethyl cyanoacetate **3** molecule, leading to chromenes **1**, depends on the previous formation of the reactant complex **CR2**, similar to **CR1** (**Scheme 12**). Thus, another molecule of **3** is located close to both electrophile faces comprising the C=C of the iminochromene **I3** to give the diastereomeric mixtures of chromenes **1**, as sets of the corresponding pairs of

enantiomers (*RR,SS* and *RS,SR*). The calculated TS, **TS_{I3-1(RR)}** and **TS_{I3-1(RS)}**, present energetic differences -1.7 Kcal/mol lower for **TS_{I3-1(RS)}**, leading to the most stable isomer of chromenes **1**—, as expected. It is important to remark that the selected model does not represent a realistic situation, only allowing to study the effect of active centres in the reaction, CaO in this case, without any confinement restrictions.

III.2 CONCLUSIONS

We report herein, for the first time, a novel family of catalysts comprising composites of calcium oxide or calcium hydroxide and carbon materials, PET/CAL, active and selective in the green efficient synthesis of 2-amino-4*H*-chromenes **1** from 2-hydroxybenzaldehydes **2** and ethyl cyanoacetate **3**, under mild and solvent-free conditions. These types of oxygenated heterocyclic compounds are especially relevant for the pharmaceutical industry due to their biological properties.

The composites PET/CAL were synthesized by direct thermal pyrolysis of mixtures of both PET and CAL as sources of carbon and CaO, respectively, using different PET/CAL ratios. The investigated hybrid materials showed basic properties and developed micro and mesoporosity. Different Ca-phases, CaO or Ca(OH)₂, were independently detected, since CaO/carbon composites initially formed can be easily hydrated, under atmospheric conditions, but also dehydrated by re-calcination. Obviously, the presence of Ca phases in explored composites contributes to the basicity of the samples whereas carbon material significantly increases the porosity of the materials. Both Ca phases were active in the investigated reaction, even for the samples showing the highest PET/CAL ratio. However, CaO-containing samples showed enhanced catalytic performance. Therefore, the obtained results strongly suggest that the reaction is mainly controlled by the basicity of the catalysts. The methodology herein reported opens the possibility of synthesizing valuable compounds from carbon-based catalysts, prepared by using plastic residues as PET source, selectively affording 2-amino-4*H*-chromenes **1** with high conversions as a sustainable alternative framed in circular economy domain.

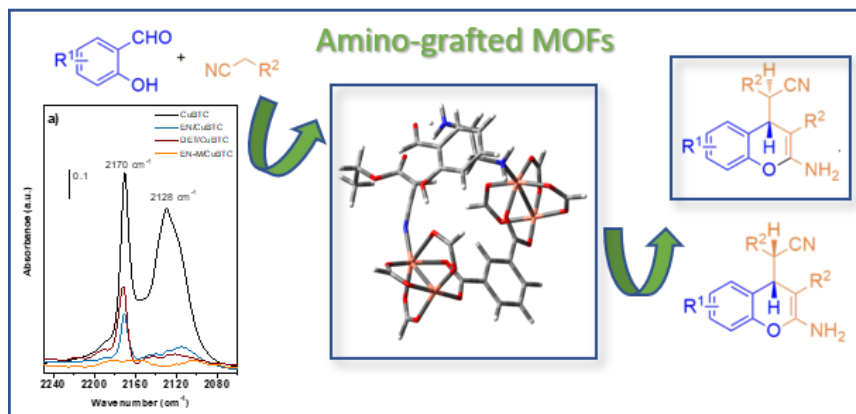
The understanding of the reaction mechanism was rationalized by using computational methods. This study reveals that the catalysed synthesis of 2-amino-4*H*-chromenes **1** takes place through cascade reactions, following the sequence: i) aldolization of both chemisorbed reagents, ii) heterocyclization and iii) dehydration, both assisted by one water molecule and, finally, iv) Michael addition of a second molecule of ethyl cyanoacetate **3**. The crucial stages are CR1 and CR2 formation, where both nucleophile and electrophile are activated. Our experimental and theoretical studies demonstrate that the presence of CaO provokes a strong kinetic effect.

CAPÍTULO IV

REDES METALOORGÁNICAS DE Cu Y Sc FUNCIONALIZADAS CON GRUPOS AMINO IMPLICADAS EN LA SÍNTESIS VERDE DE 2- AMINO-4H-CROMENOS

CAPÍTULO IV. REDES METALOORGÁNICAS DE Cu Y Sc FUNCIONALIZADAS CON GRUPOS AMINO IMPLICADAS EN LA SÍNTESIS VERDE DE 2-AMINO-4H-CROMENOS

CHAPTER IV. AMINO-GRAFTED Cu AND Sc METAL-ORGANIC FRAMEWORKS INVOLVED IN THE GREEN SYNTHESIS OF 2-AMINO-4H-CHROMENES



ABSTRACT

A new methodology for the eco-synthesis of 2-amino-4H-chromenes **1** is reported, from 2-hydroxybenzaldehydes and cyano compounds, under solvent-free and mild conditions, using amino-grafted MOFs as catalysts. The selected MOFs —commercial CuBTC and MIL-100(Sc), this last previously synthesized in our laboratories— can be easily functionalized with amines of different nature showing notable differences in their composition and textural properties. The total or partial functionalization of the metal centres in MOFs is strongly depending on the functionalization method used. Our results indicate that the catalytic performance is mainly conditioned by the type and concentration of basic sites, the porosity of the samples barely showing any influence. The methodology herein reported could be considered as an environmentally friendly alternative for the selective chromene synthesis, which allows to achieve high yields in relatively short reaction times —up to 90% over 1h—, using notably small amounts of the catalysts. Furthermore, our experiments in combination with theoretical calculations strongly suggest that basic sites in ethylenediamine functionalized catalysts can act either as individual catalytic sites, or in cooperation with the closest metal centers in samples partially functionalized, as in the case of EN/CuBTC.

IV. 1 RESULTS AND DISCUSSION

In this chapter, two new families of amino-grafted MOFs were prepared, characterized and applied to the green and efficient synthesis of 2-amino-4*H*-chromenes **1**, from 2-hydroxybenzaldehyde **2** and ethyl cyanoacetate **3**, under mild and solvent-free conditions. These materials are easily prepared by functionalization of MOFs —MIL-100 (Sc) previously prepared in our laboratories and CuBTC commercialized by Sigma-Aldrich and named Basolite® C300™— with polyamines of different nature, by using the post-synthetic method, as commented below. Additionally, the actuation mode of the most representative catalysts was theoretically investigated for the first elementary step of the reaction, consisting of aldolic condensation between reagents, by using computational methods.

IV.1.1 Synthesis and characterization of the catalysts

The MIL-100 (Sc) material was synthesized following the adapted experimental procedure previously reported by Zhu *et al*²⁶³. Both materials —MIL-100 (Sc) and CuBTC— were functionalized by following two different methods, as detailed in *Chapter VII (Section VII.3.1)*.

Two series of amino-grafted MOFs were then prepared depending on the selected method: i) materials denoted as amine-M/MOF using the adapted methodology described by Hwang *et al (Method A)*²⁶⁴ and ii) amine/MOF according to the methodology reported by Das *et al (Method B)*²⁶⁵. Then, it was prepared different materials such as EN-M/MIL-100(Sc), MMEN-M/MIL-100(Sc) and EN-M/CuBTC (*Method A*) and EN/CuBTC and DET/CuBTC (*Method B*) where EN is ethylenediamine, MMEN is N,N'-dimethylenediamine, and DET is diethylenetriamine.

Figure 39 shows the XRD patterns of CuBTC and MIL-100(Sc) before and after amine grafting. The CuBTC and MIL-100(Sc) samples showed good crystallinity and all diffraction lines could be assigned to the corresponding structural types. After the grafting process, the almost unchanged powder diffractograms of the samples indicate the preservation of the MOFs structure, except in the case of the EN-M/CuBTC sample, in which a slight variation of crystallinity is observed.

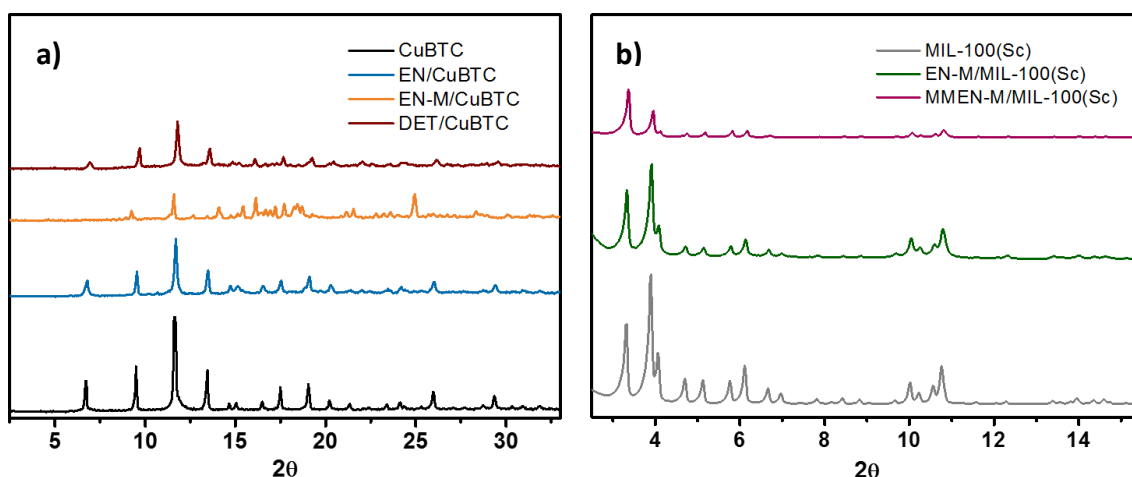


Figure 39. X-Ray diffractograms of amino-grafted a) CuBTC and b) MIL-100(Sc) samples.

Nitrogen adsorption-desorption isotherms were collected at 77 K for CuBTC (**Figure 40a**) and MIL-100(Sc) (**Figure 40b**) samples and were analysed using the BET and 2D-NLDFT methods. The measured BET surface areas and pore volumes of bare MOFs (**Table 10**) are in agreement with previous results. Amine-grafted samples show a notable reduction of the specific surface area and pore volume, especially for MIL-100(Sc) samples, for which these parameters are 2 and 3 times lower than those of the bare sample, indicating a partial occupation of the space inside the pores by the amine molecules. The particularly low value of the surface area of EN-M/CuBTC sample is probably due to the high amine loading reached in this case (*see below*). The pore size distributions (**Figure 40c** and **Figure 40d**) demonstrate the presence of micropores in CuBTC samples and a multimodal distribution in MIL-100(Sc) samples and confirm the decreased porosity in the functionalized materials.

Table 10. Catalyst textural properties.

Catalyst	S_{BET} ($\text{m}^2\cdot\text{g}^{-1}$)	V_p ($\text{cm}^3\cdot\text{g}^{-1}$)	Pore width (Å)
CuBTC	640	0.46	8.7
EN/CuBTC	546	0.23	9.3
DET/CuBTC	615	0.24	9.5
EN-M/CuBTC	6	0.016	-
MIL-100(Sc)	1590	0.72	10.9/16.7/19.9
EN-M/MIL-100(Sc)	444	0.23	10.8/16.7/19.0
MMEN-M/MIL-100(Sc)	736	0.41	10.4/16.7/19.0

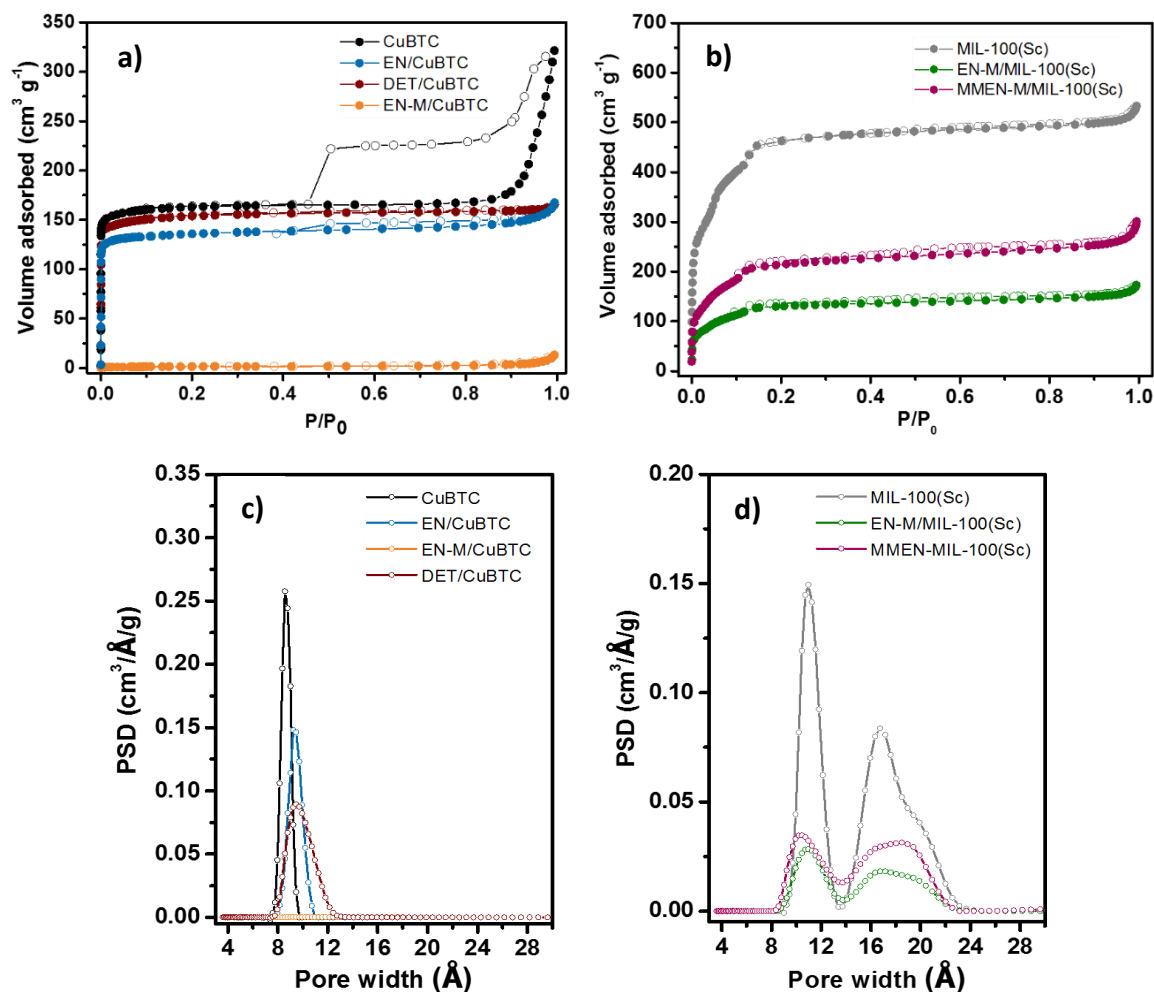


Figure 40. Nitrogen adsorption-desorption isotherms for amino-grafted a) CuBTC and b) MIL-100(Sc) samples. Pore size distributions for amino-grafted c) CuBTC and d) MIL-100(Sc).

The amine grafting of CuBTC and MIL-100(Sc) MOFs was also studied by FTIR. As shown in **Figure 41**, all the amine-grafted samples exhibit additional absorption bands in the range of 3450 to 2800 cm^{-1} , which are assigned to N–H and C–H stretching vibrations²⁶⁶, confirming the incorporation of the amine molecules in the prepared samples. The functionalization with amine molecules of coordinatively unsaturated copper (CuBTC) and scandium (MIL-100(Sc)) cations were also checked by infrared spectroscopy of carbon monoxide adsorbed at 100 K. After the activation of the samples, a saturation dose of CO was introduced into the IR cell and the corresponding spectra were recorded. The IR spectra of CO adsorbed on the bare MOFs (**Figure 42**) shows an IR absorption band centred at 2170 cm^{-1} for CuBTC and 2183 cm^{-1} for MIL-100(Sc) that comes from the fundamental C–O stretching mode of carbon monoxide interacting, through the carbon atom, with the Cu^{II} and Sc^{III} cations, respectively²⁶⁷. Additionally, in the case of CuBTC, another IR band near 2128 cm^{-1} is observed, which according to the

literature corresponds to the CO interacting with Cu^I species formed during the activation treatment of the sample²⁶⁸. The IR spectra of the grafted CuBTC samples (**Figure 42a**) show the IR absorption band at 2170 cm^{-1} , although much less intense, indicating that the open copper sites in the CuBTC are partially grafted by the amine molecules. In the case of the EN-M/CuBTC, the IR absorption band at 2170 cm^{-1} completely disappears (**Figure 42a**) which, together with the porosity results and compositional data, confirm the high incorporation of amine molecules in this sample. However, in the spectrum of the functionalized MIL-100(Sc) samples (**Figure 42b**), the band assigned to the CO stretching vibration of carbon monoxide adsorbed on Sc^{III} is not observed, indicating that in these samples the most of the metal centres are coordinated to the amine molecules.

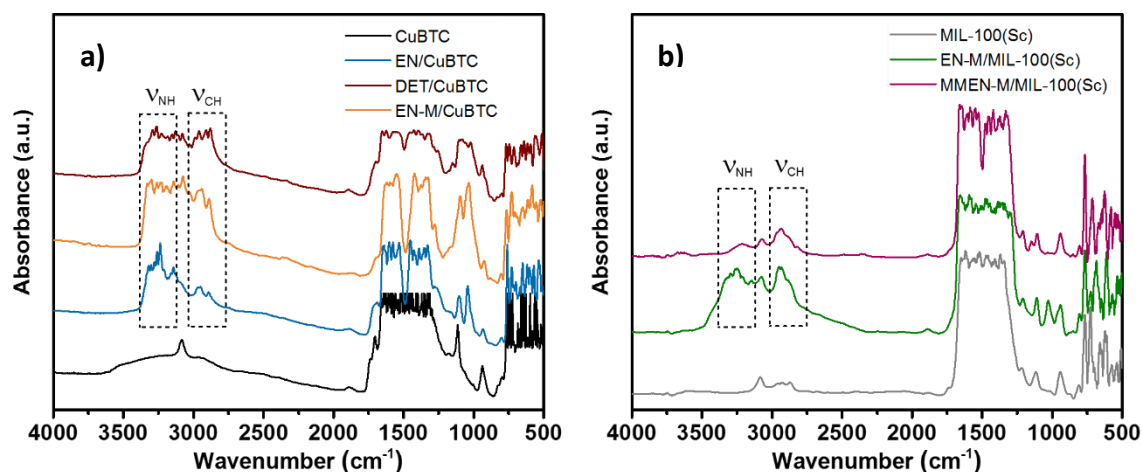


Figure 41. FTIR spectra for amino-grafted a) CuBTC and b) MIL-100(Sc) samples.

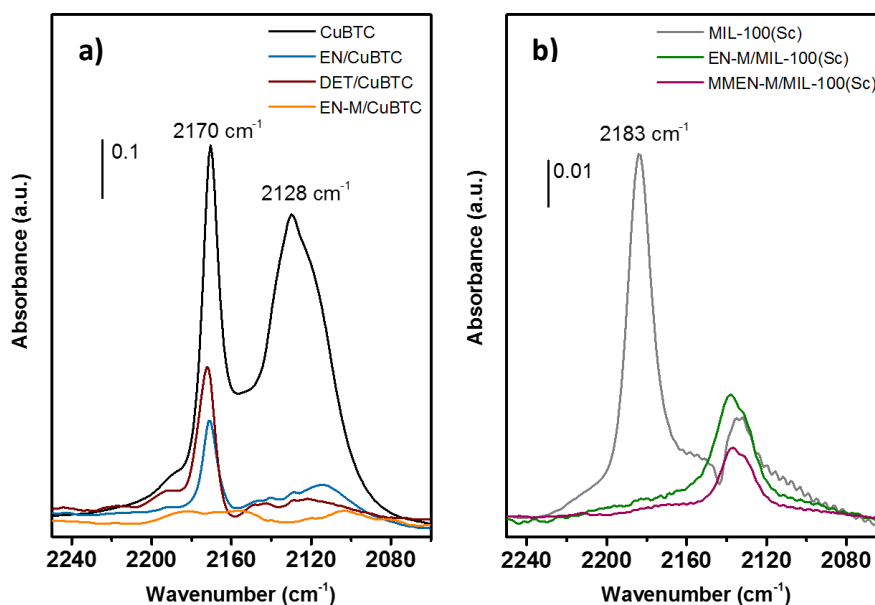


Figure 42. FTIR spectra of CO adsorbed at 100 K on bare and amino-grafted a) CuBTC and b) MIL-100(Sc) samples. IR absorption bands in 2240-2080 cm^{-1} region.

Considering these results, we also carried out elemental analysis of prepared samples confirming the presence of N (**Table 11**). It can be observed remarkable differences between the synthesized catalysts depending on the method used for their functionalization. Assuming that only one $-\text{NH}_2$ group per EN molecule is coordinated to a unique metal centre in the MOF, EN/CuBTC and DET/CuBTC samples showed a N content considerably smaller than the Cu loading, which increases in the case of using a double amount of DET (2DET/CuBTC sample), although still remaining lower than the metal loading. However, in the case of EN-M/CuBTC, the N content is notably higher indicating that part of the EN molecules are coordinated to all available Cu atoms, while the rest are probably interacting with $-\text{CO}_2\text{H}$ defects present in the framework. Therefore, it can be affirmed that the functionalization of the MOFs under study with N-containing ligands strongly depends on the method used. Modification by using the *Method A* produces the total saturation of Coordinatively Unsaturated Metal Sites (CUS), while partially functionalized MOF samples are obtained when applying *Method B*.

Table 11. Composition of the amino-grafted MOFs catalysts under study.

<i>Sample</i>	N^{c} ($\text{mmol}\cdot\text{g}^{-1}$)	Cu^{d} ($\text{mmol}\cdot\text{g}^{-1}$)
EN/CuBTC ^a	0.33	0.45
DET/CuBTC ^a	0.42	0.34
2DET/CuBTC ^a	0.58	0.31
EN-M/CuBTC ^b	1.20	0.29
EN-M/MIL-100(Sc) ^b	0.43	--
MMEN-M/MIL-100(Sc) ^b	0.30	--

Prepared by using the ^a*Method B*, ^b*Method A*. Determined by ^celemental analysis and ^dICP-OES.

These results are supported by the information provided by thermogravimetric analysis. The CuBTC support material showed two different weight losses between 373 K and 453 K, corresponding to the removal of water physically absorbed and coordinated with metal atoms^{269, 270}. After that, the main loss appeared between 573 K and 623 K, attributed to the CuBTC decomposition in BTC ligands, corresponding to the collapse of

MOF structure. EN-M/CuBTC material showed additional peaks, at 473-573 K, probably indicating two types of N interactions (**Figure 43**).

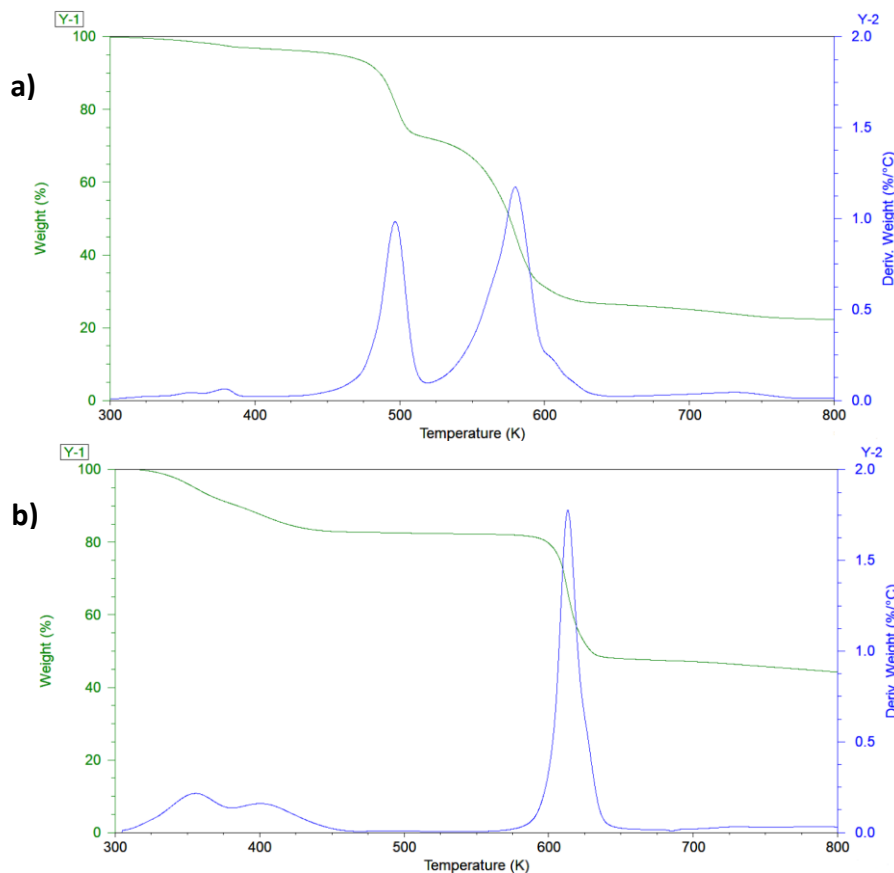


Figure 43. Thermogravimetric profile of a) EN-M/CuBTC sample and b) CuBTC sample.

IV.1.2 Catalytic performance

The amino-grafted MOFs were tested in the synthesis of 2-amino-4*H*-chromenes **1**, from 2-hydroxybenzaldehyde **2** and ethyl cyanoacetate **3**, under solvent-free conditions (**Scheme 9**). Firstly, for comparison, we explored the catalytic performance of the EN-grafted catalysts, at 323 K. It is important to remark that both supports, CuBTC and MIL-100(Sc), resulted totally inactive in this transformation even at high temperatures.

Figure 44 shows the conversion values of 2-hydroxybenzaldehyde **2** to chromenes **1** vs time in the presence of amino-grafted catalysts. It can be observed that the highest conversion values to chromenes **1** —up to 90 % after 2h—, as mixtures of the corresponding diastereoisomers **1a/1b** in approximately 2:1 ratio, are obtained when using EN-M/CuBTC, the non-porous sample presenting the superior amount of EN ligand anchored to CuBTC, as confirmed by FTIR and elemental analysis —%N: 1.20

mmol·g⁻¹— (**Figure 44a**). Considering that an unique -NH₂ function in EN ligand is coordinated to the corresponding metal centre in CuBTC or MIL-100(Sc), as mentioned above, differences in the catalytic behaviour of EN-functionalized samples could be firstly attributed to the presence of available catalytic active sites, comprising free -NH₂ functions—0.60, 0.17 and 0.22 mmol·g⁻¹ for EN-M/CuBTC, EN/CuBTC and EN-M/MIL-100(Sc) respectively (**Table 11**)—. Regarding the porosity of the catalysts, EN/CuBTC and EN-M/MIL-100(Sc) samples present similar V_p —0.23 cm³ g⁻¹—, however, EN/CuBTC sample shows larger S_{BET} —546 vs 444 m²·g⁻¹—, which could be behind the slightly higher conversion values obtained at the shortest reaction times when using this sample (**Figure 44a**, **Table 11**). In the same context, EN-M/CuBTC and EN-M/MIL-100(Sc) catalysts are able to promote the reaction at lower reaction temperature. At 303 K, EN-M/CuBTC affords chromenes **1** in 91% of conversion, after 2h of reaction time, with maintained selectivity towards chromene **1a**, as thermodynamically stable isomer (**Figure 44b**). These results strongly suggest that free-amine functions in the investigated catalysts are the active specie promoting the reaction. In fact, EN/CuBTC sample with the lowest concentration of available amine groups resulted active in the chromene synthesis although reaching the lowest conversions (**Figure 44a**) (see computational section).

We also checked the catalytic behaviour of MOFs modified with amine of different nature, MMEN-M/MIL-100(Sc) and DET/CuBTC (**Figure 44c** and **d**). MMEN-M/MIL-100(Sc), having a similar concentration of N than DET/CuBTC, resulted active in the investigated transformation, at 323 K (**Figure 44c**), yielding the corresponding chromenes **1** in 82%, after 3h of reaction time, the conversion values being notably higher compared to those obtained for EN-M/MIL-100(Sc) (**Figure 44a**). Enhanced catalytic performance observed for MMEN-M/MIL-100(Sc) sample could be attributed to the presence of free secondary amine groups, -NH-CH₃, with increased basicity in comparison with primary amine functions in EN ligand. In the same context, we also tested the DET/CuBTC catalyst, affording chromenes **1** in 78% in only 30 min of reaction time (**Figure 44c**). The same trend was observed when the reaction was carried out at 303 K observing the formation of chromenes **1** with lower conversion as expected (**Figure 44d**). Then these results indicate that the reaction is mainly controlled by the

basicity of the samples. On the other hand, MMEN-M/MIL-100(Sc) shows superior S_{BET} —736 vs 615 $\text{m}^2\cdot\text{g}^{-1}$ — and V_p —0.41 vs 0.24 $\text{cm}^3\cdot\text{g}^{-1}$ — than DET/CuBTC catalyst, therefore, in this case, texture of the catalysts does not seem to influence the catalytic performance.

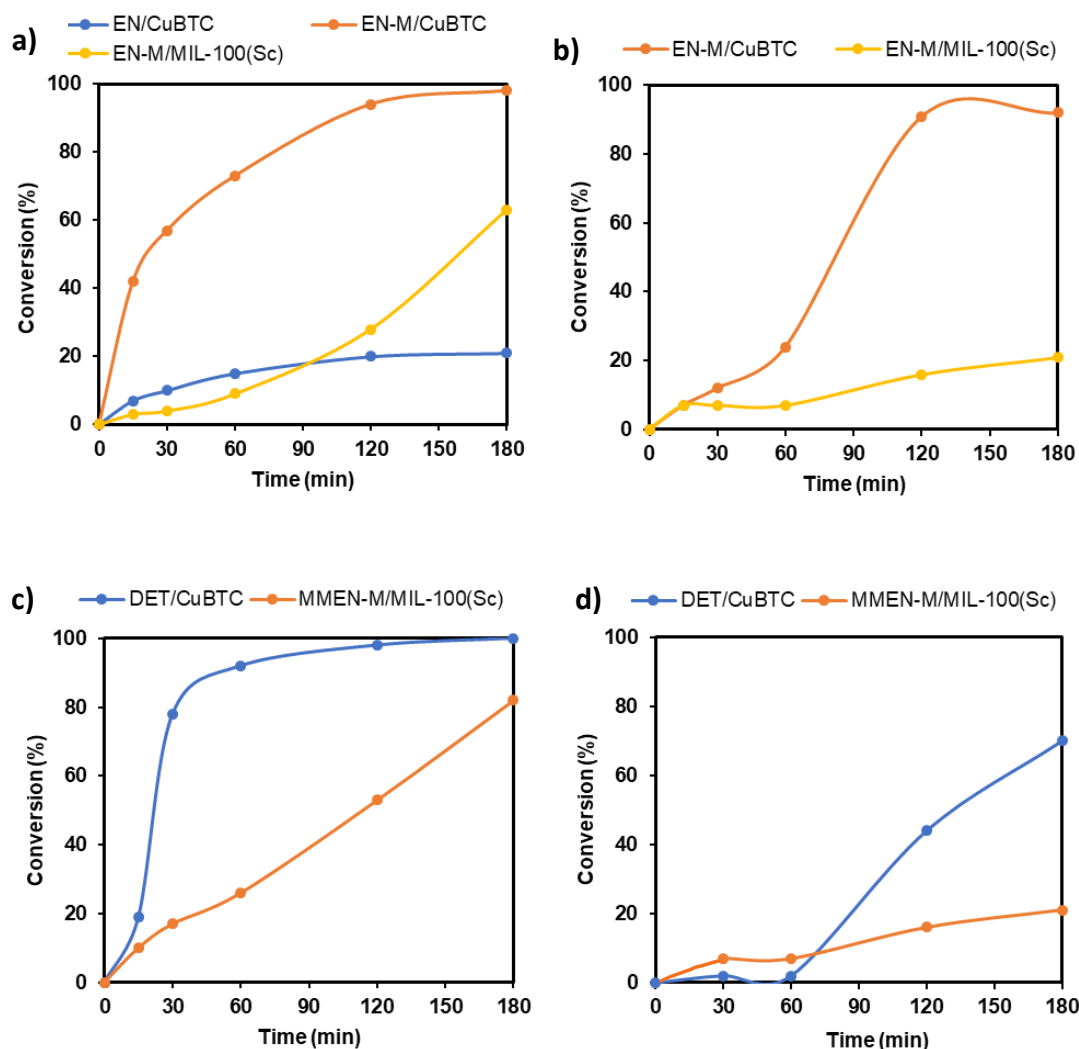


Figure 44. Synthesis of 2-amino-4*H*-chromenes **1**, from 2-hydroxybenzaldehyde **2** and ethyl cyanoacetate **3**, catalysed by a) amino-grafted CuBTC and MIL-100(Sc) at 323 K, b) EN-M/CuBTC and EN-M/MIL-100(Sc) at 303 K, c) DET/CuBTC and MMEN-M/MIL-100(Sc) at 323 K and d) DET/CuBTC and MMEN-M/MIL-100(Sc) at 303 K. Reaction conditions: 25 mg of catalysts, **2/3** molar ratio = 2:4, solvent-free conditions.

Assuming the interaction of DET with Cu centres in CuBTC through one of the terminals $-\text{NH}_2$ groups²⁶⁵, which are sterically less hindered, the secondary amine functions comprising the central N substituted with ethylene bridges in DET should be responsible of the observed reactivity. It is important to note that although the primary and secondary amine functions are able to catalyse the reaction (**Figure 44**) and that

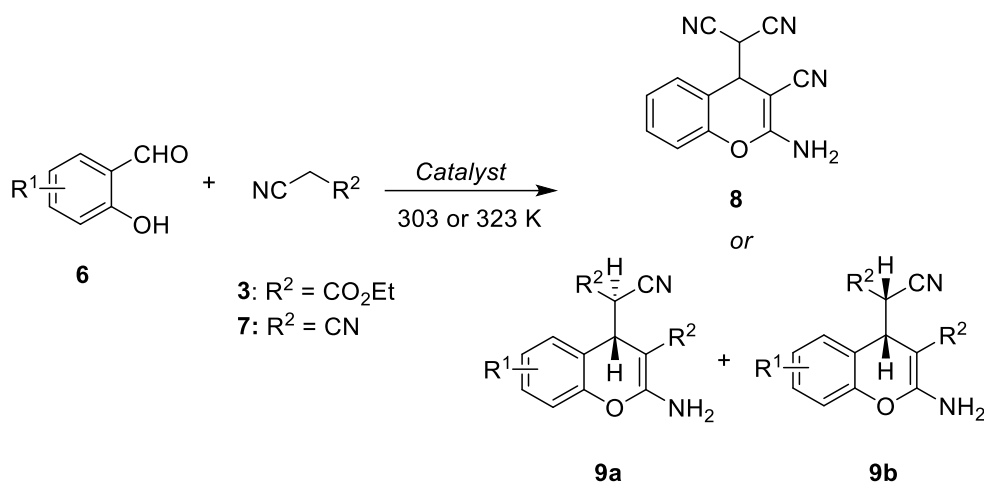
DET/CuBTC shows the presence of both groups, it seems reasonable to think that both cannot independently and simultaneously work. In fact, taken into account that both samples, MMEN-M/MIL-100(Sc) and DET/CuBTC, show similar concentration of available secondary amine groups, additional factors should be behind the extraordinarily high conversion values to chromenes **1** observed when using DET/CuBTC catalyst (see computational section). 2DET/CuBTC sample presenting increased N loading showed a catalytic behaviour quite similar to DET/CuBTC.

Considering all these results, although -NH₂ functions in EN-M/CuBTC or EN-M/MIL-100(Sc) are able to catalyse the reaction yielding the corresponding chromene derivatives, acting as individual active sites, the presence of CUS in EN/CuBTC or DET/CuBTC could suggest that both samples can operate as bifunctional catalysts, in which amine functions and free-metal centres could be responsible for the nucleophile and electrophile activations. This hypothesis is especially relevant when comparing the conversion values observed in the presence of EN-M/CuBTC and DET/CuBTC catalysts. While the reaction catalysed by EN-M/CuBTC, with the highest concentration of amine groups, led to chromene **1** in 57% after 30 min of reaction time, notably superior conversion values (78%, 30 min) were observed in the presence of DET/CuBTC sample.

The influence of the catalyst amount was explored in the reaction by using 2DET/CuBTC sample, observing an increase in conversion values to **1** from 14% —25 mg of the catalyst— to 82% —50 mg of the catalyst—, after only 15 min of reaction time. The same trend was also observed when using another less active catalyst such as MMEN/MIL-100(Sc), affording chromenes **1** in 96% —50 mg of the catalyst— of conversion, after 3h of reaction time, compared to 82% —when using 25 mg of the catalyst— (**Figure 44c**).

The scope of the methodology was investigated by using different substituted 2-hydroxybenzaldehydes **6** but also another cyano compound such as malononitrile **7** (**Table 12, Scheme 13**). In all the cases, chromenes **8** or **9** were selectively synthesized in good-to-excellent yields in the presence of amino-grafted investigated MOFs. Particularly chromene **8** (R¹ = H and R² = CN) was obtained in quantitatively yield in the presence of EN-M/MIL-100(Sc) in only 15 min of reaction time under mild condition (303 K) (**Table 12, entry 2**). Even when using EN/CuBTC, the sample with minor concentration

of -NH₂ functions, the corresponding chromene derivative was obtained in almost 90%, due to the strong reactivity of malononitrile **7** (Table 12 entry 1). The influence of substitution at position 5- in the aromatic ring of 2-hydroxybenzaldehydes **6** was investigated in the presence of the most active catalyst, DET/CuBTC, obtaining, in all the cases, the corresponding chromene derivatives **9** in good-to-excellent conversions (**9a/9b** 2:1 ratio) (Table 12, entries 3-6). The observed reactivity order is as follows: H \approx NO₂ > Br > OMe. It seems then that the presence of electrowithdrawing substituents at position 5- in 2-hydroxybenzaldehyde favours the reaction. Based on our previous studies concerning the use of amino-grafted mesoporous silicas as catalysts involved in the synthesis of coumarins from 2-hydroxybenzaldehyde and ethyl acetoacetate²²⁷, the substitution in 2-hydroxybenzaldehyde affects not only the electrophilicity of -CHO functions but also the acidity of the *para* -OH group. Although the presence of electrodonating substituents on the aromatic ring should favour the first step of the reaction comprising the aldolic reaction between reagents, electrowithdrawing substituents at position 5- produce an increment of acidity of phenol groups probably driving the heterocyclization step, since when R¹ is NO₂ group the reaction takes place even at lower temperatures, affording mixtures of chromenes **9** with increased selectivity to **9a** (**9a/9b** 3:1 ratio). Interestingly, ethyl 2-amino-6-bromo-4-(1-cyano-2-ethoxy-2-oxoethyl)-4*H*-chromene-3-carboxylate **4** (HA 14-1)^{256, 257} which is expressed in most types of cancer, can be efficiently synthesized, as a diastereomeric mixture in a 2:1 ratio, in 90% of conversion after 3h of reaction time (Table 12, entry 4).



Scheme 13. Synthesis of chromenes **8** and **9** from 5-substituted 2-hydroxybenzaldehydes and cyano compounds, at 303 or 323 K, under solvent-free conditions.

Table 12. Synthesis of chromenes **7** and **8** from 2-hydroxybenzaldehydes **6** and cyano compounds **3** or **7** catalysed by amino-grafted CuBTC. Reaction conditions: 25 mg of catalysts, 303 K or 323 K, **6/3** and **6/7** molar ratio = 2:4, solvent-free conditions.

Entry	Catalyst	R ¹	R ²	Temperature (K)	Time (min)	Conversion (%)
1	EN/CuBTC	H	CN	303	15	87
2	EN-M/MIL-100(Sc)	H	CN	303	15	99
3	DET/CuBTC	H	CO ₂ Et	323	60 (120)	92 (98)
4	DET/CuBTC	Br	CO ₂ Et	323	180	87
5	DET/CuBTC	OMe	CO ₂ Et	323	180	52
6	DET/CuBTC	NO ₂	CO ₂ Et	323	60 (120)	84 (99)

Reaction conditions: 2-hydroxybenzaldehyde (2 mmol), cyano compound (4 mmol), catalyst (25 mg).

IV.1.3 Computational study

In order to rationalize the obtained results, the aldolization reaction, as the first elementary step in the synthesis of chromenes **1**, catalysed by amino-grafted CuBTC, was theoretically analysed. Considering previous studies concerning the Friedländer reaction catalysed by CuBTC¹⁷⁷, the reduced models representing CuBTC but also functionalized with the corresponding amines were selected (**Figure 45**). In these models it was observed a slight increment of the Cu-Cu distance in amino-grafted catalysts regarding the bare CuBTC – 2.4746 Å (**Figure 45a**), 2.5575 Å (**Figure 45b**), 2.5570 Å (**Figure 45c**) – the Cu-NH₂ distance maintained in approximately 2.146 Å.

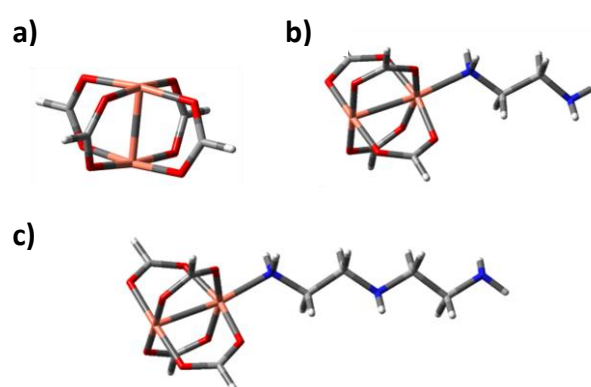


Figure 45. Reduced models simulating a) bare CuBTC, b) EN or EN-M/CuBTC and c) DET/CuBTC catalysts.

Since the reaction is also catalysed by basic species, as experimentally demonstrated, the transition structures for the uncatalysed reaction or in the presence

of bare CuBTC have not been investigated. Having in mind our previous studies analysing amino-grafted mesoporous silicas^{222, 223}, we explored the aldolization reaction between ethyl cyanoacetate **3** and 2-hydroxybenzaldehyde **2**, in which compound **3** is able to donate a proton to amine functions in the catalyst, through *keto* or *enol* forms, this proton subsequently activating the carbonyl acceptor, the –CHO group in compound **2**. Comparing both optimized TS when using the reduced model b or c (**Figure 45**) simulating EN/CuBTC (**Figure 46** and **47**) and DET/CuBTC catalysts (**Figure 46** and **47**), respectively, it can be observed, in both cases, a more advanced TS when ethyl cyanoacetate **3** is involved as *enol* form (**Figure 47**). This was confirmed by computed C-C bond forming distances —2.5499 vs 2.1761 for EN/CuBTC catalyst (**Figure 46a** and **47a**) and 2.6186 vs 2.1274 for DET/CuBTC catalyst (**Figure 46b** and **47b**)—. In the same context, the formation of TS-EN_B (*enol* form, **Figure 47a**) requires lower free energy barrier in 14.10 kcal/mol than TS-EN_A (*keto* form, **Figure 46a**) observing the same trend for TS-DET_B —16.61 kcal/mol more stable than TS-DET_A (**Figure 46b**)—. Both observations suggested that ethyl cyanoacetate **3** reacts with 2-hydroxybenzaldehyde **2** through its *enol* form (**Figure 47**). However, the small free energy differences do not justify the catalytic behaviour observed for both EN/CuBTC and DET/CuBTC catalysts, probably indicating that additional factors could determine the catalytic performance.

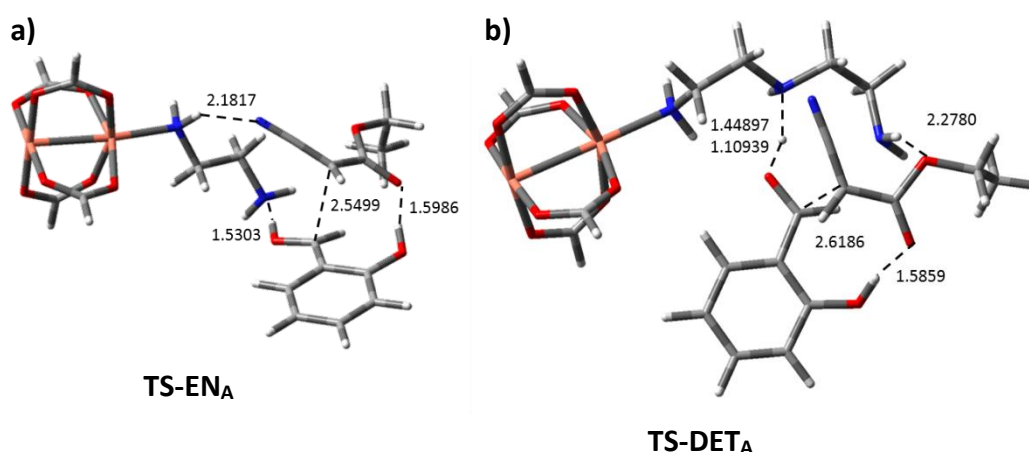


Figure 46. Optimized TS for the aldolization reaction between 2-hydroxybenzaldehyde **2** and ethyl cyanoacetate **3** (*keto* form) catalysed by a) EN/CuBTC and b) DET/CuBTC. Relevant distances are expressed in Å.

Motivated because both catalysts, EN/CuBTC and DET/CuBTC, showed only a few Cu sites grafted with the corresponding amines, the computational and experimental results suggest that amine functions and CUS in these catalysts could act in cooperation.

Investigating this possibility, we firstly analysed the interaction modes of reactants with uncoordinated Cu centres using the reduced model showed in **Figure 46a**. As it can be observed from **Table 13**, the most stable optimized structures comprise the interaction between ethyl cyanoacetate **3** through lone pairs from C=O or C≡N functions with Cu centres showing slight free energy deviation.

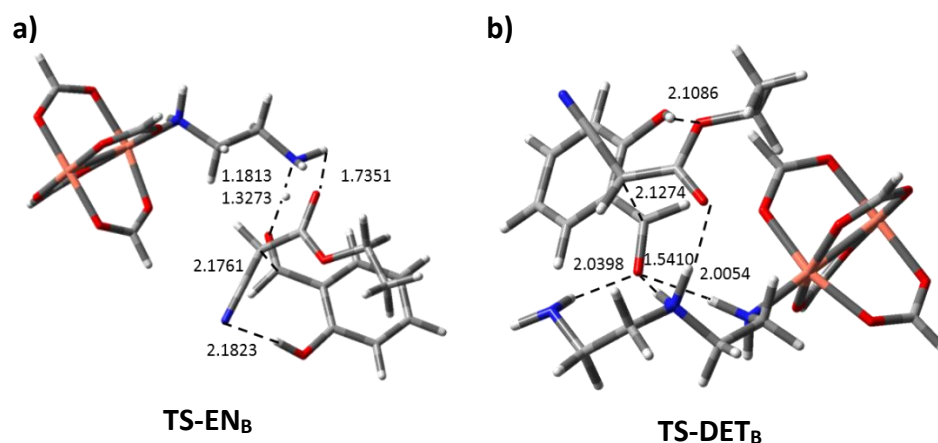


Figure 47. Optimized TS for the aldolization reaction between 2-hydroxybenzaldehyde **2** and ethyl cyanoacetate **3** (*enol* form) catalysed by a) EN/CuBTC and b) DET/CuBTC. Relevant distances are expressed in Å.

Table 13. Interactions of the reagents with metal centres in remaining CUS for amino-grafted CuBTC.

Interactions	Compound	ΔG (Kcal/mol)
Model a (Cu...O=C)	2	5.92
Model a (Cu...O-H)	2	9.04
Model a (Cu...O=C-O)	3	-1.08
Model a (Cu...N≡C)	3	-0.48
Model a (Cu...O-C=O)	3	3.21

In order to prove our hypothesis, we select an extended cluster simulating CuBTC in which one Cu atom is functionalized with amine groups of EN ligand whereas the closest Cu atom is interacting with ethyl cyanoacetate **3** through either C=O (**Figure 48a**) or C≡N groups (**Figure 48b**) as the most stable interactions. Briefly, the computed free energy value for TS-EN(Cu-C=O) were approximately 10 kcal/mol lower compared to TS-EN_A (**Figure 46a**) showing similar interaction modes except for -OH function now forming a strong hydrogen bonding with the CuBTC cluster. However, small free energy barrier, less than 1 kcal/mol, was observed when comparing TS-EN_B (**Figure 47a**) and TS-EN(Cu-C≡N) (**Figure 48b**), TS-EN_B being a more advanced transition structure as demonstrated by C-C bond forming distances —2.1761 vs 2.5418 Å for TS-EN_B and TS-

EN(Cu-C≡N), respectively—. Note that EN-M/CuBTC catalyst showed the absence of unsaturated Cu centres and, therefore, the superior concentration of free -NH₂ functions (**Table 13**) able to promote the reaction, probably acting as individual catalytic sites through TS-EN_B (**Figure 47a**), being this feature behind of its enhanced catalytic performance (**Figure 44a**). In the case of EN/CuBTC catalyst showing a low %Cu centres functionalized with amine groups as experimentally demonstrated, the most probable TS could be TS-EN(Cu-C≡N), acting as a bifunctional catalyst, in which the free amine function in EN is able to abstract a proton of **3**, through its enol form, this proton activating the carbonyl acceptor in 2-hydroxybenzaldehyde **2**, whereas -CN function is interacting with neighbouring unsaturated Cu centre. Thus, low conversion values of **2** obtained in the presence of EN/CuBTC could be attributed to the presence of a lower concentration of -NH₂ active centres in this catalyst but also to the interaction of ethyl cyanoacetate **3** through C=O or C≡N functional groups with bare Cu centres, inhibiting the reaction with the time as experimentally observed (**Figure 44a**).

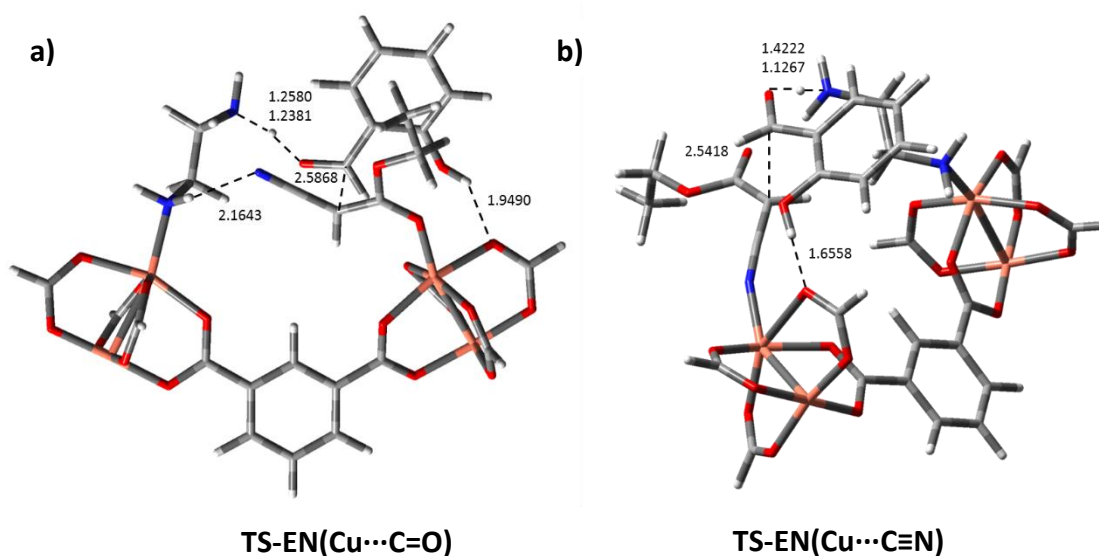


Figure 48. Optimized TS for the aldolization reaction between 2-hydroxybenzaldehyde **2** and ethyl cyanoacetate **3** catalysed by EN/CuBTC. a) Cu...O=C and b) Cu...N≡C interactions. Relevant distances are expressed in Å.

Considering these results, DET/CuBTC could act as a bifunctional catalyst where ethyl cyanoacetate **3** would donate its acidic proton to secondary amine groups whereas simultaneously interacting with neighbouring Cu CUS through -C≡N functions, -NH functions in each amine groups participating in the activation of carbonyl acceptor in 2-hydroxybenzaldehyde **2** as shown in TS-DET_B (**Figure 47b**).

IV.2 CONCLUSIONS

We report herein for the first time a novel family of amino-grafted MOFs able to catalyse the synthesis of 2-amino-4*H*-chromenes **8**, from 2-hydroxybenzaldehydes and cyano compounds, under solvent-free and mild conditions. The catalysts were easily prepared by reacting the corresponding metal-organic network with organic amines, the functionalization of selected MOFs strongly depending on the used method. Our results demonstrate that the catalytic performance is mainly conditioned by the type and concentration of basic sites. It is supported by the catalytic behaviour of EN-M/CuBTC and EN/CuBTC catalysts, being EN-M/CuBTC the most efficient catalyst, which shows a high concentration of basic catalytic sites coordinating each metal centres in CuBTC. In the same context, the presence of secondary amine functions in DET/CuBTC or MMEN-M/MIL-100(Sc) samples favours the reaction. Since the porosity of the samples barely shows any influence on the catalytic performance, the reaction would be then mainly controlled by the basicity of the samples.

Our experimental and theoretical results strongly suggest that available amine groups in EN functionalized catalysts can act either as individual catalytic sites or in cooperation with the nearest CUS in samples partially functionalized, such is the case of EN-M/CuBTC and EN/CuBTC catalyst respectively. In the case of using DET/CuBTC, the additional stabilization of the corresponding transition structure for the aldolization reaction, as the first elementary step in the formation of chromenes, involving strong hydrogen bonding $\text{NH}\cdots\text{O}=\text{C}$ as responsible for the electrophile activation, could be behind of its superior catalytic performance.

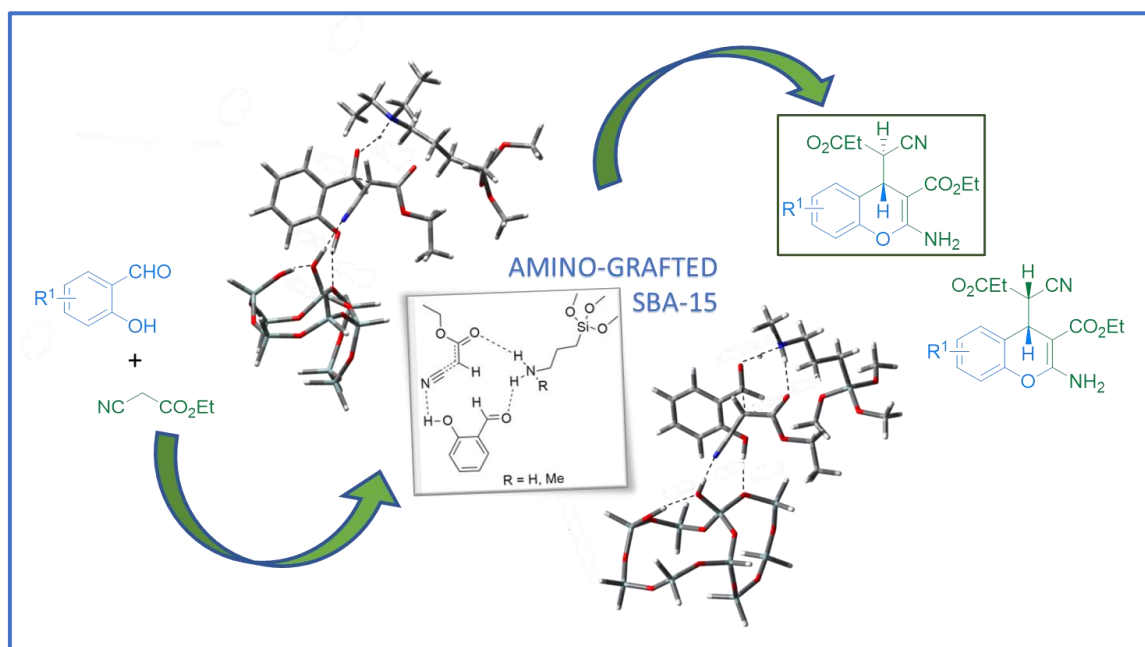
In comparison with the catalysts previously reported, the amino-grafted MOF catalysts allow to obtain the 2-amino-4*H*-chromenes **8** with similar conversion values but using notably less amount of catalyst.

CAPÍTULO V

SÍLICES MESOPOROSAS BÁSICAS EN LA SÍNTESIS VERDE DE 2-AMINO-4H-CROMENOS

CAPÍTULO V. SÍLICES MESOPOROSAS BÁSICAS EN LA SÍNTESIS VERDE DE 2-AMINO-4H-CROMENOS

CHAPTER V. BASIC MESOPOROUS SILICAS IN THE GREEN SYNTHESIS OF 2-AMINO-4H-CHROMENES



ABSTRACT

A new family of amino-grafted mesoporous silica materials active in the synthesis of 2-amino-4H-chromenes **1**, from 2-hydroxybenzaldehydes and cyano compounds, under solvent-free and mild conditions, is reported. The catalysts can be easily prepared by a post-synthetic method, by functionalizing the SBA-15 silica with the corresponding amino silanes. As reported in previous chapters, the obtained results indicate that the catalytic performance is mainly conditioned by the type and concentration of the corresponding basic sites.

The experimental results are also supported with theoretical calculations, which suggest that the rate-limiting step of the reaction, comprising the aldolization reaction between reagents, requires the presence of bases, but also the silica matrix favouring this initial reaction.

V.1 RESULTS AND DISCUSSION

In this chapter, a new family of amino-grafted SBA-15 mesoporous silicas was prepared, characterized and applied to the green and efficient synthesis of 2-amino-4H-chromenes, from 2-hydroxybenzaldehydes **6** and ethyl cyanoacetate **3**, under mild and solvent-free conditions. These materials are easily prepared by functionalization of SBA-15, previously synthesized, with amino silanes showing amine groups of different nature, by using the post-synthetic method, as commented below. Additionally, the mechanism understanding was investigated by using computational methods.

V.1.1 Synthesis and characterization of the catalysts

The mesoporous silica-based catalysts were synthesized by following the experimental procedure previously reported by Zhao *et al*^{181, 271}. SBA-15 mesoporous silica, previously prepared in our laboratory, was functionalized by grafting according to the experimental protocol reported by López-Sanz *et al*²⁷², as described in *Chapter VII (Section VII.3.1)*.

The selected silane compounds used for functionalizing the mesoporous SBA-15 were (3-aminopropyl)triethoxysilane (APTES), [3-(diethylamino)propyl]trimethoxysilane (DEAPTMS), (3-methylaminopropyl)trimethoxysilane (MAPTMS), and [3-(2-aminoethylamino)propyl]trimethoxysilane (2APTMS), then, affording the catalysts denoted as APTES/SBA-15, DEAPTMS/SBA-15, MAPTMS/SBA-15 and 2APTMS/SBA-15, respectively. This type of catalysts has been previously investigated in our research group and tested in the synthesis of coumarins²²³.

All the materials showed a type IVa isotherm accompanied by an H1 hysteresis loop. As expected, the synthesized SBA-15 matrix shows a predominantly mesoporous structure and high surface area (**Figure 49** and **Table 14**). After functionalization, micro- and mesoporosity are notably decreased in all the materials as demonstrated by V_{micro} and V_{meso} (**Table 14**), probably due to a partial blockage of the pores. This also generates a pronounced diminution in surface area from $579 \text{ m}^2 \cdot \text{g}^{-1}$ to $269 \text{ m}^2 \cdot \text{g}^{-1}$ in the case of 2APTMS/SBA-15 sample. The pore diameter is slightly lower with respect to SBA-15 sample in a range of 68 to 57 Å as expected, notably decreased for the materials with higher N content (**Table 14**).

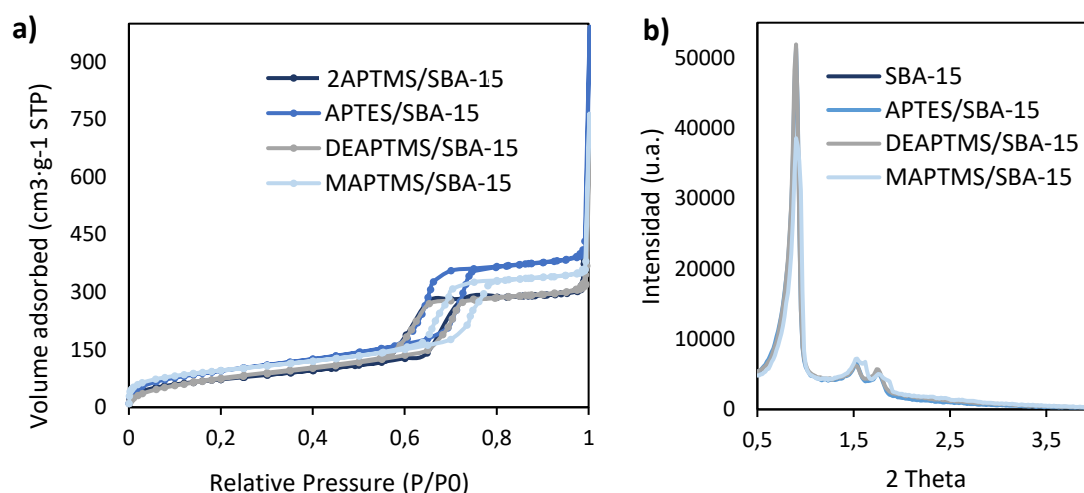


Figure 49. a) Adsorption/desorption isotherms of amino-grafted SBA-15 catalysts. b) XRD patterns for SBA-15 and amino-grafted SBA-15 catalysts.

Table 14. Amount of nitrogen and textural parameters in SBA-15 samples.

Catalyst	BET	($p/p_0 = 0,95$)	Dubinin-Radushkevich		BJH	N loading
	S_{BET} ($\text{m}^2 \cdot \text{g}^{-1}$)	V_{T} ($\text{cm}^3 \cdot \text{g}^{-1}$)	V_{micro} ($\text{cm}^3 \cdot \text{g}^{-1}$)	V_{meso} ($\text{cm}^3 \cdot \text{g}^{-1}$)	D (Å)	($\text{mmol} \cdot \text{g}^{-1}$)
SBA-15	579	0.97	0.04	0.93	68	-
APTES/SBA-15	332	0.63	0.00	0.63	62	2.19
DEAPTMS/SBA-15	271	0.50	0.00	0.50	57	1.72
MAPTMS/SBA-15	326	0.56	0.01	0.55	67	0.42
2APTMS/SBA-15	269	0.47	0.05	0.42	61	2.8

S_{BET} : BET surface, V_{T} : total pore volume, V_{micro} : microporous volume, V_{meso} : mesoporous volume, D (Å): diameter.

The SBA-15 sample is mainly composed of SiO_2 , with minimum traces of C, H, N and S. The results of the elemental analysis for amino functionalized samples confirm the presence of N (**Table 14**). As it can be seen, different concentration of amine groups anchored to the silica surface was observed. The lower content for DEAPTMS/SBA-15 samples would be related to the presence of higher C% in the starting silane by the presence of ET groups. In the same context, the highest N loading for 2APTMS/SBA-15 catalyst is attributed to the presence of primary and secondary amine functions. It is surprising the low concentration of amine groups in MAPTMS/SBA-15 sample. This feature could be due to the interaction of basic amine function with silica matrix by hydrogen bonding inhibiting the grafting processes. These interactions for 2APTMS/SBA-15 and DEAPTMS/SBA-15 samples should be weak because of the presence of bulking substituents.

On the other hand, XRD diffractograms for the SBA-15 matrix and amino-grafted materials showed well-resolved diffraction lines at low angles evidencing the hexagonal structure of the samples (**Figure 49b**).

Samples under study were also investigated through FTIR spectroscopy (**Figure 50**). It was observed the almost total disappeared band at 3745 cm^{-1} , assigned to isolated silanol groups²⁷³, indicating a high functionalization degree for the samples APTES/SBA-15, DEAPTMS/SBA-15 and 2APTMS/SBA-15 (**Figure 50**). It can be an example depicted in **Figure 50a** which shows the comparison between APTES/SBA-15 and SBA-15 matrix. However, MAPTMS/SBA-15 sample showed a lower functionalization degree exhibiting an FTIR profile quite like SBA-15 (**Figure 50b**). All these results are in accordance with compositional data shown in **Table 14**. The broad adsorption band in the range of $3700\text{--}3250\text{ cm}^{-1}$, assigned to Si-OH stretching mode of hydrogen-bonded silanols²⁷⁴, is present in all the explored samples, suggesting the presence of neighbouring silanols at the silica surface. In the case of the samples APTES/SBA-15 and MAPTMS/SBA-15 (**Figure 50a** and **50b**), the bands corresponding to amine groups (1595 cm^{-1})²⁷⁵ indicate the formation of hydrogen bonds between amine functions and silanol groups acting as hydrogen acceptors and donors, respectively. For the 2APTMS/SBA-15 sample additional bands, at 3362 and 3301 cm^{-1} , assigned to asymmetric and symmetric -NH_2 stretch hydrogen bonded amino group were observed as expected²⁷⁶. On the other hand, it was identified the presence of unreacted -OCH_3 groups as demonstrated by the presence of bands at 2973 and 2884 cm^{-1} corresponding to asymmetric and symmetric -CH_3 stretch²⁷⁷.

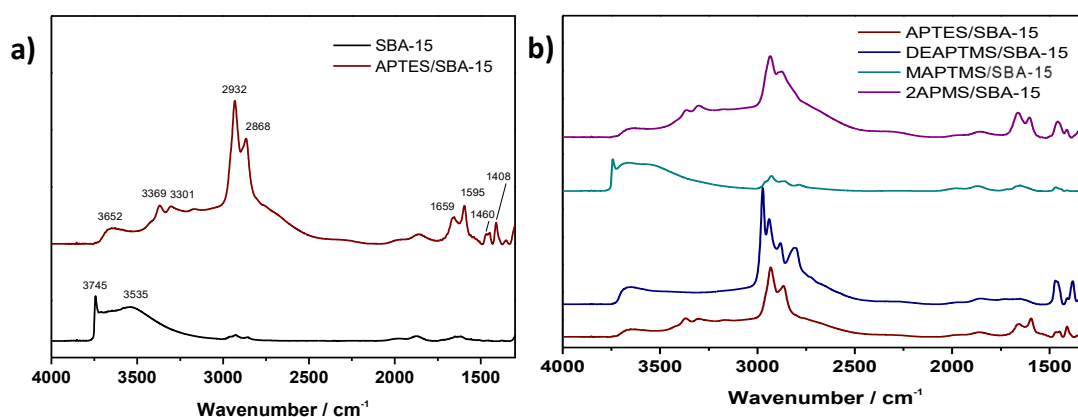


Figure 50. FTIR spectra for amino-grafted SBA-15 samples.

Thermogravimetric analysis of the samples indicated that these materials are thermally stable from room temperature to approximately 473 K. In the case of SBA-15 matrix, it was observed a mass loss lower than 5 % until 373 K, attributed to the removal of physically adsorbed water in pores. For amino-grafted samples additionally, there is a weight loss in the temperature range of 523-773 K because of the decomposition of organic moieties confirming the functionalization at the surface of SBA-15 matrix²⁷⁸. The differences in the mass losses between the catalysts are in good agreement with the elemental analysis results.

V.1.2 Catalytic performance

Subsequently, we study the catalytic behaviour of the investigated materials in the synthesis of 2-amino-4H-chromenes **1**, between 2-hydroxybenzaldehyde **2** and ethyl cyanoacetate **3**, under solvent-free conditions (**Scheme 9**). Based on our previous studies and for comparison purposes, we firstly carried out the reaction at 323 K. All the catalysts led to the corresponding chromene derivatives with conversion values to **1** up to 87 % in only 60 min of reaction time except for APTES/SBA-15 sample, which reached to lower conversions at the shortest reaction times. Note that a pure sample of chromenes **1** was obtained in all cases after 3 h (**Figure 51a**).

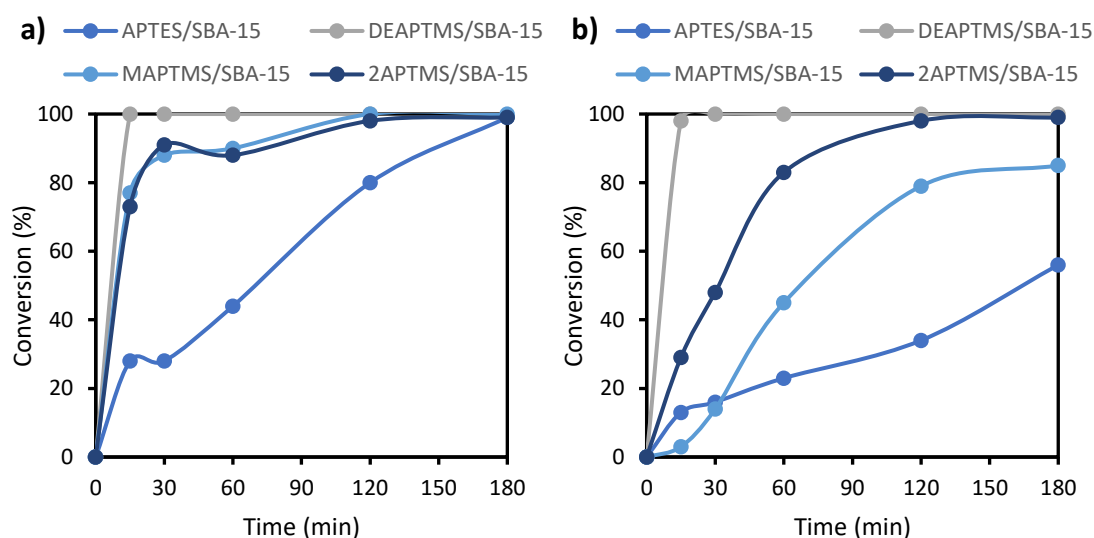


Figure 51. Synthesis of 2-amino-4H-chromenes **1** catalysed by amino-grafted/SBA-15 catalysts at a) 323 K and b) 303 K. Reaction conditions: 25 mg of catalysts, **2/3** molar ratio = 2:4, solvent-free conditions.

It is noteworthy that all the active catalysts provided diastereomeric mixtures of chromenes **1a/1b** in approximately 2:1 ratio, the major compound being the most thermodynamically stable isomer **1a**, as expected. Having in mind these results, it could be thought that the basicity of the catalysts is an important factor to be considered. Taking into account the high conversion values to **1** in the presence of these amino-grafted SBA-15 mesoporous silicas, even at shortest reaction times, and in order to establish differences between catalysts, we explore the catalytic behaviour of those at a lower temperature, 303 K (**Figure 51b**).

In this case, all the catalysts were also active in the synthesis of chromenes **1**, giving the corresponding chromenes with lower conversions, as expected, but showing significant differences. As anticipated, by one side, it was observed that the conversion strongly depends on the basicity of the samples following this reactivity order: APTES/SBA-15 < MAPTMS/SBA-15 < 2APTMS/SBA-15 < DEAPTMS/SBA-15 (see computational section). In general, it is well-known that alkyl-substituted amines behave as stronger bases as their number of substituents increases, due to the inductive effects of alkyl groups on the nitrogen atom²⁷⁹. On the other hand, the catalytic behaviour is also influenced by the N content. In this context, an example to be mentioned is the catalytic behaviour of MAPTMS/SBA-15 sample compared to APTES/SBA-15. In this case, it is observed a clear influence of basicity of the amine groups; while APTES/SBA-15 shows a considerably higher N content (2.19 vs 0.42 mmol·g⁻¹) and similar S_{BET} (~330 m²·g⁻¹) and pore size distribution (**Table 14, Figure 49a**), MAPTMS/SBA-15 exhibited an enhancement of the catalytic performance —45 % of conversion vs 23 % observed for APTES/SBA-15 after only 60 min—. Considering the SBA-15 grafted with secondary amines, MAPTMS/SBA-15 and 2APTMS/SBA-15 samples, and assuming that although 2APTMS/SBA-15 contains primary and secondary amine groups and both functions should not simultaneously work, as already motivated in *Chapter V*, notably available -NH- functions in 2APTMS/SBA-15 are probably behind of the enhanced conversion values observed. The same consideration in combination with the higher basicity of tertiary amine groups can be made for DEAPTMS/SBA-15. Regarding the texture parameters of the samples, it seems that porosity does not influence the catalytic performance probably because the pore sizes of the catalysts, in

all the cases, are large enough to allow the appropriated diffusion of reactants and products. It is important to mention that SBA-15 sample was also tested resulting completely inactive by itself in the synthesis of chromenes **1**, even at the highest temperature (323 K), as expected. Therefore, SBA-15 mesoporous silica acts as a support of active phases, in our case differently substituted amine functions.

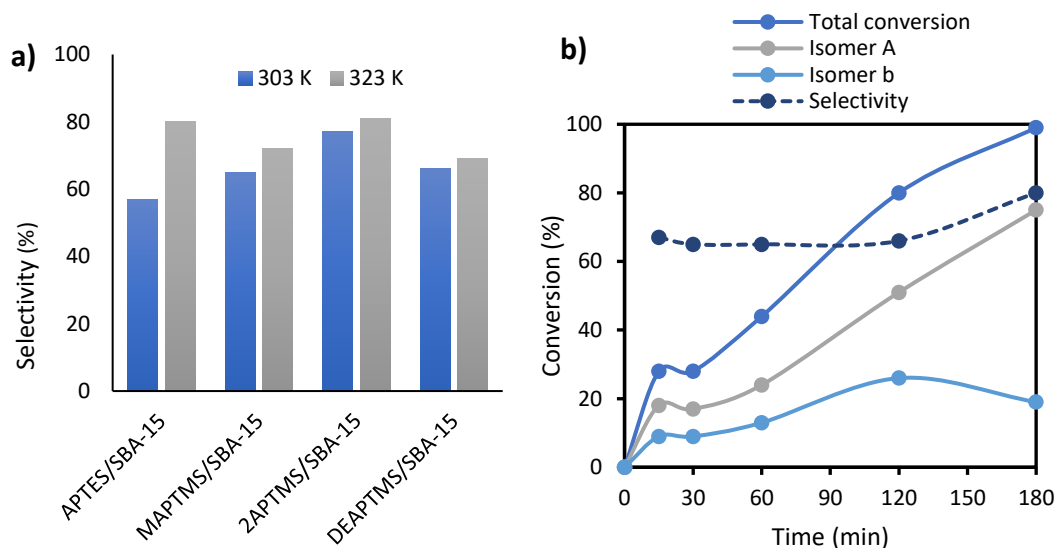


Figure 52. Synthesis of chromenes **1** catalysed by amino-grafted SBA-15 catalysts, a) selectivity after 180 min of reaction time, at 323 and 303 K. b) Conversion values and selectivity variation to isomer **1a** using APTES/SBA-15 as catalyst at 323 K. Reaction conditions: 25 mg of catalysts, **2/3** molar ratio = 2:4, solvent-free conditions.

In all the investigated cases, chromene **1a** was the major isomer, conversion to **1a** being in a range 57-77 % (at 303 K) or 69-81 % (at 323 K) depending on the catalysts and the reaction temperature, both after 3h of reaction time (**Figure 52a**). It can be observed a slightly diminished selectivity to **1a**, at 303 K, compared to that at superior temperature, 323 K. The notable increase in selectivity (80 %) in the presence of APTES/SBA-15 catalyst, at 323 K, could be attributed to epimerization of isomer **1b** to **1a** as previously observed when using other basic metallosilicates⁵⁷. Although selectivity to **1a** increased with the reaction time in all the investigated cases, this effect was considerably enhanced in the presence of APTES/SBA-15 catalyst, at 323 K (**Figure 52b**). In this case, APTES/SBA-15 was the catalyst with the highest S_{BET} ($332 \text{ m}^2 \cdot \text{g}^{-1}$) and V_{meso} ($0.63 \text{ cm}^3 \cdot \text{g}^{-1}$) probably allowing the isomer interconversion (**Table 14**). The superior selectivity to **1a** (81 % at 323 K) when using 2APTMS/SBA-15 ($S_{\text{BET}} = 269 \text{ m}^2 \cdot \text{g}^{-1}$ and $V_{\text{meso}} = 0.42 \text{ cm}^3 \cdot \text{g}^{-1}$) could be then due to some type of confinement effect. Thus, it seems that the diastereoselectivity to **1a** is depending on the texture of the samples, mainly of

the mesoporosity, in such a manner that high diastereoselectivity was observed when using the samples with lower V_{meso} values (**Figure 52b**).

The influence of the catalyst amount in the reaction was also explored by modifying, in this case, the reactant molar ratio but maintaining the catalyst amount at 25 mg. Three experiments were carried out by increasing the reactant amounts (2-hydroxybenzaldehyde **2**/ethyl cyanoacetate **3** ratio (mmol)): a) **2/3** = 2:4, b) **2/3** = 4:8 and c) **2/3** = 6:12. Thus, the amount of the corresponding catalyst was reduced from 3.5 % to 1.7 % and 1.2 % expressed in wt. % regarding total reactant amounts. As it can be observed from **Figure 53**, the conversion values were decreased when increasing the reactant amounts, as expected, most of the catalysts remaining actives (**Figure 53**). Remarkably, DEAPTMS/SBA-15 afforded chromenes **1** with quantitative conversion after 1 h and 2 h when the reactant molar ratio was 4:8, and 6:12, respectively. However, APTES/SBA-15 catalyst was found to be almost inactive when the reactant amount was increased.

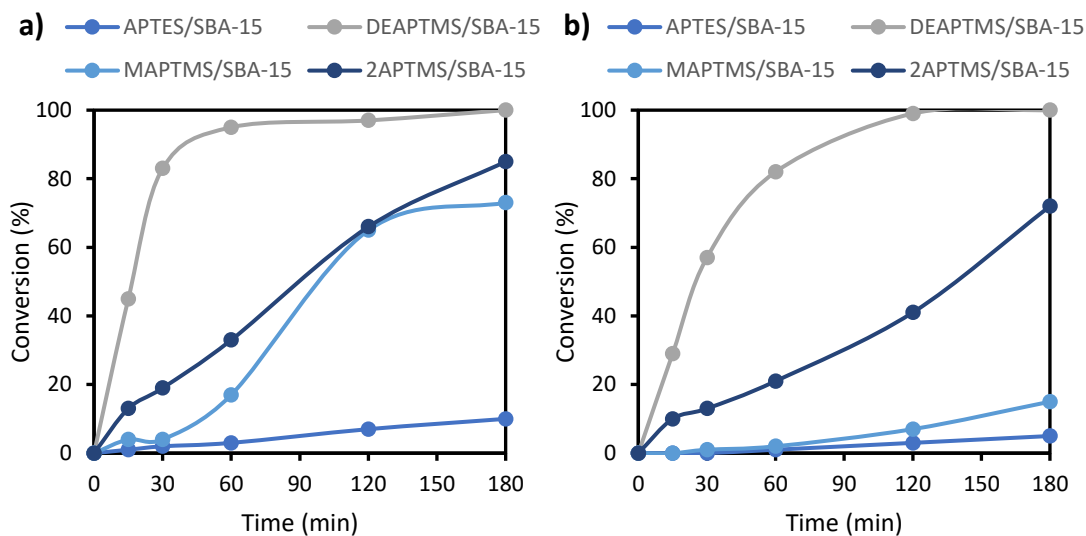
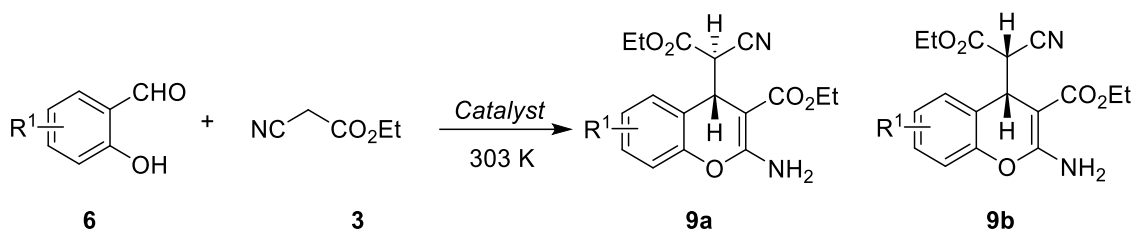


Figure 53. Catalyst amount influence in the synthesis of chromenes **1** catalysed by amino-grafted SBA-15 materials: a) **2/3** molar ratio = 4:8, b) **2/3** molar ratio = 6:12. Reaction conditions: 25 mg of catalysts, 303 K, solvent-free conditions.

Finally, the scope of the reaction was investigated from differently 5-substituted-2-hydroxybenzaldehydes **6** (**Scheme 14**) in the presence of the most efficient catalyst, DEAPTMS/SBA-15, under the same reaction conditions, at 303 K.



Scheme 14. Synthesis of 5-substituted-2-hydroxybenzaldehydes **9** from different 5-substituted-2-hydroxy-aldehydes **6** and **3**, at 303 K, under solvent-free conditions.

The reactivity order of 5-substituted-2-hydroxybenzaldehydes **6** is H > Br > OMe > NO₂ (**Figure 54**). The obtained results show that the 5-substituted chromenes **9** can be easily synthesized with good to excellent conversion values (up 95 % after 1h). Interestingly, the methodology herein reported constitutes a highly efficient alternative for the synthesis of ethyl 2-amino-6-bromo-4-(1-cyano-2-ethoxy-2-oxoethyl)-4H-chromene-3-carboxylate **4** (**HA 14-1**), where R¹ is Br, in 98 % of conversion and 70 % of selectivity to **4a**, as a potential drug to be used in cancer treatment as mentioned in previous chapters.

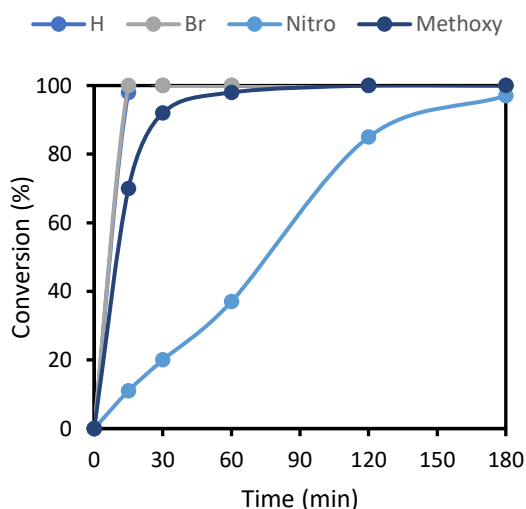


Figure 54. Synthesis of 4H-chromenes **9** by using different 5-substituted-2-hydroxy-aldehydes **5** and ethyl cyanoacetate **3**, catalysed by DEAPTMS/SBA-15. Reaction conditions: 25 mg of catalysts, 303 K, **6/3** molar ratio = 2:4, solvent-free conditions.

It is noteworthy that the presence of substituents on the aromatic ring of **6** modifies the acidity of –OH group but also the electrophilicity of –CHO function influencing the reactivity as demonstrated in previous studies²²³. While the presence of –NO₂ group in 5-substituted-2-hydroxybenzaldehydes **6** increase the acidity of –OH function, –OMe group increases the electrophilicity of –CHO moiety. Both referred

effects should then affect the reactivity affording the corresponding chromenes **9** with increased conversions. In our case, the presence of –OMe and –Br substituents do not significantly affect conversion values regarding unsubstituted 2-hydroxybenzaldehyde **2** (Figure 54). However, in accordance with previous studies reported by some of us the presence of nitro group at 5-position difficulted the reaction leading to chromenes **9** with diminished conversion (37 % after 1h) becoming 97 % after 3h of reaction time. The positive trend observed in this case in comparison with those observed when using amino-grafted MOFs (Chapter IV) could be attributed to the different interaction modes reagents-catalysts.

IV.1.3 Computational study

We also try to rationalize the obtained experimental results through theoretical calculations. Based on our previous studies concerning the mechanistic considerations in the synthesis of 2-amino-4H-chromenes⁵⁶ but also those recently reported by us and discussed in this Thesis Chapter III (Section III.1.3)²⁸⁰, we analysed the first elementary step of the reaction consisting of the aldol condensation between reagents. In this context, we follow two different approaches involving i) only the basic centers of the catalysts comprising the amine functions, then acting as individual catalytic sites, but also ii) analysing the influence of the mesoporous silica as catalyst support, without considering the confinement restrictions if any. To this end, considering the first approach, we select the reduced models shown in Figure 55a studying the catalytic behaviour of amine functions – primary, secondary and tertiary amines –.

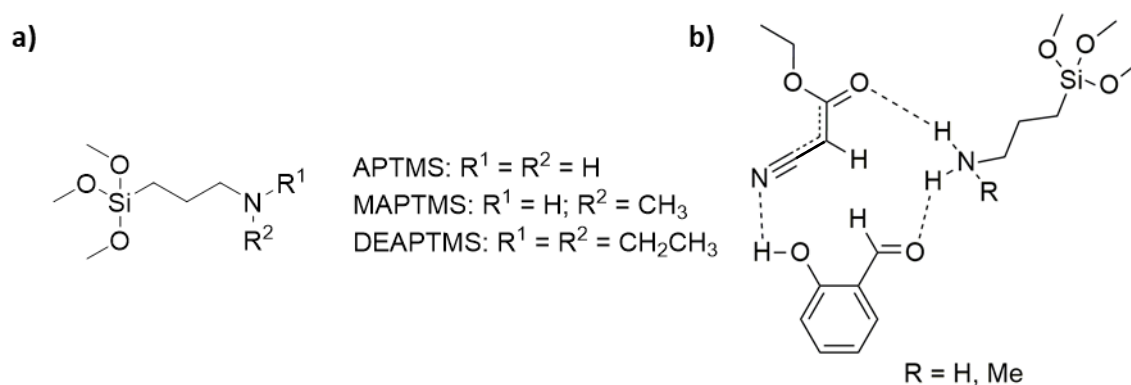


Figure 55. a) Reduced models of amine-based catalysts. b) Reactant complexes indicating the reactants-amine interactions.

Considering the first step of the reaction as the rate-limiting step since it requires the presence of bases, as anticipated in previous chapters, the amine function role is the activation of nucleophile by abstracting the acidic proton in ethyl cyanoacetate **3**. Starting from this hypothesis, we investigated the different possibilities for the reactants-catalyst interactions involving the distinct catalysts concluding that the most probable interactions are those shown in **Figure 55b**. Particularly, in the case of APTMS and MAPTMS catalysts, it was observed the spontaneous formation of the corresponding initial reactant complexes (RC) (**Figure 55b**) with free energy barrier values of -4.8 and -6.7 Kcal/mol respectively, favouring the reactant approach. For **a)** $\text{N}^{\text{C}}\text{-MAPTMS}$ ($\text{R}^2 = \text{Me}$), the acidic proton in **3** was almost total transferred to amine function, confirming the major basic character of MAPTMS regarding APTMS. Thus, a serie of H-migrations occurs from ethyl cyano acetate **3**, as enol form, to amine function which are able to activate the electrophile, in this case 2-hydroxybenzaldehyde **2**, by protonation of the $-\text{CHO}$ group whereas ethyl cyanoacetate **3** interacting with $-\text{OH}$ group in 2-hydroxybenzaldehyde **2** by hydrogen bonding. Note that this possibility is prevented in the case of DEAPTMS. This feature was already reported in our previous studies when investigating the amino-grafted SBA-15 materials as dual acid-base catalysts involved in the synthesis of coumarin derivatives from ethyl acetoacetate²²³.

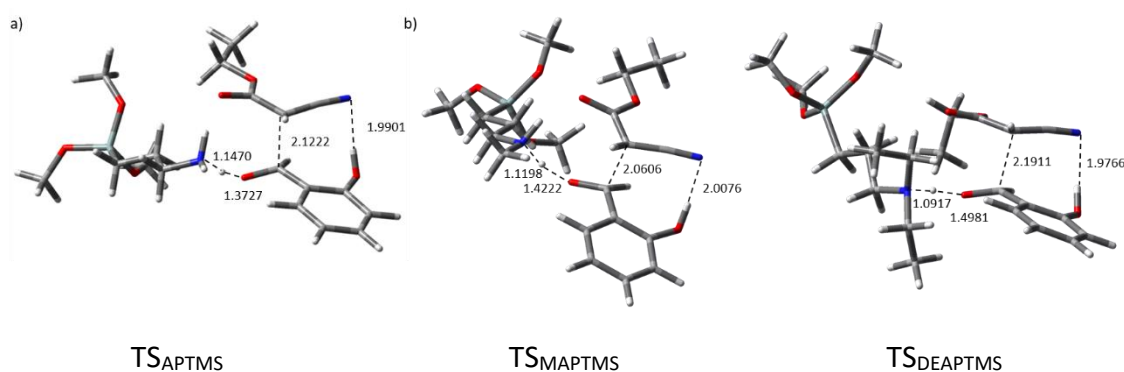


Figure 56. Optimized TS for the aldol reaction between 2-hydroxybenzaldehyde **2** and ethyl cyanoacetate **3** catalyzed by amino-grafted mesoporous silicas when amine function acting as individual catalytic sites: a) TS_{APTMS} , b) $\text{TS}_{\text{MAPTMS}}$, and c) $\text{TS}_{\text{DEAPTMS}}$. Relevant distances are expressed in Å.

The preliminary inspection of the optimized TS for the aldolization reaction catalyzed by amines according to the models of our choice (**Figure 56a**) revealed an increase of the $\text{H}\cdots\text{O}=\text{CH}$ distances depending on the amine nature (**Figure 56**). The marked basic character of MAPTMS and DEAPTMS is in good agreement with larger

H \cdots O=CH distances, 1.4222 and 1.4981 Å, respectively, vs 1.3727 Å observed for TS_{APTMS}. However, the most advanced TS was TS_{MAPTMS} which presented the shortest C-C bond distance (2.0606 Å). The variation of C-C bond distances in TS followed a similar trend than that observed for free-energy values (TS_{DEAPTMS} > TS_{APTMS} > TS_{MAPTMS}) (**Figure 57a**) suggesting that the MAPTMS should exhibit the best catalytic performance. Additionally, we also computed the TS when using diethylamine as a catalyst. The TS_{DIETHYLAMINE} was quite similar to TS_{MAPTMS} (C-C distance of 2.0442 Å) although showing a superior free-energy barrier up to 3.4 Kcal/mol compared to TS_{MAPTMS}. On the other hand, the highest free-energy barrier was observed for TS_{DEAPTMS}, 10.5 Kcal/mol higher than that observed for TS_{MAPTMS}, probably due to steric effects.

These results are in contrast with the observed catalytic performance for the sample functionalized with a tertiary amine, DEAPTMS/SBA-15, which exhibited the best conversion to products after the shortest reaction times. This circumstance could be firstly due to the high concentration of basic catalytic sites as confirmed by N loading determined by elemental analysis (**Table 14**).

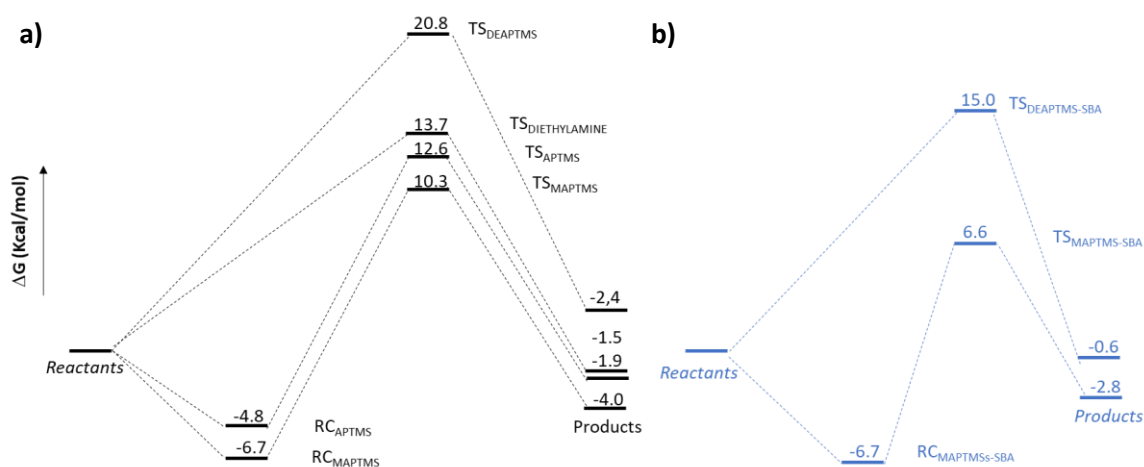


Figure 57. Free-energy profiles for the aldolization reaction between 2-hydroxybenzaldehyde **2** and ethyl cyanoacetate **3** catalyzed by amino-grafted mesoporous silicas. a) Amines as individual catalytic sites. b) Amines with the assistance of the silica matrix.

We also studied the effect of the possible participation of the silica matrix in the reaction. With this aim, we select the structural unit shown in **Figure 58a** as the most suitable model cluster of SBA-15 molecular sieve²⁸¹. In this context, it is in good agreement with the FTIR experiments above reported in which it is commented the presence of associated silanols. Firstly, we studied the possible interactions of ethyl

cyanoacetate **3** with the silica cluster. The computed free-energy values when the cyano group in **3** is interacting with the selected silica model, by hydrogen bonding with the free-hydrogen of silanol, resulted in 3.0 or 3.6 Kcal/mol lower when compared to O- or C=O interactions. Considering these results, we found the optimized TS shown in **Figure 58b-c** maintaining the initial structures suggested above (**Figure 56**), where the amine functions are responsible for the activation of both nucleophile **3** and electrophile **2** at the same time that silica cluster is involved retaining both species by strong hydrogen bondings between cyano group in **3** and silanol, $-C\equiv N\cdots H-O-Si\equiv$, and phenolic hydrogen in **2** with basic centers, $O-H\cdots O\equiv Si$. Taken into account the spontaneous formation of $RC_{MAPTMS-SBA}$, the free-energy barrier of both, $TS_{MAPTMS-SBA}$ and $TS_{DEAPTMS-SBA}$, just differs in 1.7 Kcal/mol lower for $TS_{MAPTMS-SBA}$, but also that $TS_{DEAPTMS-SBA}$ is a more advanced transition state, as deduced from the C-C distance 2.1094 Å vs 2.3020 Å computed for $TS_{MAPTMS-SBA}$. These results are in accordance with the experimental results. Remarkably, the silica participation notably reduces the free-energy values from 20.8 Kcal/mol (**Figure 57a**) to 15 Kcal/mol for $TS_{DEAPTMS}$ and $TS_{DEAPTMS-SBA}$, respectively. Similar energetic differences were also observed for $TS_{MAPTMS-SBA}$. Considering this scenario, it seems that the most probable TS for the aldolization of **2** with **3** is that in which amine functions are behind the observed reactivity but with the assistance of the silica matrix allowing the reactant approach more accused in the case of $TS_{DEAPTMS-SBA}$.

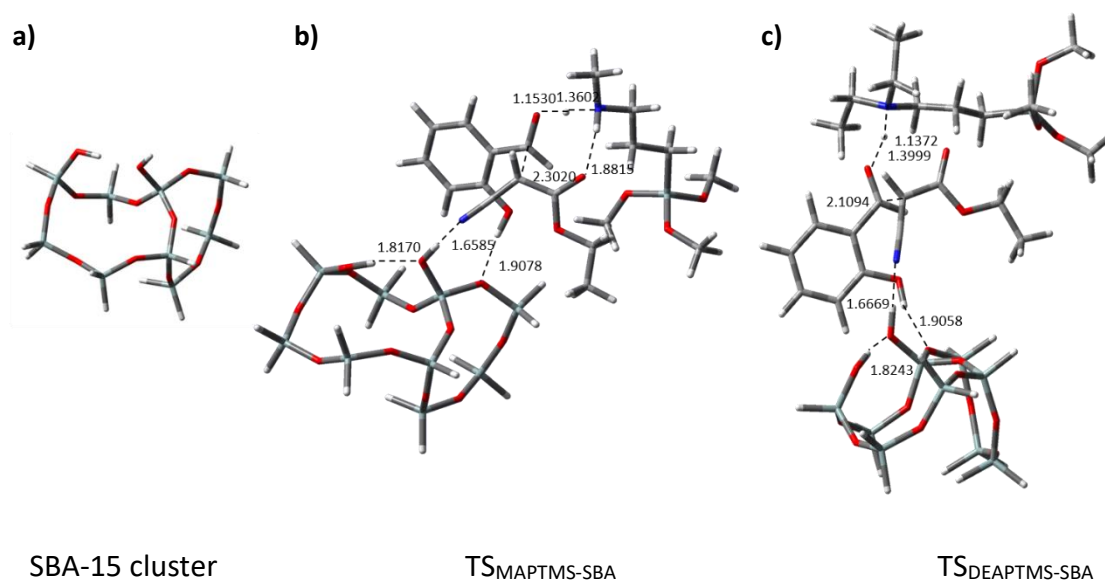


Figure 58. Influence of catalytic support. Optimized TS for the aldol reaction between 2-hydroxybenzaldehyde **2** and ethyl cyanoacetate **3** catalyzed by amino-grafted mesoporous silicas. a) Silica cluster, b) $TS_{MAPTMS-SBA}$, and c) $TS_{DEAPTMS-SBA}$. Relevant distances are expressed in Å.

Based on both experimental and theoretical results, amino-grafted mesoporous silicas can be considered as interesting and more sustainable alternative catalysts, particularly DEAPTMS/SBA-15 sample with a high concentration of active catalytic sites.

V.2 CONCLUSIONS

We report herein a new family of amino-grafted SBA-15 catalysts, useful in the eco-efficient synthesis of 2-amino-4*H*-chromenes **9**, from different 5-substituted 2-hydroxybenzaldehydes and ethyl cyanoacetate, under solvent-free and mild conditions. The catalysts were prepared by a post-synthetic method (grafting), functionalising the silica support with the corresponding aminosilanes.

Our experimental results demonstrate that the catalytic performance mainly depends on the basicity of the catalyst, being DEAPTMS/SBA-15 the most active catalyst, presenting the highest concentration of basic sites.

Our theoretical calculations supported these results. Considering the first step of the reaction as the rate-limiting step since it requires the presence of bases, the amine function role is the activation of nucleophile by abstracting the acidic proton in ethyl cyanoacetate **3**. It was found that the silica support participates in the reaction by reducing the free-energy values of the corresponding optimized TS. It suggests that the most probable TS for the aldolization step is that in which amine functions are behind the observed reactivity but with the assistance of the silica matrix allowing the reactant approach. All these results strongly indicate that the silica matrix acts not only as support of the basic catalytic species, in our case the amine functions, but also contributing to the stabilization of the suggested TS.

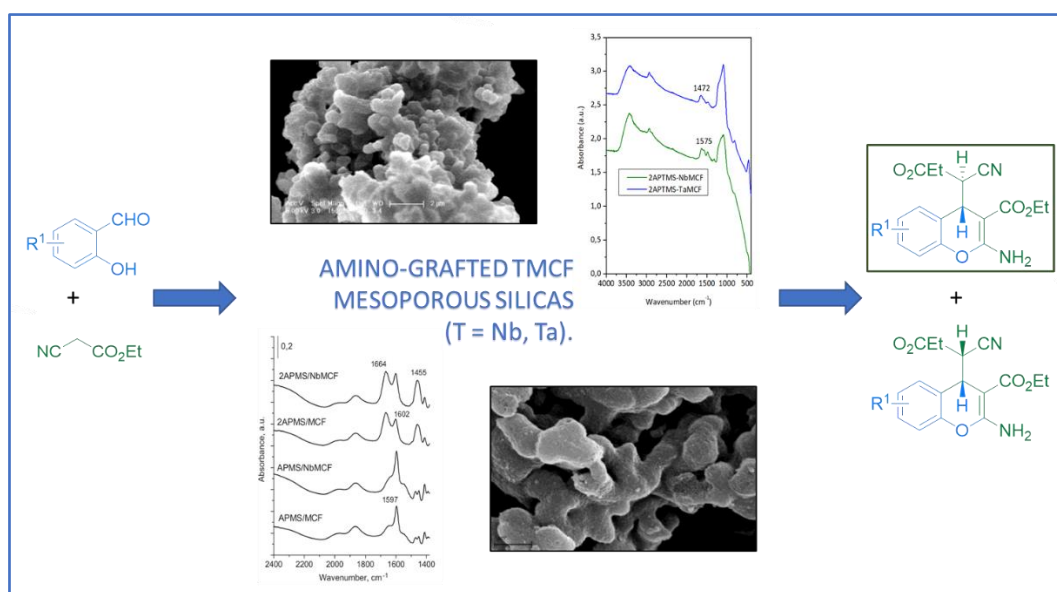
In summary, the amino-grafted SBA-15 catalysts reported in this chapter, particularly DEAPTMS/SBA-15, emerge as an eco-friendly alternative to other basic carbon materials (*Chapter III*) or amino-grafted MOFs (*Chapter V*), previously described, showing notably superior catalytic performance affording the corresponding chromenes with almost quantitative conversion values even at shorter times and using less amount of catalyst.

CAPÍTULO VI

***SÍLICES MESOPOROSAS TMCF (T = Nb, Ta)
FUNCIONALIZADAS CON GRUPOS AMINO. UN
TIPO DE CATALIZADORES ALTAMENTE
EFICIENTES EN LA SÍNTESIS DE 2-AMINO-4H-
CROMENOS***

CAPÍTULO VI. SÍLICES MESOPOROSAS TMCF (T = Nb, Ta) FUNCIONALIZADAS CON GRUPOS AMINO. UN TIPO DE CATALIZADORES ALTAMENTE EFICIENTES EN LA SÍNTESIS DE 2-AMINO-4H-CROMENOS

CHAPTER VI. AMINO-GRAFTED TMCF MESOPOROUS SILICAS (T = Nb, Ta). A TYPE OF HIGHLY PERFORMANT CATALYSTS FOR THE SYNTHESIS OF 2-AMINO-4H-CHROMENES



ABSTRACT

In this chapter, a new family of bifunctional mesoporous silica materials is presented. The synthesis of the materials was carried out from the corresponding TMCF (T = Nb or Ta) mesoporous silicas, previously prepared, by reacting with aminosilanes —3-aminopropyl-trimethoxysilane (APTMS) or 2APTMS—.

These materials are highly efficient and selective catalysts in the 2-amino-4H-chromenes **1** synthesis, operating under mild reaction conditions and without any solvent. These are catalysts more efficient and stereoselective than its analogous modified with metal alkaline oxides, Me/NbMCF (Me = Na or Cs), previously reported in our group, allowing the obtaining of 2-amino-4H-chromenes with excellent yields and at short reaction times, using less catalyst than 2% of total weight.

VI.1 RESULTS AND DISCUSSION

Having in mind the extraordinary catalytic performance observed for the amino-grafted SBA-15 mesoporous silicas in the synthesis of 2-amino-4*H*-chromenes, described in the *Chapter VII (Section VII.3.1)*, but also considering our previous results concerning the use of the metallosilicates as promising bifunctional catalysts active in the synthesis of quinolines, through Friedländer reaction²²¹, and more recently in the preparation of chromene derivatives^{57, 58}, in this chapter we explore the catalytic behaviour of different families of metallosilicates based on MFC mesoporous silicas incorporating or not Nb or Ta in its structure and functionalized with differently substituted amine groups.

VI.1.1 Synthesis and characterization of the catalysts

Firstly, we carried out the preparation of the corresponding mesoporous silicas — MCF¹⁹², NbMCF(*Ox*) and NbMCF(*Et*)⁵⁸ and TaMCF(*Et*)⁵⁷—. The samples marked as *Ox* or *Et* differ in the metallic source used in each synthesis; *Ox* is referred to ammonium niobate(V) oxalate hydrate (C₄H₄NNbO₉) while *Et* means the corresponding metal ethoxide.

Subsequently, the prepared silicas were modified by grafting according to the experimental protocol previously reported by Zhang *et al*²⁸². Then, the samples denoted as APTMS/MCF, 2APTMS/MCF, APTMS/NbMCF(*Ox*), 2APTMS/NbMCF(*Ox*), 2APTMS/NbMCF(*Et*), 2APTMS/TaMCF(*Et*) were synthesized where APTMS is 3-aminopropyl-trimethoxysilane and 2APTMS is [3-(2- aminoethylamino) propyl] trimethoxysilane. In addition, 2APTMS/Cs/NbMCF catalyst was prepared from NbMCF(*Ox*) by treatment with CH₃COOCs. It was carried out by filling the outgassed NbMCF(*Ox*) with an aqueous solution of CH₃COOCs and subsequent functionalization as shown in the corresponding experimental part section.

The catalysts were characterized by several techniques. Textural parameters and N loading of the samples are summarized in **Table 15**.

Table 15. Textural parameters and N content for the samples under study.

Catalizador	BET surface (m ² ·g ⁻¹)	Pore volume (cm ³ ·g ⁻¹) BdB FHH adsorption	Pore diameter (nm) BdB FHH adsorption	N loading (mmol·g ⁻¹)
MCF	626	2.7	35.7	--
APTMS/MCF	338	2.1	34.1	1.31
2APTMS/MCF	309	1.9	33.5	2.34
NbMCF(Ox)	682	2.7	37.2	--
APTMS/NbMCF(Ox)	339	1.9	36.3	0.93
2APTMS/NbMCF(Ox)	328	1.7	32.0	2.72
NbMCF(Et)	717	2.8	27.9	--
2APTMS/NbMCF(Et)	266	1.4	20.5	4.43
TaMCF	556	2.1	17.9	--
2APTMS/TaMCF(Et)	61	0.2	17.3	4.05

As it can be seen from **Table 15**, unmodified mesoporous silica exhibited high S_{BET} in a range of 556-717 m²·g⁻¹ and pore volumes between 2.1 and 2.8 cm³·g⁻¹. As previously reported and cited above, the N₂ adsorption/desorption isotherms of MCF and TMCF supports are typical of mesostructured cellular foams exhibiting an H1 type hysteresis loop at relatively high pressure (p/p^0) with parallel adsorption and desorption branches¹⁹². As an example, the isotherm for TaMCF sample is shown in **Figure 59a**. It is important to note that the inclusion of Nb into MFC structure increased S_{BET} and the pore volume. Regarding the composition of the samples, the loading of Nb and Ta are expressed as Si/Nb and Si/Ta ratios determined by XRF. In general, the loading of Nb in NbMCF (Si/Nb ratio = 260 and 169 for NbMCF(Ox) and NbMCF(Et), respectively) is lower than the assumed one (Si/Nb ratio = 260) whereas Ta content is notably higher (Si/Ta ratio = 96)^{57, 58}. It is in accordance with literature data, describing that the introduction of Nb into the framework of molecular sieves is more difficult than in the case of Ta affording materials with low Nb concentration^{283, 284}. In all the cases, the functionalization of the different mesoporous MCF materials notably reduced the S_{BET} the pore volume and pore diameter, as expected, probably due to a partial collapse of the structure and also a partial block of the channels. This reduction is notably lower in

the case of the 2APTMS/TaMCF(Et) sample (61 vs 266-339 $\text{m}^2\cdot\text{g}^{-1}$) (**Figure 59b** and **Table 15**).

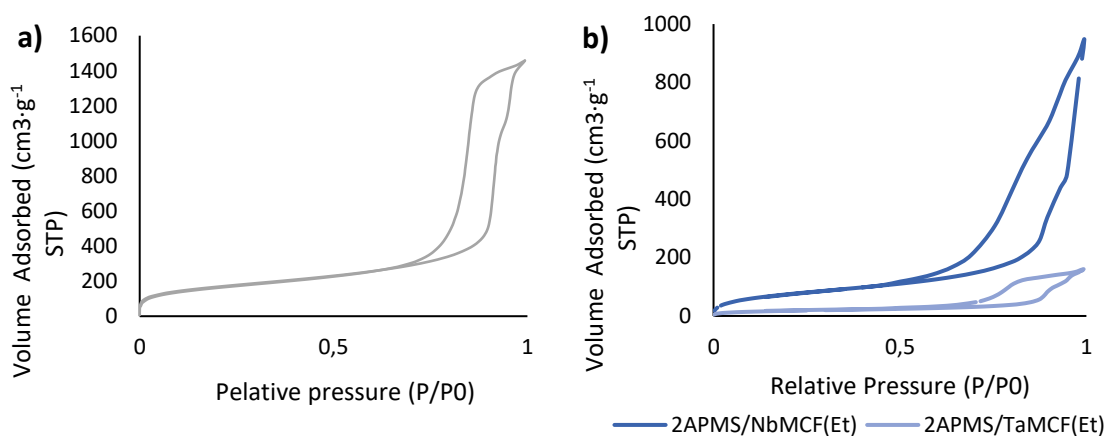


Figure 59. Adsorption/desorption isotherms of a) TaMCF(Et), b) 2APTMS/NbMCF(Et) and 2APTMS/TaMCF(Et) catalysts.

Analysing the compositional data obtained from elemental analysis (**Table 15**), both MCF and NbMCF(Ox) samples showed similar functionalization degree whereas TMCF(Et) (where T is Nb or Ta) present considerably higher concentration of amine groups, these results in good agreement with the notably S_{BET} diminution, particularly for 2APTMS/TaMCF ($61 \text{ m}^2\cdot\text{g}^{-1}$).

Thermogravimetry/Differential Thermal Analysis (TG/DTA) was carried out to confirm the grafting on MCF samples and to study the thermal stability of the samples. **Figure 60** shows as examples the TG/DTA curves, recorded under air atmosphere, for 2APTMS/TaMCF(Et) and 2APTMS/NbMCF(Et) samples. Weight loss in the range of 400-900 K is related to the removal of 2APTMS²⁸⁵. DTA curves of 2APTMS/NbMCF and 2APTMS/TaMCF catalysts have two exothermic peaks at this range. The first signal, near to 500 K, is assigned to the removal of terminal amine groups NH_2 . The second one, at approximately 600 K in 2APTMS/NbMCF and 700 K for 2APTMS/TaMCF, is assigned to the removal of secondary amine groups. It is noteworthy that the stability of $-\text{NH}_2$ groups is similar in all the materials and it does not depend on the nature of support, whereas the stability of NH groups in 2APTMS loaded on TaMCF is higher than those anchored at NbMCF surface. Moreover, it should be remarked that for the 2APTMS/NbMCF(Et) sample one endothermic effect, at approximately 350 K, is clearly observed in DTA curve, attributed to the water desorption which was not observed for

two other samples. This effect is accompanied by a mass loss observed in the thermogravimetric curve and should be attributed to a different hydrophilic/hydrophobic character of both samples.

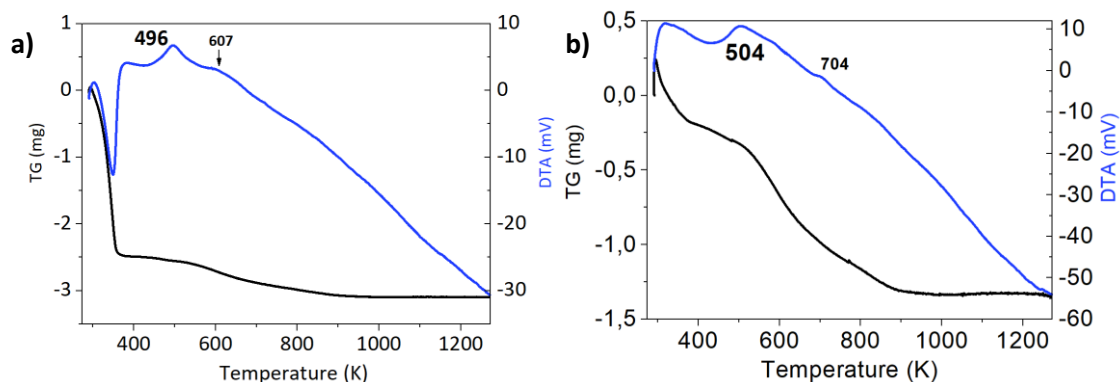


Figure 60. TG/DTA curves for a) 2APTMS/NbMCF(Et), and b) 2APTMS/TaMCF(Et). Curves normalized to 5 mg of the sample.

The referred samples were also characterized by FT-IR spectroscopy in order to confirm the presence of amino and methoxy groups in the investigated materials. Spectra of MCF, TaMCF(Et) and NbMCF(Et) supports show the bands characteristic of Si-O-Si vibrations in silica —1240, 1090, 800 and 460 cm^{-1} — (**Figure 61a**). Moreover, for MCF sample the band from isolated silanol groups, Si-OH, is observed at 3740 cm^{-1} .

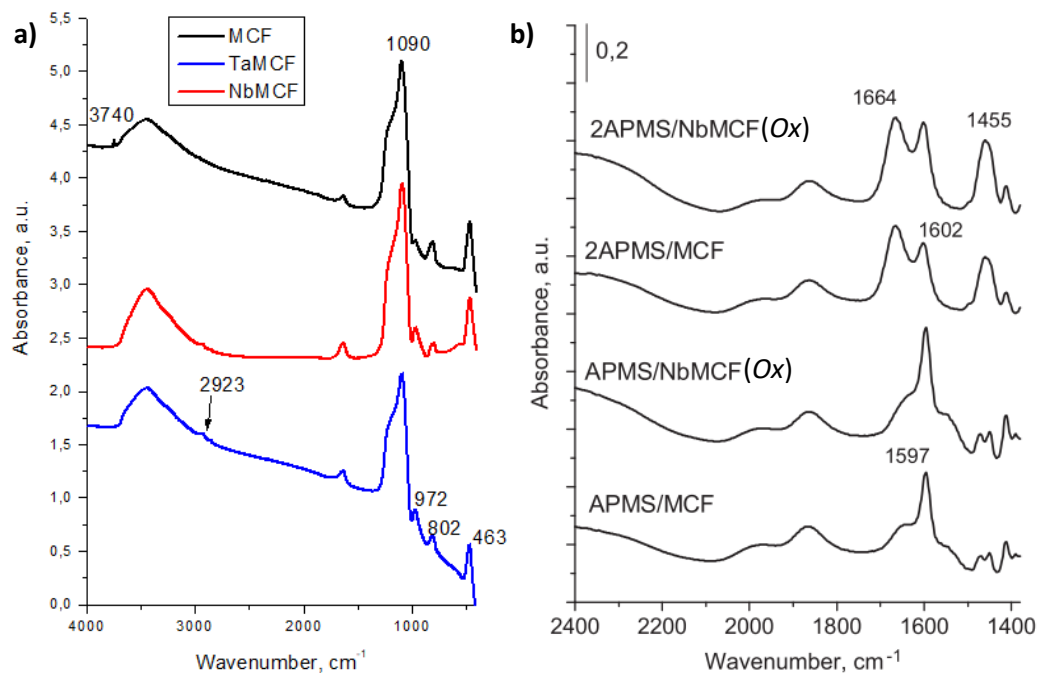


Figure 61. FTIR spectra of a) MCF supports and b) MCF and NbMCF(Ox) materials after evacuation at 373 K²²².

The grafting of organosilanes is produced by the interaction between silanol hydroxyl groups, provided by the support, and alkoxy groups from the silane molecules. In the case of MCF and NbMCF(Ox) catalysts, the IR spectra (**Figure 61b**) suggest, as previously reported Smuszkiewicz *et al*²²², the presence of methoxy species —band at 1455 cm^{-1} — in the catalysts functionalized with 2APTMS, it indicating the presence of free methoxy groups not anchored to the silica surface. However, in APTMS materials most of the methoxy species are bonded to the surface of the mesoporous support. The bands present in all the catalysts at approximately 1600 cm^{-1} are due to the primary amines, and the other one at 1660 cm^{-1} , which only appears in 2APTMS catalysts, is assigned to the secondary amines.

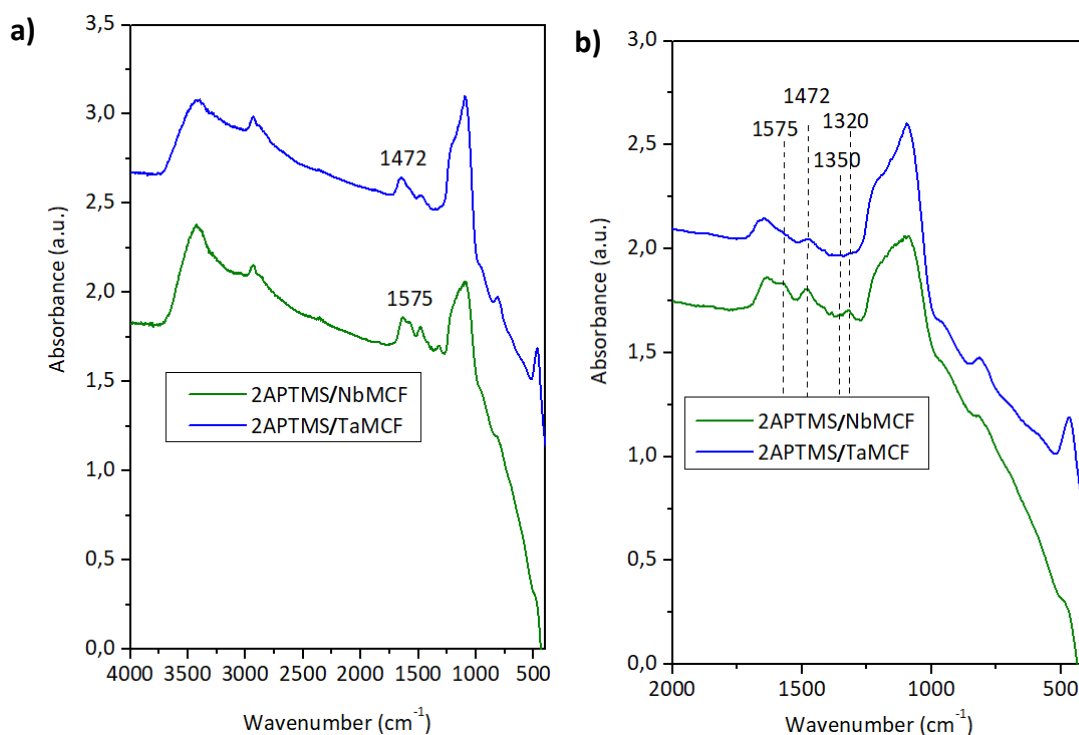


Figure 62. FTIR spectra of 2APTMS/NbMCF(Et) and 2APTMS/TaMCF(Et) after evacuation at 373 K: a) from 500 cm^{-1} until 4000 cm^{-1} and b) from 500 cm^{-1} until 2000 cm^{-1} .

IR spectra of NbMCF(Et) and TaMCF(Et) modified samples proved the 2APTMS loading. All spectra show the bands assigned to C–H stretching vibrations at 2933 cm^{-1} , and to C–H bending vibrations at 1472 cm^{-1} and 1350 cm^{-1} ($1472\text{-}\delta_{\text{as}}(\text{CH}_3)$ vibrational mode in methoxy groups, $1350\text{-}\delta_{\text{s}}(\text{CH}_3)$ vibrational mode in methoxy groups^{286, 287} (**Figure 62**). Moreover, the band at 1575 cm^{-1} coming from N–H vibrations is visible, being this band the most pronounced for 2APTMS/NbMCF(Et), as the sample with the

highest N loading. All bands indicated above come from (aminoethylamino)propyl anchored on the surface of mesoporous support.

The metal coordination in NbMCF(Ox), NbMCF(Et) and TaMCF(Et) catalysts modified with 2APTMS was studied by UV-Vis spectroscopy (**Figure 63**). The UV-Vis spectrum of NbMCF shows the presence of two UV bands at 230 and 270 nm. The first band corresponds to a charge transfer in tetrahedrally coordinated niobium species located in a silica skeleton^{288, 289}. The second band should be assigned to pentacoordinated niobium species located in the silica framework as was previously reported by Tranca *et al*²⁹⁰. The presence of an octahedral niobium species in NbMCF is suggested by the presence of a signal at 300 nm. In the spectra of 2APTMS-NbMCF the band at 270 nm is not observed due to the interactions between Nb-OH and APTMS. Moreover, the band at 340 nm is more pronounced, because of the presence of extra niobium framework.

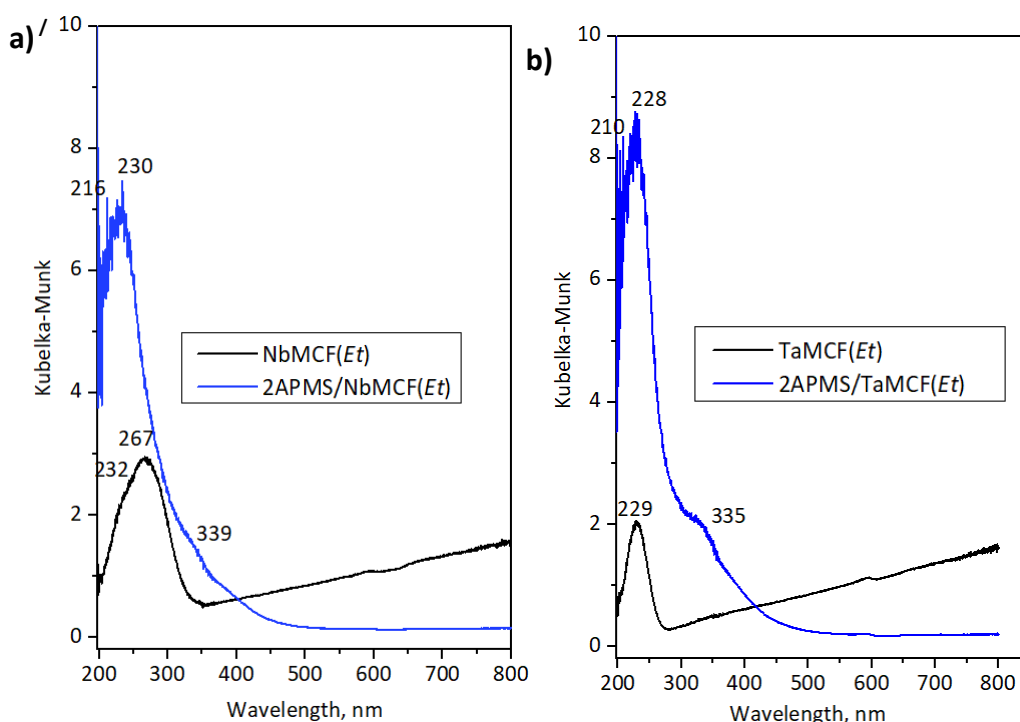


Figure 63. UV-Vis spectra of a) NbMCF(Et) and b) TaMCF(Et) catalysts dried at 373 K.

The UV-vis spectrum of TaMCF(Et) shows the symmetric band at 230 nm typically associated with tetracoordinated Ta species. After the modification with 2APTMS, in 2APTMS/TaMCF(Et) sample, this band becomes wider. Moreover, low intensity band at 330-350 nm appears, which indicates the presence of octahedral tantalum species in

TaMCF(Et) after modification, due to the removal of tantalum from the framework during the modification with APTMS or due to a probable coordination of Ta atoms in the structure with the silane molecules.

The morphology of the materials was also investigated by SEM and TEM microscopy. All the observed MCF catalysts showed coral-type morphology in the SEM microphotographs (**Figure 64**). The TEM images suggested the typical MCF strutlike structure, regular structure in cellular foams²²².

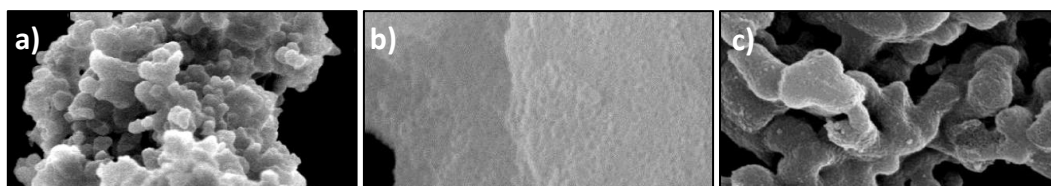


Figure 64. SEM images from a) MCF, b) NbMCF(Ox) and c) 2APTMS/NbMCF(Ox).

VI.1.2 Catalytic performance

The catalytic behaviour of the synthesized mesoporous silicas was checked in the synthesis of 2-amino-4H-chromenes **1**, between 2-hydroxybenzaldehyde **2** and ethyl cyanoacetate **3**, under mild and solvent-free conditions, at 323 K, for comparison purposes (**Scheme 9**). Obviously, the investigated silica supports tested under these experimental conditions have not shown any catalytic activity, as expected.

In **Figure 65** it is depicted the conversion values to chromenes **1**, at 323 K, vs time. All the catalysts led to chromenes **1** as diastereomeric mixtures, in approximately 2:1 ratio, compound **1a** being the major diastereomer as expected. Among the most efficient catalysts highlight 2APTMS/MCF and 2APTMS/NbMCF(Ox), reaching almost quantitative conversion values at short reaction times (30 min) (**Figure 65a**). Remarkably, these catalysts show similar amine functions —primary and secondary amine groups—, textural parameters and N loading. However, it is clear the influence of the presence of Nb in APTMS catalysts affording the corresponding chromenes with conversion up to 87% after 2h. Remarkably, differences were barely observed in the presence of APTMS/Nb(Cs)MCF, prepared from NbMCF by exchange with Cs salt solution and subsequent functionalization with the corresponding silane as previously reported⁵⁸. The results obtained when using APTMS/MCF catalyst then strongly suggest

that the nature of amine functions together with the presence of Nb in materials under study conditioned the catalytic performance.

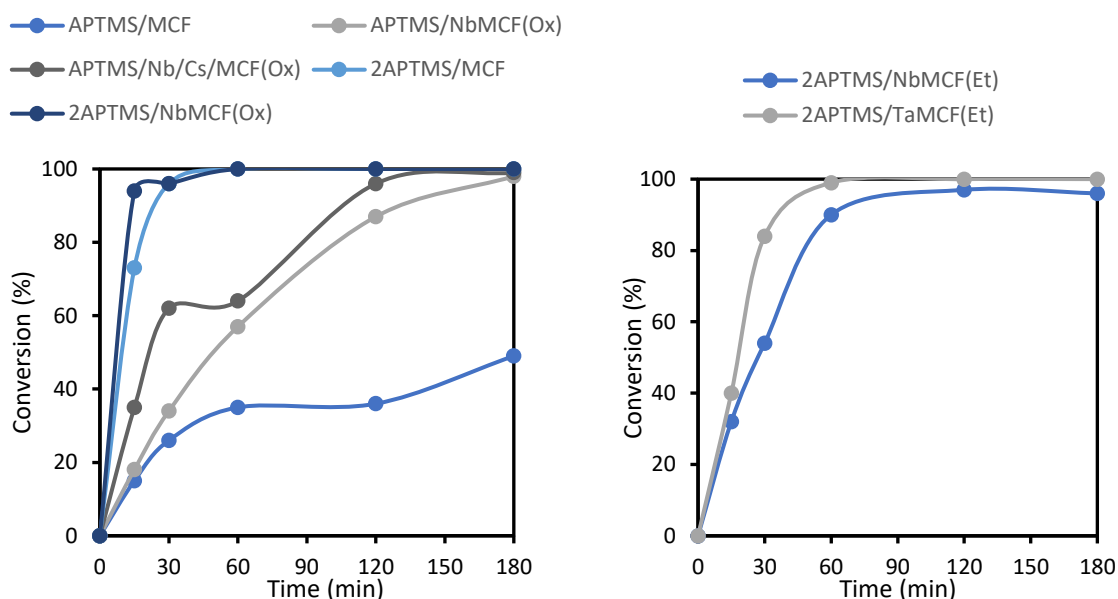


Figure 65. Synthesis of 2-amino-4H-chromenes **1**, catalysed by a) amino-grafted MCF and NbMCF(Ox), and b) amino-grafted NbMCF(Et) and TaMCF(Et) catalysts. Reaction conditions: 25 mg of catalysts, 323 K, 2:4, **2/3** molar ratio = 2:4, solvent-free conditions.

We also checked the catalytic behaviour of samples of the *Et* serie, 2APTMS/NbMCF(*Et*) and 2APTMS/TaMCF(*Et*), in this case observing a notable enhancement of conversion to **1** in the presence of 2APTMS/TaMCF(*Et*) at short reaction times (54% vs 84% after 30 min). It should be reasonable to think that a superior concentration of amine functions available to interact the reactants or intermediate species should enhance the conversion to **1**. However, if we compare the reactivity of 2APTMS/NbMCF catalysts, *Ox* or *Et*, the 2APTMS/NbMCF(*Ox*) sample showing lower N loading (2.71 vs 4.43 mmol·g⁻¹) and notably higher Si/Nb (260 vs 169) reached significant higher conversion values to **1** (96% vs 54 % after 30 min) (**Figure 65b**). This enhanced catalytic performance could be then attributed to its higher S_{BET} ($V_{\text{meso}} = 1.7$ vs 1.4 cm³·g⁻¹ and diameter = 32 vs 20.5 nm) which allow the fast and efficient diffusion of reactant and products (**Table 15**). All these results indicate that these amino-grafted NbMCF samples can act as bifunctional catalysts as previously reported for the quinoline synthesis through Friedländer reaction²²¹. In the case of the catalyst 2APTMS/TaMCF(*Et*) the almost absence of porosity and the high concentration of amine functions suggest

that the organic groups are probably located in the open mouth of the pores acting as individual catalytic active sites.

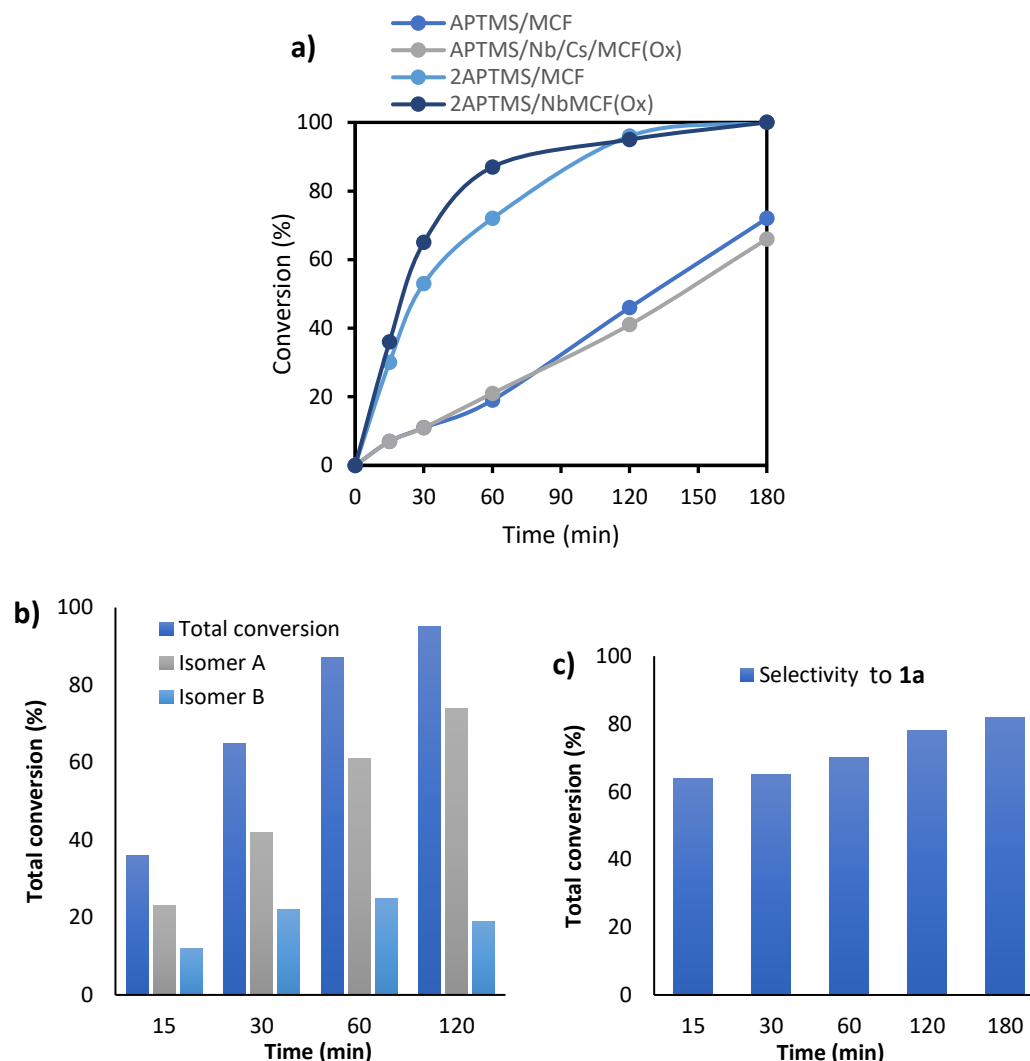


Figure 66. Synthesis of 2-amino-4H-chromenes **1** a) catalysed by MCF and NbMCF(Ox) catalysts. b) Conversion of **1a** and **1b** and c) selectivity to **1a** catalysed by 2APTMS/NbMCF(Ox). Reaction conditions: 25 mg of catalysts, 303 K, $2/3$ molar ratio = 2:4, solvent-free conditions.

In order to establish possible differences between the most efficient samples, 2APTMS/MCF and 2APTMS/NbMCF(Ox), the reaction was investigated at a lower temperature (303 K) (**Figure 66**). All the catalysts remained active, chromenes **1** being obtained in around 40% of conversion, after 2h, when using the APTMS samples. Remarkably, both APTMS catalysts reached conversion values close to 70 % after 180 min. In the case of 2APTMS catalysts, it was observed a slight enhancement of conversion values (65% vs 53% after 30 min) for the 2APTMS/NbMCF(Ox) sample attributed to the incorporation of Nb in silica network, as expected. Both samples led to

chromenes **1** with quantitative conversions after 2h of reaction time. **Figure 66b** depicts the selectivity to isomer **1a** with the time. While the conversion values to **1a/1b** were maintained in 2:1 ratio, at the shortest reaction times, selectivity to **1a** is increased to 73%, after 2h, probably due to the interconversion of **1b** to **1a**, becoming 82 % after 3h of reaction time, when using 2APTMS/NbMCF(Ox) catalyst (**Figure 66c**).

The samples of Et serie follow a similar trend than that observed at a higher temperature. Accordingly, 2APTMS/TaMCF(Et) gave superior conversion values to chromenes **1** (45%) in comparison with 2APTMS/NbMCF(Et) sample (15%), both after 1h of reaction time (**Figure 67**). Then, it seems that a compromise between Si/T ratio (T = Nb or Ta) and N loading is required. Furthermore, the porosity notably diminished in 2APTMS/TaMCF(Et) could be behind of the decreased conversion values to **1** (**Table 15**). It is important to note that chromenes **1** was obtained with conversion up to 95%, in the presence of amino-grafted TaMCF(Et) samples, after 120 min of reaction time.

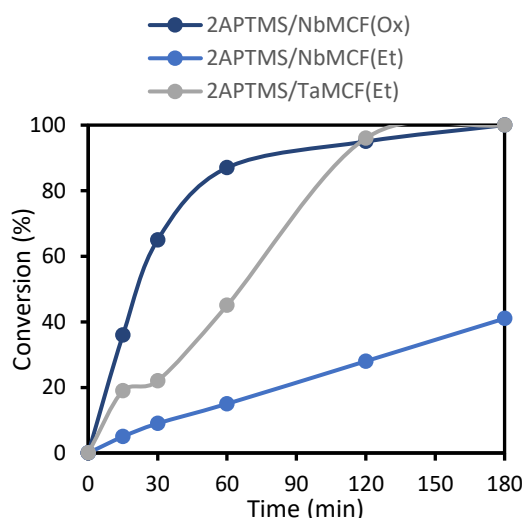


Figure 67. Synthesis of 2-amino-4H-chromenes **1** catalysed by amino-grafted NbMCF(Ox), NbMCF(Et) and TaMCF(Et) catalysts at a) 303 K. Reaction conditions: 25 mg of catalysts, **2/3** molar ratio = 2:4, solvent-free conditions

The influence of the catalyst amount was checked by following two strategies: i) increasing the reactant **2/3** molar ratio to 4:8 but maintaining the catalyst amount at 303 K (**Figure 68a**), and ii) maintaining the molar **2/3** molar ratio in 2:4 and increasing the catalyst amount to 50 mg (**Figure 68b**).

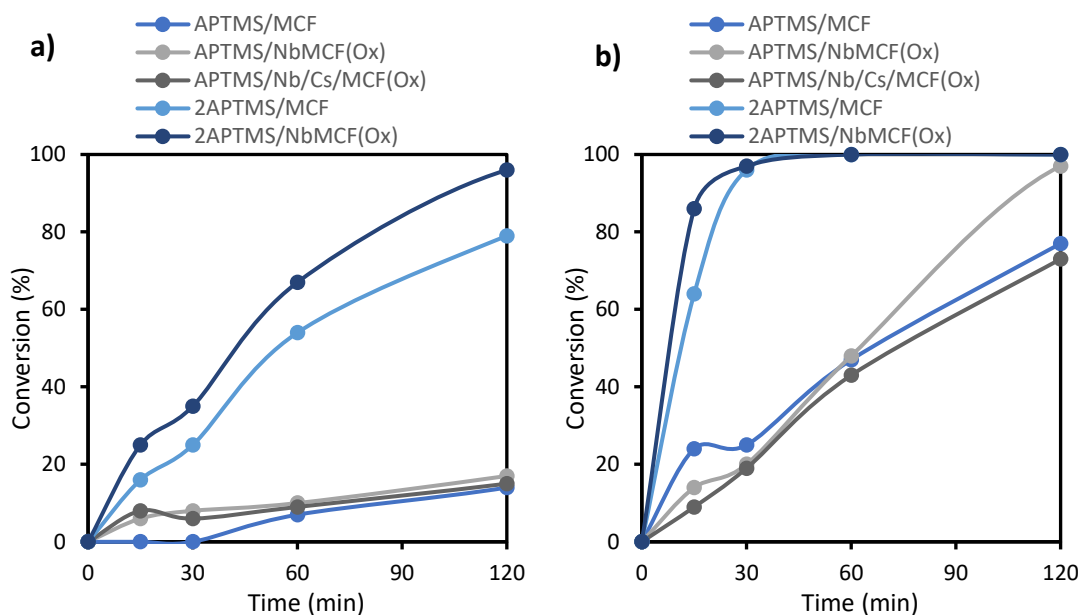


Figure 68. Catalyst amount influence in the synthesis of chromenes **1** catalysed by amino-grafted MCF and Nb/MCF catalysts: a) **2/3** molar ratio = 4:8 (catalyst amount: 25 mg) and b) **2/3** molar ratio = 2:4 (catalyst amount: 50 mg). Reaction conditions: 303 K, solvent-free conditions.

In the first approach, when using the worst reaction conditions (**Figure 68a**), all the catalysts were active maintaining the reactivity order. Even under these reaction conditions, the most active catalysts, 2APTMS/NbMCF(Ox) and 2APTMS/MCF, showed excellent conversion values, particularly the first one, leading to chromenes **1** in almost quantitative yield in 2h (**Figure 68a**). It is important to note the increase of the selectivity to chromene **1a** after 2h of reaction time, in the case of 2APTMS/NbMCF(Ox) and 2APTMS/MCF catalysts —from 2:1 ratio of **1a/1b** to 8:1—. On the other hand, when increasing the catalyst amount to 50 mg, maintaining the **2/3** molar ratio in 2:4 (**Figure 68b**), an increment in conversion values to chromenes **1** was observed as expected.

Finally, the reaction was also scoped by using different substituted 2-hydroxybenzaldehydes **6** in the presence of 25 mg of 2APTMS/NbMCF(Et) as a catalyst, at 323 K (**Scheme 13**). In all cases, chromenes **9** were selectively synthesized reaching good to excellent yields, reactivity differences barely being observed. Certainly, the substitution at position 5 in the aromatic ring in 2-hydroxybenzaldehyde provoked notably diminution in conversion values to **9**. At the higher reaction times, the following reactivity order was observed: H > NO₂ > Br > OMe, concluding that the presence of electrowithdrawing substituents at position 5 in 2-hydroxybenzaldehyde strongly favours the reaction (**Figure 69**).

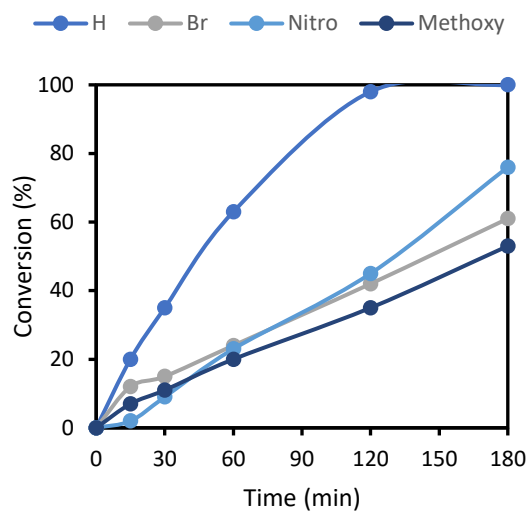


Figure 69. Synthesis of 2-amino-4*H*-chromenes **9** catalysed by 2APTMS/NbMCF(Et). Reaction conditions: 25 mg of catalysts, 323 K, 6/3 molar ratio = 2:4, solvent-free conditions.

As commented in previous chapters, the observed differences when using 5-substituted 2-hydroxybenzaldehydes seems strongly depending on the used catalysts and, therefore, related to the reactant-catalysts interactions.

VI.2 CONCLUSIONS

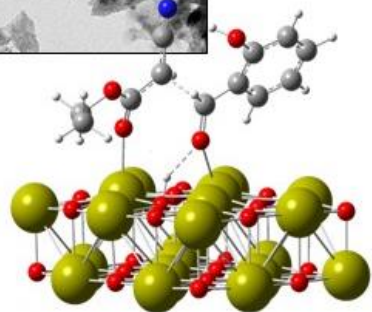
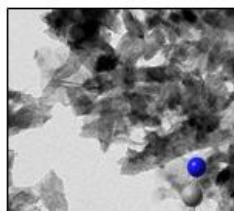
We report herein a new family of amino-grafted MCF catalysts with Nb and Ta metal sites inserted on the silica matrix, being all of them selective and active in the green efficient synthesis of 2-amino-4*H*-chromenes **1** and **9** from 2-hydroxybenzaldehydes and ethyl cyanoacetate, under mild and solvent-free conditions. TMCF mesoporous silica (where T is Nb or Ta) were prepared by using different metal sources —ethoxides and oxalates—. Subsequently, the mesoporous silicas were functionalized by grafting with the corresponding amino silanes —APTMS and 2APTMS—.

Our experimental results demonstrate that the catalytic performance is depending on the basicity of the catalysts, being the most active the ones that present the highest concentration of basic sites, particularly 2APTMS/TMCF samples. The presence of metal centres in the structure of the mesoporous silica framework contributes to significantly improve the conversion values to chromenes, even when using diminished catalyst amount and operating at a lower temperature.

The obtained results indicate that the amino-grafted TMCF catalysts could act as bifunctional catalysts as suggested by the highest catalytic performance obtained. In the case of 2APTMS/TaMCF sample, the high concentration of amino groups in combination with its lower porosity, suggest that the basic functions are mainly located at the open mouth of the pores, probably acting as individual catalytic sites.

In summary, the amino-grafted MCF catalysts reported herein allow to obtain the 2-amino-4*H*-chromenes **1** and **9** reaching quantitative conversion values even at shorter times, using less amount of catalyst at a reaction temperature close to room temperature. These materials can be considered as an interesting and sustainable alternative to other porous catalysts reported in previous chapters.

ESQUEMA INTEGRADOR

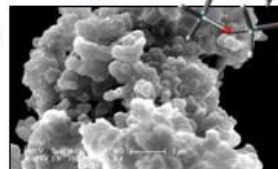
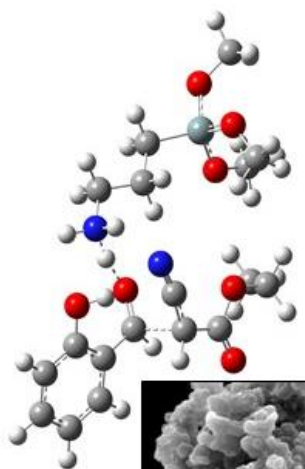
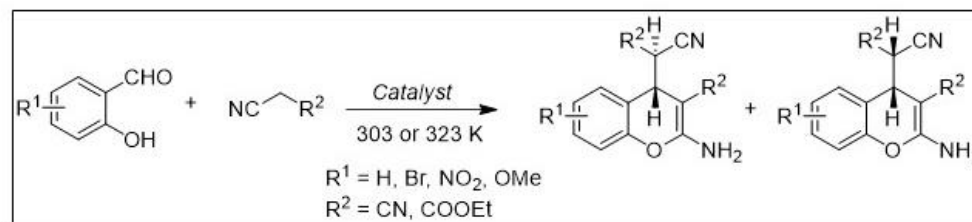


Basic carbon nanocatalysts: PET/CAL, PET/MAG and PET/DOL

- One pot synthesis.
- Different catalytic species: CaO, Ca(OH)₂ and MgO.
- Carbonaceous support barely contributes to the catalytic activity.
- Bifunctional acid-base catalysts.
- Efficient and selective to **1** at 323 K and using 50 mg of catalyst.
- Valorization of plastic residues.

Amino-grafted Cu and Sc MOFs: CuBTC and MIL-100 (Sc)

- Two different methodologies of synthesis and different MOF supports: CuBTC and MIL-100(Sc).
- Post-synthetic functionalization (grafting).
- Partial or total functionalization depending on the support and post-synthetic method.
- Bifunctional acid-base catalysts.
- Efficient and selective to **1** at 303 K and using 25 mg of catalyst.
- CUS and amine functions could work in cooperation.



Amino-grafted SBA-15 catalysts

- Post-synthetic functionalization (grafting).
- High functionalization degree.
- Efficient and selective to **1** at 303 K and using 25 mg of catalyst.
- Catalytic activity depending on the N content.
- Influence of the silica support

Amino-grafted T/MCF (T = Nb, Ta) catalysts

- Structural Nb and Ta atoms from different sources.
- Post-synthetic functionalization (grafting).
- Efficient and selective to **1** at 303 K and using 25 mg of catalyst at short reaction times.
- Catalytic activity depending on the N content.
- Probable contribution of the metal atoms to the catalytic activity.

CAPÍTULO VII

SECCIÓN EXPERIMENTAL

*CHAPTER VII. EXPERIMENTAL SECTION*CAPÍTULO VII. SECCIÓN EXPERIMENTALVII.1 EQUIPMENTS***Atomic Emission Spectroscopy***

ICP-OES PlasmaQuant PQ 9000 (Analytik Jena) spectrometer

Catalytic Activity Studies

Starfish Multirreaction equipment (Heidolph Instruments)

Elemental analysis

Elemental analyser LECO CHNS-932

Elemental analyser Vario EL III

FTIR

Bruker Vertex 80v spectrometer equipped with an MCT cryodetector

N₂ adsorption/desorption

ASAP 2020 (Micromeritics) physisorption analyser

Tristar II 3020 (Micromeritics) gas analyser

NMR

Bruker XRD 400 (9.4 Tesla, 400.13 MHz for ¹H) spectrometer with a 5-mm inverse-detection H-X probe equipped with a z-gradient coil, at 300 K

pH_{PZC} determination

GLP 22 Milimeter pHmeter (CRISON)

SEM

Zeiss Evo 40 Microscope

Thermogravimetric analysis

SDT Q600 Thermal Analyzer (TA Instruments)

TEM

JEOL JEM1010 apparatus equipped with a Gatan Orius 200 SC digital camera

JEOL 2000 Electron Microscope

UV-Vis

Varian-Cary 300 Scan UV-Visible spectrophotometer

XRD

Bruker D8 Advance diffractometer

Siemens D5000 diffractometer

Panalytical X'Pert PRO Theta/Theta diffractometer

XRF

MiniPal Energy-Dispersive X-Ray Fluorescence (Philips)

VII.2 CHEMICAL REAGENTS AND SOLVENTS

The used materials in this research were all commercially available.

Synthesis of the catalysts

1,3,5-Benzenetricarboxylic acid, (Trimesic acid): SIGMA-ALDRICH, 95%

1,3,5-Trimethylbenzene: SIGMA-ALDRICH, ≥99,99%

Ammonium fluoride: SIGMA-ALDRICH, ≥99.99%

Chloridric Acid: PANREAC, 36%

Copper benzene-1,3,5-tricarboxylate, (Basolite® C 300): BASF

Dolomite: mined from deposits located near Ząbkowice (Poland), supplied by PPUH "DOLOMIT" Kopalnia "Ząbkowice" S.A.

Hydrochloric acid: SIGMA-ALDRICH, 36.5-38.0%

Limestone: mined from deposits located near Czatkowice (Poland), supplied by "Czatkowice" Limestone Mine, Ltd.

Magnesite: mined from deposits located near Grochów (Poland), supplied by Magnezyty Grochów S. A

Niobium ammonium niobate (V) oxalate hydrate: SIGMA-ALDRICH, 99.99%

Niobium ethoxide: SIGMA-ALDRICH, 99.95%

Poly(ethylene glycol)-*block*-poly(propylene glycol)-*block*-poly(ethylene glycol), (Pluronic P123): SIGMA-ALDRICH, ≥99.99%

Poly(ethylene terephthalate) (PET): Elana S. A. (Poland), 99.999%

Scandium(III) nitrate hydrate: SIGMA-ALDRICH, 99.9%

Tantalum(V) ethoxide: SIGMA-ALDRICH, 99.98%

Tetraethyl orthosilicate (TEOS): SIGMA-ALDRICH o Fluka, >99%

Catalyst functionalization

(3-Aminopropyl)triethoxysilane, (APTES): SIGMA-ALDRICH, 99%

(3-Aminopropyl)trimethoxysilane, (APTMS): SIGMA-ALDRICH, 99%

N-(2-Aminoethyl)-3-amiopropyltrimethoxysilane, (2APTMS): SIGMA-ALDRICH, 99%

[3-(Diethylamino)propyl]trimethoxysilane, (DEAPTMS): ALFA AESAR, 98%

Diethylenetriamine, (DET): SIGMA-ALDRICH, 99%

N,N'-Dimethylethylenediamine, (MMEN): SIGMA-ALDRICH, 98%

Ethylenediamine, (EN): SIGMA-ALDRICH, 99%

[3-(Methylamino)propyl]trimethoxysilane, (MAPTMS): ALFA AESAR, 98%

Catalytic Activity

5-Bromo-2-hydroxybenzaldehyde: ALFA AESAR, 98%

Ethyl cyanoacetate: ALFA AESAR, >98%

2-Hydroxybenzaldehyde: ALFA AESAR, 99%

2-Hydroxy-5-methoxybenzaldehyde: ALFA AESAR, 98%

2-Hydroxy-5-nitrobenzaldehyde: ALFA AESAR, 98%

Malononitrile: SIGMA-ALDRICH, 99%

Solvents

Anhydrous toluene: CARLO ERBA, 99.8%

Cloroform-*d*: EURISO-TOP, 99.8%

Dichloromethane: SIGMA-ALDRICH, >99.8%

Diethyl ether: SIGMA-ALDRICH, 98%

Dimethylformamide, (DMF): SIGMA-ALDRICH, 99.8%

Dimethyl sulfoxide-*d*₆: CARLO ERBA, 99.8%

Ethanol: PANREAC, 99.8%

Ethyl acetate: ALFA AESAR, 99%

n-Hexane: PANREAC, 99%

Gasses

Nitrogen: PREMIER X50S, CARBUROS METÁLICOS

Helium: PREMIER X50S, CARBUROS METÁLICOS

Synthetic air: PREMIER X50S, CARBUROS METÁLICOS

VII.3 GENERAL PROCEDURES

VII.3.1 Synthesis and functionalization

Basic-carbon nanocatalysts

The materials were synthesized according to the experimental protocol reported by Przepiórski *et al*²⁵¹. Following this methodology, four different homogeneous PET/CAL mixtures were prepared, varying the PET:CAL ratio. In short, 10 g of PET and several CAL amounts —2.0, 4.3, 10.0 and 23.3 g— were used to obtain the corresponding catalysts: PET/CAL 83:17, PET/CAL 70:30, PET/CAL 50:50 and PET/CAL 30:70. Two extra materials were also prepared for comparison reasons: PET/MAG 30:70 and PET/DOL 30:70, by mixing 10 g of PET with 23.3 g of MAG or DOL.

Each mixture was previously dried in air atmosphere at 393 K during 24 h. Then, they were heated from room temperature to 538 K during 1 h, by using a slope of 10 K/min, under nitrogen atmosphere. The gas flow was set at 100 cm³/min. This first heating stage was done in order to disperse on a uniformly way the selected mineral — CAL, MAG or DOL— over the PET matrix. After that, the mixtures were cooled back until room temperature and powdered. Subsequently, the samples were submitted to additional thermal treatment by heating until 1123 K, using the ramp and gas flow previously selected. The obtained carbonaceous materials were milled and sieved below 0.025 mm.

Additionally, samples from exclusively PET, MAG, DOL or CAL —10 g each— as raw materials were also prepared. Finally, the catalyst PETb/CAL 30:70 was synthesized by using a commercially available plastic bottle and under the same experimental conditions described below.

Amino-grafted Cu and Sc Metal-Organic Frameworks

MIL-100-Sc was prepared by adapting the experimental procedure reported by Zhu *et al*²⁹¹. In essence, MIL-100-Sc was prepared by mixing 0.61 g of Sc(NO₃)₃·H₂O and 0.25 g of trimesic acid in 45 mL of DMF. The obtained mixture was stirred at room temperature for 30 min. After that, it was introduced into a Teflon-lined autoclave (100 mL), at 423

K, and it was heated for 36 h. The obtained product was filtered off and washed with DMF. Finally, it was dried at room temperature.

The synthesized MOF material MIL-100-Sc was functionalized adapting and following the experimental protocol reported by Hwang *et al*²⁶⁴. In short, 1.0 g of as-synthesized MIL-100-Sc was immersed in ethanol, at 373 K for 20 h before being activated at 453 K during 12 h, under N₂ atmosphere to remove the terminal solvent molecules on the open metal sites. After activation, MIL-100-Sc material was suspended in 100 mL of anhydrous toluene. Then, 1.0 mL of the corresponding amine was added, and the reaction was refluxed under N₂ atmosphere for 12 h. After that, the resulting solid was filtered and washed with hexane to remove the unreacted amine. Finally, it was dried at room temperature.

Following this protocol, two amino-grafted MIL-100-Sc catalysts were prepared, by using ethylenediamine (EN) or N,N'-dimethylethylenediamine (MMEN) denoted as EN-M/MIL-100-Sc and MMEN-M/MIL-100-Sc, respectively.

On the other hand, amino-grafted CuBTC materials have been prepared, from commercial reagents, by using two different methodologies. **Method A**, involves the same experimental protocol described above, used for the synthesis and functionalization of MIL-100-Sc catalyst. Following this method, EN-M/CuBTC samples were prepared from CuBTC by reacting with EN. For comparison purposes, **Method B** was followed to prepare analogous sample EN/CuBTC. The material was prepared in the presence of refluxing diethyl ether as a solvent²⁹². To sum up, 0.6 g of commercial CuBTC was refluxed in 20 mL of diethyl ether with 1.5 mmol of the corresponding amine under vigorous stirring during 72 h. The obtained catalyst was washed with diethyl ether to remove the unreacted amine (5 x 5 mL) and dried at 323 K. Following the Method B, two amino-grafted CuBTC samples were prepared by using ethylenediamine (EN) or diethylenetriamine (DET) denoted as EN/CuBTC and DET/CuBTC, respectively. Besides, 2DET/CuBTC was also prepared by using a double amount of DET.

Amino-grafted SBA-15 catalysts

Mesoporous SBA-15 silica was prepared following the experimental protocol proposed by Zhao *et al*^{181, 271}. In short, 30 mL of deionized water and 4 g of Pluronic P123 were

added to a 120 g HCl solution (2 M). The mixture was stirred until a homogeneous solution is obtained. Then, it was heated until 313 K and TEOS (tetraethyl ortosilicate) was added. After that, the mixture remains stirring during 24 h. Subsequently, the solution was introduced into a Teflon autoclave at constant pressure and 373 K during 48 h, under static conditions. The obtained material was filtered off and washed with water until neutral pH and dried at room temperature. Finally, the solid was calcined at 823 K, setting the heating range in 1 K/min and remaining the temperature during 6 h.

Amino-grafted SBA-15 was functionalized by following the reported methodology by López-Sanz *et al*²⁷². To sum up, the corresponding amount of silane (6.65 mmol, in excess) was added to a suspension of dried 2 g of SBA-15 in 35 mL of toluene. The mixture was stirred during 5 h at room temperature. Then, the material was filtered off and washed with 20 mL of toluene in order to extract the unreacted silane. Finally, the solid was dried in vacuum at room temperature.

Selected compounds to carry out the grafting were APTES, DEAPTMS, MAPTMS and 2APTMS, obtaining the corresponding catalysts APTES/SBA-15, DEAPTMS/SBA-15, MAPTMS/SBA-15 and 2APTMS/SBA-15, respectively.

Amino-grafted MCF, TaMCF and NbMCF silica catalysts

The experimental methodology followed for the synthesis of MCF support material was previously reported by Smuszkiwicz *et al*²²². Briefly, 8 g of Pluronic 123 (poly(ethylene glycol)-*block*-poly(propylene glycol)-*block*-poly(ethylene glycol)) were dissolved into HCl solution (0.7 M) at a temperature range of 308-313 K. After that, 12 g of 1,3,5 trimethylbenzene and 0.0934 g of NH₄F were added. The mixture was stirred during 2h. Then, 17.054 g of TEOS were added and the solution was stirred in the same temperature range for 24 h. Once this process was finished, the mixture was transferred into a polypropylene bottle and heated at 373 K under static conditions for 24h. The obtained material was filtered off and washed with distilled water. Finally, once the solid was dried at room temperature, the template was calcined at 773 K, using a heating range of 1 K/min, during 8 h under static conditions.

NbMCF(Ox), NbMCF(Et) and TaMCF(Et) materials were prepared following the same experimental protocol but including the corresponding metal sources: niobium

ammonium niobate(V) oxalate hydrate for NbMCF(Ox), and niobium ethoxide or tantalum ethoxide as niobium and tantalum sources, respectively, 10 minutes after TEOS addition for NbMCF(Et) and TaMCF(Et) samples, respectively. This addition was made keeping constant the TEOS/Nb or TEOS/Ta ratio in 64, assuming Si/Nb and Si/Ta molar ratio = 64.

The synthesized mesoporous silicas were functionalized by grafting with 3-aminopropyl-trimethoxysilane (APTMS) and [3-(2-aminoethylamino) propyl] trimethoxysilane (2APTMS). According to the experimental protocol previously reported by Zhang *et al*²⁸², 2 g of the corresponding silica powder were refluxed in 200 mL of a dry toluene solution. Then, 10 mL of the corresponding silane were added, and the solution was stirred during 373 K for 18 h. After that, catalyst was filtered off and washed with 200 mL of dry toluene, 100 mL of water and 20 mL of acetonitrile to remove the unreacted silane. Finally, the solid was dried in an oven at 373 K. The obtained catalysts were named as APTMS/MCF, 2APTMS/MCF APTMS/NbMCF(Ox), 2APTMS/NbMCF(Ox), 2APTMS/NbMCF(Et) and 2APTMS/TaMCF(Et).

VII.3.2 Characterization techniques

Elemental analysis

The content of C, H and O in the solids was carried out with an Elemental Analyser LECO CHNS-932. In addition, the copper amount was determined by Atomic Emission Spectroscopy (AES), using an ICP-OES PlasmaQuant PQ 9000 (Analytik Jena) spectrometer.

For amino-grafted MCF catalysts, the used equipment to determine the content of N, C, O and H in the catalysts was an Elementar Analysis Vario EL III.

These analyses were made in the Transmission Electron Microscopy Laboratory in the SIDI (Servicio Interdepartamental de Investigación, Universidad Autónoma de Madrid).

FT-IR

Fourier transform infrared spectra were determined using a Bruker Vertex 80v spectrometer, with an MCT cryodetector coupled. To sum up, these measurements were carried out in a thin, self-supported wafer of the samples. These wafers were previously outgassed for their activation inside the IR cell under dynamic vacuum at 423 K during 6 h. After activation treatment, coordinatively unsaturated metal sites were determined by dosing carbon monoxide into cells under study.

In case of SBA-15 catalysts, they were activated by outgassing them at 403 K under dynamic vacuum during 8 h. In case of amino-grafted MCF materials, they were studied by using a Vertex 70 spectrometer. Previously, the samples were pressed in wafers ($5 \text{ mg}\cdot\text{cm}^{-1}$) and placed in a vacuum cell, evacuated at 373 K for 2 h. The spectra were obtained at room temperature, with the resolution set at 4 cm^{-1} and the number of the scans fixed in 64.

Nitrogen adsorption

Adsorption/desorption isotherms in carbon and silica materials were obtained by using an analysing equipment ASAP 2020 (Micromeritics). Carbonaceous samples were previously degasified during 1080 min, at 573 K, under high vacuum. After degasification

process, the adsorption process was carried out with N_2 at 77 K. The isotherms data were analysed by using the BET method to determine the specific surface area and the two dimensional non local density functional theory (2d-NLDFT) model for the determination of pore volume and pore size distribution. Micropore surface area (S_{micro}), external surface area (S_{ext}) and total surface (S_{total}) were determined by α_s method. The Dubinin-Radushkevich method was used to obtain the micropore volume (V_{micro}) from the adsorption branches of the measured isotherms. Total pore volume (V_T) was determined from the nitrogen amount absorbed at relative pressure p/p_0 of 0.95. The difference between these volumes corresponds to the mesopore volume (V_{meso}).

For MOF catalysts, samples were previously outgassed at 413 K overnight, under dynamic vacuum at, approximately, 10^{-6} mbar. Isotherms of MOF samples were obtained with a Tristar II 3020 (Micromeritics) gas analyser.

In case of amino-grafted SBA-15 catalysts, samples were previously outgassed before carrying out the measurements, at 353 K overnight. BJH method was followed to determine windows parameters.

For amino-grafted MCF catalysts, samples were previously outgassed, at 383-393 K overnight, until obtaining a residual pressure lower than 0.7 Pa. BdB-FHH method was followed to determine cells diameters.

pH_{PZC} determination

The PZC was determined by following the described methodology in the literature^{293, 294}, corresponding to the equilibrium pH when the material is dispersed in H_2O at room temperature. They were measured with GLP 22 Milimeter pHmeter (CRISON).

Thermogravimetric Analysis and Differential Thermal Analysis

All the samples were studied by thermogravimetric analysis by using an SDT Q600 Thermal Analyzer (TA Instruments), where 45 mg of the corresponding material were heated from room temperature until 1223 K. The selected slope depends on the material and the temperature range under study, but it is usually set at 10 K/min. The analyses were made under two different atmospheres: He as an inert medium and synthetic air as an oxidant medium. The gas flow was fixed at 100 mL/min.

Transmission Electron Microscopy

The morphology of the materials was investigated by TEM using JEOL JEM1010 apparatus operating at 100 kV and equipped with a digital camera Gatan Orius 200 SC model. In the previous preparation of the samples, each material was suspended in water (2.5 mg in 50 mL). Then, they were homogenized in an ultrasonic bath, during 15 min at 40 KHz. After that, the samples were deposited over a carbon lined grid and dried.

For amino-grafted MCF catalysts, TEM studies were carried out by using a JEOL 2000 electron microscope operating at 80 kV. The powdered samples were deposited on a grid covered with a holey thin carbon film.

These analyses were made in the Transmission Electron Microscopy Laboratory in the SIDI (Servicio Interdepartamental de Investigación, Universidad Autónoma de Madrid) and in the Unidad de Apoyo a la Investigación in the ICP (Instituto de Catálisis y Petroleoquímica).

Scanning Electron Microscopy

For SEM measurements, a Zeiss Evo 40 microscope was used, operating at 17 Kv. The samples were previously deposited on a grid with a holey thin carbon film.

X-Ray Diffraction

MOF samples were studied by XRD by using both, Bruker D8 Advance diffractometer or Siemens D5000 diffractometer. In this crystallographic analysis, samples were powdered and studied under a $\text{CuK}\alpha$ ($\lambda = 1.5418 \text{ \AA}$) radiation.

Amino-grafted SBA-15 materials were studied by XRD by using a Panalytical X'Pert PRO Theta/Theta diffractometer at 45 kV.

These analyses were made in the Transmission Electron Microscopy Laboratory in the SIDI (Servicio Interdepartamental de Investigación, Universidad Autónoma de Madrid).

X-Ray Fluorescence

Amino-grafted TMCF materials were investigated by X-Ray Fluorescence with a MiniPal Energy-Dispersive X-Ray Fluorescence instrument (Philips). The calibration curves prepared from mixtures of silica and Nb₂O₅ (Si/Nb from 5 to 300) were used.

VII.3.3 Catalytic performance

The catalytic activity of the synthesized materials was checked in 2-amino-4*H*-chromene synthesis. *In a typical experiment*, the corresponding amount of the catalysts were added to a mixture of 2-hydroxybenzaldehyde (2 mmol) and ethyl cyanoacetate (4 mmol), and the reaction mixture was stirred, at the corresponding temperature, for 3 h (**Scheme 9**). The reactions were carried out in a Starfish Multireaction Equipment, in liquid phase, under atmospheric pressure and solvent-free conditions. Samples of reacting mixtures were taken at fixed reaction times —15, 30, 60, 120 and 180 min— in order to analyse them by Proton Nuclear Magnetic Resonance (¹H NMR). The collected samples were diluted with CH₂Cl₂ (1 mL) and the catalyst was filtered off with a glass syringe equipped with a microfilter (Millipore, 0.45 μm HV). Then, the solvent was evaporated *in vacuo*.

Qualitative monitorization of the reaction progress was obtained by thin layer chromatography (TLC) performed on a DC-Aulofolien/Kieselgel 60 F₂₄₅ (Merck), using CH₂Cl₂/EtOH (98:2) mixture as eluent.

Conversion values are defined as the fraction of the corresponding 2-hydroxybenzaldehyde reactant transformed each reaction time into chromenes determined by ¹H NMR. Reaction products were also characterized by this technique, by using a Bruker XRD 400 (9.4 Tesla, 400.13 MHz for ¹H) spectrometer with a 5-mm inverse-detection H-X probe equipped with a z-gradient coil, at 300 K. Chemical shifts (δ in ppm) are given from internal solvent, CDCl₃ 7.26 for ¹H.

VII.3.4 Computational studies

All the calculations were performed by using the Gaussian 09 software package²⁹⁵, in gas phase, at 298 K. In order to optimize geometries, B3LYP hybrid functional was used, in combination with 6-31G(d,p) basis set, this functional being a methodology used to study nanostructures^{296,297}. Stationary points were characterized

by the analyse of the harmonic vibrational frequency, and the TS were confirmed to be first-order saddle points. To represent the desired reaction coordinate, the imaginary frequency was inspected in all TS. To check the correct connection between reactants and products, IRC was followed in key TS²⁹⁸.

Basic-carbon nanocatalysts

Based on our experimental observations and recent publications —reporting that the most stable isomers for $(\text{CaO})_n$ when $n > 3$ show 3D structures, particularly cubic structures— the selected size of the cluster in the calculations was $(\text{CaO})_n$, being $n = 20$. This number was selected because it is large enough to contain all reactant structures.

We studied the most probable pathway comprising i) aldol reaction between reactants, ii) heterocyclization, iii) dehydration and finally iv) Michael addition of a second molecule of ethyl cyanoacetate **3** yielding chromenes **1** as mixtures of the corresponding diastereoisomers.

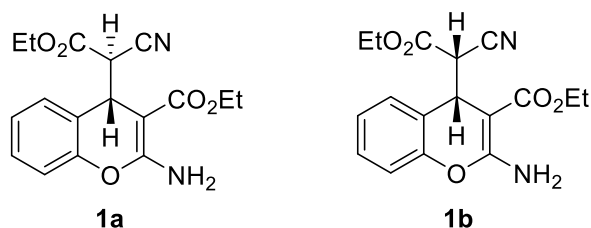
Amino-grafted Cu and Sc Metal-Organic Frameworks

We studied the first elementary step of the reaction consisting on aldolization reaction between reagents **2** and **3**. The reduced models selected are represented in **Figure 44**.

Amino-grafted SBA-15 catalysts

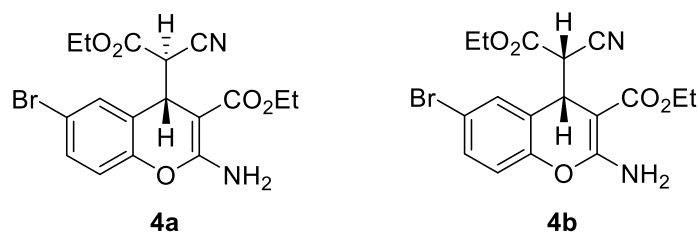
We studied the first elementary step of the reaction consisting on aldolization reaction between reagents **2** and **3**. The reduced model when investigating the influence of silica support in the reaction is depicted in **Figure 54**, as the most probable model cluster.

VII.4 SPECTROSCOPIC DATA

Ethyl 2-amino-4-(1-cyano-2-ethoxy-2-oxoethyl)-4H-chromene-3-carboxylate (1)

(1a): ^1H NMR (400 MHz, CDCl_3 , 298 K) δ (ppm)=7.29–7.24 (m, 1H, aromatic), 7.11–7.04 (m, 3H, aromatic), 6.49 (br s, 2H, NH_2), 4.70 (d, J (H,H)=3.6 Hz, 1H, CH), 4.28–4.20 (m, 4H, CH_2), 3.97 (d, J (H,H)=3.7 Hz, 1H, CH), 1.33 (t, J (H,H)=7.2 Hz, 3H, CH_3), 1.27 (t, J (H,H)=7.2 Hz, 3H, CH_3). ^{13}C NMR (100 MHz, CDCl_3 , 298 K) δ (ppm)= 168.11 (CO), 165.20 (CO), 162.63 ($\text{C}=\text{C}-\text{COOC}_2\text{CH}_5$), 150.56 (ArC), 129.36 (ArCH), 128.23 (ArCH), 124.71 (ArCH), 120.25 (ArC), 116.65 (ArCH), 115.53 (CN), 73.41 ($\text{C}=\text{C}-\text{COOC}_2\text{CH}_5$), 62.73 (CH_2), 59.96 (CH_2), 46.85 (CH), 36.99 (CH), 14.58 (CH_3), 14.00 (CH_3).

(1b): ^1H NMR (400 MHz, CDCl_3 , 298 K) δ (ppm)=7.48 (dd, J (H,H)=7.8, 1.5 Hz, 1H aromatic), 7.29–7.24 (m, 1H, aromatic), 7.17 (m, 1H, aromatic), 6.98 (dd, J (H,H)=7.8, 1.5 Hz, 1H aromatic), 6.50 (br s, 2H, NH_2), 4.61 (d, J (H,H)=3.5 Hz, 1H, CH), 4.28–4.20 (m, 2H, CH_2), 4.02 (q, J (H,H)=7.2 Hz, 2H, CH_2), 3.78 (d, J (H,H)=3.5 Hz, 1H, CH), 1.34 (t, J (H,H)=7.8 Hz, 3H, CH_3), 1.12 (t, J (H,H)=7.8 Hz, 3H, CH_3). ^{13}C NMR (100 MHz, CDCl_3 , 298 K) δ (ppm)= 168.21 (CO), 164.82 (CO), 162.42 ($\text{C}=\text{C}-\text{COOC}_2\text{CH}_5$), 150.23 (ArC), 129.16 (ArCH), 128.76 (ArCH), 124.96 (ArCH), 120.86 (ArC), 116.32 (ArCH), 116.15 (CN), 73.51 ($\text{C}=\text{C}-\text{COOC}_2\text{CH}_5$), 62.51 (CH_2), 59.97 (CH_2), 45.45 (CH), 37.32 (CH), 14.59 (CH_3), 13.71 (CH_3).

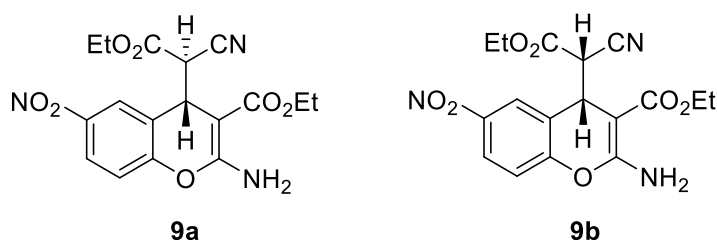
Ethyl 2-amino-6-bromo-4-(1-cyano-2-ethoxy-2-oxoethyl)-4H-chromene-3-carboxylate (4)

(4a): ^1H NMR (400 MHz, CDCl_3 , 298 K) δ (ppm) = 7.39 (m, 1H, aromatic), 7.23 (d, J (H,H)=2.2 Hz, 1H, aromatic), 6.96 (d, J (H,H)=8.7 Hz, 1H, aromatic), 6.50 (br s, 2H, NH_2),

4.65 (d, J (H,H)=3.5 Hz, 1H, CH), 4.34-4.20 (m, 4H, CH₂), 3.97 (d, J (H,H)=3.5 Hz, 1H, CH), 1.33-1.29 (m, 6H, CH₃).

(4b): ¹H NMR (400 MHz, CDCl₃, 298 K) δ (ppm) = 7.58 (d, J (H,H)=2.1 Hz, 1H, aromatic), 7.40-7.37 (m, 1H, aromatic), 6.89 (d, J (H,H)=8.7 Hz, 1H, aromatic), 6.50 (br s, 2H, NH₂), 4.57 (d, J (H,H)=3.7 Hz, 1H, CH), 4.34-4.20 (m, 2H, CH₂), 4.07 (q, J (H,H)=7.2 Hz, 2H, CH₂), 3.74 (d, J (H,H)=3.7 Hz, 1H, CH), 1.33-1.29 (m, 3H, CH₃), 1.16 (t, J (H,H)=7.2 Hz, 3H, CH₃).

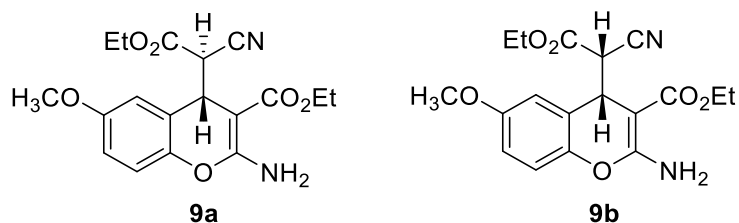
Ethyl 2-amino-4-(1-cyano-2-ethoxy-2-oxoethyl)-6-nitro-4H-chromene-3-carboxylate ($R^1 = \text{NO}_2$, **9**)



(9a): ¹H NMR (400 MHz, CDCl₃, 298 K) δ (ppm) = 8.21 (dd, J (H,H)=2.4, 9 Hz, 1H, aromatic), 8.07 (d, J (H,H)=2.4 Hz, 1H, aromatic), 7.18 (d, J (H,H)=9 Hz, 1H, aromatic), 6.50 (br s, 2H, NH₂), 4.80 (d, J (H,H)=3.3 Hz, 1H, CH), 4.37-4.22 (m, 4H, CH₂), 4.04 (d, J (H,H)=3.3 Hz, 1H, CH), 1.37-1.29 (m, 6H, CH₃).

(9b): ¹H NMR (400 MHz, CDCl₃, 298 K) δ (ppm) = 8.41 (dd, J (H,H)=2.3 Hz, 1H, aromatic), 8.21 (dd, J (H,H)=2.4, 9 Hz, 1H, aromatic), 7.17 (d, J (H,H)=9 Hz, 1H, aromatic), 6.50 (br s, 2H, NH₂), 4.68 (d, J (H,H)=3.6 Hz, 1H, CH), 4.37-4.22 (m, 4H, CH₂), 4.11 (q, J (H,H)=7.2 Hz, 2H, CH₂), 3.82 (d, J (H,H)=3.6 Hz, 1H, CH), 1.37-1.29 (m, 3H, CH₃), 1.19 (t, J (H,H)=7.2 Hz, 3H, CH₃).

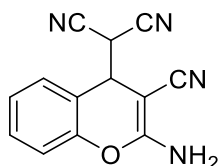
Ethyl 2-amino-4-(1-cyano-2-ethoxy-2-oxoethyl)-6-methoxy-4H-chromene-3-carboxylate ($R^1 = \text{OCH}_3$, **9**)



(9a): ^1H NMR (400 MHz, CDCl_3 , 298 K) δ (ppm) = 7.00 (m, 1H, aromatic), 6.84 (m, 1H, aromatic), 6.62 (d, J (H,H)=3.0 Hz, 1H, aromatic), 6.50 (br s, 2H, NH_2), 4.69 (d, J (H,H)=3.7 Hz, 1H, CH), 4.29-4.22 (m, 4H, CH_2), 3.97 (d, J (H,H)=3.7 Hz, 1H, CH), 3.75 (s, 3H, OCH_3), 1.34 (t, J (H,H)=7.2 Hz, 3H, CH_3), 1.30 (t, J (H,H)=7.2 Hz, 3H, CH_3).

(9b): ^1H NMR (400 MHz, CDCl_3 , 298 K) δ (ppm) = 7.00 (m, 1H, aromatic), 6.93 (d, J (H,H)=9.0 Hz, 1H, aromatic), 6.82 (m, 1H aromatic), 6.50 (br s, 2H, NH_2), 4.60 (d, J (H,H)=3.7 Hz, 1H, CH), 4.29-4.22 (m, 2H, CH_2), 4.04 (q, J (H,H)=7.2 Hz, 2H, CH_2), 3.81 (s, 3H, OCH_3), 3.80 (d, J (H,H)=3.7 Hz, 1H, CH), 1.34 (t, J (H,H)=7.2 Hz, 3H, CH_3), 1.14 (t, J (H,H)=7.2 Hz, 3H, CH_3).

2(-2-Amino-3-cyano-4H-chromen-4-yl)malononitrile (8)



^1H NMR (400 MHz, CDCl_3 , 298 K) δ (ppm)=7.52 (d, J (H,H)=6.8, 1.5 Hz, 1H aromatic), 7.45 (d, J (H,H)=6.8, 1.5 Hz, 1H aromatic), 7.31 (d, J (H,H)=6.8, 1.5 Hz, 1H aromatic), 7.15 (d, J (H,H)=7.0, 1.5 Hz, 1H aromatic), 6.50 (br s, 2H, NH_2), 4.31 (d, J (H,H)=3.4, 1.5 Hz, 1H, CH), 4.01 (d, J (H,H)=3.5, 1.5 Hz, 1H, CH).

BIBLIOGRAFÍA

-
- ¹ Radiografía del Sector Químico Español 2020 (feiQue).
<https://www.feique.org/pdfs/radiografiasectorial.pdf> (accessed February 3, 2020).
- ² INE. Encuesta Industrial de Empresas 2019. (accessed February 3, 2020).
- ³ Hagen, J. *Industrial Catalysis: A Practical Approach*, 3rd Edition. Wiley-VCH Verlag GmbH & Co., 2011.
- ⁴ Asamblea de las Naciones Unidas sobre el Medio Ambiente del Programa de las Naciones Unidas para el Medio Ambiente. <https://papersmart.unon.org/resolution/uploads/k1900126.pdf> (accessed February 3, 2020).
- ⁵ Cybulski, A.; Moulijn, J. A.; Sharma, M. M.; Sheldon, R. A. *Fine Chemicals Manufacture: Technology and Engineering*; Elsevier Science B.V.: Amsterdam, 2001; pp. 1-9.
- ⁶ Pollak, P. *Fine Chemicals – The Industry and the Business*, 2nd. rev. ed.; J. Wiley & Sons, 2011.
- ⁷ Trost, B. M. Atom Economy: A Search for Synthetic Efficiency. *Science* **1991**, 254, 1471-1477.
- ⁸ Trost, B. M. Atom Economy - A Challenge for Organic Synthesis: Homogeneous Catalysis Leads the Way. *Angew. Chem. Int. Ed.* **1995**, 34, 259-281.
- ⁹ Sheldon, R. A. Atom efficiency and catalysis in organic synthesis, *Pure App. Chem.* **2000**, 72, 1233-1246.
- ¹⁰ Sheldon, R. A. The E Factor: 15 Years On, *Green Chem.* **2007**, 9, 1261-1381.
- ¹¹ Sheldon, R. A. E factors, Green chemistry and catalysis: An odyssey, *Chem. Commun.* **2008**, 3352-3365.
- ¹² Arends, I.; Sheldon, R.; Hanefeld, U., *Green Chemistry and Catalysis*; WILEY-VCH Verlag GmbH & Co. KGaA: Weinheim, 2007; pp. 2-5.
- ¹³ Anastas, P. T.; Warner, J. C. *Green Chemistry: Theory and Practice*; Oxford University Press: New York, 1998, p. 30.
- ¹⁴ Nelson, W. N. *Green Solvents for Chemistry: Perspectives and Practice*; Oxford University Press: New York, 2003.
- ¹⁵ Lancaster, M. *Green Chemistry: An introductory Text*, University of York, RSC, 2002.
- ¹⁶ Marlack, A. S., *Introduction to Green Chemistry*, Marcel Dekker, 2001.
- ¹⁷ Sustainable Development Goals. United Nations.
<https://www.un.org/sustainabledevelopment/es/sustainable-development-goals/> (accessed February 15, 2020).
- ¹⁸ Erythropel, H. C.; Zimmerman, J. B.; de Winter, T. M.; Petitjean, L.; Melnikov, F.; Lam, C. H.; Lounsbury, A. W.; Mellor, K. E.; Janković, N.Z.; Tu, Q.; Pincus, L. N.; Falinski, M. M.; Shi, W.; Coish, P.; Plata, D. L.; Anastas, P. T. The Green ChemisTREE: 20 years after taking root with the 12 principles. *Green Chem.* **2018**, 20, 1929-2160
- ¹⁹ Belwal, C. K.; Patel, J. Synthetic Methods for Simvastatin – an Overview, *J. Pharm. Appl. Chem.* **2019**, 5, 23-43.

- ²⁰ Presidential Green Chemistry Challenge: 2010 Greener Reaction Conditions Award. Merck & Co., Inc. Codexis, Inc. <https://www.epa.gov/g-1reenchemistry/presidential-green-chemistry-challenge-2010-greener-reaction-conditions-award>. (accessed February 15, 2020).
- ²¹ Wells, P.B. *Catalysis Encyclopedia of Materials: Science and Technology*, 2nd. Ed., 2001; pp. 1020-1025.
- ²² Davis, M. E. and Suib, S. L. *Selectivity in Catalysis*. ACS Symposium Series, 517. Washington DC, 1993.
- ²³ Circular economy: definition, importance and benefits. News. European Parliament. <https://www.europarl.europa.eu/news/en/headlines/economy/20151201STO05603/circular-economy-definition-importance-and-benefits> (accessed February 19, 2020).
- ²⁴ Industrial Catalyst Market: Global Industry Trends, Share, Size, Growth, Opportunity and Forecast 2019-2024. <https://www.researchandmarkets.com/reports/4775802/industrial-catalyst-market-global-industry> (accessed March 06, 2020).
- ²⁵ Armor, J. North American Catalysis Society, NSF workshop report on "Future Directions in Catalysis", 2012. <http://www.nacatsoc.org/educatalysis.asp> (accessed March 06, 2020).
- ²⁶ Catlow, C. R.; Davidson, M.; Hardacre, C.; Hutchings, G. J. Catalysis making the world a better place. *Phil. Trans. R. Soc. A*. **2016**, 374.
- ²⁷ Smith, B. E. Nitrogenase Reveals Its Inner Secrets. *Science* **2002**, 297, 1654-1655.
- ²⁸ Smil, V. Detonator of the population explosion. *Nature* **1999**, 415.
- ²⁹ Fryzuk, M. D. Ammonia transformed. *Nature* **2004**, 427, 489-299.
- ³⁰ Ritchie, H. How many people does synthetic fertilizer feed? 2017. <https://ourworldindata.org/how-many-people-does-synthetic-fertilizer-feed#:~:text=As%20a%20result%2C%20the%20Haber,to%203.5%20billion%20people%20today> (accessed March 12, 2020).
- ³¹ Costa, M.; Dias, T. A.; Brito, A.; Proença, F. Biological importance of structurally diversified chromenes. *Eur. J. Med. Chem.* **2016**, 123, 487-507.
- ³² Vukovic, N.; Sukdolak, S.; Solujic, S.; Niciforovic. Substituted imino and amino derivatives of 4-hydroxycoumarins as novel antioxidant, antibacterial and antifungal agents: synthesis and in vitro assessments. *Food Chem.* **2010**, 120, 1011-1018.
- ³³ Hayes, J. E.; Allen, P.; Brunton, N.; O'Grady, M. N.; Kerry, J. P. Phenolic Composition and in Vitro Antioxidant Capacity of Four Commercial Phytochemical Products: Olive Leaf Extract (*Olea europaea*), Lutein, Sesamol and Ellagic Acid. *Food Chem.* **2011**, 126, 948-955.
- ³⁴ Lipkus, A. H.; Yuan, Q.; Lucas, K. A.; Funk, S. A.; Bartelt, W. F.; Schenck, R. J.; Trippe, A. J. Structural Diversity of Organic Chemistry. A Scaffold Analysis of the CAS Registry. *J. Org. Chem.* **2008**, 73, 4443-4451.
- ³⁵ Ellis, G.P. Chromenes, Chromanones, and Chromones. In *The Chemistry of Heterocyclic Compounds*. John Wiley & Sons, Inc., 1977; Vol. 31

- ³⁶ Torres-Barajas, L.; Rojas, J.; Buitrago, A.; Morales, A. Natural products and semisynthetic derivatives obtained from *Ageratina jahnii* and *Ageratina pichinchensis* (Asteraceae) species. *Revista Ciencia e Ingeniería* (Universidad de los Andes) **2019**, *40*, 77-86.
- ³⁷ Chavarría, M.; Castro, V.; Poveda, L.; Murillo, R. Four new compounds from the non-polar extract of the plant *Amyris brenesii* (Rutaceae) from Costa Rica. *Rev. Biol. Trop.* **2008**, *56*, 1043-1051.
- ³⁸ Borroto, A.; Reyes-Garau, D.; Jimenez, M. A.; Carrasco, E.; Moreno, B.; Martinez-Pasamar, S.; B. Cortés, J.R.; Perona, A.; Abia, D.; Blanco, S.; Fuentes, M.; Arellano, I.; Lobo, J.; Heidarieh, H.; Rueda, J.; Esteve, P.; Cibrián, D.; Martínez-Riaño, A.; Mendoza, P.; Prieto, C.; Calleja, E.; Oeste, C. L.; Orfao, A.; Fresno, M.; Sánchez-Madrid, F.; Alcamí, A.; Bovolenta, P.; Martín, P.; Villoslada, P.; Morreale, A.; Messeguer, A.; Alarcón, B. First-in-class inhibitor of the T cell receptor for the treatment of autoimmune diseases. *Sci. Transl. Med.* **2016**, *8*, 370ra 184.
- ³⁹ Dubal, K. N.; Ghorpade, P. N.; Kale, M. V. Studies on bioactive compounds of *Tectaria Coadunata* (Wall. Ex Hook. & Grev.). *Asian J. Pharm. Clin. Res.* **2013**, *6*, 11-15.
- ⁴⁰ Llewellyn, B. D. Hematoxylin Formulae. 2013.
- ⁴¹ UVigo. Histological techniques. General staining, 2019. <https://mmegias.webs.uvigo.es/6-tecnicas/5-general.php>. (accesed March 26, 2020).
- ⁴² Wang, J. L.; Liu, D.; Zhang, Z. J.; Shan, S.; Han, X.; Srinivasula, S. M.; Croce, C. M.; Alnemri, E. S.; Huang, Z. Structure-based discovery of an organic compound that binds Bcl-2 protein and induces apoptosis of tumor cells. *Proc. Natl. Acad. Sci.* **2000**, *97*, 7124-7129.
- ⁴³ Kumar Verma, R.; Kumar Prajapati, V.; Kumar Verma, G.; Chakraborty, D.; Sundar, S.; Madhujar, R.; Kumar Dubey, V.; Shankar Singh, M.; Molecular Docking and in Vitro Antileishmanial Evaluation of Chromene-2-thione Analogues. *ACS Med. Chem. Lett.* **2012**, *3*, 243-247.
- ⁴⁴ Batista Jr., J. M.; Lopes, A. A.; Ambrosio, D. L.; Regasini, L.O.; Kato, M. J.; Bolzani, V.D.S.; Cicarelli, R. M.; Furlan, M., Natural chromenes and chromene derivatives as potential anty-trypanosomal agents. *Biol. Pharm. Bull.* **2008**, *31*, 1983-1985.
- ⁴⁵ Kidwai, M.; Saxena, S.; Khan, K. R.; Thukral, S. S., Aqua mediated synthesis of substituted 2-amino-4H-chromenes and in vitro study as antibacterial agents. *Bioorg. Med. Chem. Lett.* **2015**, *15*, 4295-4298.
- ⁴⁶ Kesten, S. R.; Heffner, T. G.; Johnson, S. J.; Pugsley, J. L.; Wright, D. L.; Wise, D. L. Design, synthesis, and evaluation of chromen-2-ones as potent and selective human dopamine D4 antagonists. *J. Med. Chem.* **1999**, *42*, 3718-3725.
- ⁴⁷ Bruhlmann, C.; Ooms, F.; Carrupt, P.; Testa, B.; Catto, M.; Leonetti, Altomare, C.; Cartti, A. Coumarins derivatives as dual inhibitors of acetylcholinesterase and monoamine oxidase. *J. Med. Chem.* **2001**, *44*, 3195-3198.
- ⁴⁸ Lalleman, B. Hair dyeing process using a chromene or chromane dye. WO 2011020857 A2, February 24, 2011. U.S. Patent No. 8,518,126. Washington, DC: U.S. Patent and Trademark Office.

- ⁴⁹ Elinson, M.N.; Nasybullin, R.F.; Ryzhkov, F.V.; Zaimovskaya, T.A.; Egorov, M.P. Solvent-free cascade assembling of 2-hydroxybenzaldehydes and cyanoacetates: fast and efficient approach to medicinally relevant 2-amino-4H-chromene scaffold. *Monatsh. Chem.* **2014**, 145, 605-610.
- ⁵⁰ Kulkarni, M.A.; Pandit, K.S.; Desai, U.V.; Lad, U.P.; Wadgaonkar, P.P. Diethylamine: A smart organocatalyst in eco-safe and diastereoselective synthesis of medicinally privileged 2-amino-4H-chromenes at ambient temperature. *Comp. Rend. Chim.* **2013**, 16, 689-695.
- ⁵¹ Curini, M.; Epifano, F.; Chimichi, S.; Montanari, F.; Nocchetti, M.; Rosati, O. Potassium exchanged layered zirconium phosphate as catalyst in the preparation of 4H-chromenes. *Tetrahedron Lett.* **2005**, 46, 3497-3499.
- ⁵² Yadav, J.S.; Reddy, B.V.S.; Gupta, M.K.; Prathap, I.; Pandey, S.K. Amberlyst A-21[®]: An efficient, cost-effective and recyclable catalyst for the synthesis of substituted 4H-chromenes. *Catal. Commun.* **2007**, 8, 2208-2211.
- ⁵³ Constantino, U.; Curini, M.; Montanari, F.; Nocchetti, M.; Rosati, O. Hydrotalcite-like compounds as heterogeneous catalysts in liquid phase organic synthesis. II. Preparation of 4H-chromenes promoted by hydrotalcite doped with hydrous tin(IV) oxide. *Micropor. Mesopor. Mat.* **2008**, 107, 16-22.
- ⁵⁴ Yu, N.; Aramini, J.M.; Germann, M.W.; Huang, Z. Reactions of 2-hydroxybenzaldehydes with alkyl cyanoacetates on the surface of solid catalysts: syntheses of 4H-chromene derivatives. *Tetrahedron Lett.* **2002**, 41, 6993-6996.
- ⁵⁵ Zhu, J.; Bienayme, H. *Multicomponent Reactions*; WILEY-VCH Verlag GmbH & Co. KGaA: Weinheim, 2005.
- ⁵⁶ Velasco, J.; Pérez-Mayoral, E.; Calvino-Casilda, V.; López-Peinado, A.J.; Bañares, M.A.; Soriano, E. Imidazolium sulfonates as environmental-friendly catalytic systems for the synthesis of biologically active 2-amino-4H-chromenes: mechanistic insights. *J. Phys. Chem. B.* **2015**, 119, 12042-12049.
- ⁵⁷ Smuszkiewicz, A.; López-Sanz, J.; Sobczak, I.; Martín-Aranda, R.M.; Ziolk, M.; Pérez-Mayoral, E. Tantalum vs Niobium MCF nanocatalysts in the green synthesis of chromene derivatives. *Catal. Today.* **2019**, 325, 47-52.
- ⁵⁸ Smuszkiewicz, A.; López-Sanz, J.; Sobczak, I.; Ziolk, M.; Martín-Aranda, R.M.; Soriano, E.; Pérez-Mayoral, E. Mesoporous niobiosilicate NbMCF modified with alkali metals in the synthesis of chromene derivatives. *Catal. Today* **2016**, 277, 133-142.
- ⁵⁹ Velázquez-Herrera, F. D.; González-Rodal, D.; Fetter, G.; Pérez-Mayoral, E. Enhanced catalytic performance of highly mesoporous hydrotalcite/SBA-15 composites involved in chromene multicomponent synthesis. *Micropor. Mesopor. Mat.* **2020**, 309, 110569.
- ⁶⁰ Velázquez-Herrera, F. D.; González-Rodal, D.; Fetter, G.; Pérez-Mayoral, E. Towards highly efficient hydrotalcite/hydroxyapatite composites as novel catalysts involved in eco-synthesis of chromene derivatives. *App. Clay Sci.* **2020**, 198, 105833.

- ⁶¹ Ioannidou, O.; Zabaniotou, A. Agricultural residues as precursors for activated carbón production-A review. *Renew. Sust. Energ. Rev.* **2007**, *11*, 1966-2005.
- ⁶² Bandosz, T. J. *Activated Carbon Surfaces in Environmental Remediation, Vol. 7*. Academic Press, 2006.
- ⁶³ Pérez-Mayoral, E.; Matos, I.; Bernardo, M.; Fonseca, I. M. New and Advanced Porous Carbon Materials in Fine Chemical Synthesis. Emerging Precursors of Porous Carbons. *Catalysts* **2019**, *9*, 133.
- ⁶⁴ Marsh, H.; Rodríguez-Reinoso, F. Activated Carbon (Origins). In *Activated Carbon*. Elsevier Science, 2006, pp. 13–86.
- ⁶⁵ Stoeckli, H. F. Microporous carbons and their characterization: The present state of the art. *Carbon*, **1990**, *28*, 1–6.
- ⁶⁶ Kurzweil, P. CAPACITORS | *Electrochemical Double-Layer Capacitors: Carbon Materials*. In *Encyclopedia of electrochemical power sources Vol 3*; Garche J, Dyer CK, Moseley PT, Ogumi Z, Rand DAJ, Scrosati B, Eds.; Elsevier: Amsterdam, 2009; pp 634–648.
- ⁶⁷ Calvino-Casilda, V.; López-Peinado, A. J.; Durán-Valle, C. J.; Martín-Aranda, R. M. Last Decade of Research on Activated Carbons as Catalytic Support in Chemical Processes. *Catal. Rev.* **2010**, *52*, 325–380.
- ⁶⁸ Activated carbon applications. <http://www.nordicwatersa.com/activatedcarbon/applications.htm> (accessed April 17, 2020).
- ⁶⁹ Thommes, M.; Kaneko, K.; Neimark, A. V.; Oliver, J. P.; Rodriguez-Reinoso, F.; Rouquerol, J.; Sing, K. Physisorption of gases, with special reference to the evaluation of surface area and pore size distribution. *Pure Appl. Chem.* **2015**, *87*, 1051–1069.
- ⁷⁰ Othman, Z. A. Review: Fundamental Aspects of Silicate Mesoporous Materials. *Materials* **2012**, *5*, 2874–2902.
- ⁷¹ Wang, R.; Sang, S.; Zhu, D.; Liu, S.; Yu, K. Pore characteristics and controlling factors of the Lower Cambrian Hetang Formation shale in Northeast Jiangxi, China. *Energ. Explor. Exploit.* **2018**, *36*, 43–65.
- ⁷² Radovic, L. R.; Rodríguez Reinoso, F. *Chemistry and Physics of Carbon*. Thrower, P. A., Ed.; Marcel Dekker: New York, 1996, pp. 243–358.
- ⁷³ Yang, Ralph T. Active carbon. By H. Jankowska, A. Swiatkowski, and J. Choma, Ellis Horwood, West Sussex, England, and Prentice-Hall, Englewood Cliffs, NJ, 1991, 280 pp. *AICHE J.* **1992**, *38*.
- ⁷⁴ Chingombe, P.; Saha, B.; Wakeman, R.J. Surface modification and characterisation of a coal-based activated carbon. *Carbon* **2005**, *43*, 3132–3143.
- ⁷⁵ Gorgulho, H.F.; Mesquita, J.P.; Gonçalves, F.; Pereira, M.F.R.; Figueiredo, J.L. Characterization of the surface chemistry of carbon materials by potentiometric titrations and temperature-programmed desorption. *Carbon* **2008**, *46*, 1544–1555.
- ⁷⁶ Benzigar, M.R.; Talapaneni, S.N.; Joseph, S.; Ramadass, K.; Singh, G.; Scaranto, J.; Ravon, U.; Al-Bahily, K.; Vinu, A. Recent advances in functionalized micro and mesoporous carbon materials: Synthesis and applications. *Chem. Soc. Rev.* **2018**, *47*, 2680–2721.

- ⁷⁷ Activated Carbon Producers Association (ACPA): Brussels, Belgium. <https://activatedcarbon.org/index.php/activated-carbon> (accessed 13 July, 2020).
- ⁷⁸ Ghouma, I.; Mejdi, J.; Sophie, D.; Limousy, L.; Ghimbeu, C. M.; Ouederni, A. Activated carbon prepared by physical activation of olive stones for the removal of NO₂ at ambient temperature. *Int. Chem. Eng.* **2015**, *18*, 63-74.
- ⁷⁹ Yahya, M.A.; Al-Qodah, Z.; Ngah, C.W.Z. Agricultural bio-waste materials as potential sustainable precursors used for activated carbon production: A review. *Renew. Sustain. Energy Rev.* **2015**, *46*, 218–235.
- ⁸⁰ González-García, P. Activated carbon from lignocellulosics precursors: A review of the synthesis methods, characterization techniques and applications. *Renew. Sustain. Energy Rev.* **2018**, *82*, 1393–1414.
- ⁸¹ Tan, X.; Liu, S.; Liu, Y.; Gu, Y.; Zeng, G.; Hu, X.; Wang, X.; Liu, S.; Jiang, L. Biochar as potential sustainable precursors for activated carbon production: Multiple applications in environmental protection and energy storage. *Bioresour. Technol.* **2017**, *227*, 359–372.
- ⁸² Ioannidou, O.; Zabaniotou, A. Agricultural residues as precursors for activated carbon production—A review. *Renew. Sustain. Energy Rev.* **2007**, *11*, 1966–2005.
- ⁸³ Kim, H.S.; Kang, M.S.; Yoo, W.C. Highly Enhanced Gas Sorption Capacities of N-Doped Porous Carbon Spheres by Hot NH₃ and CO₂ Treatments. *J. Phys. Chem. C* **2015**, *119*, 28512–28522.
- ⁸⁴ Xiong, Z.; Shihong, Z.; Haiping, Y.; Tao, S.; Yingquan, C.; Hanping, C. Influence of NH₃/CO₂ Modification on the Characteristic of Biochar and the CO₂ Capture. *Bionergy Res.* **2013**, *6*, 1147–1153.
- ⁸⁵ Zhang, X.; Zhang, S.; Yang, H.; Feng, Y.; Chen, Y.; Wang, X.; Chen, H. Nitrogen enriched biochar modified by high temperature CO₂–ammonia treatment: Characterization and adsorption of CO₂. *Chem. Eng. J.* **2014**, *257*, 20–27.
- ⁸⁶ Wachowski, L.; Hofman, M. Thermogravimetric and textural studies of modified carbonaceous materials. *Thermochim. Acta* **2005**, *437*, 82–86.
- ⁸⁷ Sivaraj, R.; Rajendran, V.; Gunalan, G. S. Preparation and Characterization of Activated Carbons from Parthenium Biomass by Physical and Chemical Activation Techniques. *J. Chem.* **2010**, *7*, 1314-1319.
- ⁸⁸ Díaz-Terán, J. Aplicación de las técnicas de análisis térmico a velocidad controlada, CRTA, en el estudio y preparación de carbones activados químicamente de origen lignocelulósico. Ph.D. Dissertation, Universidad Nacional de Educación a Distancia, 2006.
- ⁸⁹ Canales-Flores, R.A.; Prieto-García, F. Activation Methods of Carbonaceous Materials Obtained from Agricultural Waste. *Chem. Biodivers.* **2016**, *13*, 261–268.
- ⁹⁰ Jain, A.; Balasubramanian, R.; Srinivasan, M.P. Hydrothermal conversion of biomass waste to activated carbon with high porosity: A review. *Chem. Eng. J.* **2016**, *283*, 789–805.
- ⁹¹ Ao, W.; Fu, J.; Mao, X.; Kang, Q.; Ran, C.; Liu, Y.; Zhang, H.; Gao, Z.; Li, J.; Liu, G.; et al. Microwave assisted preparation of activated carbon from biomass: A review. *Renew. Sustain. Energy Rev.* **2018**, *92*, 958–979.

- ⁹² Enterría, M.; Figueiredo, J.L. Nanostructured mesoporous carbons: Tuning texture and surface chemistry. *Carbon* **2016**, *108*, 79–102.
- ⁹³ Rojas-Cervantes, M.L. Some strategies to lower the production cost of carbon gels. *J. Mater. Sci.* **2015**, *50*, 1017–1040.
- ⁹⁴ Rey-Raap, N.; Arenillas, A.; Menéndez, J.A. Carbon Gels and Their Applications: A Review of Patents. In *Submicron Porous Materials*; Springer: Cham, Switzerland, 2017, pp. 25–52.
- ⁹⁵ Lee, J.; Kim, J.; Hyeon, T. Recent Progress in the Synthesis of Porous Carbon Materials. *Adv. Mater.* **2006**, *18*, 2073–2094.
- ⁹⁶ Zhang, X.; Li, W.; Lu, A. Designed porous carbon materials for efficient CO₂ adsorption and separation. *New Carbon Mater.* **2015**, *30*, 481–501.
- ⁹⁷ Chuenchom, L.; Kraehnert, R.; Smarsly, B.M. Recent progress in soft-templating of porous carbon materials. *Soft Matter*. **2012**, *8*, 10801-10812.
- ⁹⁸ Dutta, S.; Bhaumik, A.; Wu, K.C.W. Hierarchically porous carbon derived from polymers and biomass: Effect of interconnected pores on energy applications. *Energy Environ. Sci.* **2014**, *7*, 3574–3592.
- ⁹⁹ Bhatnagar, A.; Hogland, W.; Marques, M.; Sillanpää, M. An overview of the modification methods of activated carbon for its water treatment applications. *Chem. Eng. J.* **2013**, *219*, 499-511.
- ¹⁰⁰ Ozsoy, H. D.; van Leeuwen, J. H. Removal of color from fruit candy waste by activated carbon adsorption. *J. Food Eng.* **2010**, *101*, 106-112.
- ¹⁰¹ Durán, I.; Álvarez-Gutiérrez, N.; Rubiera, F.; Pevida, C. Biogas purification by means of adsorption on pine sawdust-based activated carbon: Impact of water vapor. *Chem. Eng. J.* **2018**, *353*, 197-207.
- ¹⁰² Giraudet, S.; Boulinguez, B.; Le Cloirec, P. Adsorption and Electrothermal Desorption of Volatile Organic Compounds and Siloxanes onto an Activated Carbon Fiber Cloth for Biogas Purification. *Energy Fuels* **2014**, *28*, 3924–3932.
- ¹⁰³ Alvarez-Pitti, J.; Rodríguez-Varela, A.; Morales-Carpi, C.; Lurbe, E.; Estañ, L. Naphazoline intoxication in children. *Eur. J. Pediatr.* **2006**, *165*, 815-816.
- ¹⁰⁴ Valente Nabais, J. M.; Ledesma, B.; Laginhas, C. Removal of amitriptyline from simulated gastric and intestinal fluids using activated carbons. *J. Pharm. Sci.* **2011**, *100*, 5096-5099.
- ¹⁰⁵ Liu, J.; Zeng, S. International Workshop on Ventilation, Comfort, and Health in Transport Vehicles. *Build. Environ.* **2012**, *47*, 357-367.
- ¹⁰⁶ Monser, L.; Adhoum, N. Modified activated carbon for the removal of copper, zinc, chromium and cyanide from wastewater. *Sep. Purif. Technol.* **2002**, *26*, 137-146.
- ¹⁰⁷ Adebajo, M.; Frost, R.; Kloprogge, J.; Carmody, O.; Kokot, S. Porous Materials for Oil Spill Cleanup: A Review of Synthesis and Absorbing Properties. *J. Porous Mater.* **2003**, *10*, 159–170.
- ¹⁰⁸ Matos, I.; Bernardo, M.; Fonseca, I. Porous carbon: A versatile material for catalysis. *Catal. Today*, **2017**, *285*, 194-203.

- ¹⁰⁹ a) Pérez-Mayoral, E.; Calvino-Casilda, V.; Godino, M.; López-Peinado, A.; Martín-Aranda, R. M. Porous Catalytic Systems in the Synthesis of Bioactive Heterocycles and Related Compounds. In *Green Synthetic Approaches for Biologically Relevant Heterocycles*. Brahmachari, G. Ed.; Elsevier: Amsterdam, 2015, pp. 378-403.; b) Pérez-Mayoral, E.; López-Peinado, A. J. Porous Catalytic Systems in the Synthesis of Bioactive Heterocycles and Related Compounds. In *Green Synthetic Approaches for Biologically Relevant Heterocycles*. 2nd Edition. Brahmachari, G. Ed.; Elsevier: Amsterdam, 2021, pp. 97-164.
- ¹¹⁰ Pérez-Mayoral, E.; Soriano, E.; Martín-Aranda, R. M.; Maldonado-Hódar, F. J. Mesoporous Catalytic Materials and Fine Chemistry. In *Comprehensive Guide for Mesoporous Materials. Volume 1: Synthesis and Characterization*, ed. Aliofkhazrae, M. Ed.; Nova Science Publishers, Inc., 2015, pp. 83-118.
- ¹¹¹ Pérez-Mayoral, E.; Calvino-Casilda, V.; Soriano, E. Metal-supported carbón-based materials: opportunities and challenges in the synthesis of valuable products. *Catal. Sci. Technol.* **2016**, 6, 1265-1291.
- ¹¹² J. López Sanz, E. Pérez-Mayoral, E. Soriano, D. Omenat-Morán, C.J. Durán, R.M. Martín-Aranda, I. Matos, I. Fonseca. Acid-Activated Carbon Materials: Cheaper Alternative Catalysts for the Synthesis of Substituted Quinolines. *ChemCatChem* **2013**, 5, 3736–3742.
- ¹¹³ Godino-Ojer, M.; Soriano, E.; Calvino-Casilda, V.; Maldonado-Hódar, F. J.; Pérez-Mayoral, E. Metal-free synthesis of quinolines catalyzed by carbon aerogels: Influence of the porous texture and surface chemistry. *Chem. Eng. J.* **2017**, 314, 488–497.
- ¹¹⁴ Marco-Contelles, J.; Pérez-Mayoral, E.; Samadi, A.; Carreiras, M. do C.; Soriano, E. Recent Advances in the Friedländer Reaction. *Chem. Rev.* **2009**, 109, 2652-2671.
- ¹¹⁵ Godino-Ojer, M.; Matos, I.; Bernardo, M.; Carvalho, R.; Soares, O.S., Durán-Valle, C.; Fonseca, I.M.; Pérez Mayoral, E. Acidic porous carbons involved in the green and selective synthesis of benzodiazepines, *Catal.Today* **2020**, 357, 64-73.
- ¹¹⁶ Godino-Ojer, M.; Blazquez-García, R.; Matos, I.; Bernardo, I.; Fonseca, I.M.; Pérez-Mayoral, E. Porous carbons-derived from vegetal biomass in the synthesis of quinoxalines. Mechanistic insights. *Catal. Today* **2020**, 354, 90–99.
- ¹¹⁷ Godino-Ojer, M.; López-Peinado, A. J.; Maldonado-Hódar, F. J.; Pérez-Mayoral, E. Highly Efficient and Selective Catalytic Synthesis of Quinolines Involving Transition-Metal-Doped Carbon Aerogels. Back cover. *ChemCatChem* **2017**, 9, 1422-1428.
- ¹¹⁸ Godino-Ojer, M.; Martín-Aranda, R. M.; Maldonado-Hódar, F. J.; Pérez-Cadenas, A. F.; Pérez-Mayoral, E. Developing strategies for the preparation of Co-carbon catalysts involved in the free solvent selective synthesis of aza-heterocycles. *Mol. Catal.* **2018**, 445, 223-231.
- ¹¹⁹ Godino-Ojer, M.; López-Peinado, A. J.; Maldonado-Hódar, F. J.; Bailón-García, E.; Pérez-Mayoral, E. Cobalt oxide-carbon nanocatalysts with highly enhanced catalytic performance for the green synthesis of nitrogen heterocycles through the Friedländer condensation. *Dalton Trans.* **2019**, 48, 5637-5648.

- ¹²⁰ Godino-Ojer, M.; López-Peinado, A. J.; Martín-Aranda, R. M.; Przepiórski, J.; Pérez-Mayoral, E.; Soriano, E. Eco-Friendly Catalytic Systems Based on Carbon-Supported Magnesium Oxide Materials for the Friedländer Condensation. *ChemCatChem* **2014**, *6*, 3440-3447.
- ¹²¹ Durán-Valle, C. J.; Carvalho, R. C. S.; Omenat-Morán, D.; Botet-Jiménez, A. B. Activated carbons as catalyst in the synthesis of fine chemicals. *Bol. Grupo Español Carbón* **2016**, 7-10.
- ¹²² Durán-Valle, C. J.; Ferrera-Escudero, S.; Calvino-Casilda, V.; Díaz-Terán, J.; Martín-Aranda, R. M. The effect of ultrasound on the catalytic activity of alkaline carbons: preparation of N-alkyl imidazoles. *Appl. Surf. Sci.* **2004**, *238*, 97–100.
- ¹²³ López-Pestaña, J. M.; Díaz-Terán, J.; Avila-Rey, M. J.; Rojas-Cervantes, M. L.; Martín-Aranda, R. M. N-alkylation of imidazole by alkaline carbons. *Micropor. Mesopor. Mater.* **2004**, *67*, 87–94.
- ¹²⁴ Calvino-Casilda, V.; Martín-Aranda, R. M.; López-Peinado, A. J. Microwave assisted green synthesis of long-chain 1-alkylimidazoles and medium-chain 1-alkyl-2-methylimidazoles with antiviral properties catalyzed by basic carbons. *Catal. Lett.* **2009**, *129*, 281–286.
- ¹²⁵ Calvino-Casilda, V.; López-Peinado, A. J.; Martín-Aranda, R. M.; Ferrera-Escudero, S.; Durán-Valle, C. J. Ultrasound-promoted N-propargylation of imidazole by alkaline-doped carbons. *Carbon* **2004**, *42*, 1363–1366.
- ¹²⁶ Ferrera-Escudero, S.; Perozo-Rondón, E.; Calvino-Casilda, V.; Casal, B.; Martín-Aranda, R. M.; López-Peinado, A. J.; Durán-Valle, C. J. The effect of ultrasound on the N-alkylation of imidazole over alkaline carbons: Kinetic aspects. *Appl. Catal. A* **2010**, *378*, 26–32.
- ¹²⁷ Calvino-Casilda, V.; Martín-Aranda, R. M.; López-Peinado, A. J. Alkaline carbons as effective catalysts for the microwave-assisted synthesis of N-substituted-gamma-lactams. *Appl. Catal. A* **2011**, *398*, 73–81.
- ¹²⁸ Foo, M. L.; Matsuda, R.; Kitagawa, S. Functional hybrid porous coordination polymers. *Chem. Mater.* **2014**, *26*, 310-322.
- ¹²⁹ Eddaoudi, M.; Moler, D. B.; Li, H.; Chen, B.; Reineke, T. M.; O’Keeffe, M.; Yaghi, O. M. Modular Chemistry: Secondary Building Units as a Basis for the Design of Highly Porous and Robust Metal–Organic Carboxylate Frameworks. *Acc. Chem. Res.* **2001**, *34*, 319-330.
- ¹³⁰ Suh, M. P.; Park, H. J.; Prasad, T. K.; Lim, D. W. Hydrogen storage in metal–organic frameworks. *Chem. Rev.* **2012**, *112*, 782-835.
- ¹³¹ Monge, Á.; Gándara, F.; Gutiérrez-Puebla, E.; Snejko, N. Lanthanide, Y and Sc MOFs: where amazing crystal structures meet outstanding material properties. *CrystEngComm* **2011**, *13*, 5031-5044.
- ¹³² Hashemi, B.; Zohrabi, P.; Raza, N.; Kim, K.H. Metal-organic frameworks as advanced sorbents for the extraction and determination of pollutants from environmental, biological, and food media. *Trends Analyt. Chem.* **2017**, *97*, 65-82.
- ¹³³ Kitagawa, S.; Kitaura, R.; Noro, S.I. Functional porous coordination polymers. *Angew. Chem. Int. Ed.* **2004**, *43*, 2334-2375.

- ¹³⁴ Web of Science. Fundación Española para la Ciencia y la Tecnología. 2020. <http://www.wos.fecyt.es> (accessed 25 July, 2020)
- ¹³⁵ Wang, Z.; Cohen, S. M. Postsynthetic covalent modification of a neutral metal–organic framework. *J. Am. Chem. Soc.* **2007**, *129*, 12368–12369.
- ¹³⁶ Férey, G. Hybrid porous solids: past, present, future. *Chem. Soc. Rev.* **2008**, *37*, 191–214.
- ¹³⁷ Furukawa, H.; Cordova, K. E.; O’Keeffe, M.; Yaghi, O. M. The chemistry and applications of metal–organic frameworks. *Science* **2013**, *341*, 6149.
- ¹³⁸ Eddaoudi, M.; Moler, D. B.; Li, H.; Chen, B.; Reineke, T. M.; O’Keeffe, M.; Yaghi, O. M. Modular Chemistry: Secondary Building Units as a Basis for the Design of Highly Porous and Robust Metal–Organic Carboxylate Frameworks. *Acc. Chem. Res.* **2001**, *34*, 319–330.
- ¹³⁹ Yaghi, O. M.; O’Keeffe, M.; Ockwig, N. W.; Chae, H. K.; Eddaoudi, M.; Kim, J. Reticular synthesis and the design of new materials. *Nature* **2003**, *423*, 705–714.
- ¹⁴⁰ Baerlocher, C.; McCusker, L. B.; Olson, D. H. *Atlas of zeolite framework types*. Elsevier: Amsterdam, 2007.
- ¹⁴¹ Rowsell, J. L.; Yaghi, O. M. Metal–organic frameworks: a new class of porous materials. *Micropor. Mesopor. Mat.* **2004**, *73*, 3–14.
- ¹⁴² Stock, N.; Biswas, S. Synthesis of Metal–Organic Frameworks (MOFs): Routes to Various MOF Topologies, Morphologies, and Composites. *Chem. Rev.* **2011**, *112*, 933–969.
- ¹⁴³ Jiang, H.L.; Xu, Q. Nanoporous Metal–Organic Frameworks. In *Nanoporous materials: synthesis and applications*; Xu, Q. Ed.; CRC Press, 2013; pp. 71–97.
- ¹⁴⁴ Tranchemontagne, D. J.; Hunt, J. R.; Yaghi, O. M. Room temperature synthesis of metal–organic frameworks: MOF-5, MOF-74, MOF-177, MOF-199, and IRMOF-0. *Tetrahedron* **2008**, *64*, 8553–8557.
- ¹⁴⁵ Hwang, Y. K.; Chang, J. S.; Park, S. E.; Kim, D. S.; Kwon, Y. U.; Jhung, S. H.; Hwang, J. S.; Park, M. S. Microwave fabrication of MFI zeolite crystals with a fibrous morphology and their applications. *Angew. Chem. Int. Ed.* **2005**, *44*, 556–560.
- ¹⁴⁶ Kappe, C. O.; Dallinger, D. Controlled microwave heating in modern organic synthesis: highlights from the 2004–2008 literature. *Mol. Divers.* **2009**, *13*, 71–193.
- ¹⁴⁷ Jiang, H. L.; Xu, Q. Porous metal–organic frameworks as platforms for functional applications. *Chem. Commun.* **2011**, *47*, 3351–3370 3351.
- ¹⁴⁸ Klinowski, J.; Paz, F. A. A.; Silva, P.M.; Rocha, J. Microwave-assisted synthesis of metal–organic frameworks. *Dalton Trans.* **2011**, *40*, 321–330.
- ¹⁴⁹ Fidalgo-Marijuan, A.; Barandika, G.; Bazán, B.; Urtiaga, M. K.; Arriortua, M. I. Self-assembly of iron TCPP (meso-tetra (4-carboxyphenyl) porphyrin) into a chiral 2D coordination polymer. *Polyhedron* **2011**, *30*, 2711–2716.
- ¹⁵⁰ Meek, S. T.; Greathouse, J. A.; Allendorf, M. D. Metal–organic frameworks: A rapidly growing class of versatile nanoporous materials. *Adv. Mater.* **2011**, *23*, 249–267.

- ¹⁵¹ Chen, D.; Sharma, S.K.; Mudhoo, A. *Handbook on Applications of Ultrasound, Sonochemistry for Sustainability*. Ed. Taylor & Francis: London, New York, 2012.
- ¹⁵² Pichon, A.; James, S. L. An array-based study of reactivity under solvent-free mechanochemical conditions-insights and trends. *CrystEngComm* **2008**, *10*, 1839-1847.
- ¹⁵³ Pichon, A.; Lazuen-Garay, A.; James, S. L. Solvent-free synthesis of a microporous metal-organic framework. *CrystEngComm* **2006**, *8*, 211-214.
- ¹⁵⁴ Cubillas, P.; Anderson, M.W. Synthesis mechanism: crystal growth and nucleation. In *Zeolites and Catalysis, Synthesis, Reactions and Applications*; Cejka, J.; Corma, A.; Zones, S. Eds. Verlag GmbH & Co. KGaA: Weinheim, 2010; pp. 1-55.
- ¹⁵⁵ Bazán, B.; Barandika, G.; Calderón-Casado, A.; Fidalgo-Marijuan, A.; Llano-Tomé, F. Urtiaga, M. K.; Arriortua, M. I. Metodologías Sintéticas para la Obtención de Compuestos de Coordinación Metal-Orgánicos. *Macla, Revista de la sociedad española de mineralogía* **2012**, *16*, 162-163.
- ¹⁵⁶ Cudney, R.; Patel, S.; McPherson, A. Crystallization of macromolecules in silica gels. *Acta Crystallogr D Biol Crystallogr.* **1994**, *50*, 479-483.
- ¹⁵⁷ Deria, P.; Mondloch, J. E.; Karagiari, O.; Bury, W.; Hupp, J. T.; Farha, O. K. Beyond post-synthesis modification: evolution of metal-organic frameworks via building block replacement. *Chem. Soc. Rev.* **2014**, *43*, 5896-5912.
- ¹⁵⁸ Zhou, G. J.; Wong, W. Y. Organometallic acetylides of PtII, AuI and HgII as new generation optical power limiting materials. *Chem. Soc. Rev.* **2011**, *40*, 2541.
- ¹⁵⁹ Kumar, G.; Gupta, R. Molecularly designed architectures – the metalloligand way. *Chem. Soc. Rev.* **2013**, *42*, 9403.
- ¹⁶⁰ Horcajada, P.; Serre, C.; Vallet-Regí, M.; Sebba, M.; Taulelle, F.; Férey, G. Metal-Organic Frameworks as Efficient Materials for Drug Delivery. *Angew. Chem. Int.* **2006**, *45*, 5974-5978.
- ¹⁶¹ Cui, Y.; Yue, Y.; Qian, G.; Chen, B. Luminescent functional metal-organic frameworks. *Chem. Rev.* **2012**, *112*, 1126-62.
- ¹⁶² Sorribas, S.; Téllez, C. MOFs: Properties and application in more efficient separations. *Bol. Grupo Español Carbón* **2016**, 19-22.
- ¹⁶³ Furukawa, H.; Ko, N.; Go, Y. B.; Aratani, N.; Choi, S. B.; Choi, E.; Yazaydin, A. Ö.; Snurr, R. Q.; O’Keffe, M.; Kim, J.; Yaghi, O. M. Ultrahigh Porosity in Metal-Organic Frameworks. *Science* **2010**, *329*, 424-428.
- ¹⁶⁴ BASF to showcase metal organic frameworks (MOFs) for energy storage at NGV Americas Conference. <https://www.basf.com/us/en/media/news-releases/2013/11/p-13-452.html> (accessed 07 August, 2020).
- ¹⁶⁵ Farha, O. K.; Özgür-Yazaydin, A.; Eryazici, I.; Malliakas, C. D.; Hauser, B. G.; Kanatzidis, M. G.; Nguyen, S. T.; Snurr, R. Q.; Hupp, J. T. De novo synthesis of a metal-organic framework material featuring ultrahigh surface area and gas storage capacities. *Nat. Chem.* **2010**, *2*, 944-948.

- ¹⁶⁶ Mulfort, K. L.; Farha, O. K.; Stern, C. L.; Sarjeant, A. A.; Hupp, J. T. Post-Synthesis Alkoxide Formation Within Metal–Organic Framework Materials: A Strategy for Incorporating Highly Coordinatively Unsaturated Metal Ions. *J. Am. Chem. Soc.* **2009**, *131*, 3866-3868.
- ¹⁶⁷ Sun, Y.; Wang, L.; Amer, W. A.; Yu, H.; Ji, J.; Huang, L.; Shan, J.; Tong, R. Hydrogen Storage in Metal–Organic Frameworks. *J. Inorg. Organomet. Polymer Mat.* **2012**, *23*, 270-285.
- ¹⁶⁸ Phan, A.; Czaja, A. U.; Gándara, F.; Knobler, C. B.; Yaghi, O. M. Metal–Organic Frameworks of Vanadium as Catalysts for Conversion of Methane to Acetic Acid. *Inorg. Chem.* **2011**, *50*, 7388-7390.
- ¹⁶⁹ Seo, J. S.; Whang, D.; Lee, H.; Jun, S. I.; Oh, J.; Jeon, Y. J.; Kim, K. A homochiral metal–organic porous material for enantioselective separation and catalysis. *Nature* **2000**, *404*, 982-986.
- ¹⁷⁰ Wu, C.D.; Hu, A.; Zhang, L.; Lin, W. A Homochiral Porous Metal–Organic Framework for Highly Enantioselective Heterogeneous Asymmetric Catalysis. *J. Am. Chem. Soc.* **2005**, *127*, 8940-8941.
- ¹⁷¹ Lee, J. Y.; Farha, O. K.; Roberts, J.; Scheidt, K. A.; Nguyen, S. B. T.; Hupp, J. T., Metal-organic framework materials as catalysts. *Chem. Soc. Rev.* **2009**, *38*, 1450-1459.
- ¹⁷² Cho, S. H.; Ma, B.; Nguyen, S. T.; Hupp, J. T.; Albrecht-Schmitt, T. E. A Metal–Organic Framework Material that Functions as an Enantioselective Catalyst for Olefin Epoxidation. *ChemInform* **2006**, *25*, 2563-2565.
- ¹⁷³ Alkordi, M. H.; Liu, Y.; Larsen, R. W.; Eubank, J. F.; Eddaoudi, M. Zeolite-like Metal–Organic Frameworks as Platforms for Applications: On Metalloporphyrin-Based Catalysts. *J. Am. Chem. Soc.* **2008**, *130*, 12639-12641.
- ¹⁷⁴ Gascon, J. *Metal organic frameworks as heterogeneous catalysts (No. 12)*. Royal Society of Chemistry, 2013.
- ¹⁷⁵ Pérez-Mayoral, E.; Čejka, J. [Cu₃(BTC)₂]: a metal-organic framework catalyst for the Friedländer reaction. *ChemCatChem* **2011**, *3*, 157-159.
- ¹⁷⁶ Pérez-Mayoral, E.; Musilová, Z.; Gil, B.; Marszalek, B.; Položij, M.; Nachtigall, P.; Čejka, J. Synthesis of quinolines via Friedländer reaction catalyzed by CuBTC metal–organic-framework. *Dalton Trans.* **2012**, *41*, 4036-4044.
- ¹⁷⁷ Položij, M.; Pérez-Mayoral, E.; Čejka, J.; Hermann, J.; Nachtigall, P. Theoretical investigation of the Friedländer reaction catalysed by CuBTC: Concerted effect of the adjacent Cu²⁺ sites. *Catal. Today* **2013**, *204*, 101-107.
- ¹⁷⁸ Godino-Ojer, M.; Shamzhy, M.; Čejka, J.; Pérez-Mayoral, E. Basolites: A type of metal organic frameworks highly efficient in the one-pot synthesis of quinoxalines from α -hydroxy ketones under aerobic conditions. *Catal. Today* **2020**, *345*, 258-266.
- ¹⁷⁹ Chiola, V.; Ritsko, J. E.; Vanderpool, C. D. Process for producing low-bulk density silica. U. S. Patent, 3556725, 1971.

- ¹⁸⁰ Beck, J. S.; Vartuli, J. C.; Roth, W. J.; Leonowicz, M. E.; Kresge, C. T.; Schmitt, K. D.; Chu, C. T. W.; Olson, D. H.; Sheppard, E. W.; McCullen, S. B.; Higgins, J. B.; Schlenker, J. L. A new family of mesoporous molecular sieves prepared with liquid crystal templates. *J. Am. Chem. Soc.* **1992**, *114*, 10834-10834.
- ¹⁸¹ Zhao, D. Y.; Feng, J. L.; Huo, Q. S.; Melosh, N.; Fredrickson, G. H.; Chmelka, B. F.; Stucky, G. D. Triblock Copolymer Syntheses of Mesoporous Silica with Periodic 50 to 300 Angstrom Pores. *Science* **1998**, *279*, 548-552.
- ¹⁸² Khodakov, Y.; Zholobenko, V. L.; Bechara, R.; Durant, D. Impact of aqueous impregnation on the long-range ordering and mesoporous structure of cobalt containing MCM-41 and SBA-15 materials. *Micropor. Mesopor. Mat.* **2005**, *79*, 29-39.
- ¹⁸³ Linssen, T.; Cassiers, K.; Cool, P.; Vansent, E. F. Mesoporous templated silicates: an overview of their synthesis, catalytic activation and evaluation of the stability. *Adv. Colloid Interface Sci.* **2003**, *103*, 121-147.
- ¹⁸⁴ Xue, G.; Yurun, F.; Li, M.; Dezhi, G.; Jie, J.; Jincheng, Y.; Sun, H.; Gong, H.; Yujun, Z. Phosphoryl functionalized mesoporous silica for uranium adsorption. *Appl. Surf. Sci.* **2017**, *402*, 53–60.
- ¹⁸⁵ Cattaneo, A. S.; Ferrara, C.; Villa, D. C.; Angioni, S.; Milanese, C.; Capsoni, D.; Grandi, S.; Mustarelli, P.; Allodi, V.; Mariotto, G.; Brutti, S.; Quartarone, E. SBA-15 mesoporous silica highly functionalized with propylsulfonic pendants: A thorough physico-chemical characterization. *Micropor. Mesopor. Mat.* **2016**, *219*, 219-229.
- ¹⁸⁶ Dragoi, B.; Dumitriu, E.; Guimon, C.; Auroux, A. Acidic and adsorptive properties of SBA-15 modified by aluminum incorporation. *Micropor. Mesopor. Mat.* **2009**, *121*, 7-17.
- ¹⁸⁷ Sonwane, C. G.; Ludovice, P. J. A note on micro-and mesopores in the walls of SBA-15 and hysteresis of adsorption isotherms. *J. Mol. Catal. A.* **2005**, *238*, 135-137.
- ¹⁸⁸ Xue, G.; Yurun, F.; Li, M.; Dezhi, G.; Jie, J.; Jincheng, Y.; Sun, H.; Gong, H.; Yujun, Z. Phosphoryl functionalized mesoporous silica for uranium adsorption. *App. Surf. Sci.* **2017**, *402*, 53–60.
- ¹⁸⁹ Zelenak, V.; Badanicova, M.; Halamova, D.; Cejka, J.; Zukal, A.; Murafa, N.; Goerigk, G. Amine-modified ordered mesoporous silica: Effect of pore size on carbon dioxide capture. *Chem. Eng. J.* **2008**, *144*, 336-342.
- ¹⁹⁰ Hesemann, P.; Nguyen, T. P.; Hankari, S. E. Precursor mediated synthesis of nanostructured silicas: from precursor-surfactant ion pairs to structured materials. *Materials* **2014**, *7*, 2978-3001.
- ¹⁹¹ Huirache-Acuña, R.; Nava, R.; Peza-Ledesma, C. L.; Lara-Romero, J.; Alonso-Núñez, G.; Pawelec, B.; Rivera-Muñoz, E. M. SBA-15 mesoporous silica as catalytic support for hydrodesulfurization catalysts. *Materials* **2013**, *6*, 4139-4167.
- ¹⁹² Lettow, J. S.; Han, Y. J.; Schmidt-Winkel, P.; Yang, P.; Zhao, D.; Stucky, G. D.; Ying, J. Y. Hexagonal to mesocellular foam phase transition in polymer-templated mesoporous silicas. *Langmuir* **2000**, *16*, 8291-8295.

- ¹⁹³ Schmidt-Winkel, P.; Lukens, W. W.; Yang, P.; Margolese, D. I.; Lettow, J. S.; Ying, J. Y.; Stucky, G. D. Microemulsion templating of siliceous mesostructured cellular foams with well-defined ultralarge mesopores. *Chem. Mater.* **2000**, *12*, 686-696.
- ¹⁹⁴ Stawicka, K.; Sobczak, I.; Trejda, M.; Sulikowski, B.; Ziolk, M. Organosilanes affecting the structure and formation of mesoporous cellular foams. *Micropor. Mesopor. Mat.* **2012**, *155*, 143-152.
- ¹⁹⁵ Schmidt-Winkel, P.; Lukens, W. W.; Zhao, D.; Yang, P.; Chmelka, B. F.; Stucky, G. D. Mesocellular siliceous foams with uniformly sized cells and windows. *J. Am. Chem. Soc.* **1999**, *121*, 254-255.
- ¹⁹⁶ Wisniewska, J.; Ziolk, M. Formation of Pt-Ag alloy on different silicas - surface properties and catalytic activity in oxidation of methanol. *RSC Advances*, **2017**, *7*, 9534-9544.
- ¹⁹⁷ Stein, A.; Melde, B. J.; Schrodin, R. C. Hybrid Inorganic-Organic Mesoporous Silicates—Nanosopic Reactors Coming of Age. *Adv. Mater.*, **2000**, *12*, 1403-1419.
- ¹⁹⁸ AlOthman, Z. A Review: Fundamental Aspects of Silicate Mesoporous Materials. *Materials*, **2012**, *5*, 2874-2902.
- ¹⁹⁹ Gierada, M.; Petit, I.; Handzlik, J.; Tielens, F. Hydration in silica based mesoporous materials: a DFT model. *Phys. Chem. Chem. Phys.* **2016**, *18*, 32962-32972.
- ²⁰⁰ Pérez-Mayoral, E.; Godino-Ojer, M.; González-Rodal, D. Bifunctional Porous Catalysts in the Synthesis of Valuable Products. In *Nanocatalysis: Applications and Technologies*. Calvino-Casilda, V.; López-Peinado, A. J.; Martín-Aranda, R. M.; Pérez-Mayoral, E., Eds.; CRC Press, 2018, pp. 25-61.
- ²⁰¹ Kelut, P.; Kulkarni, K.; Kulkarni, A. D. CO₂ adsorption by various catalysts. *Chem. Process Eng. Res.* **2014**, *18*, 7-15.
- ²⁰² Yokoi, T.; Kubota, Y.; Tatsumi, T. Amino-functionalized mesoporous silica as base catalyst and adsorbent. *App. Catal. A* **2012**, *421*, 14-37.
- ²⁰³ Kishor, R.; Ghoshal, A. K. APTES grafted ordered mesoporous silica KIT-6 for CO₂ adsorption. *Chem. Eng. J.* **2015**, *262*, 882-890.
- ²⁰⁴ Gil, M.; Tiscornia, I.; de la Iglesia, Ó.; Mallada, R.; Santamaría, J. Monoamine-grafted MCM-48: An efficient material for CO₂ removal at low partial pressures. *Chem. Eng. J.* **2011**, *175*, 291-297.
- ²⁰⁵ Yamada, H.; Dao, D. S.; Chowdhury, F. A.; Fujiki, J.; Goto, K.; Yogo, K. Development of amine-impregnated solid sorbents for CO₂ capture. *Energy Procedia* **2014**, *63*, 2346-2350.
- ²⁰⁶ Dou, B.; Hu, Q.; Li, J.; Qiao, S.; Hao, Z. Adsorption performance of VOCs in ordered mesoporous silicas with different pore structures and surface chemistry. *J. Hazard. Mater.* **2011**, *186*, 1615-1624.
- ²⁰⁷ Ushiki, I.; Ota, M.; Sato, Y.; Inomata, H. VOCs (acetone, toluene, and n-hexane) adsorption equilibria on mesoporous silica (MCM-41) over a wide range of supercritical carbon dioxide conditions: Experimental and theoretical approach by the Dubinin-Astakhov equation. *Fluid Ph. Equilibria* **2015**, *403*, 78-84.
- ²⁰⁸ Yokoi, T.; Kubota, Y.; Tatsumi, T. Amino-functionalized mesoporous silica as base catalyst and adsorbent. *App. Catal. A* **2012**, *421*, 14-37.

- ²⁰⁹ Zhang, Y.; Zhang, J.; Jiang, T.; Wang, S. Inclusion of the poorly water-soluble drug simvastatin in mesocellular foam nanoparticles: Drug loading and release properties. *Int. J. Pharm.* **2011**, *410*, 118–124.
- ²¹⁰ Moritz, M.; Geszke-Moritz, M. Mesoporous materials as multifunctional tools in biosciences: Principles and applications. *Mater. Sci. Eng. C* **2015**, *49*, 114–151.
- ²¹¹ Vallet-Regi, M.; Rámila, A.; Del Real, R. P.; Pérez-Pariente, J. A new property of MCM-41: drug delivery system. *Chem. Mater.* **2001**, *13*, 308–311.
- ²¹² Basaldella, E. I.; Legnoverde, M. S. Functionalized silica matrices for controlled delivery of cephalexin. *J. Sol-Gel Sci. Technol.* **2010**, *56*, 191–196.
- ²¹³ Popova, M. D.; Szegedi, Á.; Kolev, I. N.; Mihály, J.; Tzankov, B. S.; Momekov, G. T.; Lambov, N. G.; Yoncheva, K. P. Carboxylic modified spherical mesoporous silicas as drug delivery carriers. *Int. J. Pharm.* **2012**, *436*, 778–785.
- ²¹⁴ Lu, J.; Li, Z.; Zink, J. I.; Tamanoi, F. In vivo tumor suppression efficacy of mesoporous silica nanoparticles-based drug-delivery system: enhanced efficacy by folate modification. *Nanomedicine* **2012**, *8*, 212–220.
- ²¹⁵ Moritz, M.; Geszke-Moritz, M. Mesoporous materials as multifunctional tools in biosciences: principles and applications. *Mater. Sci. Eng. C* **2015**, *49*, 114–151.
- ²¹⁶ Chen, H. T.; Trewyn, B. G.; Wiench, J. W.; Pruski, M.; Lin, V. S. Y. Urea and thiourea-functionalized mesoporous silica nanoparticle catalysts with enhanced catalytic activity for Diels–Alder reaction. *Top Catal.* **2010**, *53*, 187–191.
- ²¹⁷ Huang, Y.; Trewyn, B. G.; Chen, H. T.; Lin, V. S. Y. One-pot reaction cascades catalyzed by base- and acid-functionalized mesoporous silica nanoparticles. *New J. Chem.* **2008**, *32*, 1311–1313.
- ²¹⁸ Huang, Y.; Xu, S.; Lin, V. S. Y. Bifunctionalized Mesoporous Materials with Site-Separated Brønsted Acids and Bases: Catalyst for a Two-Step Reaction Sequence. *Angew. Chem. Int. Ed.* **2011**, *50*, 661–664.
- ²¹⁹ Corma, A.; Boronat, M.; Climent, M.; Iborra, S.; Montón, R.; Sabater, M. J. A recyclable bifunctional acid–base organocatalyst with ionic liquid character. The role of site separation and spatial configuration of site separation and spatial configuration on different condensation reactions. *Phys. Chem.* **2011**, *13*, 17255–17261.
- ²²⁰ Martínez, C.; Corma, A. Inorganic molecular sieves: preparation, modification and industrial application in catalytic processes. *Coord. Chem. Rev.* **2011**, *255*, 1558–1580.
- ²²¹ Smuszkiewicz, A.; Pérez-Mayoral, E.; Soriano, E.; Sobczak, I.; Ziolk, M.; Martín-Aranda, R. M.; López-Peinado, A. J. Bifunctional mesoporous MCF materials as catalysts in the Friedländer condensation. *Catal. Today* **2013**, *218*, 70–75.
- ²²² Smuszkiewicz, A.; López-Sanz, J.; Pérez-Mayoral, E.; Soriano, E.; Sobczak, I.; Ziolk, M.; Martín-Aranda, R. M.; López-Peinado, A. J. Amino-grafted mesoporous materials based on MCF structure involved in the quinoline synthesis. Mechanistic insights. *J. Mol. Catal. A Chem.* **2013**, *378*, 38–46.

- ²²³ Aider, N.; Smuszkiewicz, A.; Pérez-Mayoral, E.; Soriano, E.; Martín-Aranda, R. M.; Halliche, D.; Menad, S. Amino-grafted SBA-15 material as dual acid–base catalyst for the synthesis of coumarin derivatives. *Catal. Today* **2014**, *227*, 215-222.
- ²²⁴ Blasco-Jiménez, D.; López-Peinado, A. J.; Martín-Aranda, R. M.; Ziolk, M.; Sobczak, I. Sonocatalysis in solvent-free conditions: An efficient eco-friendly methodology to prepare N-alkyl imidazoles using amino-grafted NbMCM-41. *Catal. Today* **2009**, *142*, 283-287.
- ²²⁵ Sobczak, I.; Ziolk, M.; Pérez-Mayoral, E.; Blasco-Jiménez, D.; López-Peinado, A. J.; Martín-Aranda, R. M. Efficient isomerization of saffrole by amino-grafted MCM-41 materials as basic catalysts. *Catal. Today* **2012**, *179*, 159-163.
- ²²⁶ Zienkiewicz, Z.; Calvino-Casilda, V.; Sobczak, I.; Ziolk, M.; Martín-Aranda, R. M.; López-Peinado, A. J. The possible use of alkali metal modified NbMCM-41 in the synthesis of 1, 4-dihydropyridine intermediates. *Catal. Today* **2009**, *142*, 303-307.
- ²²⁷ Domínguez-Fernández, F.; López-Sanz, J.; Pérez-Mayoral, E.; Bek, D.; Martín-Aranda, R.M.; López-Peinado, A.J.; Cejka, J. Novel basic mesoporous catalysts for the Friedländer reaction from 2-aminoaryl ketones: Quinolin-2(1H)-ones versus quinolines. *ChemCatChem* **2009**, *1*, 241–243.
- ²²⁸ Blasco-Jiménez, D.; Sobczak, I.; Ziolk, M.; López-Peinado, A. J.; Martín-Aranda, R. M. Amino-grafted metallosilicate MCM-41 materials as basic catalysts for eco-friendly processes. *Catal. Today* **2010**, *152*, 119-125.
- ²²⁹ Pérez Mayoral, E.; Soriano, E.; Calvino-Casilda, V.; Rojas-Cervantes, M. L.; Martín-Aranda, R. M. Silica-based nanocatalysts in the C C and C-heteroatom bond forming cascade reactions for the synthesis of biologically active heterocyclic scaffolds. *Catal. Today* **2017**, *285*, 65-88.
- ²³⁰ Hehre, W. J. *A guide to molecular mechanics and quantum chemical calculations (Vol. 2)*. Irvine, CA: Wavefunction, 2003.
- ²³¹ Young, D. *Computational Chemistry: a Practical Guide for Applying Techniques to Real World Problems*, John Wiley & Sons: New York, 2001.
- ²³² Allinger, N. L. *Molecular Structure. Understanding Steric and Electronic Effects from Molecular Mechanics*; Wiley, Hoboken NJ, 2010.
- ²³³ Cramer, C. J. *Essentials of Computational Chemistry: Theory and Models*; Wiley: Chichester, 2002.
- ²³⁴ Møller, C.; Plesset, M. S. Note on an approximation treatment for many-electron systems. *Phys. Rev.* **1934**, *46*, 618–622.
- ²³⁵ Čížek, J. On the correlation problem in atomic and molecular systems. Calculation of wavefunction components in Ursell-type expansion using quantum-field theoretical methods. *J. Chem. Phys.*, **1966**, *45*, 4256–4266.
- ²³⁶ Khare, R.; Mielke, S. L.; Paci, J. T.; Zhang, J. T.; Ballarini, R.; Schatz, G. C.; Belytschko, T. Coupled quantum mechanical/molecular mechanical modeling of the fracture of defective carbon nanotubes and graphene sheets. *Phys. Rev. B*, **2007**, *75*, 075412.

- ²³⁷ Hohenberg, P.; Kohn, W. Inhomogeneous electron gas. *Phys. Rev. B* **1964**, 136, 864–871.
- ²³⁸ Charif, I. E.; Mekelleche, S. M.; Villemin, D. Solvent effects on the keto-enol tautomeric equilibrium of tetronic and ethyl acetoacetate carbon acids: a theoretical study. *J. Theor. Comput. Chem.* **2010**, 9, 1021–1032.
- ²³⁹ Kohn, W.; Sham, L. J. Self-consistent equations including exchange and correlation effects. *Phys. Rev. A.* **1965**, 140, 1133–1138.
- ²⁴⁰ Bertran-Rusca, J.; Branchadell-Gallo, V.; Moreno-Ferrer, M.; Sodupe M. *Química Cuántica*. Síntesis: Madrid, 2002.
- ²⁴¹ Nagy, B.; Jensen, F. Basis Sets in Quantum Chemistry. *Rev. Comput. Chem.* **2017**, 30, 93–149.
- ²⁴² Hehre, W. J.; Stewart, R. F.; Pople, J. A. Self-Consistent Molecular-Orbital Methods. I. Use of Gaussian Expansions of Slater-Type Atomic Orbitals. *J. Chem. Phys.* **1969**, 51, 2657.
- ²⁴³ Foresman, J.; Frish, E. *Exploring chemistry*. Gaussian Inc.: Pittsburg, 1996.
- ²⁴⁴ Dunning Jr., T. H. Gaussian basis sets for use in correlated molecular calculations. The atoms boron through neon and hydrogen. *J. Chem. Phys.* **1989**, 90, 1007–1023.
- ²⁴⁵ Kendall, R. A.; Dunning Jr., T. H.; Harrison, R. J. Electron affinities of the first-row atoms revisited. Systematic basis sets and wave functions. *J. Chem. Phys.* **1992**, 96, 6796–6806.
- ²⁴⁶ Nachtigall, P.; Sauer, J. Quantum chemistry in zeolite science. In *Introduction to Zeolite Science and Practice*. Cejka, J.; Bekkum, V.; Corma, A.; Schüth, F., Eds.; Elsevier: Amsterdam, 2007, pp. 701–736.
- ²⁴⁷ Rimola, A.; Costa, D.; Sodupe, M.; Lambert, J. F.; Ugliengo, P. Silica surface features and their role in the adsorption of biomolecules: computational modeling and experiments. *Chem. Rev.* **2013**, 113, 4216–4313.
- ²⁴⁸ Deringer, V. L.; Dronskowski, R. *Computational Methods for Solids*. Elsevier, RWTH Aachen University: Aachen, 2013.
- ²⁴⁹ Libisch, F.; Huang, C.; Carter, E. A. Embedded correlated wavefunction schemes: Theory and applications. *Acc. Chem. Res.* **2014**, 47, 2768–2775.
- ²⁵⁰ Chung, L. W.; Sameera, W. M. C.; Ramozzi, R.; Page, A. J.; Hatanaka, M.; Petrova, G. P.; Harris, T. V.; Li, X.; Ke, Z.; Liu, F.; Li, H.B.; Ding, L.; Morokuma, K. The ONIOM method and its applications. *Chem. Rev.* **2015**, 115, 5678–5796.
- ²⁵¹ Przepiórski, J.; Czyżewski, A.; Pietrzak, R.; Toyoda, M.; Morawski, A. W. Porous carbon material containing CaO for acidic gas capture: Preparation and properties. *J. Hazard. Mater.* **2013**, 263, 353–360.
- ²⁵² Morales-Flórez, V.; Santos, A.; Romero-Hermida, I.; Esquivias, L. Hydration and carbonation reactions of calcium oxide by weathering: kinetics and changes in the nanostructure. *Chem. Eng. J.* **2015**, 265, 194–200.
- ²⁵³ López Granados, M.; Martín Alonso, D.; Sádaba, I.; Mariscal, R.; Ocón, P. Leaching and homogeneous contribution in liquid phase reaction catalyzed by solids: The case of triglycerides methanolysis using CaO. *Appl. Catal. B Environ.* **2009**, 89, 265–272.

- ²⁵⁴ Przepiórski, J.; Czyzewski, A.; Toyoda, M.; Tsumura, T.; Pietrzak, R.; Morawska, A. W. MgO-loaded porous carbon for carbon dioxide sorption: Study on cyclic sorption–regeneration. *Int. J. Greenhouse Gas Control* **2012**, *10*, 164-168.
- ²⁵⁵ Przepiórski, J.; Czyzewski, A.; Pietrzak, R.; Tryba, B. MgO/CaO-loaded porous carbons for carbon dioxide capture. *J. Therm. Anal. Calorim.* **2013**, *111*, 357–364.
- ²⁵⁶ Cai, S.; Kemnitzer, W.; Drewe, J.; Jiang, S.; Zhang, H.; Zhao, J.; Crogan-Grundy, C.; Xu, L.; Lamothe, S.; Gourdeau, H.; Denis, R.; Tseng, B.; Kasibhatla, S.; Cai, S. X. Discovery of 4-Aryl-4H-chromenes as a New Series of Apoptosis Inducers Using a Cell-and Caspase-Based High-Throughput Screening Assay. Structure–Activity Relationships of Fused Rings at the 7, 8-Positions. *J. Med. Chem.* **2003**, *50*, 2858-2864.
- ²⁵⁷ Keerthy, H. K.; Garg, M.; Mohan, C. D.; Madan, V.; Kanojia, D.; Shobith, R.; Nanjundaswamy, S.; Mason, D. J.; Bender, A.; Rangappa, B. K. S.; Koeffler, H. P. Synthesis and characterization of novel 2-amino-chromene-nitriles that target Bcl-2 in acute myeloid leukemia cell lines. *PLoS One.* **2014**, *9*, 107-118.
- ²⁵⁸ Chen, M.; Thanthiriwatte, K.S.; Dixon, D.A. Structures and Stabilities of (CaO)_n Nanoclusters. *J. Phys. Chem. C* **2017**, *121*, 23025–23038.
- ²⁵⁹ Ito, T.; Tashiro, T.; Kawasaki, M.; Watanabe, T.; Toi, K.; Kobayashi, H. Adsorption of methane on magnesium oxide studied by temperature-programmed desorption and ab initio molecular orbital methods, *J. Phys. Chem.* **1991**, *95*, 4476-4483.
- ²⁶⁰ Tanabe, K.; Misono, M.; Ono, Y.; Hattori, H. New solid acids and bases: their catalytic properties. In *Studies in Surface Science and Catalysis, Vol 51*; Delmon, B.; Yates, J. T., Eds., Kodansha/Elsevier: Tokyo/Amsterdam, 1989.
- ²⁶¹ Markovits, A.; Ahdjoudj, J.; Minot, C. Theoretical Study of the TiO₂ and MgO Surface Acidity and the Adsorption of Acids and Bases. *Mol. Eng.* **1997**, *7*, 245-261.
- ²⁶² Wang, C.; Liu, X.; Yang, M.; Ma, H.; Yan, P.; Slattery, J.M.; Gao, Y. A green and efficient amine-functionalized ionic liquid/H₂O catalytic system for the synthesis of α,α'-bis(substituted benzylidene)cyclopentanones. *RSC Adv.* **2013**, *3*, 8796-8804.
- ²⁶³ Li, Y.T.; Cui, K. H.; Li, J.; Zhu, J. Q.; Wang, X.; Tian, Y. Q. The Giant Pore Metal-Organic Frameworks of Scandium Carboxylate with MIL-100 and MIL-101 Structures. *Chin. J. Inorg. Chem.* **2011**, *27*, 951-95
- ²⁶⁴ Hwang, Y. K.; Hong, D. Y.; Chang, J. S.; Jhung, S. H.; Seo, Y. K.; Kim, J.; Vimont, A.; Daturi, M.; Serre, C.; Férey, G. Amine Grafting on Coordinatively Unsaturated Metal Centres of MOFs: Consequences for Catalysis and Metal Encapsulation. *Angew. Chem. Int. Ed.* **2008**, *47*, 4144-4148.
- ²⁶⁵ Das, A.; Choucair, M.; Southon, P. D.; Mason, J. A.; Zhao, M.; Kepert, C. J.; Harris, A. T.; D'Alessandro, D. M. Application of the piperazine-grafted CuBTri metal-organic framework in postcombustion carbon dioxide capture. *Micropor. Mesopor. Mat.* **2013**, *174*, 74–80.
- ²⁶⁶ Harlick, P. J.; Sayari, A. Applications of pore-expanded mesoporous silica. 5. Triamine grafted material with exceptional CO₂ dynamic and equilibrium adsorption performance. *Ind. Eng. Chem. Res.* **2007**, *46*, 446-458.

- ²⁶⁷ Areán, C. O.; Cabello, C. P.; Palomino, G. T. Infrared spectroscopic and thermodynamic study on hydrogen adsorption on the metal organic framework MIL-100(Sc). *Chem. Phys. Lett.* **2012**, 521, 104–106.
- ²⁶⁸ Szanyi, J.; Daturi, M.; Clet, G.; Baer, D. R.; Peden, C. H. F. Well-studied Cu–BTC still serves surprises: evidence for facile Cu²⁺/Cu⁺ interchange. *Phys. Chem. Chem. Phys.* **2012**, 14, 4383.
- ²⁶⁹ Castillo, J. M.; Vlugt, T. J.; Calero, S. Understanding water adsorption in Cu-BTC metal-organic frameworks. *J. Phys. Chem. C* **2008**, 112, 15934-15939.
- ²⁷⁰ Gong, Q.; Sun, L. P.; Wu, Z.; Huo, L. H.; Zhao, H. Enhanced non-enzymatic glucose sensing of Cu-BTC-derived porous copper@ carbon agglomerate. *J. Mater. Sci.* **2018**, 53, 7305-7315.
- ²⁷¹ Zhao, D.; Sun, J.; Li, Q.; Stucky, G. D. Morphological control of highly ordered mesoporous silica SBA-15. *Chem. Mater.* **2000**, 12, 275-279.
- ²⁷² López-Sanz, J.; Pérez-Mayoral, E.; Soriano, E.; Sturm, M.; Martín-Aranda, R. M.; López-Peinado, A. J.; Čejka, J. New inorganic–organic hybrid materials based on SBA-15 molecular sieves involved in the quinolines synthesis. *Catal. Today* **2012**, 187, 97-103.
- ²⁷³ Hiyoshi, N.; Yogo, K.; Yashima, T. Adsorption characteristics of carbon dioxide on organically functionalized SBA-15. *Micropor. Mesopor. Mat.* **2005**, 84, 357-365.
- ²⁷⁴ Paul, G.; Musso, G. E.; Bottinelli, E.; Cossi, M.; Marchese, L.; Berlier, G. Investigating the interaction of water vapour with aminopropyl groups on the surface of mesoporous silica nanoparticles. *ChemPhysChem* **2017**, 18, 839-849.
- ²⁷⁵ Danon, A.; Stair, P. C.; Weitz, E. FTIR study of CO₂ adsorption on amine-grafted SBA-15: elucidation of adsorbed species. *J. Phys. Chem. C* **2011**, 115, 11540-11549.
- ²⁷⁶ Musso, G. E.; Bottinelli, E.; Celi, L.; Magnacca, G.; Berlier, G. Influence of surface functionalization on the hydrophilic character of mesoporous silica nanoparticles. *Phys. Chem. Chem. Phys.* **2015**, 17, 13882-13894.
- ²⁷⁷ White, L. D.; Tripp, C. P. Reaction of (3-aminopropyl) dimethylethoxysilane with amine catalysts on silica surfaces. *J. Colloid Interface Sci.* **2000**, 232, 400-407.
- ²⁷⁸ Albayati, T. M.; Salih, I. K.; Alazzawi, H. F. Synthesis and characterization of a modified surface of SBA-15 mesoporous silica for a chloramphenicol drug delivery system. *Heliyon* **2019**, 5, e02539.
- ²⁷⁹ Ouellette, R. J.; Rawn, J. D. Amines and amides. In *Organic Chemistry Study Guide. Key Concepts, Problems, and Solutions*. Ouellette, R. J.; Rawn, J. D. Eds.; Elsevier: Amsterdam, 2015; pp. 465-494.
- ²⁸⁰ González-Rodal, D.; Przepiórski, J.; Peinado, A. L.; Pérez-Mayoral, E. Basic-carbon nanocatalysts in the efficient synthesis of chromene derivatives. Valorization of both PET residues and mineral sources. *Chem. Eng. J.* **2020**, 382, 122795.
- ²⁸¹ Wang, Z.; Wang, D.; Zhao, Z.; Chen, Y.; Lan, J. A DFT study of the structural units in SBA-15 mesoporous molecular sieve. *Comput. Theor. Chem.* **2011**, 963, 403-411.
- ²⁸² Zhang, X.; Lai, E. S. M.; Martín-Aranda, R.; Yeung, K. L. An investigation of Knoevenagel condensation reaction in microreactors using a new zeolite catalyst. *Appl. Catal. A: Gen.* **2004**, 261, 109-118.

- ²⁸³ Trejda, M.; Wojtaszek, A.; Floch, A.; Wojcieszak, R.; Gaigneaux, E. M.; Ziolek, M. New Nb and Ta–FAU zeolites—Direct synthesis, characterisation and surface properties. *Catal. Today* **2010**, 158, 170-177.
- ²⁸⁴ Wojtaszek, A.; Ziolek, M.; Tielens, F. Probing acid–base properties in group V aluminum containing zeolites. *J. Phys. Chem. C* **2012**, 116, 2462–2468.
- ²⁸⁵ Mohamadnia, Z.; Ahmadi, E.; Ghasemnejad, M.; Hashemikia, S.; Doustgani, A. Surface modification of mesoporous nanosilica with [3-(2-Aminoethylamino) propyl] trimethoxysilane and its application in drug delivery. *Int. J. Nanosci. Nanotechnol.* **2015**, 11, 167-177.
- ²⁸⁶ Boiadjiev, V.; Tysoe, W. T. Infrared study of the surface species formed by sequential chemical vapor deposition of trimethylaluminum and methanol on a hydroxylated alumina surface. *Chem. Mater.* **1998**, 10, 334-344.
- ²⁸⁷ Stawicka, K.; Trejda, M.; Ziolek, M. The production of biofuels additives on sulphonated MCF materials modified with Nb and Ta—Towards efficient solid catalysts of esterification. *Appl. Catal. A Gen.* **2013**, 467, 325-334.
- ²⁸⁸ Nishimura, M.; Asakura, K.; Iwasawa, Y. New SiO₂-supported niobium monomer catalysts for dehydrogenation of ethanol. *J. Chem. Soc. Chem. Commun.* **1986**, 15, 1660–1661.
- ²⁸⁹ Kilos, B.; Tuel, A.; Ziolek, M.; Volta, J. C. New Nb-containing SBA-3 mesoporous materials—Synthesis, characteristics, and catalytic activity in gas and liquid phase oxidation. *Catal. Today* **2006**, 118, 416-424.
- ²⁹⁰ Tranca, D.C.; Wojtaszek-Gurdak, A.; Ziolek, M.; Tielens, F. Supported and inserted monomeric niobium oxide species on/in silica: a molecular picture. *Phys. Chem. Chem. Phys.* **2015**, 17, 22401-22411.
- ²⁹¹ Li, Y.T.; Cui, K. H.; Li, J.; Zhu, J. Q.; Wang, X.; Tian, Y. Q. The Giant Pore Metal-Organic Frameworks of Scandium Carboxylate with MIL-100 and MIL-101 Structures. *Chin. J. Inorg. Chem.* **2011**, 27, 951-956.
- ²⁹² Das, A.; Choucair, M.; Southon, P. D.; Mason, J. A.; Zhao, M.; Kepert, C. J.; Harris, A. T.; D’Alessandro, D. M. Application of the piperazine-grafted CuBTTri metal-organic framework in postcombustion carbon dioxide capture. *Micropor. Mesopor. Mat.* **2013**, 174, 74–80.
- ²⁹³ Valente Nabais, J. M.; Carrott, P. J. M. Chemical characterization of activated carbon fibers and activated carbons. *J. Chem. Educ.* **2006**, 83, 436-438.
- ²⁹⁴ Leon y Leon, C. L.; Solar, J. M.; Calemma, V.; Radovic, L. R. Evidence for the protonation of basal plane sites on carbon. *Carbon* **1992**, 30, 797-811.
- ²⁹⁵ Frisch, M.J.; Trucks, G.W.; Schlegel, H.B.; Scuseria, G.E.; Robb, M.A.; Cheeseman, J.R.; Scalmani, G.; Barone, V.; Mennucci, B.; Petersson, G.A.; Nakatsuji, H.; Caricato, M.; Li, X.; Hratchian, H.P.; Izmaylov, A.F.; Bloino, J.; Zheng, G.; Sonnenberg, J.L.; Hada, M.; Ehara, M.; Toyota, K.; Fukuda, R.; Hasegawa, J.; Ishida, M.; Nakajima, T.; Honda, Y.; Kitao, O.; Nakai, H.; Vreven, T.; Montgomery, J.A.; Peralta, J.E.; Ogliaro, F.; Bearpark, M.; Heyd, J.J.; Brothers, E.; Kudin, K.N.; Staroverov, V.N.; Kobayashi, R.; Normand, J.; Raghavachari, K.; Rendell, A.; Burant, J.C.; Iyengar, S.S.; Tomasi, J.; Cossi, M.; Rega, N.; Millam, J.M.; Klene, M.; Knox, J.E.; Cross, J.B.; Bakken, V.; Adamo, C.; Jaramillo, J.; Gomperts, R.; Stratmann, R.E.; Yazyev, O.; Austin, A.J.; Cammi, R.; Pomelli, C.; Ochterski, J.W.; Martin, R.L.; Morokuma, K.; Zakrzewski, V.G.; Voth,

G.A.; Salvador, P.; Dannenberg, J.J.; Dapprich, S.; Daniels, A.D.; Farkas, Ö.; Foresman, J.B.; Ortiz, J.V.; Cioslowski, J.; Fox, D.J. Gaussian 09, Revision B.1., Gaussian, Inc., Wallingford CT, 2009.

²⁹⁶ Moradi, M.; Peyghan, A.A.; Bagheri, Z.; Kamifiroozi, M. Cation- π interaction of alkali metal ions with C24 fullerene: a DFT study. *J. Mol. Model.* **2012**, *18*, 3535–3540.

²⁹⁷ Beheshtian, J.; Baei, M.T.; Peyghan, A.A.; Bagheri, Z. Electronic sensor for sulfide dioxide based on AlN nanotubes: a computational study. *J. Mol. Model.* **2012**, *18*, 4745–4750.

²⁹⁸ Gonzalez, C.; Schlegel, H.B. Reaction path following in mass-weighted internal coordinates. *J. Phys. Chem.* **1990**, *94*, 5523–5527.



Basic-carbon nanocatalysts in the efficient synthesis of chromene derivatives. Valorization of both PET residues and mineral sources



D. González-Rodal^a, J. Przepiórski^b, A.J. López Peinado^a, E. Pérez-Mayoral^{a,*}

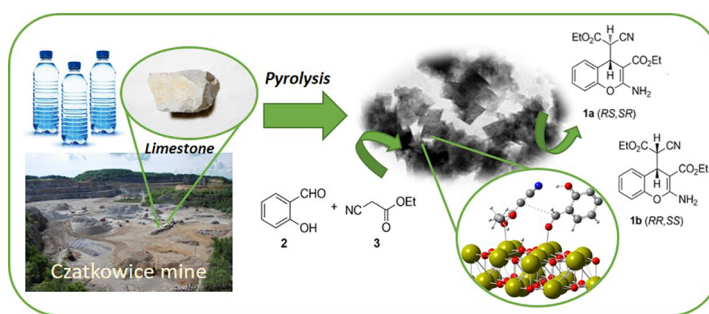
^a Departamento de Química Inorgánica y Química Técnica, Universidad Nacional de Educación a Distancia, UNED, Paseo Senda del Rey, 9, E-28040 Madrid, Spain

^b Institute of Chemical and Environmental Engineering, West Pomeranian University of Technology, Szczecin, Pulaskiego 10, 70-322 Szczecin, Poland

HIGHLIGHTS

- PET and limestone can be easily converted to carbon-based catalysts by heating.
- Polluting plastic residues are used for production of CaO supported on porous carbons.
- PET/CAL efficiently catalyzes synthesis 2-amino-4H-chromenes under mild conditions.
- The reaction is strongly favored in the presence of the CaO-containing catalysts.

GRAPHICAL ABSTRACT



ARTICLE INFO

Keywords:

Heterogeneous catalysis
Carbon-based catalysts
Cascade reactions
Multicomponent synthesis
Chromenes

ABSTRACT

Novel series of calcium oxide (calcium hydroxide)/carbon composites applied to the green and efficient synthesis of 2-amino-4H-chromenes, from salicylaldehydes and ethyl cyanoacetate, under mild and free-solvent conditions, is herein reported for the first time. These basic hybrid materials are easily prepared by direct thermal pyrolysis of limestone and PET. Different Ca-phases, CaO or Ca(OH)₂, were independently detected, since CaO/carbon composites initially formed can be easily hydrated, under atmospheric conditions, but also dehydrated by re-calcination. CaO-containing samples present enhanced catalytic performance, the observed reactivity being attributed to the catalyst basicity.

The reaction under study catalyzed by CaO probably occurs by cascade reactions through aldolization – heterocyclization – dehydration – Michael addition sequence, strongly favored by the presence of the truly active phase, CaO, as experimental and theoretical demonstrated.

The methodology herein reported can be framed in circular economy domain opening the possibility of synthesizing valuable compounds from carbon-based catalysts prepared by using plastic residues as PET source.

1. Introduction

Nowadays, the development of new nanomaterials which can be used as heterogeneous catalysts in diverse chemical processes is an active researching field with industrial repercussion. Particularly, carbon materials can be considered attractive supports for catalytic

applications as these provide the appropriate physicochemical environment for the production of fine chemicals because of their unique characteristics – high surface areas and chemical inertness and thermal stability, among others – [1,2]. In fact, in the last decades the involvement of advanced porous carbon-based materials in catalytic processes has attracted much attention of a number of teams [3–5].

* Corresponding author.

E-mail addresses: Jacek.Przepiorski@zut.edu.pl (J. Przepiórski), eperez@ccia.uned.es (E. Pérez-Mayoral).

<https://doi.org/10.1016/j.cej.2019.122795>

Received 17 July 2019; Received in revised form 7 September 2019; Accepted 9 September 2019

Available online 10 September 2019

1385-8947/ © 2019 Elsevier B.V. All rights reserved.

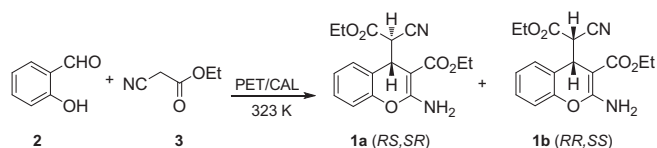
Although these materials have been used in great variety of fine chemical processes, only a few examples of those have been applied on the green synthesis of heterocyclic compounds with pharmacological interest, through cascade reactions [6]. At this regard, we have already reported different eco-friendly and efficient methodologies for the synthesis of nitrogen heterocyclic systems through Friedländer condensation, involving activated carbons exhibiting either acidic or basic character [7,8], and recently – metal-free [9] and transition metal – doped carbon aerogels [10,11]. Much more recently, we reported [12] novel composites consisting of sulfated zirconia supported over porous carbons active in the synthesis of benzodiazepines.

In this work, we seek to examine catalytic performance of a series of basic nanoporous carbonaceous catalysts prepared from poly(ethylene terephthalate) (PET), as source of carbon, and natural limestone. We have focused on the application of the materials in the catalytic synthesis of chromene derivatives, as medicinal scaffolds. The latter compounds are heterocyclic systems of natural origin and synthetic drugs [13,14]. The structures in question reveal a wide spectrum of therapeutic uses including antimicrobial, antiviral, antifungal, anti-proliferative, antioxidant, antihistaminic or antihypertensive. The chromene derivatives are also known to be biodegradable agrochemicals, among others. The synthetic methodologies reported specifically for the preparation of 2-amino-4*H*-chromenes include the use of classical homogeneous organocatalysts like organic amines [15,16] and heterogeneous ones, such as zirconium phosphate [17], base anion exchange resins like Amberlyst A-21 [18], doped hydrotalcites [19], or even molecular sieves [20], among others. Depending on the chosen methodology, syntheses often require complex isolation of a product and purification methods. It often entails use of solvents, large amounts of inorganic solids, or prolonged reaction times. All the purification methods contribute to the highly polluting waste production and increase the energy consumption. Our research group has also contributed to the development of green methodologies for the preparation of biologically active 2-amino-4*H*-chromenes in the presence of ionic liquids such as imidazolium sulfonates [21] and bifunctional mesoporous metallosilicates [22,23] as well as the mechanistic understanding of the reactions taking place during preparation processes.

In continuation with our ongoing investigations, the goal of this work is addressed at the development and examination of carbon materials revealing basic properties, highly efficient in the synthesis of 2-amino-4*H*-chromenes **1** from salicylaldehyde **2** and ethyl cyanoacetate **3** under mild and solvent-free conditions, as illustrated in Scheme 1. Conventionally, metal supported carbon materials, including catalysts are prepared by an impregnation of carbon supports with metallic salts followed by calcination or other chemical treatments [24,25]. Carbon-based catalysts herein reported are synthesized by direct pyrolysis of homogeneous mixtures of poly(ethylene terephthalate) (PET) and limestone (CAL) using different ratio of both components. The developed methodology is characterized by the easy, one-step preparation of basic catalysts from commercially available PET or troublesome wastes such as plastics but also natural sources – limestone, and additionally dolomite or magnesite for comparison. Such approach can be then framed in the circular economy domain.

2. Materials and methods

The materials used in this research were commercially available:



Scheme 1. Synthesis of 2-amino-4*H*-chromenes from salicylaldehyde **2** and ethyl cyanoacetate **3**, at 323 K, catalyzed by basic carbon materials.

Table 1

Chemical composition (in wt. %, calculated as oxides) of the minerals used in the work (based on supplier's data).

Component	Mineral		
	MAG	DOL	CAL
CaO	1,83	29,44	53,80
MgO	41,20	19,75	0,71
SiO ₂	4,21	1,43	2,13
Fe ₂ O ₃	2,57	0,14	0,11
Al ₂ O ₃	1,18	0,11	0,08

poly(ethylene terephthalate) (PET), Limestone (denoted as CAL), magnesite (denoted as MAG), and dolomite (denoted as DOL). The PET was acquired from Elana S.A. (Poland) whereas the minerals were mined from different deposits in Poland. CAL deposit was located in Czatkowice, MAG deposit was located near Grochów, and DOL was mined from deposits located near Ząbkowice. CaCO₃ and MgCO₃ are the major components for CAL (96.3%) and MAG (81.6%), respectively, whereas DOL is mainly composed of both carbonates, CaCO₃ and MgCO₃ in a 52.6/41.5 [wt.%/wt.%] ratio. The minerals contained naturally included other components, as listed in the Table 1.

Other chemical reagents and solvents used in this work were purchased from Aldrich or Alfa-Aesar.

2.1. Synthesis and characterization of carbon materials

Carbons under study have been prepared according the experimental protocol previously reported by Przepiórski et al [26–29]. Four different homogeneous PET/CAL mixtures were prepared by mixing the components at varying the PET:CAL ratio: PET/CAL 83:17, PET/CAL 70:30, PET/CAL 50:50 and PET/CAL 30:70 in which PET (10 g) and different amount of CAL (2.0, 4.3, 10.0, and 23.3 g, respectively) were used. PET/MAG 30:70 and PET/DOL 30:70 mixtures were also prepared for comparison using PET (10 g) and MAG (23.3 g) or DOL (23.3 g). Briefly, each mixture was dried in air atmosphere at 293 K during 24 h and subsequently pretreated by mean of heating from room temperature to 538 K during 1 h, under flowing (100 cm³/min), nitrogen atmosphere using a ramp of 10 K/min. This action was done in order to obtain uniform dispersion of CAL, MAG, or DOL, over the PET matrix. After cooling back to the room temperature, the mixtures were powdered, and submitted to additional thermal treatment by mean of heating from room temperature to 1123 K (for PET/CAL and PET/DOL mixtures) or 1023 K (for PET/MAG), using a temperature ramp of 10 K/min and flowing (100 cm³/min) nitrogen as an atmosphere. The product formed during this operation is milled and sieved below 0.025 mm. Samples from exclusively PET (10 g) or CAL (10 g) as raw materials were also prepared. Sample PETb/CAL 30:70 was synthesized by using a commercially available plastic bottle using the same experimental conditions described above.

Determinations of pH_{pzc} for the prepared materials were done with GLP 22 Milimeter pHmeter (CRISON) according the experimental procedure reported by Valente Nabais and Carrot [30].

XRD measurements were performed with use of a X'Pert Pro PANalytical's X-ray diffractometer using Cu K_α radiation (λ = 1.5406 Å, 45 kV, 40 mA), working within 2θ range of 4–90°, 0.005° of scan step size and 20 s of dwell time.

Textural parameters of the materials were determined from the N₂ adsorption/desorption isotherms obtained with ASAP 2020 Surface Area and Porosity analyzer (Micromeritics). Prior to N₂ adsorption, each sample was degassed at 573 K during 18 h, under high vacuum. After collecting N₂ adsorption data, BET model was applied for obtaining the specific surface area value. Total surface (S_{total}), micropore surface area (S_{micro}) and external surface area (S_{ext}) were determined by the application of α_s analysis. Micropore volume (V_{micro}) was calculated

from adsorption branches of the measured isotherms using the Dubinin-Radushkevich equation. Total pore volume (V_T) was determined from the amount of N_2 adsorbed at relative pressure p/p_0 of 0.95. Mesopore volume (V_{meso}) was calculated as a difference between the V_T and V_{micro} .

The mass changes accompanying the material synthesis were investigated by thermogravimetric analysis using a STD Q600 thermo-balance, by heating 45 mg of each sample from room temperature to 1223 K in an inert helium atmosphere. The heating rate and gas flow were set at 10 K/min and $100 \text{ cm}^3/\text{min}$, respectively.

The morphology of the materials was investigated by Transmission Electron Microscope, (TEM) using JEOL JEM1010 apparatus operating at 100 kV and equipped with a digital camera. The samples of materials were suspended in water (2.5 mg in 50 mL) and were homogenized in an ultrasonic bath, during 15 min at 40 KHz. After that, the samples were deposited over a carbon lined grid and dried.

2.2. Catalytic performance

In a typical experiment carried out at 323 K, to a mixture of salicylaldehyde **2** (2 mmol) and ethyl cyanoacetate **3** (4 mmol), a catalyst (50 mg) was added and the reaction mixture was stirred during 3 h. The reactions were carried out in the multiexperiment work station Starfish, in a liquid phase, under atmospheric pressure and solvent-free conditions. Samples of the reacting mixtures were periodically taken after certain times for analysis by ^1H NMR—15, 30, 60, 120 and 180 min. The samples were diluted with CH_2Cl_2 (1 mL) to facilitate the separation of the catalyst by filtered off using a glass syringe equipped with a microfilter (Millipore, $0.45 \mu\text{m}$ HV). Finally, the solvent was evaporated *in vacuo*.

The progress of the reactions was qualitatively monitored by thin layer chromatography (TLC) performed on a DC-Aulofolien/Kieselgel 60 F_{245} (Merck), using $\text{CH}_2\text{Cl}_2/\text{EtOH}$ (98:2) mixture as an eluent.

The yield (or conversion) of the process is defined as the fraction of reactant **2** transformed at each reaction time into compounds **1a** and **1b**, determined by Proton Nuclear Magnetic Resonance (^1H NMR).

Reaction products were characterized by ^1H NMR spectroscopy. Solution NMR spectra were recorded on a Bruker DRX 400 (9.4 Tesla, 400.13 MHz for ^1H) spectrometer with a 5-mm inverse-detection H-X probe equipped with a z-gradient coil, at 300 K. Chemical shifts (δ in ppm) are given from internal solvent, CDCl_3 7.26 for ^1H .

2.3. Computational studies

The calculations presented in this work were performed by using the Gaussian 09 software package [31], in gas phase, at 298 K. All the geometries were optimized using B3LYP hybrid functional [32,33] with 6-31G(d,p) basis set, this functional being an habitual methodology to

study nanostructures [34,35]. Recently, Chen et al. [36] reported that the most stable isomers for $(\text{CaO})_n$, when $n > 3$ present three-dimensional structures dominated by cubic structures. In this sense, based on our experimental observations, the cluster size of $(\text{CaO})_n$ in which n is 20 was selected because it is large enough to contain the reactant structures. The stationary points were characterized by means of harmonic vibrational frequency analysis. Thus, the transition structures were confirmed to be first-order saddle points. The imaginary frequency was inspected in each transition structures to ensure it represented the desired reaction coordinate. For key transition states the intrinsic reaction coordinate (IRC) was followed to ensure it connects the reactants and products [37].

3. Results and discussion

3.1. Synthesis and characterization of the catalysts

Four PET/CAL samples in which relative CAL contents increased were synthesized by direct pyrolysis of the corresponding PET/CAL mixtures, PET/CAL 83:17, PET/CAL 70:30, PET/CAL 50:50 and PET/CAL 30:70, following the experimental procedure previously reported by Przepiórski et al [26]. Additionally, carbonaceous material derived entirely from PET, (PET/CAL 100:0), or CaO from CAL, (PET/CAL 0:100), were also prepared.

Firstly, we carried out TG analysis of PET/CAL mixtures for comparison with previous studies, confirming the appearance of two mass drops at approximately 623 and 873 K, assigned to thermal degradation of PET and limestone, respectively, as reported (Fig. 1S, see Supporting information). Interestingly, PET/CAL 50:50 sample after thermal treatment and stored several days under atmospheric conditions undergoes a weight loss at approximately 625 K. At this regard, several reports describe the dehydration of $\text{Ca}(\text{OH})_2$ to CaO at closer temperatures affected by the presence of other components [38].

The investigated porous carbon catalysts were characterized by N_2 adsorption (Fig. 2S, see Supporting information). All the isotherms measured for the PET/CAL hybrid materials seem like an overlapping type I and type IV isotherms as reported [39], with a defined H3 type of hysteresis loop. It can be observed the microporous character of the samples considerably increased for the sample with higher PET/CAL ratio, PET/CAL 83:17 but also the presence of certain mesoporosity. In contrast, the carbonized PET sample in absence of CAL barely shows adsorption capacity accordingly with previous studies [26]. Table 2 summarizes the textural parameters of the investigated materials. In general, the development of the porosity is more pronounced in materials obtained from PET/CAL mixtures richer in PET component. Thus, S_{BET} (79–326 m^2/g) and V_{micro} notably increase as the CAL amount decreases, observing similar trend for S_{Total} and S_{Micro} .

The investigated samples were also characterized by XRD. Thermal

Table 2

Textural parameters for the PET/CAL samples.

Catalyst	S_{BET} (m^2/g)	t-plot			V_T (cm^3/g)	Dubinin-Radushkevich		BJH D (Å)
		S_{Total} (m^2/g)	S_{External} (m^2/g)	S_{Micro} (m^2/g)		V_{micro} (cm^3/g)	V_{meso} (cm^3/g)	
PET/CAL 0:100	33	35	35	0	0,11	0,02	0,09	142
PET/CAL 30:70	79	78	57	21	0,13	0,04	0,09	118
PET/MAG 30:70	158	176	107	69	0,32	0,07	0,25	–
PET/DOL 30:70 [27,28]	106	114	90	24	0,22	0,05	0,17	–
PETb/CAL 30:70	113	113	27	86	0,11	0,04	0,07	217
PET/CAL 50:50	131	131	67	64	0,20	0,06	0,14	112
PET/CAL 70:30	159	158	52	106	0,15	0,08	0,07	118
PET/CAL 83:17	326	327	74	253	0,26	0,16	0,10	89
PET/CAL 100:0 [26]	34	37	3	34	0,02	0,02	0,00	–
Norit RX3	1306	1468	191	1277	–	–	–	–

S_{BET} : BET surface, S_{Total} : Total surface, S_{E} : External Surface, S_{Micro} : Microporous surface, V_T : Total porous volume, V_{micro} : Microporous volume, V_{meso} : Mesoporous volume, D (Å): diameter.

Table 3
Oxide content and pH_{PZC} for PET/CAL, PET/MAG and PET/DOL samples.

Sample	CaO content (wt%)	pH_{PZC}
PET/CAL 0:100	100	–
PET/CAL 30:70	87	12.03
PET/CAL 50:50	66	12.06
PET/CAL 70:30	57	12.38
PET/CAL 83:17	35	12.12
PET/MAG 30:70	78 ^[a]	10.23
PET/DOL 30:70	88 ^[b]	12.19

^[a] MgO content.

^[b] MgO + CaO content determined by TG.

decomposition of CaCO_3 , as major compound in limestone, is confirmed by the presence of CaO in all the prepared hybrid materials as reported in elsewhere [26] together to traces of silica from raw mineral. The XRD patterns collected for three PET/CAL 30:70 samples of different history are shown in Fig. 3S (see Supporting information). PET/CAL 30:70(1) consists of hybrid material just after preparing while PET/CAL 30:70(2) and PET/CAL 30:70(3) are samples stored under atmospheric conditions several days and re-calcined PET/CAL 30:70(2) sample, respectively. PET/CAL 30:70(1) and PET/CAL 30:70(3) are mainly composed of CaO while PET/CAL 30:70(2) contains a new phase, $\text{Ca}(\text{OH})_2$, formed from CaO by hydration under atmospheric conditions [40]. These results remain in good agreement with TG experiments commented above. In all the samples, the absence of any other diffraction lines suggests a low crystallinity of the porous carbons. It is also

observed that the crystal size of the Ca phase increases as function of the CAL content on the initial mixture as previously reported.

CaO loadings determined by TG experiments and pH_{PZC} of the hybrid materials are summarized in Table 3. CaO content increases when decreasing the PET/CAL ratio whereas pH_{PZC} values are close to 12 as expected.

Morphology of the samples is also investigated by TEM. It can be observed the influence of the composition in the morphology of the materials showing significant differences (Fig. 1). All the samples show two different phases consisting of amorphous carbon and cubic structures comprising CaO or $\text{Ca}(\text{OH})_2$ heterogeneously dispersed. While in the PET/CAL 30:70 sample the amorphous carbon is deposited inside the cavities of the predominant Ca phase, when increasing the amount of PET the formation of agglomerates partially covering the CaO surface is observed. The samples with high carbon content show also the formation of threads assemblies, dispersing the CaO phase (Fig. 1 C and D).

3.2. Catalytic performance

The catalytic behavior of hybrid materials was investigated in the synthesis of 2-amino-4H-chromenes **1**, between salicylaldehyde **2** and ethyl cyanoacetate **3** under solvent-free conditions, at 323 K (Scheme 1). Remarkably, the blank experiment in absence of any catalyst lead to chromene **1** with 1% of conversion, after 3 h of reaction time.

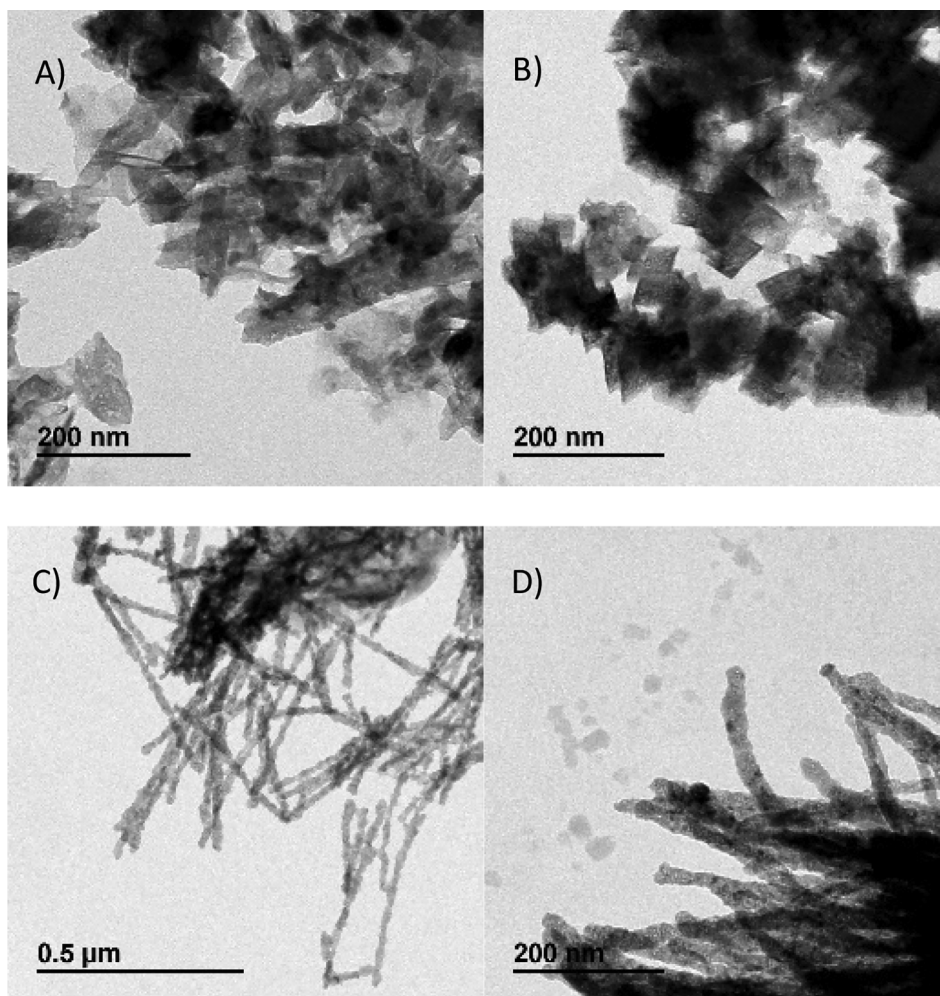


Fig. 1. TEM images of A) PET/CAL 30:70, B) PET/CAL 50:50, C) PET/CAL 70:30 y and D) PET/CAL 83:17.

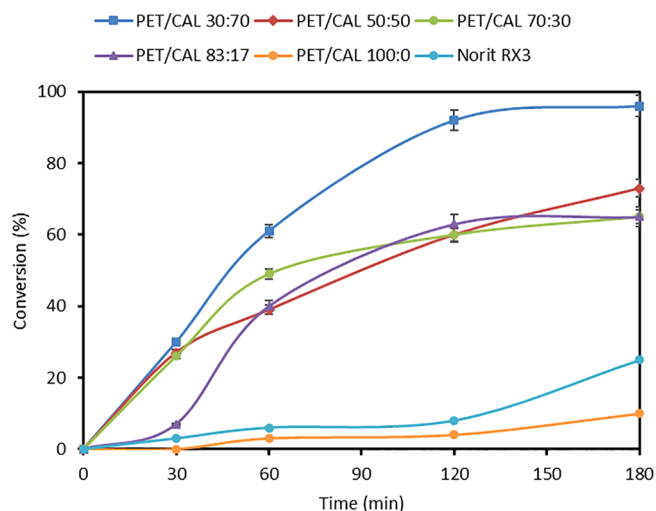


Fig. 2. Synthesis of 2-amino-4H-chromenes 1 catalyzed by A) PET/CAL hybrid materials, at 323 K, under solvent-free conditions. B) PET/CAL 100:00 and Norit RX3.

3.2.1. Catalytic behavior of PET/CAL samples

Fig. 2 depicts conversion values of salicylaldehyde 2 to chromenes 1 vs time. The conversion strongly depends on the Ca loading affording mixtures of chromenes 1a/1b (2:1 ratio in which the major compound is the most thermodynamically stable isomer) in almost quantitative conversion, after 3 h of reaction time, in the presence of PET/CAL 30:70 sample (Fig. 2). When increasing the PET/CAL ratio a diminished conversion was obtained. However, no significant differences between catalysts were observed probably due to the formed amorphous carbon is covering the surface of Ca phase. Additionally, we also tested the carbon support, prepared by pyrolysis of PET under the same experimental conditions, observing that influence of the carbon matrix in the reaction could be neglected at the shortest reaction time. We also compared with the use of a mainly microporous carbon sample, Norit RX3, observing an increase of conversion values (up to 20%) probably because of its high surface area (1306 m²/g) (Table 2). Therefore, the carbon support slightly contributes to the observed reactivity. It is important to note that raw limestone was not active in the reaction giving 3% of conversion after 2 h of reaction time.

In the same context, calcined limestone, PET/CAL 0:100, composed exclusively by CaO, was tested for comparison purposes. One of the main problems when working with metallic oxides is leaching [41]. In fact, PET/CAL 0:100 sample is totally solubilized in the reaction medium. Thus, the use of PET/CAL 0:100 sample gave quite similar results although with conversions slightly decreased than those observed for PET/CAL 30:70, the catalyst with highest Ca-content (Table 4). Additionally, we carry out the reaction in the presence of PET/CAL 30:70, in which the catalyst was removed from the reaction

Table 4

Synthesis of chromenes 1 catalyzed by PET/CAL 30:70 and CAL, at 323 K, under solvent-free conditions.

Catalysts	Time (min)			
	15	30	60	120
PET/CAL 30:70	32	42	57	92
PET/CAL 30:70*	31	35	43	57
PET/CAL 0:100	25	38	56	87

* Catalyst removed from the reaction mixture after 15 min.

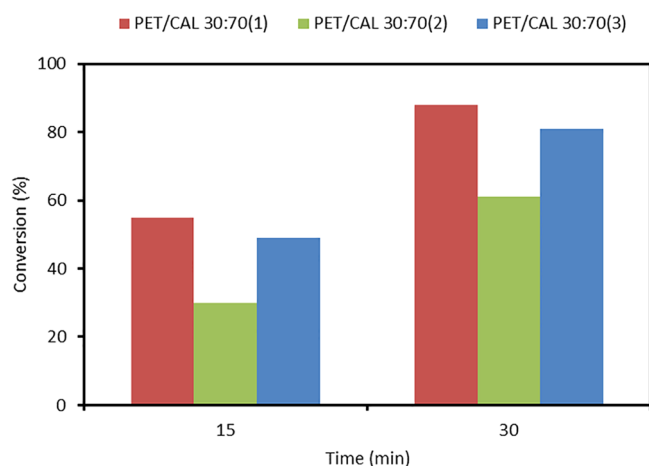


Fig. 3. Synthesis of 2-amino-4H-chromenes 1 catalyzed by PET/CAL 30:70 hybrid materials, at 323 K, under solvent-free conditions.

mixture by filtered off after 15 min of reaction time. In this case, the reaction evolves slowly indicating that leaching of active species could be although in a lesser degree. It is noteworthy that no leaching was observed in the presence of hybrid materials with increased PET/CAL ratio. All these results strongly suggest that the calcium phase in these hybrid materials is truly the active catalytic specie. However, the presence of carbon in PET/CAL samples also contributing to increase the porosity of the catalysts (Table 2) make them as heterogeneous catalysts. In this sense, similarities between samples with decreased calcium loadings could be related to the combination of active phase dispersion but also with the porosity of the materials. Obviously, in samples with high PET/CAL ratio the active centers are less accessible by the presence of amorphous carbon. However, the developed microporosity and therefore the increased surface area could both contribute to the overall conversion as suggested by the results in the presence of PET/CAL 83:17 catalyst.

Having in mind that CaO in hybrid materials under study is easily transformed into Ca(OH)₂ as demonstrated by XRD, we tested different PET/CAL 30:70 samples: i) PET/CAL 30:70(1) recently prepared and stored under inert atmosphere, ii) PET/CAL 30:70(2) prepared days ago and stored under ambient conditions (sample denoted above as PET/CAL 30:70), and iii) PET/CAL 30:70(3) prepared from PET/CAL 30:70(2) by calcination, in which the calcium phase was CaO or Ca(OH)₂ (Fig. 3S, see supporting information). Fig. 3 depicts the obtained results indicating that the most active samples are PET/CAL 30:70(1) and PET/CAL 30:70(3) in which calcium phase is CaO. The diminished conversions for PET/CAL 30:70(2) sample (60% after 30 min vs 91 and 81% for PET/CAL 30:70(1) and PET/CAL 30:70(3), respectively) could be related to the presence of Ca(OH)₂ catalyzing the reaction although in a lesser extent.

3.2.2. Influence of reaction temperature

Following ongoing investigations, we check the catalytic performance of the PET/CAL 70:30 catalyst at lower temperature, 303 K, closer to room temperature, observing the formation of chromenes 1 although in lower conversion with selectivity maintained, as expected (Fig. 4).

3.2.3. Catalytic behavior of PET/DOL and PET/MAG samples

Having all these results in mind, we also checked the catalytic behavior of PET/DOL 30:70, sample prepared by direct pyrolysis of the corresponding PET/DOL mixture (DOL = dolomite), containing both

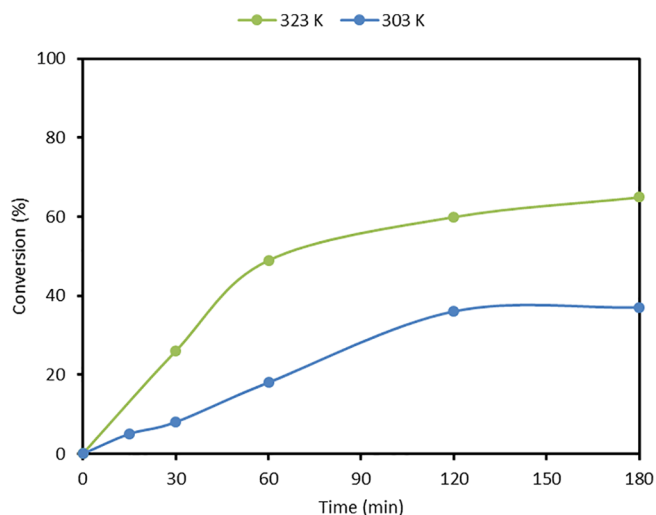


Fig. 4. Synthesis of 2-amino-4H-chromenes **1** catalyzed by PET/CAL 70:30 hybrid material, at 303 K, under solvent-free conditions.

CaO and MgO oxides (Fig. 5) [42]. As it can be observed from Fig. 5, PET/DOL 30:70 resulted as an active catalyst in the reaction affording the chromenes **1** with both diminished conversion and selectivity; almost 70% of conversion with 60% of selectivity to **1a**, after 3 h of reaction time. This result is in good agreement with those obtained for PET/CAL catalysts with inferior Ca-loading. In order to confirm that in this case the CaO is the main catalytic specie, we additionally prepared and tested the analogous PET/MAG 30:70 sample (MAG = magnesite), by using a similar experimental protocol [8,43], barely showing any activity (conversion < 5% after 3 h of reaction time). Therefore, these results strongly suggest that the reaction is mainly controlled by the basicity of the metal oxide. Thus, PET/CAL 30:70(2) and PET/DOL 30:70 with similar pH_{PZC} values closer to 12, notable differ in their catalytic behavior in comparison to PET/MAG 30:70 presenting a pH_{PZC} of 10 (Table 3). Interestingly, MAG and DOL barely are active in the reaction, as expected. Our results indicate that it is possible the transformation of mixtures of PET and mineral sources, CAL or DOL, on efficient heterogeneous catalytic systems involved in the synthesis of chromene derivatives.

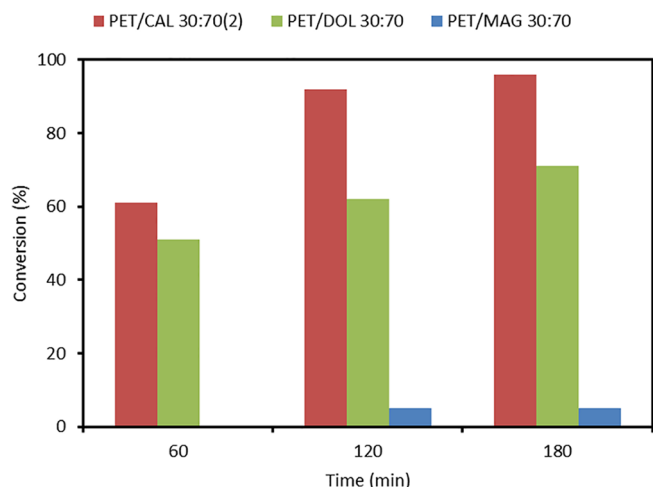


Fig. 5. Synthesis of 2-amino-4H-chromenes **1** catalyzed by PET/CAL 30:70(2), PET/DOL 30:70 and PET/MAG 30:70 hybrid materials, at 323 K, under solvent-free conditions.

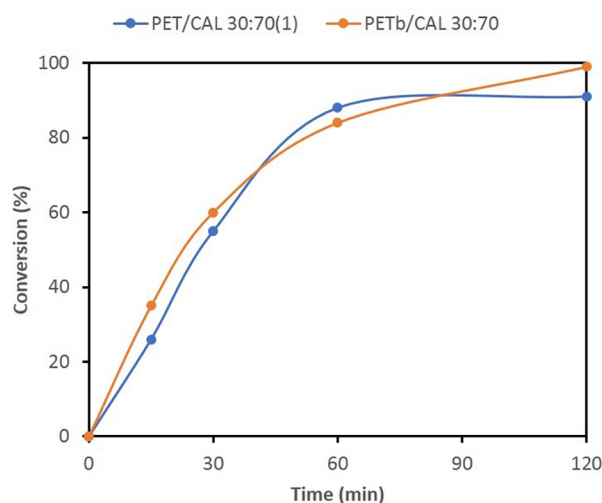


Fig. 6. Synthesis of 2-amino-4H-chromenes **1** catalyzed by PET/CAL 30:70(1) and PETb/CAL 30:70 hybrid materials, at 323 K, under solvent-free conditions.

3.2.4. Influence of catalyst amount

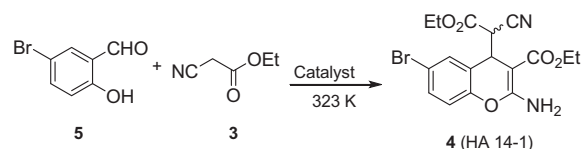
Finally, we carry out a study concerning the influence of the catalyst amount in the reaction by using 25 and 12 mg of the PET/CAL 30:70(2) catalyst. Thus, when the amount of catalyst was reduced, conversion to chromenes **1** is notably diminished (49 and 34%, after 1 h of reaction time, in the presence of 25 and 12 mg, respectively) with maintained selectivity. These results are in good agreement with those previously shown for samples with high PET/CAL ratio which point out that small amount of Ca phase can efficiently catalyze the reaction.

3.2.5. Valorization of PET residues

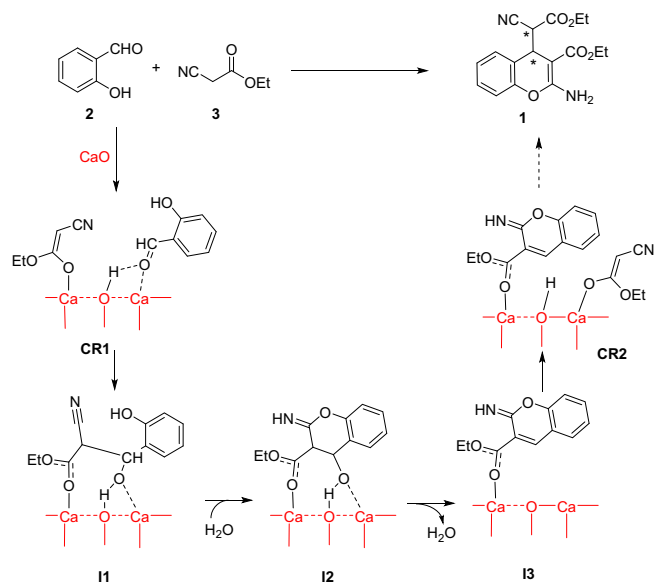
Additionally, we prepared and tested the PETb/CAL 30:70 catalyst from a commercially available plastic bottle (Fig. 6). The catalytic behavior of this sample is quite similar to that for PET/CAL 30:70(1) sample yielding the chromenes **1** with high conversions as diastereomeric mixtures **1a/1b** (approximately 2:1 ratio). These results are especially relevant due to the potential application of the highly polluting plastic residues in the preparation of efficient catalysts involved in the synthesis of valuable compounds.

3.2.6. Application of basic-carbon catalysts in the synthesis of bioactive compound **4**

Finally, PET/CAL 30:70(2) and PET/DOL 30:70 samples resulted on useful catalysts for the synthesis of ethyl 2-amino-6-bromo-4-(1-cyano-2-ethoxy-2-oxoethyl)-4H-chromene-3-carboxylate **4** (HA 14-1), from 5-bromo-2-hydroxybenzaldehyde **5** and ethyl cyanoacetate **3**, at 323 K, under solvent-free conditions, obtained with almost total conversion (99%), after only 2 h of reaction time, as diastereomeric mixture in a 2:1 ratio; compound **4** is known as antagonist for Bcl-2 protein which presents a great potential in therapy for cancer treatment (Scheme 2) [44].



Scheme 2. Synthesis of HA 14-1 **4** from 5-bromo-2-hydroxybenzaldehyde **5** and ethyl cyanoacetate **3**, at 323 K, catalyzed by PET/CAL 30:70(2) and PET/DOL 30:70.



Scheme 3. Probably reaction pathway for the synthesis of chromenes 1 catalyzed by CaO.

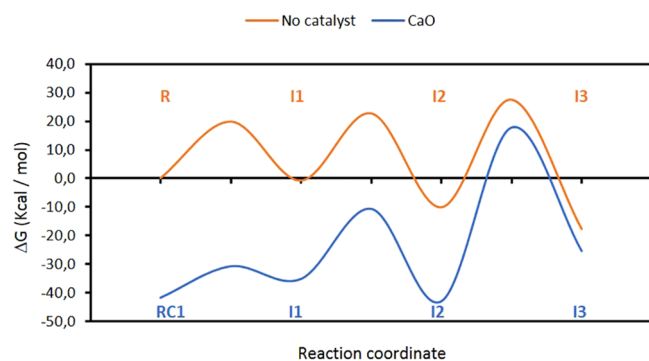


Fig. 7. Free-energy profiles computed for the uncatalyzed and catalyzed synthesis of chromenes 1.

3.3. Computational study

The role of the active phase in the investigated catalysts was theoretically studied by analyzing each reaction step as an elementary reaction, in the presence and in the absence of the catalytic specie. We select a cubic metallic cluster of $(\text{CaO})_{20}$ [36] considering that it is large enough to contain reactant structures and the most active Ca phase. Based on our previous studies when using ionic liquids as catalytic

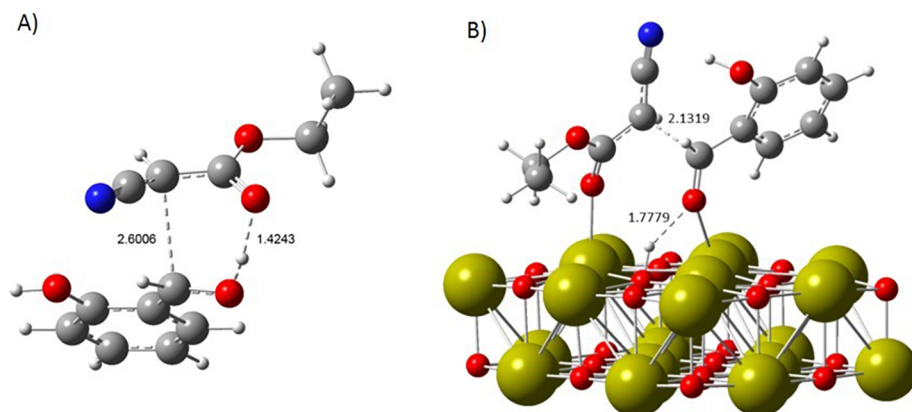


Fig. 8. Optimized transition structures $\text{TS}_{\text{R-11}}$ for the first step of the reaction in the formation of chromenes 1. A) $\text{TS}_{\text{R-11}}$ in the absence of any catalyst. B) $\text{TS}_{\text{R-11(CaO)}}$ catalyzed by CaO. Relevant distances are expressed in Å.

systems [21], it seems reasonable to think that the reaction could follow the pathway shown in Scheme 3, comprising i) aldol reaction between reactants giving I1, ii) heterocyclization to I2, iii) dehydration to I3 and finally iv) Michael addition of a second molecule of ethyl cyanoacetate 3 yielding chromenes 1 as mixtures of the corresponding diastereoisomers. Fig. 7 depicts the free-energy profiles computed for the uncatalyzed and catalyzed processes which point out the importance of the presence of the catalyst notably decreasing the free energy values during the first elementary steps of the reaction. Therefore, the presence of CaO provokes a strong kinetic effect.

Some relevant differences regarding the uncatalyzed reaction are found. Considering that alkaline earth oxides (CaO and MgO) present Lewis basicity and acidity both associated to oxygen anions [45] and Ca cations [46] at the surface, respectively, as demonstrated by adsorption experiments [47], CaO in our case could act as bifunctional acid-base catalyst activating both nucleophile, ethyl cyanoacetate 3, and electrophile, salicylaldehyde 2, at the same time. This fact was previously theoretically reported by us in the Friedländer reaction to yield quinolines catalyzed by MgO-based catalysts [8]. Based on that, we propose for the catalyzed reaction the initial formation of reactant complex, CR1, in which ethyl cyanoacetate 3 is activated by dissociative chemisorption to form the corresponding enolate anchored at the CaO surface whereas electrophile is interacting with Lewis acid center (Scheme 3). On the other side, Fig. 8 shows the computed transition structures $\text{TS}_{\text{R-11}}$ for the first step of the process comprising the aldol reaction between reagents. $\text{TS}_{\text{R-11(CaO)}}$ is notably more advanced transition structure than $\text{TS}_{\text{R-11}}$ as indicated by the C-C bond forming distances (2.1319 vs 2.6006 Å). However, while for $\text{TS}_{\text{R-11}}$ in absence of any catalyst the enolic proton is almost totally transferred to the O-carbonyl acceptor, this proton in $\text{TS}_{\text{R-11(CaO)}}$ is strongly bound to the CaO surface. Nevertheless, the catalyzed reaction occurs with decreased activation barrier, 8.8 Kcal/mol lower than calculated for the uncatalyzed process.

Both heterocyclization of I1 to I2 and subsequent dehydration to I3 are assisted by one water molecule, the presence of water being observed in all the investigated samples as demonstrated by TG experiments. In this sense, Wang et al. report a study concerning the water effect in condensation and dehydration reactions [48]. This fact has been also observed by us in the Friedländer reaction to produce quinolines catalyzed by amino-grafted mesoporous silicas [49] but also in the presence of MgO [8]. Thus, the involvement of one water molecule in $\text{TS}_{\text{I1-I2}}$ and $\text{TS}_{\text{I2-I3}}$, in absence of any catalyst, significantly reduces the activation barrier in 18.8 and 12.2 Kcal/mol, respectively, alleviating the ring strain in the proton-transfer transition state. Assuming the water participation in the catalyzed process, the transition structures $\text{TS}_{\text{I1-I2w(CaO)}}$ $\text{TS}_{\text{I2-I3w(CaO)}}$ were optimized and are shown in Fig. 9.

Interestingly, I2 intermediate changes its adsorption mode over the CaO surface for subsequent dehydration, then the -OH group being suitable for dehydration whereas the imine moiety is located

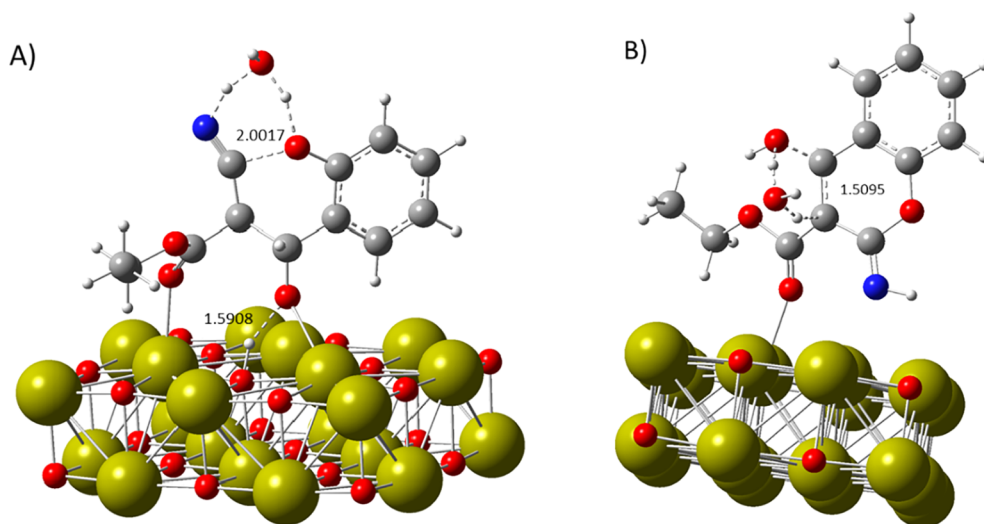


Fig. 9. Optimized transition structures TS_{11-12w} and TS_{12-13w} for the catalyzed synthesis of chromenes **1**. A) $TS_{11-12w(CaO)}$ and B) $TS_{12-13w(CaO)}$. Relevant distances are expressed in Å.

surrounding Lewis acid centers (Fig. 9 B). This new interaction is produced with notable lower free energy barrier (29.2 Kcal/mol) than those calculated for $TS_{12-13w(CaO)}$ indicating the desorption and re-adsorption before dehydration. Subsequent Michael addition of ethyl cyanoacetate **3** to **I3** leading to chromenes **1** would proceed with the strongly favored formation of reactant complex CR2, similar to CR1 (Scheme 3). The molecule of **3** is then located close to both electrophile faces comprising the C=C bond of iminochromene **I3** to yield diastereomeric mixtures of chromenes **1**, as sets of the corresponding enantiomers (*RS,SR;RR,SS*). Finally, computed transition structures for this last elementary step, $TS_{I3-1(RS)}$ and $TS_{I3-1(RR)}$ barely present energetic differences (1.7 Kcal/mol lower for $TS_{I3-1(RS)}$), yielding the chromene **1a**, the most stable isomer, as expected. At this regard, it is noteworthy that the selected model does not represent a realistic situation only allowing to study the effect of active centers in the reaction, CaO in this case, without any confinement restrictions.

4. Conclusions

In this work, we herein report for first time a family of calcium oxide (calcium hydroxide)/carbon composites involved in the efficient synthesis of 2-amino-4*H*-chromenes, a type of privileged heterocyclic scaffolds related to their biological properties, from salicylaldehydes and ethyl cyanoacetate, under mild and free-solvent conditions. These materials were synthesized by direct thermal pyrolysis of easily available precursors such as limestone and PET, exhibit basic properties and present micro and mesoporosity. All the samples are easily hydrated under ambient conditions but also dehydrated by re-calcination. Both detected Ca-phases, CaO and $Ca(OH)_2$, are active in the investigated reaction even for the samples showing the highest PET/CAL ratio. The catalysts comprising CaO present notable superior catalytic performance. Our results strongly suggest that the reaction is mainly controlled by the basicity of the catalysts.

The developed methodology can be applied by using a PET source from plastic residues which constitute an interesting environmental alternative in terms of circular economy, yielding isomer **1a** with high conversion and increase selectivity.

The reaction under study catalyzed by CaO takes place by cascade reactions probably following the sequence: i) aldolization between reagents, ii) heterocyclization and iii) dehydration, both could be assisted by one water molecule and, finally, iv) Michael addition of a second molecule of ethyl cyanoacetate **3**. The formation of reactant complexes, CR1 and CR2 for each elementary step involving ethyl cyanoacetate **3** in which both nucleophile and electrophile are activated is proposed. Our experimental and theoretical studies demonstrate that the reaction

is strongly favored in the presence of the CaO-containing catalysts.

Acknowledgments

This work has been supported by MICINN (Project CTM2014-5668-R). The authors are grateful Franchescoli Didier Velázquez Herrero for your help with the TEM images and Dr. Elena Soriano for teaching on theoretical calculations.

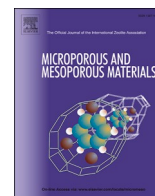
Appendix A. Supplementary data

Supplementary data to this article can be found online at <https://doi.org/10.1016/j.cej.2019.122795>.

References

- [1] J.L. Figueiredo, Application of nanocarbon materials to catalysis, in: B. Sels, M. Van de Voorde (Eds.), *Nanotechnology in Catalysis: Applications in the Chemical Industry, Energy Development, and Environment Protection*, Wiley-VCH Verlag GmbH & Co. KGaA, Weinheim, 2017, pp. 37–55.
- [2] P. Serp, J.L. Figueiredo, *Carbon Materials for Catalysis*, John Wiley & Sons, Hoboken, New Jersey, 2009.
- [3] E. Pérez-Mayoral, I. Matos, M. Bernardo, I.M. Fonseca, New and advanced porous carbon materials in fine chemical synthesis. Emerging precursors of porous carbons, *Catalysts* 9 (2019) 133, <https://doi.org/10.3390/catal9020133>.
- [4] I. Matos, M. Bernardo, I. Fonseca, Porous carbon: A versatile material for catalysis, *Catal. Today* 285 (2017) 194–203.
- [5] E. Pérez-Mayoral, V. Calvino-Casilda, E. Soriano, Metal-supported carbon-based materials: opportunities and challenges in the synthesis of valuable products, *Catal. Sci. Tech.* 6 (2016) 1265–1291.
- [6] E. Pérez-Mayoral, V. Calvino-Casilda, M. Godino, A.J. López-Peinado, R.M. Martín-Aranda, Porous catalytic systems in the synthesis of bioactive heterocycles and related compounds, in: G. Brahmachari (Ed.), *Green Synthetic Approaches for Biologically Relevant Heterocycles*, Elsevier, Amsterdam, 2015, pp. 378–403.
- [7] J. López-Sanz, E. Pérez-Mayoral, E. Soriano, D. Omenat-Morán, C.J. Durán, R.M. Martín-Aranda, I. Matos, I. Fonseca, Acid-activated carbon materials: cheaper alternative catalysts for the synthesis of substituted quinolines, *ChemCatChem* 5 (2013) 3736–3742.
- [8] M. Godino-Ojer, A.J. López Peinado, R.M. Martín Aranda, J. Przepiorski, E. Pérez-Mayoral, E. Soriano, Eco-friendly catalytic systems based on carbon-supported magnesium oxide materials for the Friedländer Condensation, *ChemCatChem* 6 (2014) 3440–3447.
- [9] M. Godino-Ojer, E. Soriano, V. Calvino-Casilda, F.J. Maldonado-Hódar, E. Pérez-Mayoral, Metal-free synthesis of quinolines catalyzed by carbon aerogels: Influence of the porous texture and surface chemistry, *Chem. Eng. J.* 314 (2017) 488–497.
- [10] M. Godino-Ojer, A.J. López Peinado, J. Maldonado-Hódar, E. Pérez-Mayoral, Highly efficient and selective catalytic synthesis of quinolines involving transition-metal doped carbon aerogels, *ChemCatChem* 9 (2017) 1422–1428.
- [11] M. Godino-Ojer, R.M. Martín-Aranda, F.J. Maldonado-Hódar, A.F. Pérez-Cadenas, E. Pérez-Mayoral, Developing strategies for the preparation of Co-carbon catalysts involved in the free solvent selective synthesis of aza-heterocycles, *Mol. Catal.* 445 (2018) 223–231.
- [12] M. Godino-Ojer, L. Milla-Diez, I. Matos, C.J. Durán-Valle, M. Bernardo, I.M. Fonseca, E. Pérez Mayoral, Enhanced catalytic properties of carbon supported

- zirconia and sulphated zirconia for the green synthesis of benzodiazepines, *ChemCatChem* 10 (2018) 5215–5223.
- [13] G.P. Ellis, *The Chemistry of Heterocyclic Compounds: Chromenes, Chromanones, and Chromones* Vol. 31 John Wiley & Sons Inc, New York, 1977.
- [14] R. Pratap, V.J. Ram, Natural and synthetic chromenes, fused chromenes, and versatility of dihydrobenzo[*h*]chromenes in organic synthesis, *Chem. Rev.* 114 (2014) 10476–10526.
- [15] M.N. Elinson, R.F. Nasybullin, F.V. Ryzhkov, T.A. Zaimovskaya, M.P. Egorov, Solvent-free cascade assembling of salicylaldehydes and cyanoacetates: fast and efficient approach to medicinally relevant 2-amino-4*H*-chromene scaffold, *Monatsh. Chem.* 145 (2014) 605–610.
- [16] M.A. Kulkarni, K.S. Pandit, U.V. Desai, U.P. Lad, P.P. Wadgaonkar, Diethylamine: A smart organocatalyst in eco-safe and diastereoselective synthesis of medicinally privileged 2-amino-4*H*-chromenes at ambient temperature, *Comp. Rend. Chim.* 16 (2013) 689–695.
- [17] M. Curini, F. Epifano, S. Chimichi, F. Montanari, M. Nocchetti, O. Rosati, Potassium exchanged layered zirconium phosphate as catalyst in the preparation of 4*H*-chromenes, *Tetrahedron Lett.* 46 (2005) 3497–3499.
- [18] J.S. Yadav, B.V.S. Reddy, M.K. Gupta, I. Prathap, S.K. Pandey, Amberlyst A-21®: An efficient, cost-effective and recyclable catalyst for the synthesis of substituted 4*H*-chromenes, *Catal. Commun.* 8 (2007) 2208–2211.
- [19] U. Constantino, M. Curinir, F. Montanari, M. Nocchetti, O. Rosati, Hydrotalcite-like compounds as heterogeneous catalysts in liquid phase organic synthesis. II. Preparation of 4*H*-chromenes promoted by hydrotalcite doped with hydrous tin(IV) oxide, *Micropor. Mesopor. Mat.* 107 (2008) 16–22.
- [20] N. Yu, J.M. Aramini, M.W. Germann, Z. Huang, Reactions of salicylaldehydes with alkyl cyanoacetates on the surface of solid catalysts: syntheses of 4*H*-chromene derivatives, *Tetrahedron Lett.* 41 (2000) 6993–6996.
- [21] J. Velasco, E. Pérez-Mayoral, V. Calvino-Casilda, A.J. López-Peinado, M.A. Bañares, E. Soriano, Imidazolium sulfonates as environmental-friendly catalytic systems for the synthesis of biologically active 2-amino-4*H*-chromenes: Mechanistic insights, *J. Phys. Chem. B* 119 (2015) 12042–12049.
- [22] A. Smuszkiewicz, J. López-Sanz, I. Sobczak, M. Ziolk, R.M. Martín-Aranda, E. Soriano, E. Pérez-Mayoral, Mesoporous niobiosilicate NbMCF modified with alkali metals in the synthesis of chromene derivatives, *Catal. Today* 277 (2016) 133–142.
- [23] A. Smuszkiewicz, J. López-Sanz, I. Sobczak, R.M. Martín-Aranda, M. Ziolk, E. Pérez-Mayoral, Tantalum vs Niobium MCF nanocatalysts in the green synthesis of chromene derivatives, *Catal. Today* 325 (2019) 47–52.
- [24] J. Przepiórski, A.W. Morawski, A. Oya, Method for preparation of copper-coated carbon material, *Chem. Mater.* 15 (2003) 862–865.
- [25] J. Przepiórski, Y. Abe, S. Yoshida, A. Oya, Preferential supporting of potassium carbonate around the peripheral region of activated carbon fibre, *J. Mater. Sci. Lett.* 16 (1997) 1312–1314.
- [26] J. Przepiórski, A. Czyżewski, R. Pietrzak, M. Toyoda, A.W. Morawski, Porous carbon material containing CaO for acidic gas capture: Preparation and properties, *J. Hazard. Mater.* 263 (2013) 353–360.
- [27] A. Czyżewski, J. Kapica, D. Moszyński, R. Pietrzak, J. Przepiórski, On competitive uptake of SO₂ and CO₂ from air by porous carbon containing CaO and MgO, *Chem. Eng. Sci.* 226 (2013) 348–356.
- [28] J. Przepiórski, A. Czyżewski, R. Pietrzak, A.W. Morawski, MgO/CaO-loaded activated carbon for carbon dioxide capture: Practical aspects of use, *Ind. Eng. Chem. Res.* 52 (2013) 6669–6677.
- [29] J. Karolczyk, M. Janus, J. Przepiórski, Removal of model contaminants from water by porous carbons obtained through carbonization of poly(ethylene terephthalate) mixed with some magnesium compounds, *J. Porous Mat.* 20 (2013) 159–170.
- [30] J.M. Valente Nabais, P.J.M. Carrott, Chemical characterization of activated carbon fibers and activated carbons, *J. Chem. Edu.* 83 (2006) 436.
- [31] M.J. Frisch, G.W. Trucks, H.B. Schlegel, G.E. Scuseria, M.A. Robb, J.R. Cheeseman, G. Scalmani, V. Barone, B. Mennucci, G.A. Petersson, H. Nakatsuji, M. Caricato, X. Li, H.P. Hratchian, A.F. Izmaylov, J. Bloino, G. Zheng, J.L. Sonnenberg, M. Hada, M. Ehara, K. Toyota, R. Fukuda, J. Hasegawa, M. Ishida, T. Nakajima, Y. Honda, O. Kitao, H. Nakai, T. Vreven, J.A. Montgomery, Jr., J.E. Peralta, F. Ogliaro, M. Bearpark, J.J. Heyd, E. Brothers, K.N. Kudin, V.N. Staroverov, R. Kobayashi, J. Normand, K. Raghavachari, A. Rendell, J.C. Burant, S.S. Iyengar, J. Tomasi, M. Cossi, N. Rega, J.M. Millam, M. Klene, J.E. Knox, J.B. Cross, V. Bakken, C. Adamo, J. Jaramillo, R. Gomperts, R.E. Stratmann, O. Yazyev, A.J. Austin, R. Cammi, C. Pomelli, J.W. Ochterski, R.L. Martin, K. Morokuma, V.G. Zakrzewski, G.A. Voth, P. Salvador, J.J. Dannenberg, S. Dapprich, A.D. Daniels, Ö. Farkas, J.B. Foresman, J.V. Ortiz, J. Cioslowski, D.J. Fox, Gaussian 09, Revision B.1., Gaussian, Inc., Wallingford CT, 2009.
- [32] A.D. Becke, Density-functional thermochemistry. III. The role of exact exchange, *J. Chem. Phys.* 98 (1993) 5648–5652.
- [33] C. Lee, W. Yang, R.G. Parr, Development of the Colle-Salvetti correlation-energy formula into a functional of the electron density, *Phys. Rev. B* 37 (1988) 785–789.
- [34] M. Moradi, A.A. Peyghan, Z. Bagheri, M. Kamifiroozi, Cation- π interaction of alkali metal ions with C₂₄ fullerene: a DFT study, *J. Mol. Model.* 18 (2012) 3535–3540.
- [35] J. Beheshtian, M.T. Baei, A.A. Peyghan, Z. Bagheri, Electronic sensor for sulfide dioxide based on AlN nanotubes: a computational study, *J. Mol. Model.* 18 (2012) 4745–4750.
- [36] M. Chen, K.S. Thanthirivatt, D.A. Dixon, Structures and Stabilities of (CaO)_n Nanoclusters, *J. Phys. Chem. C* 121 (2017) 23025–23038.
- [37] C. Gonzalez, H.B. Schlegel, Reaction path following in mass-weighted internal coordinates, *J. Phys. Chem.* 94 (1990) 5523–5527.
- [38] V. Morales-Flórez, A. Santos, I. Romero-Hermida, L. Esquivias, Hydration and carbonation reactions of calcium oxide by weathering: kinetics and changes in the nanostructure, *Chem. Eng. J.* 265 (2015) 194–200.
- [39] M. Thommes, K. Kaneko, A.V. Neimark, J.P. Olivier, F. Rodríguez-Reinoso, J. Rouquerol, K.S.W. Sing, Physisorption of gases, with special reference to the evaluation of surface area and pore size distribution (IUPAC Technical Report), *Pure Appl. Chem.* 87 (2015) 1051–1069.
- [40] D.R. Glasson, Reactivity of lime and related oxides. II. Sorption of water vapour on calcium oxide, *J. Appl. Chem.* 8 (2007) 798–803.
- [41] M. López Granados, D. Martín Alonso, I. Sádaba, R. Mariscal, P. Ocón, Leaching and homogeneous contribution in liquid phase reaction catalysed by solids: The case of triglycerides methanolysis using CaO, *App. Catal. B Environ.* 89 (2009) 265–272.
- [42] J. Przepiórski, A. Czyżewski, R. Pietrzak, B. Tryba, MgO/CaO-loaded porous carbons for carbon dioxide capture, *J. Therm. Anal. Calorim.* 111 (2013) 357–364.
- [43] J. Przepiórski, A. Czyżewski, M. Toyoda, T. Tsumura, R. Pietrzak, A.W. Morawski, MgO-loaded porous carbon for carbon dioxide sorption: study on cyclic sorption–regeneration, *Int. J. Greenhouse Gas Control* 10 (2012) 164–168.
- [44] J.L. Wang, D. Liu, Z.J. Zhang, S. Shan, X. Han, S.M. Srinivasula, C.M. Croce, E.S. Alnemri, Z. Huang, Structure-based discovery of an organic compound that binds Bcl-2 protein and induces apoptosis of tumor cells, *PNAS* 97 (2000) 7124–7129.
- [45] K. Tanabe, M. Misono, Y. Ono, H. Hattori, New solid acids and bases: their catalytic properties, in: B. Delmon, J.T. Yates (Eds.), *Studies in Surface Science and Catalysis*, Vol 51 Kodansha/Elsevier, Tokyo/Amsterdam, 1989.
- [46] T. Ito, T. Tashiro, M. Kawasaki, T. Watanabe, K. Toi, H. Kobayashi, Adsorption of methane on magnesium oxide studied by temperature-programmed desorption and ab initio molecular orbital methods, *J. Phys. Chem.* 95 (1991) 4476–4483.
- [47] A. Markovits, J. Ahdjoudj, C. Minot, Theoretical study of the TiO₂ and MgO surface acidity and the adsorption of acids and bases, *Mol. Eng.* 7 (1997) 245–261.
- [48] C. Wang, X. Liu, M. Yang, H. Ma, P. Yan, J.M. Slattery, Y. Gao, A green and efficient amine-functionalized ionic liquid/H₂O catalytic system for the synthesis of α , α' -bis (substituted benzylidene)cyclopentanones, *RSC Adv.* 3 (2013) 8796–8804.
- [49] A. Smuszkiewicz, J. López-Sanz, E. Pérez-Mayoral, E. Soriano, I. Sobczak, M. Ziolk, R.M. Martín-Aranda, A.J. López-Peinado, Amino-grafted mesoporous materials based on MCF structure involved in the quinoline synthesis. Mechanistic insights, *J. Mol. Catal. A* 378 (2013) 38–46.



Amino-grafted Cu and Sc Metal-Organic Frameworks involved in the green synthesis of 2-amino-4*H*-chromenes. Mechanistic understanding

D. González-Rodal^{a,c}, G. Turnes Palomino^{b,**}, C. Palomino Cabello^b, E. Pérez-Mayoral^{a,*}

^a Departamento de Química Inorgánica y Química Técnica, Universidad Nacional de Educación a Distancia, UNED, Facultad de Ciencias, Urbanización Monte Rozas, Avda. Esparta s/n Ctra. de Las Rozas al Escorial Km 5, Las Rozas, Madrid, E-528232, Spain

^b Departamento de Química, Universidad de las Islas Baleares, Cra. de Valldemossa km 7.5, 07122, Palma de Mallorca, Spain

^c Facultad de Ciencias Experimentales, Universidad Francisco de Vitoria, UFV, Ctra. Pozuelo-Majadahonda km 1.800, 28223, Pozuelo de Alarcn, Madrid, Spain

ARTICLE INFO

Keywords:

Amino-grafted metal-organic-frameworks
Heterogeneous catalysts
Chromene derivatives
Fine chemicals

ABSTRACT

In this work, we report for the first time a new methodology for the eco-synthesis of 2-amino-4*H*-chromenes **1**, from salicylaldehydes and cyano compounds, under solvent-free and mild conditions, using amino-grafted MOFs as catalysts. The selected MOFs – commercial CuBTC and MIL-100(Sc) previously synthesized in our laboratories – can be easily functionalized with amines of different nature showing notable differences in their composition and textural properties. The total or partial functionalization of the metal centers in starting MOFs is strongly depending on the functionalization method used. Our results indicate that the catalytic performance is mainly conditioned by the type and concentration of basic sites, porosity of the samples barely showing any influence. The methodology herein reported could be considered as an environmental friendly alternative to the selective chromene synthesis, which allows to achieve high yields in relatively short reaction times (up to 90% over 1 h), using notably small amounts of easily prepared catalysts.

Furthermore, our experiments in combination with theoretical calculations strongly suggest that free-amine groups in ethylenediamine (EN) functionalized catalysts can act either as individual catalytic sites, as for EN-M/CuBTC sample, in which all metal centers are functionalized with EN ligands and shows the highest concentration of basic catalytic sites, or acting in cooperation with the closest metal centers in samples partially functionalized, as in the case of EN/CuBTC sample.

1. Introduction

Metal-Organic Frameworks (MOFs) are fascinating organic-inorganic hybrid materials applied to a great variety of research fields such as gas storage, sensing, catalysis and even drug delivery among others [1–3]. The wide diversity of both metal ions and multidentate organic ligands available to form these 3D nanoporous networks by coordination makes possible the synthesis of these materials on demand [4].

Regarding catalytic applications, MOFs are considered promising candidates for catalyzing liquid phase reactions because of their textural properties – high surface areas and pore volumes – as well as their high concentrations of active sites accurately located [5]. In recent years, MOFs have been extensively explored as catalysts in acid-base and redox reactions [6], CO₂ chemical transformations [7], H₂ production [8] and

as multifunctional catalysts in synergistic catalysis and tandem reactions [9] but also in the production of fine chemicals [10,11] involving aldol-based reactions [12]. At this respect, we reported experimental and theoretical studies concerning the synthesis of quinolines via Friedländer reaction catalyzed by Cu₃(BTC)₂ [13–16]. Much more recently, commercial Basolites, particularly C300, F300 and Z1200, have been proposed by some of us as efficient porous catalytic active systems in the synthesis of important heterocyclic scaffolds such as quinoxalines [17].

Rostammia and col. have reported different amino-functionalized MOFs which are able to catalyze the synthesis of very different interesting compounds. Such is the case of tetrahydro-4*H*-chromenes synthesis catalyzed by IRMOF-3 (Zn₄O(H₂N-TA)₃) [18], imidazo [1,2-*a*] pyridines through Groebke–Blackburn–Bienaymé multicomponent coupling reaction in the presence of NH₂-MIL-53(Al) [19], Hantzsch

* Corresponding author.

** Corresponding author.

E-mail addresses: g.turnes@uib.es (G.T. Palomino), eperez@ccia.uned.es (E. Pérez-Mayoral).

<https://doi.org/10.1016/j.micromeso.2021.111232>

Received 30 March 2021; Received in revised form 4 June 2021; Accepted 5 June 2021

Available online 10 June 2021

1387-1811/© 2021 Elsevier Inc. All rights reserved.

condensation using Cr-MOF modified with ethylenediamine [20] and Suzuki coupling reaction catalyzed by Pd@Cu-BDC/Py-SI, a MOF consisting of palladium ions coordinated to Schiff base-decorated Cu-BDC [21]. Much more recently, the preparation of ultra-small palladium nanoparticles stabilized on diamine-modified Cr-MIL-101 has also been reported for hydrogen production from formic acid [22].

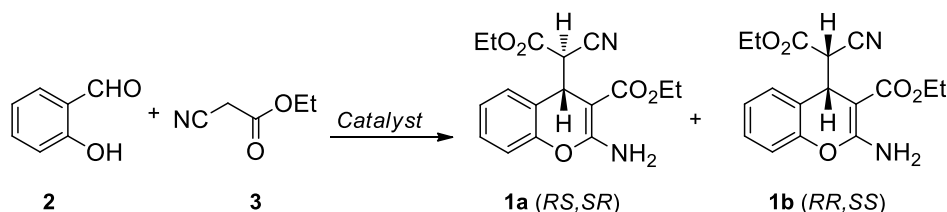
Chromene derivatives [23] are an extremely versatile class of heterocycles which has acquired especial relevance due to their therapeutic properties such as antiviral, antiproliferative, antioxidant, antihistaminic and others [24,25]. These heterocyclic compounds have been also recognized as antiapoptotic Bcl-2 proteins useful in cancer treatments to avoid the drug resistance [26,27], and for the treatment of schizophrenia [28] or Alzheimer disease [29].

Different catalysts involved in the synthesis of chromenes, particularly 2-amino-4H-chromenes, have been reported. Among the most traditional homogeneous ones stand out highly polluting organic amines [30] whereas molecular sieves [31], anion exchange resins such as Amberlyst A-21 [32], doped hydrotalcites [33] and zirconium phosphate [34], have been reported as heterogeneous catalysts. Developed methodologies so far are mostly characterized by the use of large amounts of inorganic solids and solvents, during prolonged reaction times, also requiring tedious isolation and purification steps to obtain the reaction products. These features contribute to the production of wastes, such as solid residues and liquid effluents, highly polluting, and to increase the energy consumption. In this context, we have recently reported some new and environmental-friendly catalytic systems, useful in the multicomponent synthesis of 2-amino-4H-chromenes **1** (Scheme 1) comprising ionic liquids like imidazolium sulfonates [35], bifunctional mesoporous metallosilicates [36,37] and, much more recently, CaO-carbon materials, easily prepared from poly(ethyleneterephthalate) (PET) and natural limestone allowing the valorization of both PET residues and mineral sources, mesoporous hydrotalcite/SBA-15 and hydrotalcite/hydroxyapatite composites [38–40].

The goal of this work is the development of new MOF-derived catalysts with basic properties able to promote the synthesis of 2-amino-4H-chromene derivatives from salicylaldehydes and different nitriles. The existence of coordinatively unsaturated metal sites (CUS) in the selected MOFs allows the functionalization with organic amines by coordination using a post-synthetic approach, which is an usual strategy to modify the acid-base properties of these metal-organic networks. In this context, Hwang et al. reported the preparation of an amino-grafted MIL-101 and the evaluation of its catalytic behaviour in Knoevenagel condensation, between benzaldehyde and ethyl cyanoacetate, resulting to show superior catalytic performance than amino-grafted mesoporous silica APS-SBA-15 [41]. Based on that, and in order to study the influence of both basicity and textural properties on catalytic behaviour, we select two different MOFs – Basolite C300 (CuBTC) and MIL-100(Sc) [42] –, in which metal ions Cu^{II} and Sc^{III}, respectively, are coordinated by trimesic acid (denoted as BTC) ligands, being both able to coordinate organic amines of distinct nature.

2. Materials and methods

The materials used in this research were commercially available.



Scheme 1. Synthesis of 2-amino-4H-chromenes from salicylaldehyde **2** and ethyl cyanoacetate **3** under solvent-free conditions.

Chemical reagents and solvents were purchased from Sigma-Aldrich or Alfa-Aesar. Particularly, Basolite C300 was purchased from Sigma-Aldrich.

2.1. Synthesis of MIL-100(Sc)

MIL-100(Sc) was synthesized following the experimental procedure reported by Li et al. [43]. Briefly, it was prepared by mixing Sc(NO₃)₃ · H₂O (0.61 g) and trimesic acid (0.25 g) in DMF (45 mL). The mixture was stirred at room temperature for 30 min and then introduced into a Teflon-lined autoclave (100 mL) at 423 K for 36 h. The product was filtered off, washed with DMF, and dried at room temperature.

2.2. Synthesis of amino-grafted MIL-100(Sc)

MIL-100(Sc) was functionalized following an adaptation of the experimental protocol reported by Hwang et al. [41]. As-synthesized MIL-100(Sc) (1.0 g) was immersed in ethanol, at 373 K, for 20 h before being activated at 453 K for 12 h under nitrogen atmosphere to remove the terminal solvent molecules coordinated to the open metal sites. After activation, MIL-100(Sc) was suspended in anhydrous toluene (100 mL) and the corresponding amine (1.0 mL) was added. In order to make the grafting complete, the reaction mixture was refluxed under N₂ for 12 h. The resulting solid was washed with hexane to remove the unreacted amine, and dried at room temperature.

Two amino-grafted MIL-100(Sc) samples were prepared by using ethylenediamine (EN) or N,N'-dimethylethylenediamine (MMEN) denoted as EN-M/MIL-100(Sc) and MMEN-M/MIL-100(Sc), respectively.

2.3. Synthesis of amino-grafted CuBTC

Amino-grafted CuBTC samples were prepared by using two different methodologies.

Method A: EN-M/CuBTC samples were prepared from CuBTC by reacting with EN following the experimental protocol described above and used for the functionalization of MIL-100(Sc).

Method B: For comparison purposes, analogous sample EN/CuBTC was prepared in the presence of diethyl ether as solvent [44]. Briefly, commercial CuBTC (0.6 g) was refluxed in diethyl ether (20 mL) with the corresponding amine (1.5 mmol) under vigorous stirring during 72 h. The obtained solid was washed with diethyl ether to remove the unreacted amine (5 × 5 mL) and dried at 323 K.

Following this method two amino-grafted CuBTC samples were then prepared by using ethylenediamine (EN) or diethylenetriamine (DET) denoted as EN/CuBTC and DET/CuBTC, respectively. In addition, we also prepared 2DET/CuBTC sample in which a double amount of DET was used.

2.4. Characterization of the catalysts

Textural parameters of the materials were determined from the N₂ adsorption/desorption isotherms obtained at 77 K with a TriStar II (Micromeritics) gas analyzer. The samples were previously outgassed at 413 K overnight. The data of the isotherms were analyzed by using the

Brunauer-Emmett-Teller (BET) method to determine the specific surface area and the two dimensional non-local density functional theory (2D-NLDFT) model for the determination of pore volume and pore size distribution. Powder XRD data were collected using CuK α ($\lambda = 1.5418 \text{ \AA}$) radiation on a Bruker D8 Advance diffractometer. Fourier transform infrared (FTIR) spectra were recorded using a Bruker Vertex 80v spectrometer equipped with an MCT cryodetector. For IR measurements, a thin, self-supported wafer of the samples was prepared and activated (outgassed) inside the IR cell under dynamic vacuum at 423 K for 6 h. After this activation treatment, carbon monoxide was dosed into the cell to study the coordinatively unsaturated metal centers. Elemental analyses of the solids were carried out with Elemental Analyzer LECO CHNS-932. Catalysts copper content was determined by AES (Atomic Emission Spectroscopy), using a ICP-OES PlasmaQuant PQ 9000 (Analytik Jena) spectrometer.

2.5. Catalytic performance

In a typical experiment, carried out at 323 K or 303 K, the catalyst (25 mg) was added to a mixture of salicylaldehyde **2** (2 mmol) and ethyl cyanoacetate **3** (4 mmol) and the reaction mixture was stirred during 3 h. The reactions were carried out in a multiexperiment work station Starfish, in liquid phase, under atmospheric pressure and solvent-free conditions. Samples of the reacting mixtures were periodically taken after certain times — 15, 30, 60, 120 and 180 min — for analysis by Proton Nuclear Magnetic Resonance (^1H NMR). The samples were diluted with CH_2Cl_2 (1 mL) to facilitate the separation of the catalyst by filtering off using a glass syringe equipped with a microfilter (Millipore, $0.45 \mu\text{m}$ HV). Finally, the solvent was evaporated in vacuo.

The progress of the reactions was qualitatively monitored by thin layer chromatography (TLC) performed on a DC-Aulofolien/Kieselgel 60 F245 (Merck), using $\text{CH}_2\text{Cl}_2/\text{EtOH}$ (98:2) mixture as an eluent.

The yield (or conversion) of the process is defined as the fraction of reactant **2** transformed at each reaction time into compounds, determined by ^1H NMR.

Reaction products were characterized by ^1H NMR spectroscopy. Solution NMR spectra were recorded on a Bruker DRX 400 (9.4 T, 400.13 MHz for ^1H) spectrometer with a 5-mm inverse-detection H-X probe equipped with a z-gradient coil, at 300 K. Chemical shifts (δ in ppm) are given from internal solvent, CDCl_3 7.26 for ^1H . Spectroscopic data of 2-amino-4H-chromenes **1**, **6** and **7** are in good agreement with those previously reported [30,35].

2.6. Computational methods

The calculations showed in this work were performed by using the Gaussian 09 software package [45], in gas phase, at 298 K. All the geometries were optimized using B3LYP hybrid functional [46,47] with

6-31G (d,p) basis set, this functional being a methodology used to study nanostructures [48]. The stationary points were characterized by means of harmonic vibrational frequency analysis. Thus, the transition structures were confirmed to be first-order saddle points. The imaginary frequency was inspected in each transition structures to ensure it represented the desired reaction coordinate. For key transition states the intrinsic reaction coordinate (IRC) was followed to ensure it connects the reactants and products [49].

3. Results and discussion

3.1. Characterization of the catalysts

Fig. 1 shows the X-ray diffraction patterns of CuBTC and MIL-100(Sc) before and after amine grafting. The CuBTC and MIL-100(Sc) samples showed good crystallinity and all diffraction lines could be assigned to the corresponding structural types. After the grafting process, the almost unchanged powder X-ray diffraction patterns of the samples indicate the preservation of the MOFs structure barely showing slight variations of crystallinity.

Nitrogen adsorption-desorption isotherms were collected at 77 K for CuBTC (Fig. 2a) and MIL-100(Sc) (Fig. 2b) samples and were analyzed using the BET and 2D-NLDFT methods. The measured BET surface areas and pore volumes of bare MOFs (Table 1) are in agreement with previous results. Amine-grafted samples show a notable reduction of the specific surface area and pore volume, especially for MIL-100(Sc) samples, for which these parameters are 2 and 3 times lower than those of the bare sample (Table 1), indicating a partial occupation of the space inside the pores by the amine molecules. The particularly low value of the surface area of EN-M/CuBTC sample is probably due to the high amine loading reached in this case (see below). The pore size distributions (Figure S1) demonstrate the presence of micropores in CuBTC samples and a multimodal distribution in MIL-100(Sc) samples, and confirm the decreased porosity of the functionalized materials.

The amine grafting of CuBTC and MIL-100(Sc) MOFs was also studied by FTIR spectroscopy. As shown in Fig. 3, all the amine-grafted samples exhibit additional absorption bands in the range of 3450 to 2800 cm^{-1} , which are assigned to N-H and C-H stretching vibrations [41,50–52], confirming the incorporation of the amine molecules in the prepared samples. In addition, in all the grafted samples, the observed aliphatic C–H stretching vibrations are shifted to larger values compared with those of free amine molecules, as observed when the molecule is coordinated to a Lewis center [41,53], demonstrating the selective grafting of the amines onto metal open sites of the MOFs. The functionalization with amine molecules of coordinatively unsaturated copper (CuBTC) and scandium (MIL-100(Sc)) cations was also checked by infrared spectroscopy of carbon monoxide adsorbed at 100 K. After the activation of the samples, a saturation dose of CO was introduced into

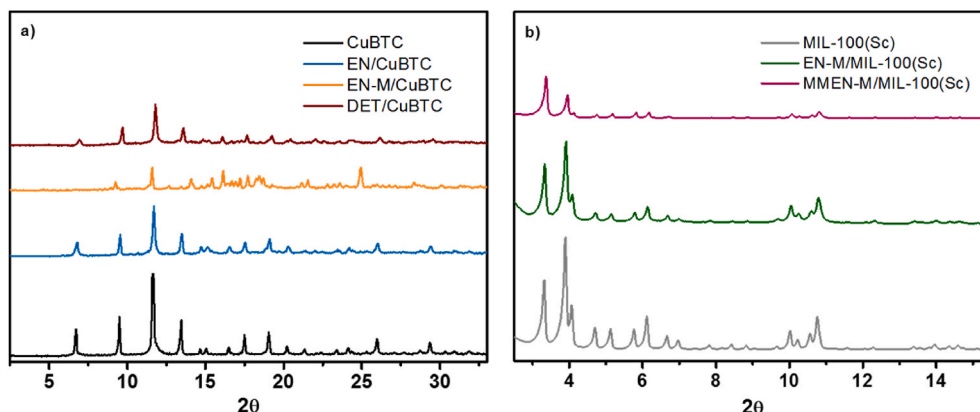


Fig. 1. X-Ray diffractograms of amino-grafted a) CuBTC and b) MIL-100(Sc) samples.

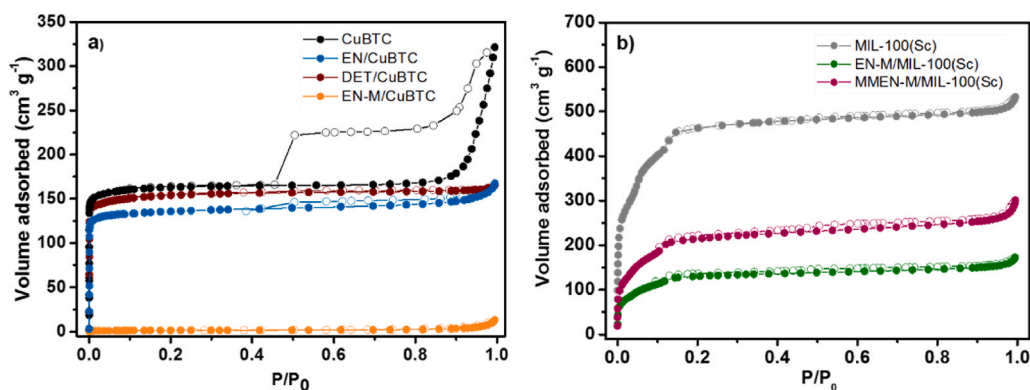


Fig. 2. Nitrogen adsorption-desorption isotherms for amino-grafted a) CuBTC and b) MIL-100(Sc) samples.

Table 1
Catalyst textural properties.

Catalyst	S_{BET} ($\text{m}^2 \text{g}^{-1}$)	V_p ($\text{cm}^3 \text{g}^{-1}$)
CuBTC	640	0.46
EN/CuBTC	546	0.23
DET/CuBTC	615	0.24
EN-M/CuBTC	6	0.016
MIL-100(Sc)	1590	0.72
EN-M/MIL-100(Sc)	444	0.23
MMEN-M/MIL-100(Sc)	736	0.41

the IR cell and the corresponding spectra were recorded. The IR spectra of CO adsorbed on the bare MOFs (Fig. 4) show an IR absorption band centred at 2170 cm^{-1} for CuBTC and 2183 cm^{-1} for MIL-100(Sc) that comes from the fundamental C-O stretching mode of carbon monoxide interacting (through the carbon atom) with the Cu^{II} and Sc^{III} cations, respectively [54]. Additionally, in the case of CuBTC, another IR band near 2128 cm^{-1} is observed, which, according to the literature, corresponds to the CO interacting with Cu^{I} species formed during the activation treatment of the sample [55]. The IR spectra of the EN/CuBTC and DET/CuBTC samples (Fig. 4a) show the IR absorption band at 2170 cm^{-1} , although much less intense, indicating that the open copper sites

in these samples are partially grafted by the amine molecules. In the case of the EN-M/CuBTC, the IR absorption band at 2170 cm^{-1} completely disappears (Fig. 4a) which, together with the porosity results and compositional data, confirm the high incorporation of amine molecules in this sample. The spectra of the functionalized MIL-100(Sc) samples (Fig. 4b) show that the band assigned to the CO stretching vibration of carbon monoxide adsorbed on Sc^{III} is not observed, indicating that in these samples, most of the metal centers are coordinated to the amine molecules.

Considering these results, we also carried out elemental analysis of the prepared samples confirming the presence of N (Table 2). Remarkable differences can be observed between the synthesized catalysts depending on the method used for their functionalization. Assuming that only one $-\text{NH}_2$ group per amine molecule is coordinated to a unique metal atom in the MOF, EN/CuBTC and DET/CuBTC samples showed a N content considerably smaller than the Cu loading, which increases in the case of using a double amount of DET (2DET/CuBTC sample), although still remaining lower than the metal loading. However, in the case of EN-M/CuBTC, the N content is notably higher indicating that part of the EN molecules are coordinated to all available Cu atoms, while the rest are probably interacting with $-\text{CO}_2\text{H}$ defects present in the framework. Therefore, it can be affirmed that the functionalization of the MOFs under study with N-containing ligands strongly depends on

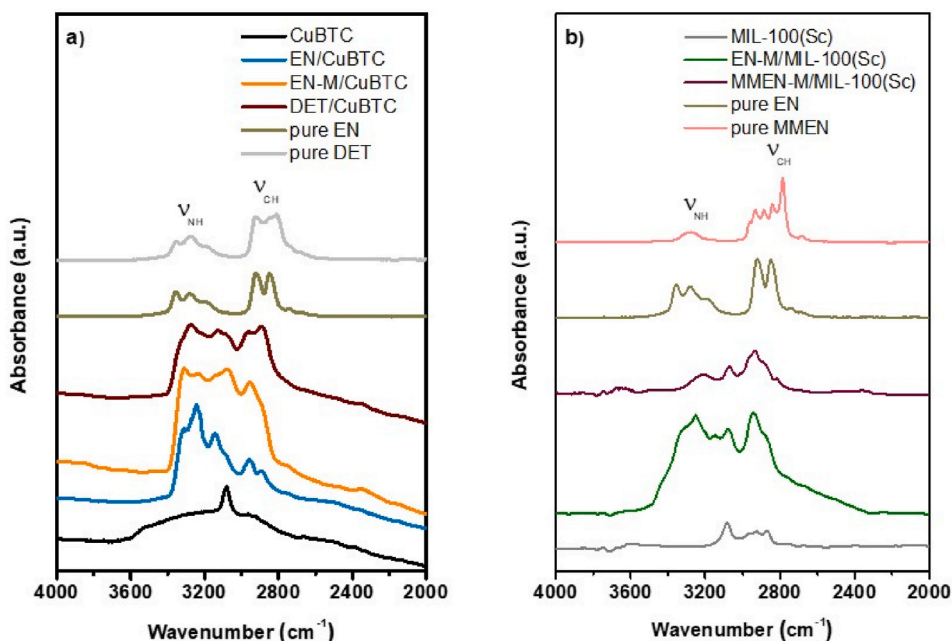


Fig. 3. FTIR spectra for amino-grafted a) CuBTC and b) MIL-100(Sc) samples.

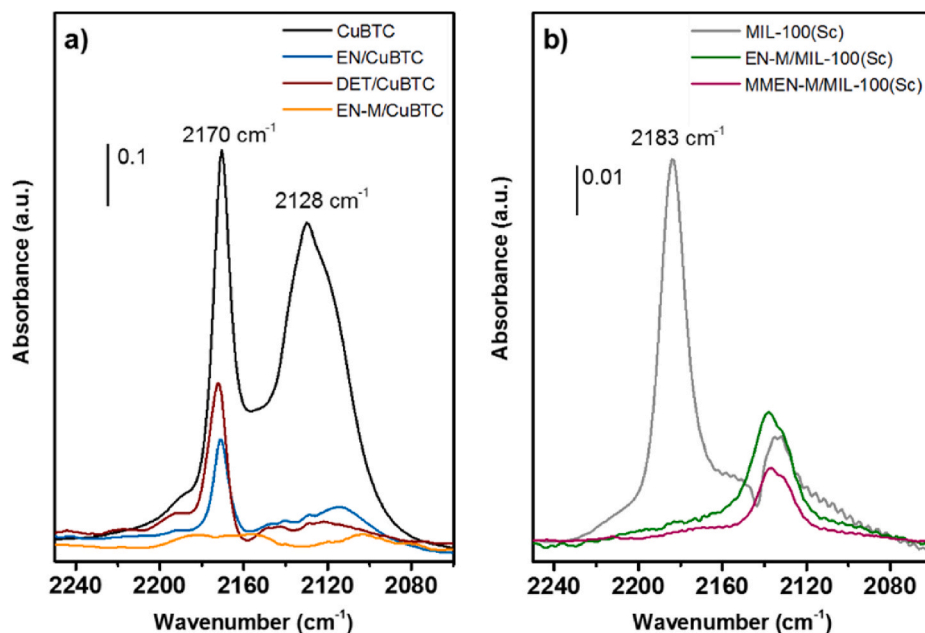


Fig. 4. FTIR spectra of CO adsorbed at 100 K on bare and amino-grafted a) CuBTC and b) MIL-100(Sc) samples. IR absorption bands in the 2240–2080 cm^{-1} region.

Table 2

Composition of the amino-grafted MOFs under study.

Sample	N ^c (mmol/g)	Cu ^d (mmol/g)
EN/CuBTC ^a	0.33	0.45
DET/CuBTC ^a	0.42	0.34
2DET/CuBTC ^a	0.58	0.31
EN-M/CuBTC ^b	1.20	0.29
EN-M/MIL-100(Sc) ^b	0.43	–
MMEN-M/MIL-100(Sc) ^b	0.30	–

Prepared by using the ^a Method B and ^b Method A. Determined by ^c Elemental analysis and ^d ICP-OES.

the method used. Modification by using the method A produces the total saturation of CUS, while partially functionalized MOF samples are obtained when applying method B.

3.2. Catalytic performance

The amino-grafted MOFs were tested in the synthesis of 2-amino-4H-chromenes **1**, from salicylaldehyde **2** and ethyl cyanoacetate **3**, under solvent-free conditions (Scheme 1). Firstly, for comparison, we explored the catalytic performance of the EN-grafted catalysts, at 323 K. It is important to remark that both supports, CuBTC and MIL-100(Sc), resulted totally inactive in this transformation even at high temperatures.

Fig. 5 shows conversion values of salicylaldehyde **2** to chromenes **1** vs time in the presence of amino-grafted catalysts. It can be observed that the highest conversion values to chromenes **1** (up to 90% after 2 h), as mixtures of the corresponding diastereoisomers **1a/1b** in approximately 2:1 ratio, are obtained when using EN-M/CuBTC, the non-porous sample presenting the superior amount of EN ligand anchored to CuBTC, as confirmed by FTIR and elemental analysis (%N: 1.20 mmol/g) (Fig. 5a). Considering that a unique $-\text{NH}_2$ function in EN ligand is coordinated to the corresponding metal center in CuBTC or MIL-100(Sc), as mentioned above, differences in the catalytic behaviour of EN-functionalized samples could be firstly attributed to the presence of available catalytic active sites, comprising free $-\text{NH}_2$ functions groups (0.60, 0.17 and 0.22 mmol/g for EN-M/CuBTC, EN/CuBTC and EN-M/MIL-100(Sc) respectively, Table 2). Regarding the porosity of the catalysts, EN/CuBTC and EN-M/MIL-100(Sc) samples present similar V_p ($0.23 \text{ cm}^3 \text{ g}^{-1}$), however

EN/CuBTC sample shows larger S_{BET} (546 vs $444 \text{ m}^2 \text{ g}^{-1}$), which could be behind the slightly higher conversion values obtained at the shortest reaction times when using this sample (Fig. 5a, Table 1). In the same context, EN-M/CuBTC and EN-M/MIL-100(Sc) catalysts are able to promote the reaction at lower reaction temperature; at 303 K, EN-M/CuBTC affords chromenes **1** in 91% of conversion, after 2 h of reaction time, with maintained selectivity towards chromene **1a**, as thermodynamically stable isomer (Fig. 5b). These results strongly suggest that free-amine functions in the investigated catalysts are the active specie promoting the reaction. In fact, EN/CuBTC sample with the lowest concentration of available amine groups resulted active in the chromene synthesis although reaching the lowest conversions (Fig. 5a) (see computational section).

We also checked the catalytic behaviour of MOFs modified with amine of different nature, MMEN-M/MIL-100(Sc) and DET/CuBTC (Fig. 5c and d). MMEN-M/MIL-100(Sc), having a similar concentration of N than DET/CuBTC, resulted active in the investigated transformation, at 323 K (Fig. 5c), yielding the corresponding chromenes **1** in 82%, after 3 h of reaction time, being the conversion values notably higher compared to those obtained for EN-M/MIL-100(Sc) (Fig. 5a). Enhanced catalytic performance observed for MMEN-M/MIL-100(Sc) sample could be attributed to the presence of free secondary amine ($-\text{NH}-\text{CH}_3$) groups with increased basicity in comparison with primary amine function in EN ligand. In the same context, we also tested the DET/CuBTC catalyst, affording chromenes **1** in 78% in only 30 min of reaction time (Fig. 5c). The same trend was observed when the reaction was carried out at 303 K observing the formation of chromenes **1** with lower conversion as expected (Fig. 5d). As mentioned above and considering that a unique $-\text{NH}_2$ function in ligands is coordinated to the corresponding metal center, the concentration of available amine groups as active catalytic sites calculated for EN/CuBTC and DET/CuBTC samples is 0.16 and 0.14 mmol/g, respectively, barely showing significant differences. These results indicate that the reaction is mainly controlled by the basicity of the samples. On the other hand, MMEN-M/MIL-100(Sc) shows superior S_{BET} (736 vs $615 \text{ m}^2 \text{ g}^{-1}$) and V_p (0.41 vs $0.24 \text{ cm}^3 \text{ g}^{-1}$) than DET/CuBTC catalyst, therefore, in this case, texture of the catalysts does not seem to influence the catalytic performance.

Furthermore, assuming the interaction of DET with Cu centers in CuBTC through one of the terminal $-\text{NH}_2$ groups [41], which are sterically less hindered, the secondary amine functions comprising the

central N, substituted with ethylene bridges, in DET should be responsible of the observed reactivity. It is important to note that although the primary and secondary amine functions are able to catalyze the reaction (Fig. 5) and that DET/CuBTC shows the presence of both groups, it seems reasonable to think that both cannot independently and simultaneously work. In fact, taken into account that both samples, MMEN-M/MIL-100 (Sc) and DET/CuBTC, show similar concentration of available secondary amine groups – 0.15 vs 0.14 mmol/g –, additional factors should be behind the extraordinarily high conversion values to chromenes **1** observed when using DET/CuBTC catalyst (see computational section). 2DET/CuBTC sample presenting increased N loading showed a catalytic behaviour quite similar to DET/CuBTC.

Taken into account all these results, although -NH_2 functions in EN-M/CuBTC or EN-M/MIL-100(Sc) are able to catalyze the reaction yielding the corresponding chromene derivatives, acting as individual active sites, the presence of CUS sites in EN/CuBTC or DET/CuBTC could suggest that both samples can operate as bifunctional catalysts, in which amine functions and free-metal centers could be responsible of the nucleophile and electrophile activations. This hypothesis is especially relevant when comparing the conversion values observed in the presence of EN-M/CuBTC and DET/CuBTC catalysts; while the reaction catalyzed by EN-M/CuBTC, with the highest concentration of amine groups, led to chromene **1** in 57% after 30 min of reaction time, notably superior conversion values (78%, 30 min) were observed in the presence of DET/CuBTC sample.

Additionally, in order to check that the amines are anchored to the metal center during the reaction, leaching test has been carried out in

the synthesis of chromene **1**, from salicylaldehyde **2** and ethyl cyanoacetate **3**, in the presence of DET/CuBTC catalyst, operating under the same experimental conditions at 323 K. After the first 15 min of the reaction time the catalyst was removed from the reaction mixture by filtering off and the resulting mixture was maintained at 323 K until completing 180 min. Chromenes **1** was obtained in 22% of conversion, then demonstrating that no leaching of DET is produced.

Reusability experiments were also carried out in the synthesis of chromenes **1** in the presence of DET/CuBTC catalyst, at 323 K. In this sense, it was observed that the conversion to **1** notably decreased during the first recycle to 36% after 3 h of reaction time. This fact could be firstly attributed to the interactions of amine centers in catalyst with acid hydrogens of chromenes **1**, but also it could be possible interactions between CN functions in **1** with CUS (see computational section). Although it is not the objective of this work, we also investigated the reusability of the catalyst in the Knoevenagel condensation between benzaldehyde (4 mmol) and malononitrile (4 mmol), at 303 K, under solvent-free conditions, affording the corresponding condensation product in almost quantitative yield during 3 consecutive cycles. The low conversion value to **1** obtained during the first recycle together these results suggest that the compounds **1** remain anchored to the amine functions in catalyst, through acid-base interactions, but also that the reusability of the catalyst depends on the nature of the products.

The influence of the catalyst amount was explored in the reaction by using 2DET/CuBTC sample, observing an increase in conversion values to **1** from 14% (catalyst: 25 mg) to 82% (catalyst: 50 mg), after only 15 min of reaction time. The same trend was also observed when using

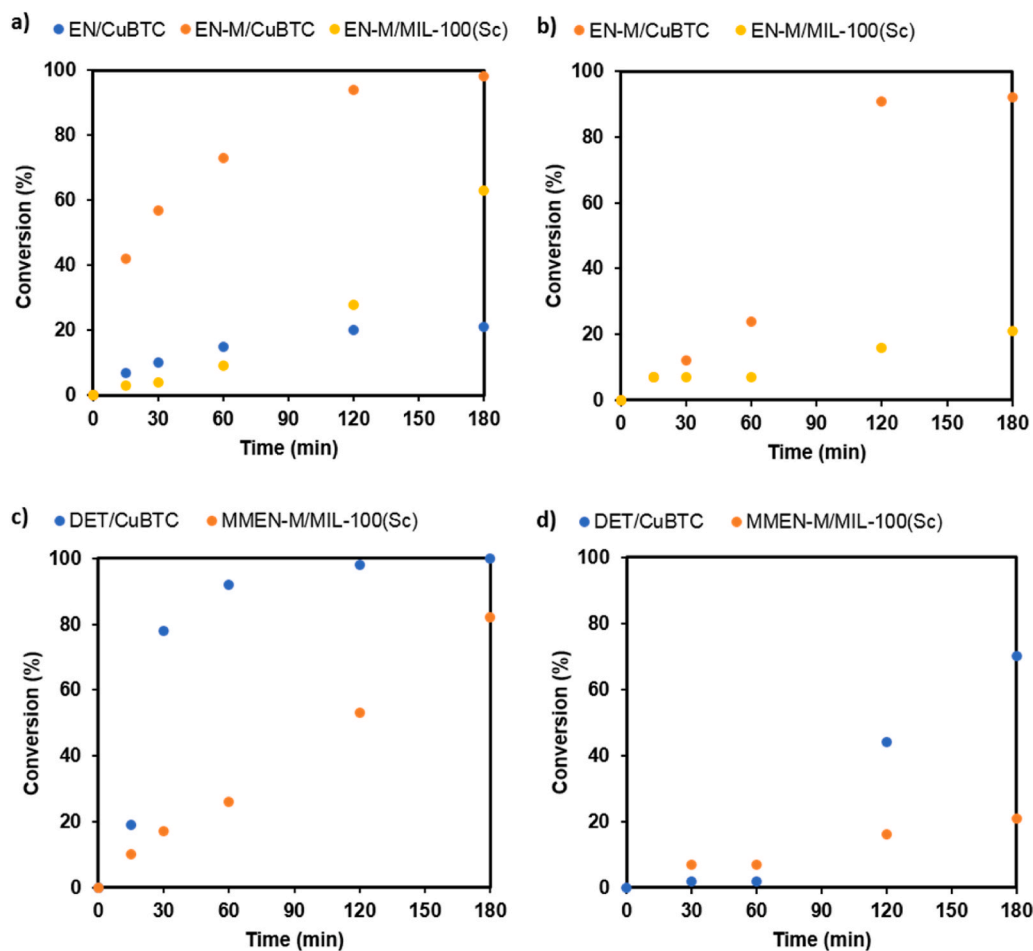


Fig. 5. Synthesis of 2-amino-4H-chromenes **1**, from salicylaldehyde **2** and ethyl cyanoacetate **3**, under solvent-free conditions, catalyzed by a) amino-grafted CuBTC and MIL-100(Sc) at 323 K, b) EN-M/CuBTC EN-M/MIL-100(Sc) at 303 K, c) DET/CuBTC and MMEN-M/MIL-100(Sc) at 323 K and d) DET/CuBTC and MMEN-M/MIL-100(Sc) at 303 K.

other less active catalyst such as MMEN/MIL-100(Sc), affording chromenes **1** in 96% (50 mg of the catalyst) of conversion, after 3 h of reaction time, compared to 82% (Figs. 5c and 25 mg of the catalyst).

The scope of the methodology was investigated by using different substituted salicylaldehydes **4** but also other cyano compound such as malononitrile **5** (Table 3, Scheme 2). In all the cases, chromenes **7** were selectively synthesized in good-to-excellent yields in the presence of amino-grafted investigated MOFs. Particularly chromene **6** ($R^1 = H$ and $R^2 = CN$) was obtained in quantitatively yield in the presence of EN-M/MIL-100(Sc) in only 15 min of reaction time under mild condition (303 K) (Table 3, entry 2). Even when using EN/CuBTC, the sample with minor concentration of $-NH_2$ functions, the corresponding chromene derivative was obtained in almost 90%, due to the strong reactivity of malononitrile **5** (Table 3 entry 1). Influence of substitution at position 5- in the aromatic ring of salicylaldehydes **4** was investigated in the presence of the most active catalyst, DET/CuBTC, obtaining, in all the cases, the corresponding chromene derivatives **7** in good-to-excellent conversions (**7a/7b** 2:1 ratio) (Table 3, entries 3–6). The observed reactivity order is as follows: $H \approx NO_2 > Br > OMe$. It seems then that the presence of electrowithdrawing substituents at position 5- in salicylaldehyde favours the reaction. Based on our previous studies concerning the use of amino-grafted mesoporous silicas as catalysts involved in the synthesis of coumarins from salicylaldehyde and ethyl acetoacetate [56], the substitution in salicylaldehyde affects not only to the electrophilicity of $-CHO$ functions but also to the acidity of the *para* $-OH$ group. Although the presence of electrodonating substituents on aromatic ring should favor the first step of the reaction comprising the aldolic reaction between reagents, electrowithdrawing substituents at position 5- produces an increment of acidity of phenol groups probably driving the heterocyclization step, since when R^1 is a NO_2 group the reaction takes place even at lower temperatures affording mixtures of chromenes **7** with increased selectivity to **7a** (**7a/7b** 3:1 ratio).

Interestingly, ethyl 2-amino-6-bromo-4-(1-cyano-2-ethoxy-2-oxoethyl)-4H-chromene-3-carboxylate **7** (**HA 14-1**), where R^1 is Br and R^2 is CO_2Et , as an agonist for Bcl-2 protein [26,27] which is expressed in most types of cancer, can be efficiently synthesized, as a diastereomeric mixture in a 2:1 ratio, in 90% of conversion after 3 h of reaction time (Table 3, entry 4).

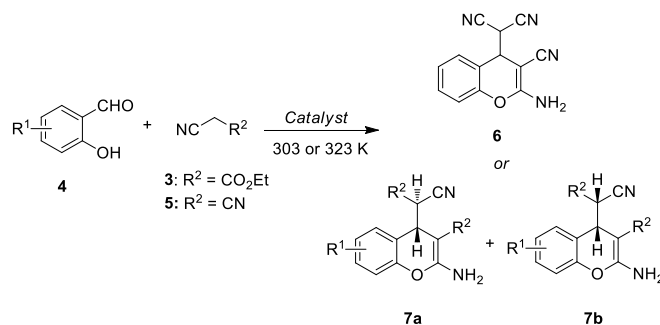
Summarizing, Table 4 shows the results reported for the chromene synthesis from salicylaldehydes **2** and **4** ($R^1 = Br$) and ethyl cyanoacetate **3** (Schemes 1 and 2). As it can be seen, the catalysts reported herein, particularly DET/CuBTC is found to catalyze selectively the synthesis of 2-amino-4H-chromenes **1** and **7** in excellent yields, after short reaction times, under solvent-free and mild reaction conditions, by using the smallest catalyst amount (25 mg), starting from higher reactant amounts.

Table 3

Synthesis of chromenes **1**, **6** and **7** from salicylaldehydes and cyano compounds catalyzed by amino-grafted CuBTC.

Entry	Catalyst	R^1	R^2	Temperature (K)	Time (min)	Conversion to 6 or 7 (%)
1	EN/CuBTC	H	CN	303	15	87
2	EN-M/MIL-100(Sc)	H	CN	303	15	99
3	DET/CuBTC	H	CO_2Et	323	60 (120)	92 (98)
4	DET/CuBTC	Br	CO_2Et	323	180	87
5	DET/CuBTC	OMe	CO_2Et	323	180	52
6	DET/CuBTC	NO_2	CO_2Et	323	60 (120)	84 (99)

Reaction conditions: Salicylaldehyde (2 mmol), cyano compound (4 mmol), catalyst (25 mg).



Scheme 2. Synthesis of chromenes **6–8** from salicylaldehydes and cyano compounds, at 303 or 323 K, under solvent-free conditions.

3.3. Computational study

In order to rationalize the obtained results, the aldolization reaction, as rate-limiting step in the synthesis of chromenes **1**, catalyzed by amino-grafted CuBTC, was theoretically analyzed. Considering previous studies concerning the Friedländer reaction catalyzed by CuBTC [15], reduced models representing CuBTC but also functionalized with the corresponding amines were selected (Fig. 6). In these models it was observed a slightly increment of the Cu–Cu distance in amino-grafting catalysts regarding the bare CuBTC -2.4746 \AA (Figs. 6a), 2.5575 \AA (Figure 6b), 2.5570 \AA (Fig. 6c) –while the Cu– NH_2 distance maintained in approximately 2.146 \AA .

Since the reaction is catalyzed by basic species, as experimentally demonstrated, the transition structures for the uncatalyzed reaction or in the presence of bare CuBTC have not been investigated. Having in mind our previous studies analyzing amino-grafted mesoporous silicas [56,57], we explored the aldolization reaction between ethyl cyanoacetate **3** and salicylaldehyde **2**, in which compound **3** is able to donate a proton to amine functions in catalyst, through *keto* or *enol* forms, this proton subsequently activating the carbonyl acceptor, the $-CHO$ group in compound **2**. Comparing both optimized transition structures when using the reduced model b or c (Fig. 6) simulating EN/CuBTC (Figs. 7a and 8a) and DET/CuBTC catalysts (Figs. 7b and 8b), respectively, it can be observed, in both cases, more advanced transition structures when ethyl cyanoacetate **3** is involved as enol form (Fig. 8) as confirmed by computed C–C bond forming distances (2.1761 vs 2.5499 for EN/CuBTC catalyst and 2.1274 vs 2.6186 for DET/CuBTC catalyst). In the same context, the formation of $TS-EN_B$ (*enol* form, Fig. 8a) requires lower free energy barrier in 14.10 kcal/mol than $TS-EN_A$ (*keto* form, Fig. 7a) observing the same trend for $TS-DET_B$ – 16.61 kcal/mol more stable than $TS-DET_A$ (Fig. 7a) –; this diminution is probably due to the stabilization of the TS by hydrogen bondings involving $-NH_2$ functions. Both observations suggested that ethyl cyanoacetate **3** reacts with salicylaldehyde **2** through its enol form (Fig. 8). However, the small free energy differences do not justify the catalytic behaviour observed for both EN/CuBTC and DET/CuBTC catalysts, probably indicating that additional factors could determine the catalytic performance.

As both catalysts, EN/CuBTC and DET/CuBTC, showed only a few Cu sites grafted with the corresponding amines, the computational and experimental results seem to suggest that amine functions and metal CUS in these catalysts could act in cooperation. To investigate this possibility we firstly analyzed the interaction modes of reactants with uncoordinated Cu centers using the reduced model showed in Fig. 6a. As it can be observed from Table 5, the most stable optimized structures comprise the interaction between ethyl cyanoacetate **3** through lone pairs from $C=O$ or $C\equiv N$ functions with Cu centers showing slight free energy deviation.

In order to probe our hypothesis, we select an extended cluster simulating CuBTC in which one Cu atom was functionalized with an amine group of an EN ligand whereas the closest Cu atom was

Table 4
Heterogeneous catalysts active in the chromene synthesis from salicylaldehydes and ethyl cyanoacetate.

Catalysts	R ¹	Reaction conditions	T (K)	Catalyst amount (g)	Time (h)	Conversion (%)	Ref.
Molecular sieve 3A	Br	Salicylaldehyde (0.010 mol), ethyl cyanoacetate (0.022 mol), EtOH(30 ml)	r.t.	3	14	86	31
SnMgAl-1	H	Salicylaldehyde (1 mmol), ethyl cyanoacetate (2 mmol)	333	0.05	1	94	33
MgAl	H				24	88	
Zr(KPO ₄) ₂	H				2	88	34
	Br				3	97	
Na/NbMCF	H	Salicylaldehyde (2 mmol), ethyl cyanoacetate (4 mmol)	298	0.05	4	93	36
	Br				5	72	
Li/NbMCF	H				3	97	37
PET/CAL 30:70	H	Salicylaldehyde (2 mmol) and ethyl cyanoacetate (4 mmol)	323	0.05	2	92	38
	Br				2	99	
HT30-SBA	Br			0.166	4	92	39
HTHA composites	H			0.05	2	93	40
DET/CuBTC	H			0.025	1	93	This work
	Br			0.025	2	99	This work

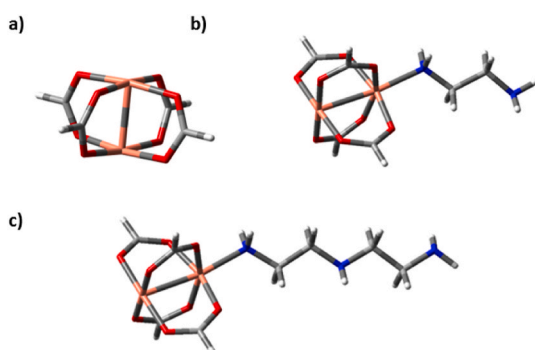


Fig. 6. Reduced model simulating a) bare CuBTC, b) EN or EN-M/CuBTC and c) DET/CuBTC.

interacting with ethyl cyanoacetate **3** through either C=O (Fig. 9a) or C≡N groups (Fig. 9b) as the most stable interactions. We used the most reduced models functionalized with EN molecules in order to reduce the computational cost. Slightly differences between both TS were observed concerning to C–C distances (2.5868 vs 2.5418 Å for TS-EN(Cu–CO) and TS-EN(Cu–C≡N) respectively) and free-energy barrier, TS-EN(Cu–C≡N) being 5 kcal/mol more stable TS-EN(Cu–CO). These features make us to suspect that TS-EN(Cu–C≡N) is probably the operative TS. Considering these results and those previously obtained, the computed free energy value for TS-EN(Cu–CO) was approximately 10 kcal/mol lower compared to TS-EN_A (Fig. 7a) showing similar interaction modes with the exception of –OH function now forming a strong

hydrogen bond with the CuBTC cluster. However, small free energy barrier, less than 1 kcal/mol, was observed when comparing TS-EN_B (Fig. 7b) and TS-EN(Cu–C≡N) (Fig. 9b), TS-EN_B being a more advanced transition structure as demonstrated by C–C bond forming distances (2.1761 vs 2.5418 Å for TS-EN_B and TS-EN(Cu–C≡N), respectively). Note that EN-M/CuBTC catalyst did not contain unsaturated Cu centers and, therefore, presented a superior concentration of free –NH₂ functions and, therefore, presented a superior concentration of free –NH₂ functions able to promote the reaction, probably acting as individual catalytic sites through TS-EN_B (Fig. 8a), being this feature behind of its enhanced catalytic performance (Fig. 5a). In the case of EN/CuBTC catalyst showing a low %Cu centers functionalized with amine groups, as experimentally demonstrated, the most probable transition structure could be TS-EN(Cu–C≡N), acting as bifunctional catalyst, in which the free amine function in EN could be able to abstract a proton of **3**, through its enol form, this proton activating the carbonyl acceptor in salicylaldehyde **2**, whereas –CN function is interacting with neighbouring unsaturated Cu centers. Thus, low conversion values of **2** obtained in the presence of EN/CuBTC sample could be attributed to a lower concentration of –NH₂ active centers in this catalyst but also to the interaction of ethyl cyanoacetate **3** through C=O or C≡N functional groups with bare Cu centers, inhibiting the reaction with the time as experimentally observed (Fig. 5a).

Considering these results, DET/CuBTC could act as bifunctional catalyst where ethyl cyanoacetate **3** would donate its acidic proton to secondary amine groups whereas simultaneously interacting with neighbouring CUS through –C≡N functions, –NH– groups in each amine group participating in the activation of carbonyl acceptor in salicylaldehyde **2** as shown in TS-DET_B (Fig. 8b). The presence of additional –NH₂ functions in this case should stabilize the corresponding TS,

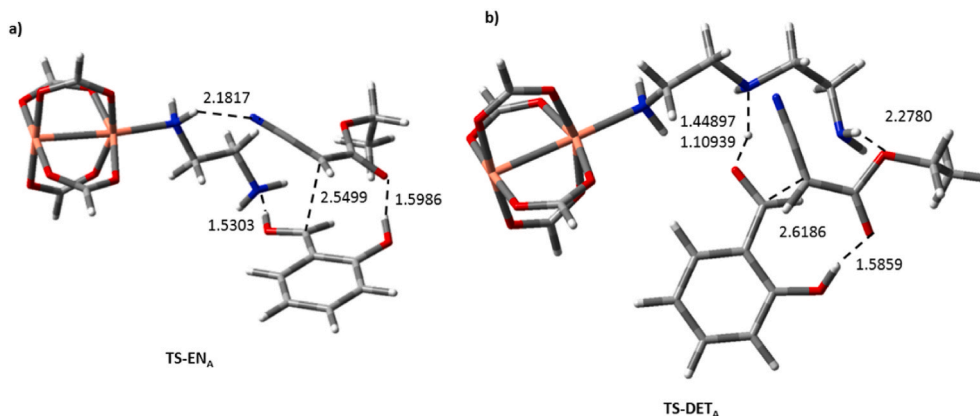


Fig. 7. Optimized transition structures for the aldolization reaction between salicylaldehyde **2** and ethyl cyanoacetate **3** (*keto* form) catalyzed by a) EN/CuBTC and b) DET/CuBTC. Relevant distances are expressed in Å.

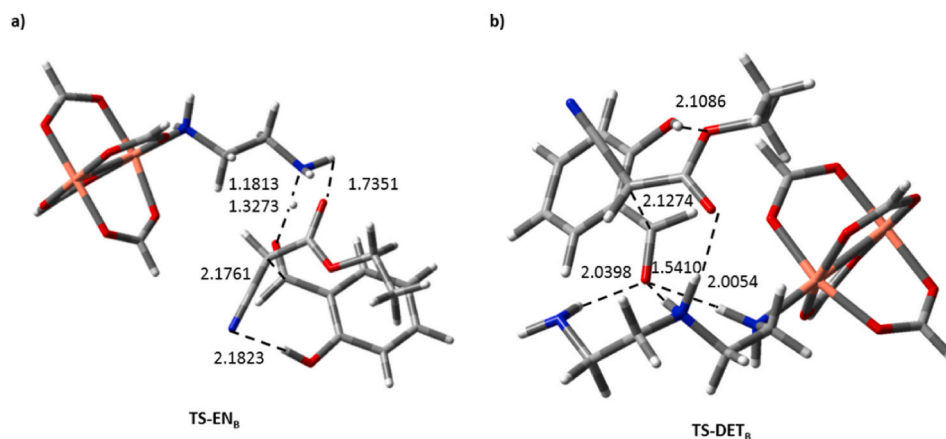


Fig. 8. Optimized transition structures for the aldolization reaction between salicylaldehyde **2** and ethyl cyanoacetate **3** (*enol* form) catalyzed by a) EN/CuBTC and b) DET/CuBTC. Relevant distances are expressed in Å.

Table 5

Interactions of the reagents with metal centers in remaining metal CUS sites for amino-grafted CuBTC.

Interactions	Compound	ΔG (Kcal/mol)
Model a (Cu...O=C)	2	5.92
Model a (Cu...O-H)	2	9.04
Model a (Cu...O=C-O)	3	-1.08
Model a (Cu...N≡C)	3	-0.48
Model a (Cu...O-C=O)	3	3.21

diminishing the free energy barrier as observed in TS-DET_B (Fig. 8B).

4. Conclusions

We report herein for the first time a novel family of amino-grafted MOFs able to catalyze the synthesis of 2-amino-4*H*-chromenes **1**, from salicylaldehydes and cyano compounds, under solvent-free and mild conditions. The catalysts were easily prepared by reacting the corresponding metal-organic network with organic amines, the functionalization of selected MOFs strongly depending of the used method. Our results demonstrate that the catalytic performance is mainly conditioned by the type and concentration of basic sites. It is supported by the catalytic behaviour of EN-M/CuBTC and EN/CuBTC catalysts, being EN-M/CuBTC the most efficient catalyst, which shows high concentration of basic catalytic sites coordinating each metal center in CuBTC. In the

same context, the presence of secondary amine functions in DET/CuBTC or MMEN-M/MIL-100(Sc) samples favors the reaction. Since the porosity of the samples barely shows influence in catalytic performance, the reaction is then mainly controlled by the basicity of the samples.

Our experimental and theoretical results strongly suggest that available amine groups in EN functionalized catalysts can act either as individual catalytic sites or in cooperation with the nearest CUS in samples partially functionalized; such is the case of EN-M/CuBTC and EN/CuBTC catalysts, respectively. In the case of using DET/CuBTC, the additional stabilization of the corresponding transition structure for the aldolization reaction, as the first elementary step in the formation of chromenes, involving strong hydrogen bonds NH...O=C and responsible of electrophile activation, could be behind of its superior catalytic performance.

CRediT authorship contribution statement

D. González-Rodal: Validation, Investigation, Writing – original draft. **G. Turnes Palomino:** Conceptualization, Methodology, Writing – review & editing, Supervision. **C. Palomino Cabello:** Validation, Investigation, Writing – original draft. **E. Pérez-Mayoral:** Conceptualization, Methodology, Writing – review & editing, Supervision, Funding acquisition.

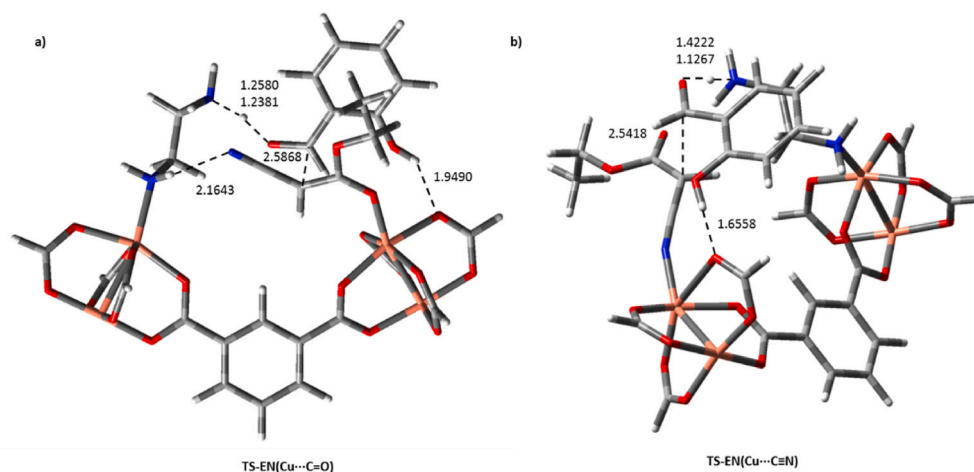


Fig. 9. Optimized transition structure for the aldolization reaction between salicylaldehyde **2** and ethyl cyanoacetate **3** catalyzed by EN/CuBTC. a) Cu...O=C and b) Cu...N≡C interactions. Relevant distances are expressed in Å.

Declaration of competing interest

The authors declare that they have no known competing financial interests or personal relationships that could have appeared to influence the work reported in this paper.

Acknowledgments

This work has been supported by Spanish Ministry (Ministerio de Economía y Competitividad, CTM2014-56668-R project).

Appendix A. Supplementary data

Supplementary data to this article can be found online at <https://doi.org/10.1016/j.micromeso.2021.111232>.

References

- [1] D. Farrusseng, S. Aguado, C. Pinel, Metal-organic frameworks: opportunities for catalysis, *Angew. Chem. Int. Ed.* 48 (2009) 7502–7513, <https://doi.org/10.1002/anie.200806063>.
- [2] R.E. Morris, J. Čejka, Exploiting chemically selective weakness in solids as a route to new porous materials, *Nat. Chem.* 7 (2015) 381–388, <https://doi.org/10.1038/nchem.2222>.
- [3] M. Almäši, V. Zelenák, M. Opanasenko, J. Čejka, A novel nickel metal-organic framework with fluorite-like structure: gas adsorption properties and catalytic activity in Knoevenagel condensation, *Dalton Trans.* 43 (2014) 3730–3738, <https://doi.org/10.1039/c3dt52698d>.
- [4] P.Z. Moghadam, A. Li, S.B. Wiggan, A. Tao, A.G.P. Maloney, P.A. Wood, S.C. Ward, D. Fairen-Jimenez, Development of a cambridge structural database subset: a collection of Metal-Organic frameworks for past, present, and future, *Chem. Mater.* 29 (2017) 2618–2625, <https://doi.org/10.1021/acs.chemmater.7b00441>.
- [5] J. Liang, Z. Liang, R. Zou, Y. Zhao, Heterogeneous catalysis in zeolites, mesoporous silica, and metal-organic frameworks, *Adv. Mater.* 29 (2017), 1701139, <https://doi.org/10.1002/adma.201701139>.
- [6] A. Dhakshinamoorthy, A.M. Asiric, H. Garcia, Catalysis by metal-organic frameworks in water, *Chem. Commun.* 50 (2014) 12800–12814, <https://doi.org/10.1039/c4cc04387a>.
- [7] H. He, J.A. Perman, G. Zhu, S. Ma, Metal-organic frameworks for CO₂ chemical transformations, *Small* 12 (2016) 6309–6324, <https://doi.org/10.1002/smll.201602711>.
- [8] A. Rossin, G. Tuci, L. Luconi, G. Giambastiani, Metal-organic frameworks as heterogeneous catalysts in hydrogen production from lightweight inorganic hydrides, *ACS Catal.* 7 (2017) 5035–5045, <https://doi.org/10.1021/acscatal.7b01495>.
- [9] Y.-B. Huang, J. Liang, X.-S. Wang, R. Cao, Multifunctional metal-organic framework catalysts: synergistic catalysis and tandem reactions, *Chem. Soc. Rev.* 46 (2017) 126–157, <https://doi.org/10.1039/c6cs00250a>.
- [10] M. Opanasenko, Catalytic behavior of metal-organic frameworks and zeolites: rationalization and comparative analysis, *Catal. Today* 243 (2015) 2–9, <https://doi.org/10.1016/j.cattod.2014.06.040>.
- [11] A. Dhakshinamoorthy, M. Opanasenko, J. Čejka, H. Garcia, Metal organic frameworks as heterogeneous catalysts for the production of fine chemicals, *CATTECH Mag. Catal. Sci. Technol. Innovation* 3 (2013) 2509–2540, <https://doi.org/10.1039/c3cy00350g>.
- [12] A. Dhakshinamoorthy, M. Opanasenko, J. Čejka, H. Garcia, Metal organic frameworks as solid catalysts in condensation reactions of carbonyl groups, *Adv. Synth. Catal.* 355 (2013) 247–268, <https://doi.org/10.1002/adsc.201200618>.
- [13] E. Pérez-Mayoral, J. Čejka, [Cu₃(BTC)₂]: a metal-organic framework catalyst for the friedländer reaction, *ChemCatChem* 3 (2011) 157–159, <https://doi.org/10.1002/cctc.201000201>.
- [14] E. Pérez-Mayoral, Z. Musilová, B. Gil, B. Marszałek, M. Polozij, P. Nachtigall, J. Čejka, Synthesis of quinolines via Friedländer reaction catalyzed by CuBTC metal-organic-framework, *Dalton Trans.* 41 (2012) 4036–4044, <https://doi.org/10.1039/C2DT11978A>.
- [15] M. Polozij, E. Pérez-Mayoral, J. Čejka, J. Hermann, P. Nachtigall, Theoretical investigation of the Friedländer reaction catalyzed by CuBTC: concerted effect of the adjacent Cu²⁺ sites, *Catal. Today* 204 (2013) 101–107, <https://doi.org/10.1016/j.cattod.2012.08.025>.
- [16] M. Godino-Ojer, A.J. López-Peinado, F.J. Maldonado-Hódar, E. Pérez-Mayoral, Highly efficient and selective catalytic synthesis of quinolines involving transition-metal-doped carbon aerogels, *ChemCatChem* 9 (2017) 1422–1428, <https://doi.org/10.1002/cctc.201601657>.
- [17] M. Godino-Ojer, M. Shamzhy, J. Čejka, E. Pérez-Mayoral, Basolites: a type of Metal Organic Frameworks highly efficient in the one-pot synthesis of quinoxalines from α -hydroxy ketones under aerobic conditions, *Catal. Today* 345 (2019), <https://doi.org/10.1016/j.cattod.2019.08.002>.
- [18] S. Rostamnia, A. Morsali, Size-controlled crystalline basic nanoporous coordination polymers of Zn₄O(H₂N-TA)₃: catalytically study of IRMOF-3 as a suitable and green catalyst for selective synthesis of tetrahydro-chromenes, *Inorg. Chim. Acta.* 411 (2014) 113–118, <https://doi.org/10.1016/j.ica.2013.12.002>.
- [19] S. Rostamnia, M. Jafari, Metal-organic framework of amine-MIL-53(Al) as active and reusable liquid-phase reaction inductor for multicomponent condensation of Ugi-type reactions, *Appl. Organomet. Chem.* (2016) 1–6, <https://doi.org/10.1002/aoc.3584>.
- [20] S. Rostamnia, H. Alamgholiloo, M. Jafari, Ethylene diamine post-synthesis modification on open metal site Cr-MOF to access efficient bifunctional catalyst for the Hantzsch condensation reaction, *Appl. Organomet. Chem.* (2018), e4370, <https://doi.org/10.1002/aoc.4370>.
- [21] S. Rostamnia, H. Alamgholiloo, X. Liu, Pd-grafted open metal site copper-benzene-1,4-dicarboxylate metal organic frameworks (Cu-BDC MOF's) as promising interfacial catalysts for sustainable Suzuki coupling, *J. Colloid Interface Sci.* 469 (2016) 310–317, <https://doi.org/10.1016/j.jcis.2016.02.021>.
- [22] H. Alamgholiloo, S. Rostamnia, A. Hassankhani, X. Liu, A. Eftekhari, A. Hasanzadeh, K. Zhang, H. Karimi-Maleh, S. Khaksar, R.S. Varma, M. Shokouhimehr, Formation and stabilization of colloidal ultra-small palladium nanoparticles on diamine-modified Cr-MIL-101: synergistic boost to hydrogen production from formic acid, *J. Colloid Interface Sci.* 567 (2020) 126–135, <https://doi.org/10.1016/j.jcis.2020.01.087>.
- [23] G.P. Ellis, *The Chemistry of Heterocyclic Compounds: Chromenes, Chromanones, and Chromones*, John Wiley & Sons, Inc., New York, 1977.
- [24] W.P. Smith, L.S. Sollis, D.P. Howes, C.P. Cherry, D.I. Starkey, N.K. Cobley, Dihydropyranocarboxamides related to zanamivir: a new series of inhibitors of influenza virus sialidases. 1. Discovery, synthesis, biological activity and structure-activity relationships of 4-guanidino- and 4-amino-4H-pyran-6-carboxamides, *J. Med. Chem.* 29 (1998) 787–797, <https://doi.org/10.1021/jm970374b>.
- [25] A. Zonouzi, A. Mirzazadeh, M. Safavi, K.S. OArdestani, S. Emami, A. Foroumand, 2-amino-4-(nitroalkyl)-4H-chromene-3-carbonitriles as new cytotoxic agents, *Int. J. Psychol. Res.* 12 (2013) 679–685, <https://doi.org/10.1021/jm970374b>.
- [26] W. Kemnitzer, J. Drewe, S. Jiang, H. Zhang, J. Zhao, C. Crogan-Grundy, L. Xu, S. Lamothe, H. Gourdeau, R. Denis, B. Tseng, S. Kasibhatla, S. Cai, Discovery of 4-aryl-4H-chromenes as a new series of apoptosis inducers using a cell and caspase-based high throughput screening assay. 3. Structure-activity relationships of fused rings at the 7,8-positions, *J. Med. Chem.* 50 (2003) 2858–2864, <https://doi.org/10.1021/jm070216c>.
- [27] H.K. Keerthy, M. Garg, C.D. Mohan, V. Madan, D. Kanojia, R. Shobith, S. Nanjundaswamy, D.J. Mason, A. Bender, B.K.S. Rangappa, H.P. Kowffler, Synthesis and characterization of novel 2-amino-chromene-nitriles that target bcl-2 in acute myeloid leukemia cell lines, *PLoS One* 9 (2014) 107–118, <https://doi.org/10.1371/journal.pone.0107118>.
- [28] S.R. Kesten, T.G. Heffner, S.J. Johnson, T.A. Pugsley, J.L. Wright, D.L. Wise, Design, synthesis and evaluation of chromen-2-ones as potent and selective human dopamine D₄ antagonists, *J. Med. Chem.* 42 (1999) 3718–3725, <https://doi.org/10.1021/jm990266k>.
- [29] C. Bruhlmann, F. Ooms, P. Carrupt, B. Testa, M. Catto, F. Leonetti, C. Altomare, A. Cartti, Coumarins derivatives as dual inhibitors of acetylcholinesterase and monoamine oxidase, *J. Med. Chem.* 44 (2001) 3195–3198, <https://doi.org/10.1021/jm010894d>.
- [30] M.A. Kulkarni, K.S. Pandit, U.V. Desai, U.P. Lad, P.P. Wadgaonkar, Diethylamine: a smart organocatalyst in eco-safe and diastereoselective synthesis of medicinally privileged 2-amino-4H-chromenes at ambient temperature, *Compt. Rendus Chem.* 16 (2013) 689–695, <https://doi.org/10.1016/j.crci.2013.02.016>.
- [31] N. Yu, J.M. Aramini, M.W. Germann, Z. Huang, Reactions of salicylaldehydes with alkyl cyanoacetates on the surface of solid catalysts: syntheses of 4H-chromene derivatives, *Tetrahedron Lett.* 41 (2000) 6993–6996, [https://doi.org/10.1016/S0040-4039\(00\)01195-3](https://doi.org/10.1016/S0040-4039(00)01195-3).
- [32] J.S. Yadav, B.V. Subba Reddy, M.K. Gupta, I. Prathap, S.K. Pandey, Amberlyst A-21: an efficient, cost-effective and recyclable catalyst for the synthesis of unsubstituted 4h-chromenes, *Catal. Commun.* 8 (2007) 2208–2211, <https://doi.org/10.1016/j.catcom.2007.05.005>.
- [33] U. Constantino, M. Curinir, F. Montanari, M. Nocchetti, O. Rosati, Hydrotalcite-like compounds as heterogeneous catalysts in liquid phase organic synthesis. II. Preparation of 4H-chromenes promoted by hydrotalcite doped with hydrous tin (IV) oxide, *Microporous Mesoporous Mater.* 107 (2008) 16–22, <https://doi.org/10.1016/j.micromeso.2007.05.010>.
- [34] M. Curini, F. Epifano, S. Chimichi, F. Montanari, M. Nocchetti, O. Rosati, Potassium exchanged layered zirconium phosphate as catalyst in the preparation of 4H-chromenes, *Tetrahedron Lett.* 46 (2005) 3497–3499, <https://doi.org/10.1016/j.tetlet.2005.03.075>.
- [35] J. Velasco, E. Pérez-Mayoral, V. Calvino-Casilda, A.J. López-Peinado, M. A. Bañares, E. Soriano, Imidazolium sulfonates as environmental-friendly catalytic systems for the synthesis of biologically active 2-amino-4H-chromenes: mechanistic insights, *J. Phys. Chem. B* 119 (2015) 12042–12049, <https://doi.org/10.1021/acs.jpcc.5b06275>.
- [36] A. Smuszkievicz, J. López-Sanz, I. Sobczak, M. Ziolk, R.M. Martín-Aranda, E. Soriano, E. Pérez-Mayoral, Mesoporous niobiosilicate NbMCF modified with alkali metals in the synthesis of chromene derivatives, *Catal. Today* 277 (2016) 133–142, <https://doi.org/10.1016/j.cattod.2016.02.042>.
- [37] A. Smuszkievicz, J. López-Sanz, I. Sobczak, R.M. Martín-Aranda, M. Ziolk, E. Pérez-Mayoral, Tantalum vs Niobium MCF nanocatalysts in the green synthesis of chromene derivatives, *Catal. Today* 325 (2019) 47–52, <https://doi.org/10.1016/j.cattod.2018.06.038>.
- [38] D. González-Rodal, J. Przepiórski, A.J. López Peinado, E. Pérez-Mayoral, Basic-carbon nanocatalysts in the efficient synthesis of chromene derivatives. Valorization of both PET residues and mineral sources, *Chem. Eng. J.* 382 (2020), 122795, <https://doi.org/10.1016/j.cej.2019.122795>.

- [39] F.D. Velazquez-Herrera, D. Gonzalez-Rodal, G. Fetter, E. Pérez-Mayoral, Enhanced catalytic performance of highly mesoporous hydrotalcite/SBA-15 composites involved in chromene multicomponent synthesis, *Microporous Mesoporous Mater.* 309 (2020), 110569, <https://doi.org/10.1016/j.micromeso.2020.110569>.
- [40] F.D. Velazquez-Herrera, D. Gonzalez-Rodal, G. Fetter, E. Pérez-Mayoral, Towards highly efficient hydrotalcite/hydroxyapatite composites as novel catalysts involved in eco-synthesis of chromene derivatives, *Appl. Clay Sci.* 198 (2020), 105833, <https://doi.org/10.1016/j.clay.2020.105833>.
- [41] Y.K. Hwang, D.Y. Hong, J.S. Chang, S.H. Jung, Y.K. Seo, J. Kim, A. Vimont, M. Daturi, C. Serre, G. Férey, Amine grafting on coordinatively unsaturated metal centers of MOFs: consequences for catalysis and metal encapsulation, *Angew. Chem. Int. Ed.* 47 (2008) 4144–4148, <https://doi.org/10.1002/anie.200705998>.
- [42] C. Palomino Cabello, P. Rumori, G. Turnes Palomino, Carbon dioxide adsorption on MIL-100(M) (M = Cr, V, Sc) metal-organic frameworks: IR spectroscopic and thermodynamic studies, *Micropor. Mesopor. Mat.* 234–239 (2014) 190, <https://doi.org/10.1016/j.micromeso.2014.02.015>.
- [43] Y.T. Li, K.H. Cui, J. Li, J.Q. Zhu, X. Wang, Y.Q. Tian, The giant pore metal-organic frameworks of scandium carboxylate with MIL-100 and MIL-101 structures, *Chin. J. Inorg. Chem.* 27 (2011) 951–956.
- [44] A. Das, M. Choucair, P.D. Southon, J.A. Mason, M. Zhao, C.J. Kepert, A.T. Harris, D.M. D'Alessandro, Application of the piperazine-grafted CuBTri metal-organic framework in postcombustion carbon dioxide capture, *Microporous Mesoporous Mater.* 174 (2013) 74–80, <https://doi.org/10.1016/j.micromeso.2013.02.036>.
- [45] M.J. Frisch, G.W. Trucks, H.B. Schlegel, G.E. Scuseria, M.A. Robb, J.R. Cheeseman, G. Scalmani, V. Barone, B. Mennucci, G.A. Petersson, H. Nakatsuji, M. Caricato, X. Li, H.P. Hratchian, A.F. Izmaylov, J. Bloino, G. Zheng, J.L. Sonnenberg, M. Hada, M. Ehara, K. Toyota, R. Fukuda, J. Hasegawa, M. Ishida, T. Nakajima, Y. Honda, O. Kitao, H. Nakai, T. Vreven, J.A. Montgomery Jr., J.E. Peralta, F. Ogliaro, M. Bearpark, J.J. Heyd, E. Brothers, K.N. Kudin, V.N. Staroverov, R. Kobayashi, J. Normand, K. Raghavachari, A. Rendell, J.C. Burant, S.S. Iyengar, J. Tomasi, M. Cossi, N. Rega, J.M. Millam, M. Klene, J.E. Knox, J.B. Cross, V. Bakken, C. Adamo, J. Jaramillo, R. Gomperts, R.E. Stratmann, O. Yazyev, A.J. Austin, R. Cammi, C. Pomelli, J.W. Ochterski, R.L. Martin, K. Morokuma, V.G. Zakrzewski, G.A. Voth, P. Salvador, J.J. Dannenberg, S. Dapprich, A.D. Daniels, Ö. Farkas, J. B. Foresman, J.V. Ortiz, J. Cioslowski, D.J. Fox, *Gaussian 09, Revision B.1*, Gaussian, Inc., Wallingford CT, 2009.
- [46] A.D. Becke, Density-functional thermochemistry. III. The role of exact exchange, *J. Chem. Phys.* 98 (1993) 5648–5652, <https://doi.org/10.1063/1.464913>.
- [47] C. Lee, W. Yang, R.G. Parr, Development of the Colle-Salvetti correlation-energy formula into a functional of the electron density, *Phys. Rev. B* 37 (1988) 785–789, <https://doi.org/10.1103/PhysRevB.37.785>.
- [48] N.R. Dhupal, M.P. Singh, J.A. Anderson, J. Kiefer, H.J. Kim, Molecular interactions of a Cu-based Metal–Organic framework with a confined imidazolium-based ionic liquid: a combined density functional theory and experimental vibrational spectroscopy study, *J. Phys. Chem. C* 120 (2016) 3295–3304, <https://doi.org/10.1021/acs.jpcc.5b10123>.
- [49] C. Gonzalez, H.B. Schlegel, Reaction path following in mass-weighted internal coordinates, *J. Phys. Chem.* 94 (1990) 5523–5527, <https://doi.org/10.1021/j100377a021>.
- [50] P.J. Harlick, A. Sayari, Applications of pore-expanded mesoporous silica. 5. Triamine grafted material with exceptional CO₂ dynamic and equilibrium adsorption performance, *Ind. Eng. Chem. Res.* 46 (2007) 446–458, <https://doi.org/10.1021/ie060774+>.
- [51] M. Wickenheisser, F. Jeremias, S.K. Henninger, C. Janiak, Grafting of hydrophilic ethylene glycols or ethylenediamine on coordinatively unsaturated metal sites in MIL-100(Cr) for improved water adsorption characteristics, *Inorg. Chim. Acta.* 407 (2013) 145–152, <https://doi.org/10.1016/j.ica.2013.07.024>.
- [52] S.N. Kim, S.T. Yang, J. Kim, J.E. Park, W.S. Ahn, Post-synthesis functionalization of MIL-101 using diethylenetriamine: a study on adsorption and catalysis, *CrystEngComm* 14 (2012) 4142–4147, <https://doi.org/10.1039/C2CE06608D>.
- [53] A. Arnanz, M. Pintado-Sierra, A. Corma, M. Iglesias, F. Sánchez, Bifunctional metal organic framework catalysts for multistep reactions: MOF-Cu(BTC)-[Pd] catalyst for one-pot heteroannulation of acetylenic compounds, *Adv. Synth. Catal.* 354 (2012) 1347–1355, <https://doi.org/10.1002/adsc.201100503>.
- [54] C.O. Areán, C.P. Cabello, G.T. Palomino, Infrared spectroscopic and thermodynamic study on hydrogen adsorption on the metal organic framework MIL-100(Sc), *Chem. Phys. Lett.* 521 (2012) 104–106, <https://doi.org/10.1016/j.cplett.2011.11.054>.
- [55] J. Szanyi, M. Daturi, G. Clet, D.R. Baer, C.H.F. Peden, Well-studied Cu–BTC still serves surprises: evidence for facile Cu²⁺/Cu⁺ interchange, *Phys. Chem. Chem. Phys.* 14 (2012) 4383, <https://doi.org/10.1039/C2CP23708C>.
- [56] N. Aider, A. Smuszkiewicz, E. Pérez-Mayoral, E. Soriano, R.M. Martín-Aranda, D. Halliche, S. Menad, Amino-grafted SBA-15 material as dual acid–base catalyst for the synthesis of coumarin derivatives, *Catal. Today* 227 (2014) 215–222, <https://doi.org/10.1016/j.cattod.2013.10.016>.
- [57] A. Smuszkiewicz, E. Pérez-Mayoral, E. Soriano, I. Sobczak, M. Ziolk, R.M. Martín-Aranda, A.J. López-Peinado, Bifunctional mesoporous MCF materials as catalysts in the Friedländer condensation, *Catal. Today* 218–219 (2013) 70–75, <https://doi.org/10.1016/j.cattod.2013.04.034>.